# Investigating the effects of Wnt/β-catenin Signalling on Melanoma Cell Metabolism and Mitochondrial Dynamics

**Kate Brown**

A Thesis Presented for the Degree of Doctor of Philosophy from the School of Pharmacy at the University of East Anglia, Norwich, UK.

February 2015

# I. Abstract

Wnts are secreted morphogens that play pivotal roles in embryonic development, stem cell biology and a number of disease states including cancer. Most Wnts signal through a pathway that results in the stabilisation of an intracellular signalling molecule called β-catenin. In melanoma cells, Wnt/β-catenin signalling has been implicated as a key regulator of cellular invasion and metastasis.

Using both transient and stable enhancement of Wnt/β-catenin signalling, I have found that mutation–based dysregulation of PI3K signalling dictates the invasive capacity of melanoma cell lines in response to Wnt3a stimulation. I demonstrate by confocal imaging that WNT3A facilitates perinuclear localisation of mitochondria with higher levels of mitochondrial networking and they show significant changes in the proteins of mitochondrial dynamics. Observed changes in mitochondrial fusion and fission proteins including MFN1, MFN2, OPA1 and DNM1L suggest that activation of Wnt/β-catenin signalling can increase mitochondrial fusion and decrease mitochondrial fission in melanoma cells. Cellular metabolic analysis using the Seahorse Bioscience $XF^e96$ Analyzer suggests that Wnt/β-catenin mediated mitochondrial fusion may cause a global down-regulation of cellular energy metabolism in melanoma cells. This is supported by biochemical analysis of citrate synthase and lactate dehydrogenase activity.

Knockout of β-catenin removes the mitochondrial fusion effect in these cells and reverses any Wnt driven reduction in migration and metabolism suggesting that β-catenin is able to control mitochondrial function and dynamics. We show that β-catenin binds to the mitochondrial regulatory protein PARK2 in melanoma cells and subsequently blocks the autophagy dependency of melanoma cells.

In summary, we demonstrate that activation of Wnt/β-catenin signalling in melanoma cells can lead to reduced cellular metabolism coupled with highly altered mitochondrial dynamics. This novel finding, controlled by β-catenin, has potentially wide implications for understanding how certain context-dependent effects of Wnt/β-catenin signalling may be secondary to the regulation of mitochondrial dynamics and global cellular metabolism.

# II. List of Contents

# III. List of Tables

# IV. List of Figures

## V. List of Abbreviations

Ab - Antibody

Akt – Protein Kinase B

ADP – Adenosine Diphosphate

AJCC - American Joint Commission on Cancer

ADT - Adenosine Diphosphate

ATP - Adenosine Triphosphate

APC - Adenomatosis Polyposis Coli

APS - Ammonium Persulfate

BCA - bicinchoninic acid

BRAF – Gene encoding B-Raf protein

BrdU - Bromodeoxyuridine

BSA - Bovine serum albumin

CamKII - calcium-calmodulin-dependent kinase

CCCP - Carbonyl cyanide *m*-chlorophenyl hydrazine

CK1α - Casein Kinase 1α

$CO_2$ – Carbon Dioxide

CoA – Coenzyme A

CRD - cysteine rich domain

Daam1 - Dishevelled-associated activator of morphopgenesis 1

DAG - di-acyl glycerol

DCFDA - 2',7' –dichlorofluorescin diacetate

DHICA - 5,6-dihydroxyindole-2-carboxylic acid

DKK1 - Dickkopf related protein 1

DMEM - Dulbecco's modified Eagle's medium

DMSO - Dimethyl sulfoxide

DNA - Deoxyribonucleic acid

dNTPs - Deoxynucleotide Triphosphates

DOPA - 3,4-dihydroxyphenylalanine

DRP - Dynamin-1-like protein

DTT - Dithiothreitol

Dvl - Dishevelled

ECAR - Extracellular Acidification Rate

ECL - Electrochemiluminescence

EDTA - Ethylenediaminetetraacetic acid

EF-$Tu_{mt}$ – mitochondrial elongation factor Tu

EMT – Epithelial to Mesenchymal Transition

em - emmission

Edn3 - endothelin 3

ER - Endoplasmic reticulum

ERK - Extracellular regulated kinase

ETC - Electron Transport Chain

ex - Excitation

FACS - Flow Assisted Cell Sorter

FCCP - Trifluorocarbonylcyanide Phenylhydrazone

FCS - Fetal calf serum

$FAD^+$ - flavin adenine dinucleotide-oxidase

$FADH_2$ - flavin adenine dinucleotide-reduced

Fsc - Forward Scatter

Fcs-a - Forward scatter area

Fsc-h - Forward scatter height

FZD - Frizzled

GAPDH - Glyceraldehyde 3-phosphate dehydrogenase

GDP – Guanosine diphosphate

GFP - Green Fluorescent Protein

GSK3 – Glycogen Synthase Kinase 3

GTP - Guanosine-5'-triphosphate

GTPases - Gunaosine Triphosphatases

$H_20$ - Water

HBSS - Hanks buffered salt solution

HCL - Hydrochloric acid

HRP - Horseradish Peroxidase

HSP – Heavy strand promoter

HSP - Heat shock protein

$IF_{mt}$ – mitochondrial initiation factor

IgG - Immunoglobulin

IHC - Immunohistochemistry

IMM - Inner Mitochondrial Membrane

IP - Immunoprecipitation

$IP_3$ - inositol 1,4,5-triphosphate

JUK - Jun kinase

Kbp – kilobase pairs

KO - Knockout

LDH – Lactate Dehydrogenase

LDL - low-density lipoprotein

LEF1 - Lymphoid Enhancer-Binding Factor 1

LHON - Leber's hereditary optic neuropathy

LRP5/6 - Low-density lipoprotein receptor-related protein 5/6

LSP – Light strand promoter

MAPK - Mitogen activated protein kinase

MC1R – Melanocortin-1 receptor

MDM2 - Mouse double minutes 2 homolog

MELAS - mitochondrial encephalopathy, lactic acidosis and stroke-like episode syndrome

MFN - Mitofusin

MITF - Microphthalmia-associated transcription factor

mtDNA - Mitochondrial DNA

mTOR - Mammalian target of rapamycin

mtRF1a - Mitochondrial termination release factor

mtSSB - Mitochondrial-specific single-stranded DNA binding protein

$NAD^+$ - Nicotinamide adenine dinucleotide-oxidase

NADH - Nicotinamide adenine dinucleotide-reduced

$NADP^+$ - Nicotinamide adenine dinucleotide phosphate-oxidase

NADPH - Nicotinamide adenine dinucleotide phosphate-reduced

NCC – Neural Crest Cells

ND - NADH dehydrogenase

NF-κB - Nuclear factor kappa-light-chain-enhancer of activated B cells

NLK - Nemo-like kinase

NRAS - neuroblastoma RAS viral (v-ras) oncogene homolog

NOD-SCID - Non-Obese Diabetic - Severe combined immunodeficiency

ns – not significant

OCR - Oxygen Consumption Rate

OMM - Outer Mitochondrial Memebrane

OPA - optic atrophy type 1

OXPHOS - Oxidative Phosphorylation

P- Phosphorylated

PAGE - Polyacrylamide Gel Electrophoresis

PBS - Phosphate buffered saline

PCP - Planar Cell Polarity

PCR - Polymerase Chain Reaction

PDE6 - phosphodiesterase 6

PDL - Poly-D-Lysine

Pen/Strep - 100 U/mL penicillin and 100 µg/mL streptomycin (pen/strep)

PFA - Paraformaldehyde

PI3K - Phosphoinositide 3-kinase

$PIP_2$ - phosphatidylinositol 4,5-biphosphate

$PIP_3$ - phosphatidylinositol (3,4,5)-trisphosphate

PKC – Protein kinase C

PLC - phospholipase C

POLG - DNA polymerase

PolyHEMA - Poly(2-hydroxyethyl methacrylate).

PP2A – Protein Phosphatase 2A

PTEN - Phosphatase and tensin homolog

qPCR - Quantitative polymerase chain reaction

r - Recombinant

Rac – Sub family of the Rho family of GTPases

Ras – Rat sarcoma superfamily of proteins

Rho – Sub Family of GTPases, sub family of Ras superfamily of proteins

RNA - Ribonucleic acid

ROCK - Rho-associated kinase

ROR2 - receptor tyrosine kinase-like orphan receptor 2

ROS - Reactive oxygen species

RPMI - Roswell Park Memorial Institute medium

rRNA – ribosomal RNA

RT - Room temperature

RTK - receptor-like tyrosine kinase

RT-PCR - Reverse Transcriptase Polymerase Chain Reaction

si - Small Interfering

SDS - Sodium dodecyl sulfate

SFRPs - soluble frizzled-related proteins

SNHL - non-syndromic sensorineural hearing loss

SNPs - single poly nucleotide

STA - stabilized constitutively active

TAE – Tris Acetate EDTA

TAK1 - TGFβ activated kinase

TRP - Tautomerse

TBS - Tris Buffered Saline

TBST - Tris Buffered Saline Tween

TCA cycle - tricarboxylic acid cycle

TCF4 - Transcription factor 4

TE – Tris-EDTA

TEMED - Tetramethylethylenediamine

TIM - Translocase of inner mitochondrial membrane

TMRM - Tetramethylrhodamine, methyl ester

TOM - Translocase of outer mitochondrial membrane

tRNA – transfer RNA

UV - Ultraviolet

UVR – Ultraviolet Radiation

VDAC - voltage-dependent anion channel

WIF – Wnt inhibitory factor

Wnt – Wingless Int genes

2D - Two Dimensional

3D - Three Dimensional

## VI. Acknowledgements

In writing my Ph.D. thesis, I have received support from many people, some of whom deserve a special mention. I would like to firstly thank my supervisor Dr Vicky Sherwood. I would like to thank you for encouraging my research and for allowing me to grow as a research scientist. Your advice on both research as well as on my career have been priceless. I would especially like to thank Dr Andy Chien and Prof. Randy Moon for allowing me to spend time in their labs at the University of Washington and to Rima, and the other lab members for all their help and assistance. The time I spent in Seattle including the work I carried out and the friendships I made were invaluable.

I also want to that the members of the Sherwood, Morris and Baldelli-Bombelli groups, for your friendship and help over the past 3 years. In addition, I thank the members of the O'Connell, Wheeler and Münsterberg labs for their help and generosity, and Dr Paul Thomas and Dr Darren Sexton for your technical help and guidance.

A special thanks goes to my family, for your support. Especially to my dad for your grammatical proof readings. I'd like to promise I will never ask again but I don't think I can. Finally, and most of all, I owe utmost thanks to my husband Alex. Thank you for making me laugh when I wanted to cry and letting me rant over things you didn't understand. Your unwavering confidence in me and our future gave me the strength to get through this.

# 1. INTRODUCTION

## 1.1. Melanoma

Cancer is the uncontrolled, abnormal, growth of cells that initiates due to a DNA mutation (1). There are over 200 different types of cancer that vary in their causes and symptoms, but they all have increased cell proliferation. The current statistics from Cancer Research UK state that one in two people will develop cancer, at some point throughout their lifetime and results in more than one in four deaths in the UK (2). Due to lifestyle, certain cancers have increased over the past 50 years. These include lung cancer due to smoking, liver and kidney cancers due to alcohol consumption and melanoma due to ultraviolet radiation (2). However, over the past few decades, due to increased awareness and routine screening, there has also been a dramatic reduction in some cancers, including cervical and lung cancer but, conversely, the national screening programme actually led to an increase in the number of breast cancer diagnoses (2). As well as cancer being caused by external carcinogens, there is a hereditary link to a number of cancers, including the BRCA1 gene in breast cancer and the CDKN2A mutation in melanoma (3-5). These predispositions have lead an increase in early diagnosis, as well as increased research leading to better therapies and longer life expectancies have all contributed to an overall decrease in cancer related deaths, in both the UK and the US (2, 6).

Cancer research is a very broad topic, given the number of different types of cancer and the different causes. Some main areas of research focus on factors that affect most, if not all, cancers. Tumours will initiate from one cell type but, as they grow, they will form a body that encompasses a variety of cells. Tumours will evade the immune system as they develop from our own cells and, therefore, are not recognised as foreign bodies. Current research into the tumour microenvironment, especially regulatory T cells, how these contribute to tumour growth and how they could be targeted in cancer treatments is on going (7). Another main area of cancer research focuses on angiogenesis, the process by which tumours will develop their own blood supply to provide oxygen and nutrients for growth. The blockade of the signals that initiate angiogenesis or the formation of new blood vessels is currently

under investigation (8). Another area of cancer research is that of metabolism as described in detail in section 1.3.2. The altered metabolism of cancer cells has been known since it was first described by Otto Warburg in 1924 (9). However, research into this aspect of cancer biology has grown more recently as we investigate the mechanisms that control cancer cell metabolism and, potentially, how to target it in treatments.

### 1.1.1. The Structure of the Skin

This research focuses on metastatic melanoma (MM), the worst form of skin cancer as described in detail in the following sections. Other non-melanoma skin cancers (NMSC) are more common including squamous cell carcinoma (SCC) and basal cell carcinoma (BCC) but these cause relatively few deaths, compared to those caused by MM (10-12). Melanoma is a cancer of melanocytes, the pigment producing cells predominantly found in the basal layer of the epidermis of the skin, but also, located in the hair follicle, the iris of the eye, and the inner ear (13-15). Skin is the largest organ of the body. It protects the major organs, acts as a barrier to pathogens and aids homeostasis of the body by retaining water and releasing sweat. It also acts as the best protection against ultraviolet radiation (1). The skin consists of three main layers; Figure 1.1 shows a cross section of the skin structure. The top layer is the epidermis, which is broken down into four sub-layers. The stratum corneum is the top layer, made mainly of dead skin cells, is highly hydrophobic and roughly 10-20 µm thick (16). The second layer is the stratum granulosum, formed of granular keratinocytes and the third layer is the stratum spinosum, formed of polyhedral keratinocytes (17). Within these layers, there will also be Langerhans cells (16). The fourth layer is the stratum germinativum. It is within this basal layer that the melanocytes reside with merkel cells (17). The second main layer of the skin is the dermis and the connection between the dermis and the epidermis is known as the basement membrane. The main body of the dermis is called the dermal matrix, which is full of collagen allowing the flexibility of the skin. The dermis also consists of fibroblasts, dendritic cells and a variety of immune cells, including T-cells. This thick layer of the skin will also have blood vessels, hair follicles, and sebaceous and

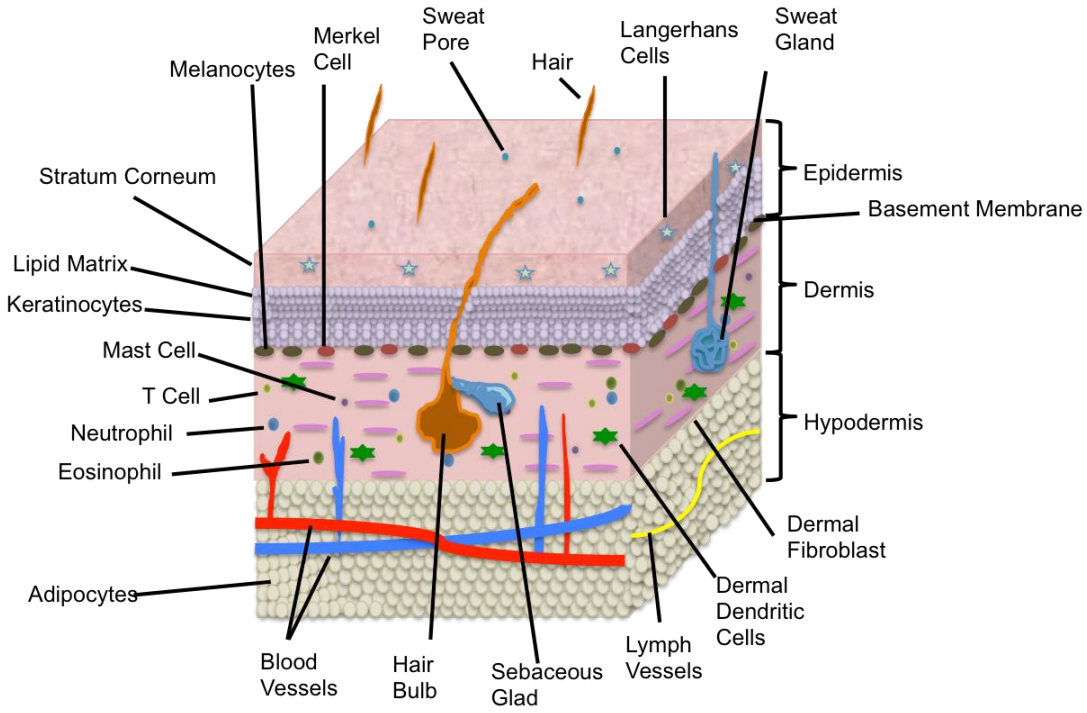


**Figure 1.1: The Structure of the Skin**

The skin is divided into three layers, the Epidermis is the top layer covered by the Stratum Corneum, which contains Langerhans cells. It is through the epidermis that sweat is secreted, and hairs protrude. The epidermis is primarily made up of keratinocytes and at the bottom is the basement membrane consisting of melanocytes and merkel cells. The second layer is the Dermis. Within the dermal matrix are the all other aspects of skin biology, it contains hair bulbs, sebaceous glands, sweat glands, and many cells types including, mast cells, T-cells, neutrophils, eosinophils, dermal fibroblasts and dendritic cells. Smaller branches of blood vessels will also protrude into the dermis from the hypodermis, the bottom layer of the skin structure. Made primarily of adipocytes the hypodermis houses the blood vessels including veins, arteries and lymph vessels. Image adapted from (1).

sweat glands. The final layer of the skin is often not, actually, considered to be part of the skin structure. The hypodermis is primarily made of adipocytes and houses the larger blood and lymphatic vessels (16).

### 1.1.2. The Development and Function of Melanocytes

Melanocytes derive from neural crest cells (18) from the ectoderm of developing embryos (17, 19, 20). The neuroectoderm forms the neural plate, which folds into the neural tube to become elements of the central nervous system. NCC arise from the neural plate boarder created by levels of bone morphogenetic proteins, Wnt and fibroblast growth factor secreted from the underlying paraxial mesoderm, as well as Wnt signals from the non-neural ectoderm (19, 21, 22). This leads to the expression of neural plate boarder specifiers including; Pax3/7, Zic, Msx1/2 and Dlx5 (23), which are precursors to the neural crest markers; Slug/Snail, FoxD3, Sox10, Sox9, AP-2 and c-Myc (17, 19, 24, 25). These genes signify the specification of the NCC as they regulate the expression of genes controlling cell cycle, epithelial to mesenchymal transition (EMT) and migration (23). Once the neural tube is formed, NCC cells form the roof plate and undergo EMT, the transcription of Slug/Snail repress expression of E-cadherin and, under non-canonical Wnt signalling, cause the progenitor cells to migrate along the dorsolateral route beneath the ectoderm to their final destination (17, 20, 22, 26). There are typically four groups of NCC, cranial, vagal, trunk and sacral, where melanocytes originate from the trunk and cranial populations and reside, mainly, in the epithelium (17, 20). As well as melanocytes, the NCC are responsible for the production of other cell lineages through the SoxE family of proteins. These include cartilage mesectoderm, neurons and glial cells. The lineage specification of NCC is dependent on their location and multiple signalling pathways. Notch and canonical Wnt signalling are both implicated in the specification of neural crest progenitor cells such as the melanocyte precursors, melanoblasts (19, 21, 25). It has been shown that melanoblasts actually have their cell lineage defined before they leave the neural tube (27), but the development of a melanoblast is controlled by Microphthalmia-associated transcription factor (MITF), together with Pax3 and Sox10 (28). As both Pax3 and Sox10 are involved in the lineage specification of other

NCC, it is MITF that is known as the master regulator of melanogenesis (29). Following their lineage determination, melanocyte survival and migration is controlled by endothelin 3 (Edn3) and its receptor Ednrb, c-KIT and MITF (19, 25), leading to the activation of the Protein kinase C (PKC) and mitogen-activated protein kinase (MAPK) pathways (30). As stated previously, MITF is the master regulator of melanocyte development and it is especially vital in melanogenesis (29, 31). MITF activates pigment producing genes such as *dct* and *tyrosinase* (32) and plays a role in melanoblast survival by upregulating the anti-apoptotic gene *bcl2* (19, 33). Adult melanocyte stem cells develop through the same process and reside primarily in the hair bulge, although it is debated as to whether they are also present in the dermis (17, 34). In the hair bulge melanocyte stem cells are activated during the regeneration of a new hair and, then, migrate to the basal layer of the epidermis where they become mature melanocytes (17).

Melanocytes produce melanin in a biochemical process termed melanogenesis (17, 35). Melanin has many beneficial properties including absorption and scattering of ultraviolet (UV) light, scavenging of free radicals, ion storage and is used in coupled oxidation-reduction reactions (36, 37). Melanin is produced in cytoplasmic organelles called melanosomes (37, 38) in response to ultraviolet radiation (UVR) (17, 35-37). These double membrane, intracellular, organelles are formed in four stages (39, 40). Firstly, intraluminal proteinaceous fibrils start to form and, in stage two, this continues and melanin synthesis begins (as described later). As melanin is produced, it is deposited on to the fibrils which causes them to thicken and darken. This stage is often referred to as maturation (39, 40). The final stage sees a loss of the fibril structure as the melanin encompasses the internal structure. Upon stimulation by sunlight, surrounding keratinocytes in the skin activate p53 by UVR, causing transcription of proopiomelanocortin and an increase in α-melanocyte stimulating hormone (α-MSH), adrenocorticotropic hormones and pro-pigment activities (41). When α-MSH binds to the melanocortin-1 receptor (MC1R), it activates the cAMP/protein kinase A (42)/CREB signalling pathway and increases the levels of MITF and subsequent melanin synthesis and pigmentation (43-45). The number of melanocytes in the epidermis is fairly constant at 1200/mm$^2$ independent

of skin colour (17, 37) but numbers increase following UVR (46). Melanocyte proliferation is controlled by factors released by the surrounding keratinocytes such as α-MSH, Edn3, granulocyte-macrophage colony-stimulating factor, steel factor, leukemia inhibitory factor, basic fibroblast growth factor, and hepatocyte growth factor (47), leading to the activation of the MAPK/extracellular regulated kinase (ERK) and phosphoinositide 3-kinase (PI3K)/AKT signalling pathways (48). Following melanogenesis, melanocytes distribute the melanin to 30-40 nearby keratinocytes (17, 20, 49). Melanocytes have dendritic formations that allow for the transfer of melanin, where it sits above the nucleus to protect the DNA from ionising radiation (17, 49, 50). Figure 1.2 shows a schematic of the melanin scattering.

Melanin comes in two different forms, the dark black/brown eumelanin and a red/yellow pheomelanin (13, 51), produced according to the availability of substrates such as cysteine and tyrosine (17). Tyrosinase converts tyrosine to 3,4-dihydroxyphenylalanine (DOPA) by hydroxylation and DOPA is then oxidised to DOPAquinone (52). If cysteine is present, it will react with DOPAquinone to produce cysteinylDOPA, oxidation of which then produces the yellow/red pheomelanin (35, 53). If cysteine is not available DOPAquinone is converted to DOPAchrome by cyclisation (53). DOPAchrome loses its carboxylic acid, becoming DHI, which, when oxidized, forms the insoluble dark brown/black DHI-melanin. DOPAchrome can, however, also be converted to 5,6-dihydroxyindole-2-carboxylic acid (DHICA) in the presence of tautomerse (TRP) 2 which is catalyzed by TRP1 to form the light brown DHICA-melanin (35, 53). Figure 1.3 shows a simple schematic of this process. There is always a mixture of melanins in human skin, but it is, typically, the levels of eumelanin that determine skin colour differences between ethnic groups (17). Eumelanin has better photoprotecting properties, including an ability to neutralise reactive oxygen species (ROS) and resistance to degradation (54). Due to its higher photoprotection there is a 30-40% decrease in risk of developing skin cancer in darker skin (53).

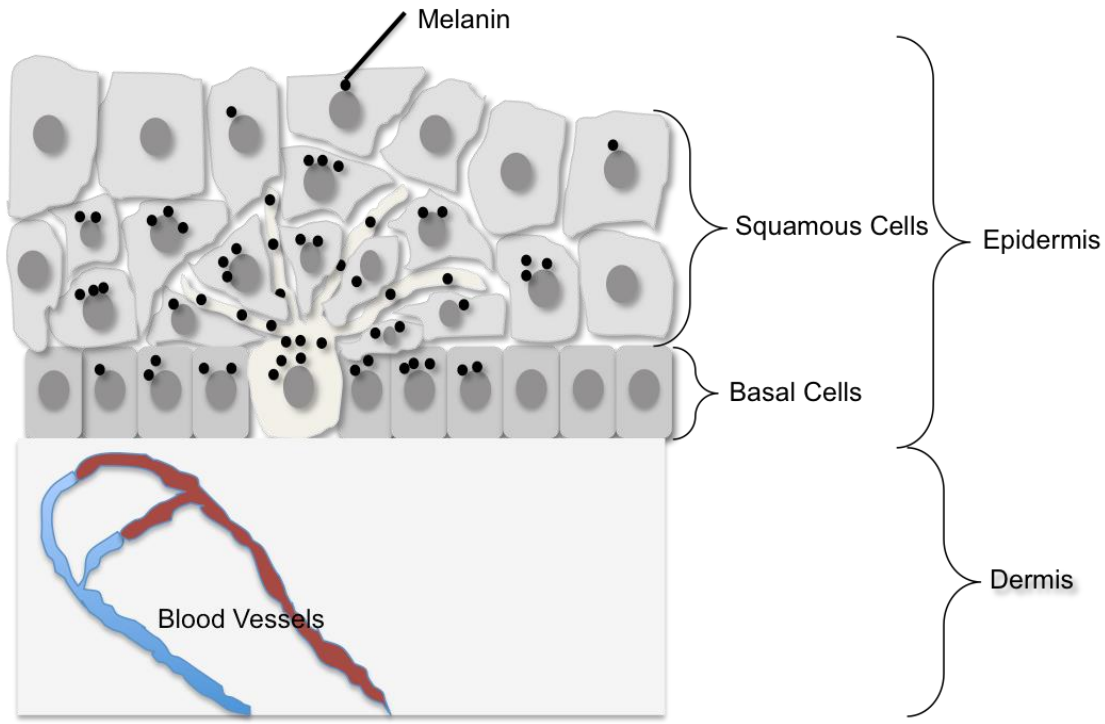


**Figure 1.2: Melanin Scattering From Melanocytes to Nearby Keratinocyte Cells**
Melanocytes sit at the base of the epidermis and dendritic formations extend around the keratinocytes to allow for transfer of melanin. Melanosomes sit atop the nucleus of cells to protect the DNA from UVR. Image adapted from (17).

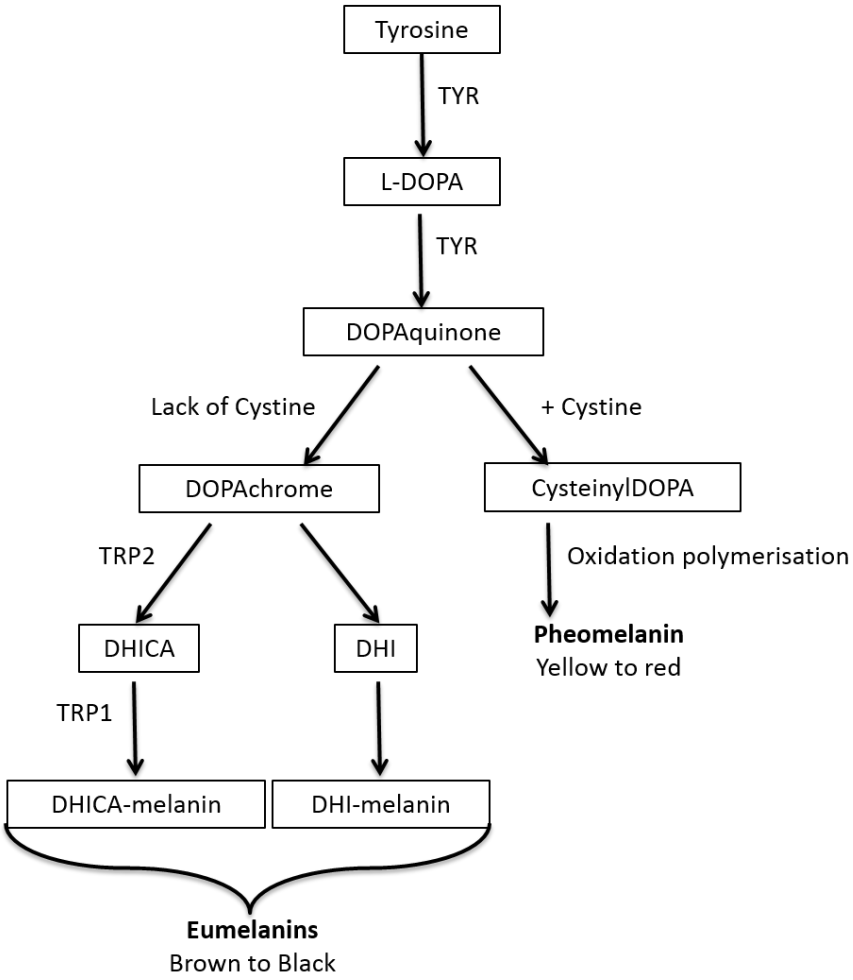


**Figure 1.3: Melanogeneis production of Pheomelanin and Eumelanin**
Melanin formation initiates from Tyrosine. Tyrosinase converts it to 3,4-dihydroxyphenylalanine (DOPA) by hydroxylation, DOPA is then oxidised to DOPAquinone. If cysteine is present it will react with DOPAquinone to produce cysteinylDOPA, oxidation of which then produces the yellow/red pheomelanin. If cysteine is not available DOPAquinone is converted to DOPAchrome by cyclisation. DOPAchrome loses its carboxylic acid becoming DHI, which when oxidized forms the insoluble dark brown/black DHI-melanin. DOPAchrome can however also be converted to 5,6-dihydroxyindole-2-carboxylic acid (DHICA) in the presence of tautomerse (TRP) 2 which is catalyzed by TRP1 to form the light brown DHICA-melanin. Image adapted from (17).

### 1.1.3. Initiation and Progression of Metastatic Melanoma

Melanoma can occur anywhere in the body. Melanocytes can proliferate and aggregate to form benign hyperplastic lesions called nevi (20). However, these are not necessarily precursors to malignant melanoma as direct transformation of melanocytes can also occur (20). Most often, nevi do not progress to malignant disease due to cellular senescence (55, 56), but melanomas acquire alterations, causing excessive proliferation and a survival benefit (19, 25). Both the MAPK/ERK, and PI3K/Akt pathways are linked to melanocyte proliferation. Therefore, it is unsurprising that the majority of mutations initiating melanomas are within these pathways (57), as described further in section 1.1.4.

Melanomas typically start progressing with a horizontal or radial growth phase (RGP) during which they can be easily excised (19). In the RGP, the tumour grows through the epidermis, but does not invade through the basement membrane, which separates the epidermal and dermal layers of skin. This is followed by a vertical growth phase where melanoma cells will invade through the basement membrane into the dermis and hypodermis. As melanoma progresses into a metastatic phase, it will eventually invade through the endothelium and into the vascular system by intravasation and travel to distant sites before extravasation and secondary tumour formation (19, 25, 58).

When checking nevi, the rule of ABCDE helps aid identification of a potential malignant melanoma. A stands for Asymmetry, B = Boarder, C = Colour, D = Diameter and E = Evolving (59). Normal benign nevi will be uniform in shape and colour, and will typically be round with a smooth border and should be no wider than the end of a pencil (6 mm). However, diversion from any of these factors can occur without diagnosis of melanoma. The indication that something is wrong with a pre-existing nevi is evolution, whether the nevi changes in size, shape or colour (60). There are alternative views to these descriptions, given the role of MITF in the pigmentation of melanoma (31), D can sometimes stand for Dark (61).

#### 1.1.3.1. Prevalence of Melanoma

Metastatic melanoma is the 5th most common cancer in the UK. It is one of the most aggressive malignancies in humans and is responsible for 60% of all deaths associated with skin cancer (49). Melanoma accounts for less than 5% of new cancer cases in the US and the UK (1, 10, 62), accounting for around 20 new cases for every 100,000 people (10, 62). However, incidence of the disease has been on the rise for the past two decades (63, 64) and it is estimated that numbers have quadrupled since the 1970s (10, 49, 65). More recently, between 1992 and 2004, melanoma incidence increased 45%, or 3.1% annually (66). This is primarily thought to be due to increased sun exposure from more frequent holidays, long-term increased sun exposure and, recently, due to the increased trend of tanning-beds (65, 67, 68). Due to this, melanoma has an unusual pattern of incidence although, as with other cancers, the majority (45%) of cases are in the over 65s, there has been an increase in cases in the under 50s population (10). The disease is more frequent in men in the over 50s age range (6) but, actually, has a ratio of 4:10, men to women, in the 20-24 age range (10). Currently, it is the most common form of cancer among adults 25-29 and the second most common amongst 15-29 year olds (69). About 65% of melanoma cases can now be attributed to UVR from the sun or sunbed use and this rises to 85% in the UK alone (70, 71). Between 1980 and 2004, the annual incidence of melanoma among young women increased by 50%, from 9.4 cases to 13.9 cases per 100,000 women (72), and this is attributed to around 100 deaths in the UK (73). UVR is a proven human carcinogen (74). Frequent tanners using new high-pressure sunlamps may receive as much as 12 times the annual UVA dose compared to the dose that they receive from sun exposure (73). The International Agency for Research on Cancer, an affiliate of the World Health Organization, includes UV tanning devices in its Group 1, a list of the most dangerous cancer-causing substances, a group that also includes agents such as plutonium, cigarettes, and solar UVR (74). A public awareness campaign, 'Sun Smart', has been running in the Australian State of Victoria since 1988 (75). Incidence rates in this region are starting to now slow and the education on sun damage is starting to take a positive effect (76). Due to this campaign, as of the beginning of this year, commercial sunbeds are now banned in

the State of Victoria. In the UK, as a result of the campaigning of famous skin type 1 individuals, the Sunbeds (Regulation) Act came into effect in 2010 to ban the use of sunbeds for under-18s. Unfortunately, despite the campaign, prevalence in Australasia is increasing rapidly, due to UVR but, it is believed, this is due to climatic change and the reduction in the ozone layer (70, 77-79).

Incidences rates in non-Caucasian populations are low (80). However, Asian American and African American melanoma patients have a greater tendency than Caucasians to present with advanced disease at time of diagnosis. While melanoma is uncommon in African Americans, Latinos, and Asians, it is frequently fatal for these populations (81). As few as 48% of melanomas in African Americans are diagnosed at an early stage, compared to 74% in Hispanics and 84% in Caucasians (82, 83). Melanomas in African Americans, Asians, Filipinos, Indonesians and native Hawaiians most often occur on non-exposed skin with less pigment, with 60-75% of tumours arising on the palms, soles, mucous membranes and nail regions (83).

#### 1.1.3.2. Pathological Staging of Melanoma

Staging of melanoma in the UK and U.S. is currently carried out according to the American Joint Commission on Cancer (AJCC) TNM system the details of which are in Table 1.1. T stands for Tumour and determines tumour growth within the skin and is defined by a number 0-4, depending on depth or thickness of the tumour as measured by the Breslow measurement. This classification will also be given a rating of a or b depending on the presence of ulceration (a-without/b-with), and/or mitotic cells. N stands for Nodes and this classification determines if the cancer has spread to the lymph nodes or the lymphatic system and is rated on a scale of 0-3 determined by spread and number. In addition, a, b or c will determine the size of metastatic lesion, a- for microscopic, b- for macroscopic and c- spread only to the local skin or lymphatic channels but has not reached the lymph nodes. M stands for Metastasised. It is based on either yes or no represented as 0 or 1. Letters a, b and c determine the location of the metastases and the levels of lactate dehydrogenase

**Table 1.1: TNM classification**

The table shows the TNM classification of melanoma. Table adapted from AJCC Melanoma Staging and Classification (84).

| Classification | | |
|---|---|---|
| **T** | **Thickness (mm)** | **Ulceration Status/Mitoses** |
| **T1** | ≤ 1.0 | a: Without ulceration and mitosis < 1/mm$^2$ |
| | | b: With ulceration or mitosis ≥ 1/mm$^2$ |
| **T2** | 1.01-2.00 | a: Without ulceration |
| | | b: With ulceration |
| **T3** | 2.01-4.00 | a: Without ulceration |
| | | b: With ulceration |
| **T4** | > 4.00 | a: Without ulceration |
| | | b: With ulceration |
| **N** | **No. of metastatic Nodes** | **Nodal Metastatic Burden** |
| **N0** | 0 | N/A |
| **N1** | 1 | a: Micrometastasis |
| | | b: Macrometastasis |
| **N2** | 2-3 | a: Micrometastasis |
| | | b: Macrometastasis |
| | | c: In transit metastases/satellites without metastatic nodes |
| **N3** | 4+ | Metastatic nodes, or matted nodes, or in transit metastases/satellites with metastatic nodes. |
| **M** | **Site** | **Serum LDH** |
| **M0** | No Distant metastasis | N/A |
| **M1a** | Distant skin, subcutaneous, or nodal metastases | Normal |
| **M1b** | Lung Metastases | Normal |
| **M1c** | All other visceral metastases | Normal |
| | Any distant metastasis | Elevated |

(LDH) in the blood (84). Table 1.2a shows how the TNM classification fits into the pathologic staging of a melanoma at diagnosis.

#### 1.1.3.3. Mortality of Melanoma

Despite the rise in incidence, the number of associated deaths has fallen and it is now the least common cause of cancer-related deaths in the UK (10). This is partly due to the ageing population extending survival rates but, mainly, due to increased awareness leading to earlier diagnosis (49). The survival rate for patients whose melanoma is detected early, before the tumour has penetrated the epidermis, is about 97% (6). The survival rate falls to 10% for those with advanced disease (6). As stated previously, the often late diagnosis in African Americans results in their overall survival rate being only 77%, compared with 91% for Caucasians (80). A detailed breakdown of survival rates defined by melanoma stage is shown in Table 1.2b.

#### 1.1.3.4. Current Treatment Options

The primary treatment for melanoma is surgery, followed by lymph node mapping to test for metastasis. Sentinel nodes are lymph nodes that are predicted to be the likely first sites of metastasis, due to their proximity to the tumour. Sentinel node biopsies, with the use of radioactive tracers, allow the identification and removal of metastatic lymph nodes (84). However, this can cause lymphedema, a swelling due to the lack of fluid removal that would have been carried out by the lymph node. This is especially common if the nodes are removed from the groin and under the arm (85, 86). It can be a lifelong problem and cause subsequent skin problems and be very painful so, therefore, a full lymph node dissection is only carried out if necessary. Following this surgery, adjuvant therapy is recommended to prevent reoccurrence. Typically, high dose interferon α2b is the initial treatment although the benefits of this have been questioned and, if it does prevent reoccurrence, the effect is minimal (87, 88). If a tumour is inoperable, regional chemotherapy may be undertaken. However, if the tumour is in a limb, hyperthermic isolated limb perfusion has been shown to extend the time of reoccurrence by up to 37 months

**Table 1.2: Pathalogic Staging of Melanoma**

**a)** Table represents the pathalogical staging of melanoma according to the TNM classification. **b)** 5 year and 10 year survival rates according to stage at time of diagnosis. Tables adapted from AJCC Melanoma Staging and Classification (84).

**a)**

| | T | N | M |
|---|---|---|---|
| IA | T1a | No | M0 |
| IB | T1b | No | M0 |
| | T2a | No | M0 |
| IIA | T2b | No | M0 |
| | T3a | No | M0 |
| IIB | T3b | No | M0 |
| | T4a | No | M0 |
| IIC | T4b | No | M0 |
| IIIA | T1-4a | N1a | M0 |
| | T1-4a | N2a | M0 |
| IIIB | T1-4b | N1a | M0 |
| | T1-4b | N2a | M0 |
| | T1-4a | N1b | M0 |
| | T1-4a | N2b | M0 |
| | T1-4a | N2c | M0 |
| IIIC | T1-4b | N1b | M0 |
| | T1-4b | N2b | M0 |
| | T1-4b | N2c | M0 |
| | Ant T | N3 | M0 |
| IV | Any T | Any N | M1 |

**b)**

| Stage | % 5 year survival | % 10 year survival |
|---|---|---|
| IA | 97 | 95 |
| IB | 92 | 86 |
| IIA | 81 | 67 |
| IIB | 70 | 57 |
| IIC | 53 | 40 |
| IIIA | 78 | 68 |
| IIIB | 59 | 43 |
| IIIC | 40 | 24 |
| IV | 15 | 10 |

(89). Chemotherapy agents such as dacarbazine have minimal effects in advanced disease, with a response seen in 5% of patients extending progression free survival by only 1.6 months (90). Temozolomide is an oral analogue of dacarbazine that has the added benefit of penetrating the central nervous system and, therefore, has beneficial effects on brain metastasis (91). Other single chemotherapeutic agents include anti-microtubular agent, paclitaxel which has around a 20% response rate but causes toxic side effects including alopecia, neuropathy and myelosupression (91). Chemotherapeutic agents with limited beneficial effects, when used in combination therapies have increased response rates. Agents that are typically not used for the treatment of melanoma such as cisplatin and tamoxifen, when combined with dacarbazine and carmustine in a treatment called the Dartmouth regimen, had a response rate of 55%. However, they had little effect on overall survival (91, 92). Once a melanoma has reached stage III or is a recurrent melanoma, treatments become more targeted (93). Biological treatments can include IL-2 and INF-α that can be used alone or in combination with chemotherapeutic agents. However, they are associated with high toxicity so their treatment is limited to advanced disease (87, 91, 94, 95).

Another biological treatment is the cytotoxic T-lymphocyte-associated antigen (CTLA-4) monoclonal antibody, ipilimumab that extended overall survival from 4 to 36 months in melanoma patients that responded to treatment (96, 97). The blockade of immune checkpoints is the most promising treatment for cancer, in general and, specifically, in melanoma, in the last decade. Immune checkpoints are necessary in normal cellular function to prevent autoimmunity and to protect tissues from excessive immune responses (98). In normal $T_{Helper}$ cells, CTLA-4 downregulates T-cell activation, by counteracting CD28 which, following antigen recognition activates T-cells (98). Tumour cells dysregulate immune checkpoint proteins as a form of immune resistance. The IgG monoclonal antibody, ipilimumab inhibits CTLA4 thereby enabling the CD28 mediated immune response and increasing the autoimmunity of tumours (99-102). Initially developed by Bristol-Myers-Sqibb, the phase III clinical trial in 2010 showed an increased median survival of 10 months, one year survival to 46% and two year survival to 18% in advanced melanoma patients

(99). This trial caused controversy as, instead of using a placebo control, they measured the drug against a trial vaccine that some claimed caused toxicity therefore making ipilimumab appear better by comparison. Despite this, ipilimumab was approved by the US in 2010 and by the UK in 2014 for the treatment of advanced melanoma. One of the major benefits of this treatment is its durability and lack of acquired resistance (97) which, as described later, is a major obstacle in melanoma treatments. To improve the response to ipilimumab, it can be used in co-immunotherapy. Nivolumab is an antibody against programme death 1 (PD-1) receptor, another immune-checkpoint receptor (99). Nivolumab compliments the effects of ipilimumab, by limiting the activity of T-cells in periphery tissues during an immune response, in trials of stage III melanoma a significant increase to patient outcomes (97, 98, 103, 104). In addition, a current phase I trial is taking place, combining the treatment of ipilimumab with bavituximab, a phosphatidylserine antibody, that is predicted to enhance the effects of ipilimumab (105). Phosphatidylserine is intracellular in normal cell but is expressed on the surface of tumour cells allowing for a very targeted treatment (106). Once bound, this will attract the immune system to target the tumour cells. Therefore, used in combination with ipilimumab will enhance this effect.

As explained in the next section, mutations within the RAS/RAF/MEK/ERK and PI3K/AKT pathways are the most common in melanoma and they pose as good targets for the treatment of melanoma (107). Treatments targeted to the BRAF mutation have proven to be very successful, including debrafenib (108) and vemurafenib (109). Response to vemurafenib is seen in 40-80% of patients with extended progression-free survival of 5.3 months (90). However, melanoma is notoriously resistant to conventional therapies and can rapidly (less than 1 year) acquire resistance to novel, promising treatments, as has been highlighted in BRAF inhibitor trials (57, 110). There are a number of mechanisms by which cancer cells can become resistance to treatments. The classic method is the removal of cytostatic substances from the cell by P-glycoprotein through a transmembrane protein. However, this is not the case in melanoma (111). Another transmembrane glycoprotein, that aids in the export of therapies from the cells, is a member of the

ABC transporter family (112), the multidrug resistance-related protein (MRP) which has been shown to be upregulated in melanoma (111). However, this upregulation has not been seen in response to chemotherapy (113, 114). Resistance to MEK inhibitors has been seen in melanoma cells due to the increased expression of the ubiquitin ligase SMURF2. This overcomes the TGFβ signalling induced by the MEK inhibitor. In addition, the increased expression of SMURF2 subsequently increased levels of MITF which also contributed to the cells resistance to cytotoxicity (57). The mechanism that led to the resistance of the BRAF inhibitor vemurafenib was the re-activation of MAPK signalling via EGFR (115). In total, there have been 22 different modes of acquired resistance described for BRAF and MEK inhibitors (57). This demonstrates that there is no one mechanism causing multi-drug resistance in patients and new therapies need to be designed with this in mind. Due to this, combination therapies targeting BRAF, along with other pathways, such as MEK (116, 117) and mTOR/PI3K (116) are utilised. However, resistance can still occur (118). To help overcome this, research into the benefits of nanoparticle-assisted treatments have led to increased response rates of 27% and reduced side effects with drugs such as paclitaxel (91). Nanoparticle-aided therapy will also allow for directly targeted treatments by endocytosis of nanoparticle encapsulated drugs and active targeting, using the overexpression of surface markers specific to each cancer type, such as MC1R on melanoma cells (119).

Most conventional anti-cancer treatments work on the assumption that cancer cells are equal in their ability to form tumours. Therefore, most therapies aim to eradicate all the cancer cells within the tumour (120, 121). However, accumulating evidence over the last decade suggests that there are subsets of cancer cells in most tumour types which are particularly effective at forming tumours and resisting conventional therapies possibly due to the upregulation of ABC transporters on melanoma cells (112). It is now believed that most relapses following initial therapeutic remission can be attributed to these subpopulations of cancer cells (122). It is, therefore, becoming increasingly apparent that effective cancer treatments of the future should target those subpopulations of cancer cells capable of initiating and maintaining the tumour mass. However, before this can be achieved, scientists must first obtain a

detailed understanding of the biological properties of these cells in order to identify suitable targeting strategies for their eradication.

### 1.1.4. The Genetics of Melanoma

UV radiation typically causes C – T prymidine dimer formations (123). However, there are a number of genetic backgrounds associated with metastatic melanoma that are distinct from UV radiation. Table 1.3 summarises some currently known mutations and states the pathway in which they function, the frequency of the mutation and potential treatment options. The MAPK/ERK pathway and PI3K/PTEN/Akt pathways are highly implicated in melanoma progression regulated by cytokines and receptor tyrosine kinases (124), Figure 1.4 shows how these pathways interact.

The MAPK/ERK pathway is also known as the RAS/RAF/MEK/ERK pathway and initiates with the small G protein RAS at the plasma membrane that becomes activated by exchanging a GDP for GTP (125). RAS then binds to the serine/threonine kinase, RAF, which translocates to the plasma membrane and becomes activated. The RAF family of kinases consists of three members, A-RAF, B-RAF and C-RAF, B-RAF becomes activated directly by the binding of RAS but other molecules are needed to activate A-RAF and C-RAF (107). Activated RAF phosphorylates, both MEK1 and MEK2, on the serine residues, leading to the activation of ERK1/2 (also known as MAPK) by phosphorylation of a Thr-Glu-Tyr motif in the activation loop (107). Phospho-ERK then translocates to the nucleus and increases the transcription of genes, regulating proliferation and cell survival (126).

The PI3K/PTEN/Akt pathway activated via a receptor protein tyrosine kinases (Class 1A), causing autophosphorylation of the tyrosine residues (107). PI3K will translocate to the membrane and bind to the receptor by its adaptor subunit, causing activation of the catalytic subunit and production of phosphatidylinositol (3,4,5)-trisphosphate ($PIP_3$) from phosphatidylinositol (4,5)-bisphosphate ($PIP_2$).

**Table 1.3: Selected known mutations in Melanoma**

Known mutations in melanoma with their associated pathways, co-mutations, frequency and potential therapeutic treatments. Table adapted from (57). NB not all known mutations are listed.

| Primary Subtypes | Pathway | Aberration | Found in Tumours with… | Frequency | Possible Therapies |
|---|---|---|---|---|---|
| BRAF | MAPK | Point mutation<br>Gene fusions | NRAS WT | 50-60%<br>rare | BRAFi+MEKi<br>BRAFi+EGFRi<br>AKTi |
| NRAS | MAPK, PI3K, RALGDS | | BRAF WT | 20-25% | MEKi+CDKi |
| KIT | MAPK, PI3K | Point mutations, amplification | NRAS BRAF WT mostly | 1% | Sunitinib, nilotinib, imatinib |
| GNAQ/ GNA11 | Family of G protein α subunits MAPK activators | Point mutations | NRAS BRAF WT | 1% | MEKi+PI3Ki, enzastaurin |
| MITF | Transcription, lineage, cell cycle | Amplification | All | 20% | HDACi |
| NF1 | MAPK, PI3K negative regulator of RAS | Mutations, loss of expression | BRAF, NRAS WT and less often in mutated | 4% | MEKi+mTORi or PI3Ki |
| TERT | Telomerase | Mutations in the promoter of catalytic subunit | ND | 70-80% | TERT inhibitors in preclinical |
| ERBB4 | PI3K, MAPK | Point mutations | All | 15-20% | Lapatinib +PI3Ki |
| MET | PI3K, MAPK | Activation by stromal HGF | All | ND | Cabozantinib |
| AKT3 | PI3K | Amplification | All | 25% | AKTi, PI3Ki, mTORi |
| PTEN | PI3K | Point mutations or deletion | BRAF mutated; BRAF and NRAS WT | 40-60% | PI3Ki |
| MAGI | PI3K; stabilizes PTEN | -- | All | -- | PI3Ki |
| TACC | Possibly stimulates PI3K AURKA signalling | -- | BRAF and NRAS mutated | 5% | PI3Ki, AURKAi |
| PREX2 | RHO/RAC/ MAPK; Rac exchange factor | Point mutations | BRAF or NRAS mutated | 14% | |
| RAC1 | RHO/RAC/ MAPK; Regulator of cell adhesion, invasion, migration | Point mutations | BRAF or NRAS mutated | 9% | |
| MAP2K1/2 | MAPK (MEK1/2) | Mutations | BRAF mutated; BRAF, NRAS WT | 5% | ERKi |

| | | | | | |
|---|---|---|---|---|---|
| MAP3K5/9 | RHO/RAC/ MAPK | Mutations, loss of heterozygocity | All | 85% and 67% | MEKi, ERKi |
| MYC | Transcription | Amplification | All | 20-40% | mTORi |
| ETV1 | Transcription | Amplification | All | 15% | |
| TP53 | Cell Cycle, apoptosis | Point mutations | All | 10-20% | |
| MDM4 | Negative regulator of p53 | Overexpression | All | 65% | p53-MDM4i |
| CDKN2A | Negative regulator of TP53 and RB | Point mutations, deletion | BRAF and NRAS mutated, KIT amplified | 30-40% | CDKi |
| BCL2 | Suppression of apoptosis | Elevated expression, amplification | All | 30% | BH3 mimetics |
| CCND1 | Cell cycle, G1/S cyclin | Amplification | More frequent in BRAF, NRAS WT | 11% | CDKi |
| CDK4 | Cell cycle, G1/S cyclin-dependent kinase | Amplification | More frequent in BRAF, NRAS WT | 3% | Selective CDKi |
| PPP6C | Catalytic unit of phosphatase, negative regulator of CCND1, Aurora | Point mutations | BRAF and NRAS mutated | 12% | AURKA CDKi |
| STK19 | Kinase; unknown function | Point mutations | BRAF and NRAS mutated | 5-10% | |
| SNX3 | Endosome protein sorting | Point mutations | BRAF mutated; BRAF, NRAS WT | 7% | |
| GRIN2A | Ionotropic glutamate-gated ion channel, NMDA binding | Point mutations | -- | 25% | |
| GRM3 | Possibly accessory MAPK signalling | Point mutations | ND | 13-18% | |
| TRRAP | Part of histone acetyltransfera se complex | Point mutations | ND | 10-13% | |
| ARID2 | SWI/SNF Chromatin remodelling, SWI/SNF comlex | Inactivating mutations | BRAF, NRAS mutated | 7-9% | |
| BAP1 | BRCA1 DNA repair | Inactivating mutations | BRAF, NRAS WT | 1% | |
| NEDD9 | Integrin adaptor, promotes EMT and migration metastasis | Amplification | All | 50-60% | |

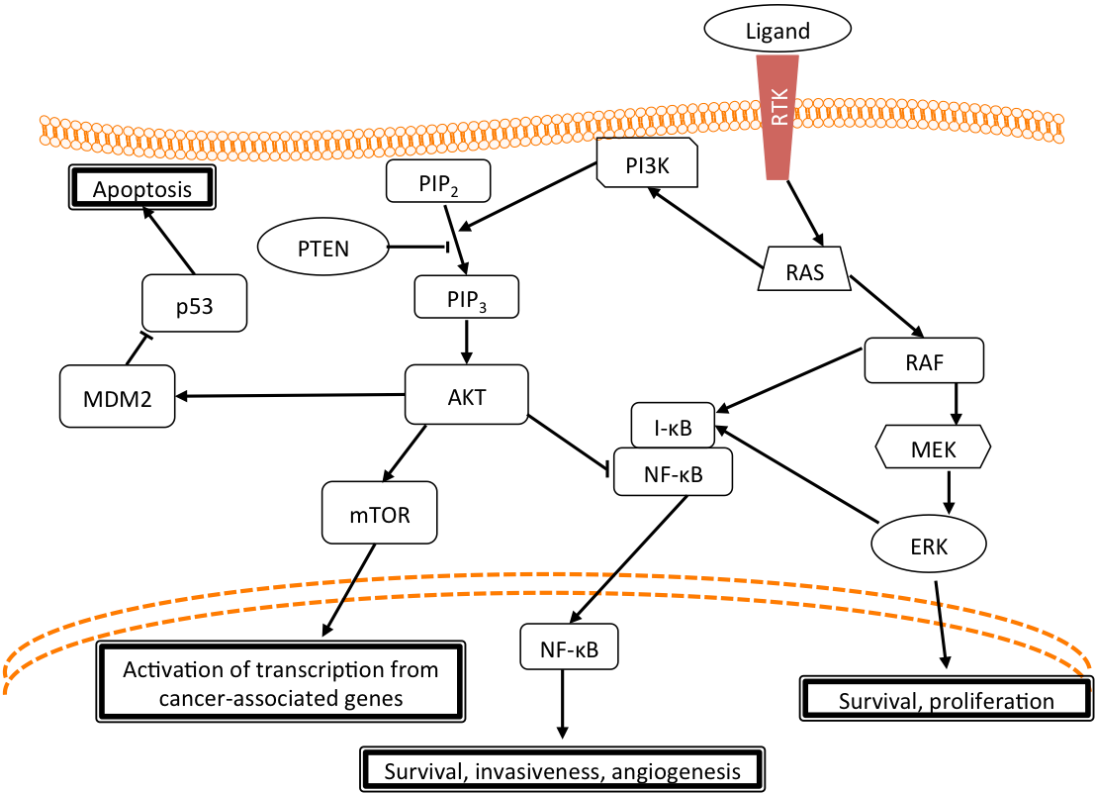


**Figure 1.4: Connections of the RAS/RAF/ERK and PI3K/PTEN/AKT pathways in melanoma.** A schematic showing the binding of a ligand to the receptor tyrosine kinase (RTK) activating the RAS/RAF/ERK and PI3K/PTEN/AKT signalling pathways. The binding of a ligand activates RAS by swapping GDP to GTP. This leads to the activation of RAF, which phosphorylates MEK, leading to the activation of ERK (also known as MAPK). Activation of this pathway leads to the transcription of genes involved in growth and division. RAF and ERK can also lead to the translocation of NF-κB to the nucleus by displacing the inhibitory I-κB, at the nucleus NF-κB turns on genes regulating the invasion, survival and angiogenesis. Ras can also lead to the activation of PI3K. This then switches $PIP_2$ to $PIP_3$, which can be reversed by PTEN thereby blocking the PI3K pathway. $PIP_3$ can bind to AKT, which can negatively regulate NF-κB but can also phosphorylate MDM2 to antagonises p53-mediated apoptosis or can activate mTOR via phosphorylation of TSC and leads to the activation of transcription of genes such as S6K. Image adapted from (125).

Active $PIP_3$ will then recruit molecules with a pleckstrin homology domain such as Akt and PDK1 (107, 127). The binding of $PIP_3$ to Akt allows PDK1 to phosphorylate Akt at T308. Fully active Akt is also phosphorylated at S437 but the mechanism by which this occurs is still unknown. Akt, itself, can enter the nucleus and activate genes regulating proliferation and survival, but it can also phosphorylate mouse double minutes 2 homolog (MDM2) to degrade p53 and increase apoptosis (128). Phosphatase and tensin homolog (PTEN) is a $PIP_3$ phosphatase and negatively regulates the Akt recruitment and can reverse $PIP_3$ to $PIP_2$. Inactivating mutations in PTEN activate $PIP_3$, causing the phosphorylation of AKT. This increases cell survival proliferation and anti-apoptotic signals via mTOR though the phosphorylation of TSC leading to transcription of genes such as S6K (129).

These pathways can however, interact. RAS can activate PI3K, thereby increasing AKT activity (130). Both pathways can regulate nuclear factor kappa-light-chain-enhancer of activated B cells (NF-κB) via RAF and ERK from the RAS/RAF/MEK/ERK pathway by displacing the inhibitory I-κB and via direct Akt inhibition. This will lead to the transcription of cancer associated genes (131). It is within members of these pathways that we see the most frequent mutations in melanoma. The most common is the BRAF mutation (123, 132-136), common in up to 53-66% of melanoma patients which causes constitutive activation of the MAPK/ERK signalling pathway (137). Of these patients, 80% have the specific mutation $BRAF^{V600E}$, whereas, 16% have $BRAF^{V600K}$, and 4% have either $BRAF^{V600D\ or\ R}$ mutation (138). The $BRAF^{V600E}$ mutation causes a 500-fold increase in BRAF kinase activity leading to increased cell division and survival (25). Less common, but with the same subsequent effect of hyperactive MAPK signalling, are mutations within NRAS. This is seen in approximately 9-29% of patients and is most often mutually exclusive to the BRAF mutation (134, 135, 137). Both BRAF and NRAS are activated by Ras with BRAF having the highest RAS activation, as well as the highest basal activity levels, causing it to be one of the most common mutations in cancer (139-141).

Other mutations are also known in melanoma, such as mutations within PTEN (142-145) seen in around 30-50% of melanoma cases (146). Mutations within the tumour

supressor PTEN are typically inactivating and cause hyperactve PI3K signalling via the Akt/PKB pathway (127), leading to loss of control over the cell growth, metabolism and survival (146, 147). Mutations within PTEN are often seen alongside BRAF mutations (142). However, they are less common in NRAS mediated melanomas (145). Other less common mutations in melanoma patients include those within Akt (148-150), the overexpression of which can switch a melanoma from its radial growth phase to the vertical growth phase (151). Inherited forms of melanoma tend to carry mutations within CDKN2A causing destabilisation of p53 (3, 49, 152, 153), whereas sun-damaged skin is more prone to mutations within C-kit (154-156). Melanocortin 1 Receptor (MC1R) gene variants can also cause a predisposition to melanoma independent from MC1Rs effects on skin tone and hair colour (157, 158). Mutations within MITF are not that common, seen in around 20% of melanoma cases (159). Typically, they are gene amplifications and they cause the constituative transcription of a number of different genes, including those involved in the cell cycle such as CDK2 (19, 160), tumour survival such as HIF1α (161), and melanocytic markers, such as SOX10 (25, 162). These muations likely infer differing effects on melanoma progression (142, 150, 163). Due to this diversity, it is important to compare how diverse mutational backgrounds affect the various characteristics of tumour cells, such as the differences between wildtype (WT) and $BRAF^{V600E}$.

An additional signalling pathway that has to be considered when discussing the genetics of melanoma is the Wnt signalling pathway. As shown in section 1.1.2, the Wnt signalling pathways are involved in the development of melanocytes and section 4.1.1 will show the roles that they play in melanoma initiation and progression. Although Wnts and β-catenin are rarely mutated in melanoma (164), aberrant Wnt signalling is common in melanoma (20, 165, 166). The following section will describe the Wnt signalling pathways.

## 1.2. WNT SIGNALLING

The Wnt signalling pathways are highly conserved regulatory pathways that play a role in embryonic development, as well as cell fate, migration and polarity (25, 167). The name Wnt comes from a combination of the *Drosophila wingless (wg)* gene

controlling segment polarity and the vertebrate homolog *Int-1* (166-169). The Wnt family consists of, at least, 19 lipid-modified, cysteine-rich, secreted glycoproteins, defined by a sequence homology (22, 25, 167). Wnts are considered unconventional morphogens as they can act in an autocrine manner over short distances or in a paracrine manner over long distances (169, 170). They all have typical features of a secreted growth factor, including the lack of a transmembrane domain, hydrophobic signal sequence and an *N*-glycosylation site (22).

It was stated previously that Wnts are lipid-modified secreted glycoproteins. The lipid modification is the addition of a palmitate moiety on the first cystine residue and is necessary for their protein function. This causes the protein to be hydrophobic and allows them to target lipid-dense regions, such as the membrane or lipid rafts and allows the N-linked glycosylation of the Wnt protein (171). These post-translational modifications occur at the ER, which is where the protein Porcipine resides and is thought to play an important role in these lipidations (172). The secretion of Wnts from the cell that produces them is regulated by *wntless* (wls) and *evenness interrupted* (evi). These encode a 7-pass transmembrane located on the Golgi and are thought to physically interact with Wnts to shuttle them to the cell surface (169, 172).

There have been three Wnt signalling pathways characterised so far; the canonical Wnt/β-catenin-dependent pathway, and two β-catenin-independent pathways, the noncanonical Wnt/calcium pathway and the noncanonical planar cell polarity (PCP) pathway (22, 25, 166-169). The canonical Wnt pathway works at the transcriptional level to control proliferation and differentiation, whereas the non-canonical pathways are linked to cell motility and cytoskeletal rearrangements (22, 25, 166). A summary of these three pathways is shown in Figure 1.5. All the pathways are activated through Frizzled (FZD) receptors although other receptors can also activate these pathways, as discussed below. In humans, there are ten FZD 7-transmembrane receptors (22, 25, 167, 173), which share topological similarities with G-protein coupled receptors (174) and, also have a number of differences (22). FZD receptors

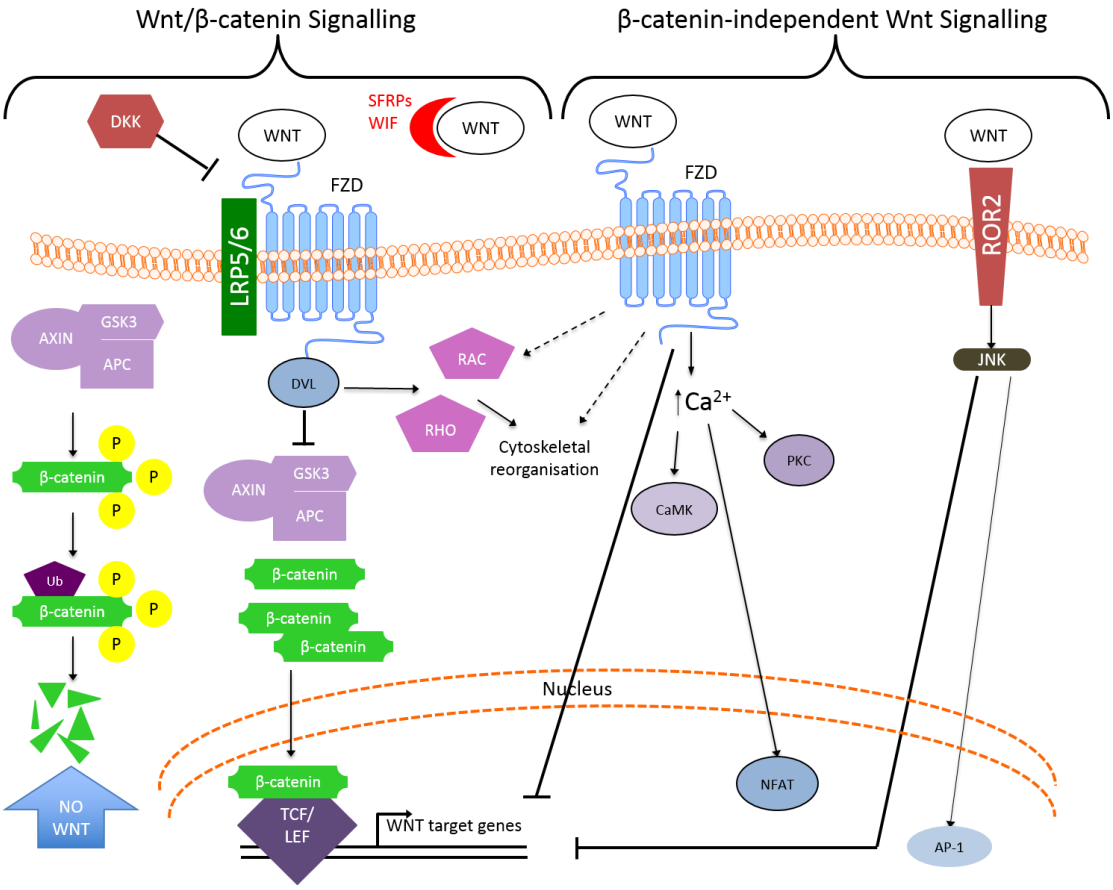


**Figure 1.5: Schematic of Wnt/β-catenin and β-catenin-independent Wnt Signalling**
A schematic of the β-catenin-dependent (175) and -independent (right) Wnt signalling pathways. The far left shows the β-catenin-dependent pathway in the absence of a Wnt ligand. The destruction complex formed of Axin, APC and GSK3 causes the phosphorylation of β-catenin in the cytoplasm, this leads to β-catenin ubiquitination and subsequent destruction by the proteasome. The binding of a Wnt ligand to the FZD receptor and the LRP 5/6 co-receptor causes the recruitment of Dvl, and inhibits the destruction complex. This allows β-catenin to accumulate in the cytoplasm and translocate to the nucleus where it activates transcription of Wnt-target genes via the TCF/LEF transcription factors. This pathway can be inhibited by DKK competitively binding to the LRP5/6 co-receptor; blocking the binding of Wnt ligands by SFRPs or WIF can also inhibit this pathway. The two branches of the β-catenin-independent signalling pathway are activated by the binding a Wnt ligand to the FZD receptor and a variety of co-receptors including ROR2. The Wnt/$Ca^{2+}$ pathway can alter intracellular $Ca^{2+}$ levels. This can block the β-catenin-dependent pathway through inhibition of TCF gene transcription but also can lead to NFAT mediated gene activation. Activation of the Wnt/PCP pathway can cause the activation of small GTPases Rho and Rac to cause cytoskeletal changes and subsequently affect cell motility. Image adapted from (173).

have sites for glycosylation and phosphorylation for PKA, PKC and CK2, as well as an N-terminus that contains a cysteine rich domain (CRD) for direct Wnt ligand binding (22, 168, 169, 174). The crystal structure of FZD8 bound to Wnt8 has already been shown by Janda *et al.* 2012 (176). The Wnt8 ligand is described as forming a hand shape with the thumb and index finger extended to grab the CRD binding site of the FZD receptor. The activation of the FZD receptor causes the recruitment of the cytosolic phosphoprotein dishevelled (Dvl) to the plasma membrane and initiates a series of intracellular signalling events (25).

As stated in section 1.1.1, Wnt signalling is intrinsically involved in embryogenesis in the formation of the neural tube, the determination of cell lineage, migration and EMT. Therefore, it is unsurprising that Wnt signalling has been linked to stem cells and self-renewal properties. Due to this, Wnt/β-catenin signalling is found in the adult tissues associated with self renewal, including the epithelium of the small intestines, hair follicles, bones, hematopoietic stem cells and, crucially, in melanocytes (168). Due to their wide-ranging effects, Wnt proteins have subsequently been linked to a number of diseases, including cancer (166, 177, 178). Mutations within low-density lipoprotein receptor-related protein (LRP) LRP5 and -6 (LRP5/6) have a number of effects including; reduced bone density in osteoporosis, familial coronary disease and late-onset Alzheimer's disease (179-181). Mutations within the non-canonical Wnt signalling pathway have also been linked to type II diabetes through Wnt5B, Wnt10B and TCF7L2 (182-184) and to end-stage polycystic kidney disease (185, 186), whereas upregulation of Wnt5a has been linked to Alzheimer's disease (187). More recent work has now started to link Wnt signalling to the control of the mitochondria and energy cell metabolism (188-196).

Almost all Wnts have been implicated in cancer. In breast, esophageal and colorectal cancers, nuclear β-catenin predicts lower patient survival and adenomatosis polyposis coli (APC) is found to be mutated in 80% of colorectal carcinomas, causing constitutive activation of the Wnt/β-catenin pathway (166, 168). Non-canonical Wnts are linked to multiple cancer types including gastric, lung and melanoma (197, 198) and are shown to increase cancer cell invasion and metastasis, specifically in

breast cancer metastasis to the brain (198, 199). However, as this research will show, along with the research of others, Wnt signalling is not always oncogenic in its nature (166, 200-203), especially as the β-catenin-independent pathway can inhibit Wnt/β-catenin signalling (166, 173). Instead, Wnt signalling, both canonical and non-canonical, is highly context-dependent in differing tumours (177, 204, 205). Due to this, it is important to investigate the roles of the differing Wnt pathways in different tumour types and in different genetic backgrounds of the same tumour.

### 1.2.1. The Wnt/β-catenin Pathway

There are three commonly canonical Wnts; Wnt-1, 3a and 8 (20, 25). However, their downstream activity is determined by which of the 10 FZD receptors they bind (206). In the absence of a Wnt ligand, Glycogen Synthase Kinase 3 (GSK3β), which forms part of a destruction complex, phosphorylates cytoplasmic β-catenin (173), which is, subsequently, ubiquitinated by the E3 ubiquitin ligase β-Trcp, leading to its proteasomal degradation (25, 167, 177, 200, 201, 207-214). Along with GSK3β, the destruction complex consists of the tumour suppressor APC, Protein phosphatase 2A (PP2A), and Casein Kinase 1α (CK1α), as well as the scaffolding protein Axin (20, 22, 25, 173). In a Wnt 'on' situation, a Wnt ligand will bind to the CRD of a FZD receptor that couples to single pass transmembrane molecule, LRP5/6 (20, 22, 166-169, 174). These, also have the ability to bind Wnt proteins and are required to mediate the canonical Wnt signal (167). LRP5/6 is phosphorylated, causing deactivation of the destruction complex by translocating Axin (a negative Wnt regulator) to the plasma membrane, thereby inhibiting its interaction with GSK3β. The binding of a Wnt ligand to a FZD receptor also causes the recruitment of Dvl to the plasma membrane, where it, also is phosphorylated and interacts directly with Axin (20, 25). Once at the plasma membrane, Axin is de-phosphorylated (215), releasing β-catenin to accumulate in the cytoplasm and, subsequently, translocates to nucleus. This translocation process is poorly understood as β-catenin has no nuclear localisation sequence and the nucleus does not require importin machinery (25, 168, 216). Once at the nucleus, β-catenin binds to transcription factors TCF/LEF, displacing Groucho and activating transcription of an estimated 70-Wnt target genes (20, 168). In order to do this, other

factors are needed. Legless and Pygopus both bind to the TCF-β-catenin complex via the N-terminus of β-catenin (217). In addition, transcription has been shown to occur independently of TCF, as this becomes altered by TAK1 and Nemo signalling (218) through activation of the MAPK pathway (described in section 1.1.4) and β-catenin binds to Pitx2 (219) or Prop1 (220). The Wnt/β-catenin pathway self-regulates both positively and negatively as the expression of LRP, *Axin2*, TCF/LEF and FZD are all controlled by the β-catenin/TCF complex (168). The Wnt/β-catenin pathway can also be activated independently of a Wnt ligand through the binding of Norrin and R-Spondin2 to the LRP5/6 receptors (167, 173).

### 1.2.2. The Non-Canonical Pathways

There are two non-canonical pathways activated by Wnt ligands (see Figure 1.5). The archetypal β-catenin-independent Wnts are Wnt5a, Wnt5b and Wnt11 (198). As stated previously, the β-catenin-independent Wnts can inhibit Wnt/β-catenin signalling. However, it has been shown in melanoma cells that Wnt5a can actually increase Wnt/β-catenin signalling by activating ARF6 via FZD4 and LRP6 receptors (221). These pathways are implicated in embryogenesis including gastrulation, neural tube closure and EMT of neural crest cells (22).

#### 1.2.2.1. The PCP Pathway

The planar cell polarity pathway (PCP) regulates actin cytoskeletal structures and cell movement (22, 198). Cell polarity is very important to normal cell function. PCP is the polarisation of cells along the plane of the epithelial layer at right angles to the apical-basal axis (22). The pathway uses FZD receptors previously described, specifically FZD3 or 6. It also utilises co-receptors including the receptor tyrosine kinase-like orphan receptor 2 (ROR2), receptor-like tyrosine kinase (RTK) and protein tyrosine kinase 7 (25). Following activation of the FZD and co-receptor, Dvl is recruited forming a complex with the Dishevelled-associated activator of morphopgenesis 1 (Daam1) which, subsequently, activates the small G-protein Rho-associated kinase (ROCK) and myosin (22, 25, 167). This pathway ultimately regulates cytoskeletal dynamics (198). However, another pathway can be activated

independent of Daam1. Instead this branch of the PCP pathway uses a separate domain of Dvl and activates small Rac GTPase which, subsequently, stimulates Jun kinase (JNK), which regulates actin rearrangement (22, 25, 198).

Due to its upregulation in a number of cancers, it has been suggested that levels of PCP/Wnt could be used for cancer prognostics (198). It has also been shown that Wnt5a inhibitors block melanoma cell invasion, indicating that they could be used as potential future treatments for melanoma or, potentially, other cancers (222). This is especially beneficial as levels of Wnt5a increase resistance to BRAF targeted treatments (223). In gastric cancer, single poly nucleotide (SNPs) mutations occur with molecules of the Wnt/PCP pathway. Therefore, sequencing for these could be used to screen for a predisposition to gastric cancer (198).

#### 1.2.2.2. The Wnt/$Ca^{2+}$ Pathway

The Wnt/$Ca^{2+}$ pathway is dependent on G-proteins and regulates the levels of intracellular calcium from the endoplasmic reticulum (ER) stores and, via PKC, also regulates cytoskeletal organisation and cell motility (22, 167). PKC in this pathway acts in a positive feedback loop with Wnt5a, as Wnt activation of this pathway leads to activated PKC but, subsequent activated PKC, leads to increased Wnt5a (22). When a Wnt ligand binds in this pathway, the FZD receptor directly interacts with a G-protein which leads to the activation of phospholipase C (PLC) that translocates to the plasma membrane (22, 167, 224, 225). This causes the hydrolysation of phosphatidylinositol 4,5-biphosphate ($PIP_2$) into inositol 1,4,5-triphosphate ($IP_3$) and di-acyl glycerol (22). $IP_3$ interacts with calcium channels on the ER and causes the release of calcium ions. The increase in calcium activates a number of calcium-dependent proteins, including calcium-calmodulin-dependent kinase (CamKII), in addition to PKC which is known to regulate processes during gastrulation (167). Both of these calcium sensitive molecules activate nuclear transcription factors NFκB and CREB (22, 224). In addition, CamKII can activate downstream effectors, including TGFβ activated kinase (TAK1) and Nemo-like kinase (NLK) which antagonise β-catenin/TCF signalling (167). The activation of the Wnt/$Ca^{2+}$ pathway can also

activate phosphodiesterase 6 (PDE6) leading to a decrease in cyclic guanosine monophosphate (25, 224, 225).

As with the previous pathways, the Wnt/$Ca^{2+}$ pathway is implicated in embryonic development and cancer (226-229) but, also, it is implicated in inflammatory diseases through its upregulation of NFκB (224, 230). Inhibition of this pathway can reduce both myocardial and Alzheimer's disease (187, 231).

### 1.2.3. Inhibitors of the Wnt Pathways

There are natural inhibitors of the Wnt signalling pathways (see Figure 1.5). This first group are extracellular secreted antagonists of the Wnt pathways. The Wnt-inhibitor protein (WIF) has been shown to bind to Wnts 3a, 4, 5a, 7a, 9a and 11. They bind through their WIF domain and block the binding of Wnts to the FZD receptors and prevent downstream signalling (232). Soluble frizzled-related proteins (SFRP) also block the Wnt pathways by mimicking the cysteine-rich binding sequences on FZD receptors or the receptor tyrosine kinases (169, 233, 234). They bind to the Wnt ligands, preventing Wnt from binding to the FZD receptor. In normal cells, SFRPs act as tumour suppressor genes and both WIF1 and SFRPs are commonly downregulated in cancers (173, 178, 235). Other extracellular antagonists of the pathways are Cerberus and its homolog Coco, that also bind to Wnts and block the downstream signalling (234). These inhibitors have been shown to bind to Wnt ligands associated with both the β-catenin-dependent and –independent pathways. The second group of inhibitors all work by competitively binding to LRP5/6 co-receptor to block signalling (20, 168, 169, 234, 236). The family of Dickkopf (DKK) proteins (236), Wise, SOST and Insulin-like growth factor binding protein (IGFBP-4) predominantly bind to LRP6 but DKK proteins have also been shown to bind to Kremem1 and Wise has been shown to bind to LRP4 (237). The final group of Wnt signalling inhibitors are transmembrane molecules that work at the plasma membrane. These include Shisa, Waif1, APCDD1 and Tiki1. They are classed as one family as they are all transmembrane molecules. However, this family do not all function in the same manner. For example, Waif1 binds to the LRP6 receptor, whereas APCDD1 binds to

Wnt ligands and LRP5 and Tiki1 modifies Wnt ligands to remove 8 amino residues and inhibit its function (237).

## 1.3. THE MITOCHONDRION AND ITs FUNCTION

This project investigates the effects of the Wnt/β-catenin signalling pathway on melanoma cell metabolism. Therefore, it is necessary to understand the mitochondria and the processes of energy metabolism that they carry out.

Mitochondria are semi-autonomous organelles that produce the majority of the required energy of eukaryotic cells through the processes of adenosine triphosphate (ATP) synthesis by oxidative phosphorylation (OXPHOS) and the tricarboxylic acid (TCA) cycle (238-241). However, they are also involved in a number of other cellular processes, including intracellular calcium homeostasis and are vital for cell growth, division and apoptosis (239). Mitochondria play a central role in the sensing and production of cellular energy levels and, along with transcription factors, hormones and kinases, they measure ratios of (nicotinamide adenine dinucleotide) $NAD^+$ to NADH, ADP to ATP and levels of acetyl CoA and adjust their response accordingly (242). The number, size and location of mitochondria are tightly controlled and can vary between cell types (240, 243, 244), but can also vary according to the metabolic function of the cell (245). Specifically, cells such as hepatocytes have a high-energy demand and, therefore, have many mitochondria (246), whereas erythrocytes produce all their energy through glycolysis and, therefore, have no need for mitochondria and, through evolution, have lost them (238, 247, 248). It has been shown that mitochondria do not increase their numbers according to the energy demand but, instead, increase their mass in order to induce OXPHOS and ATP production (242). It has also been shown that mitochondria can exist in a number of formations: individual, heterogeneous or as interconnected networks (239, 245, 249).

### 1.3.1. Shape and Structure of Mitochondria

Mitochondria are semi-autonomous, double membrane, organelles, the structure of which is shown in Figure 1.6. Mitochondria vary in shape from punctate structures

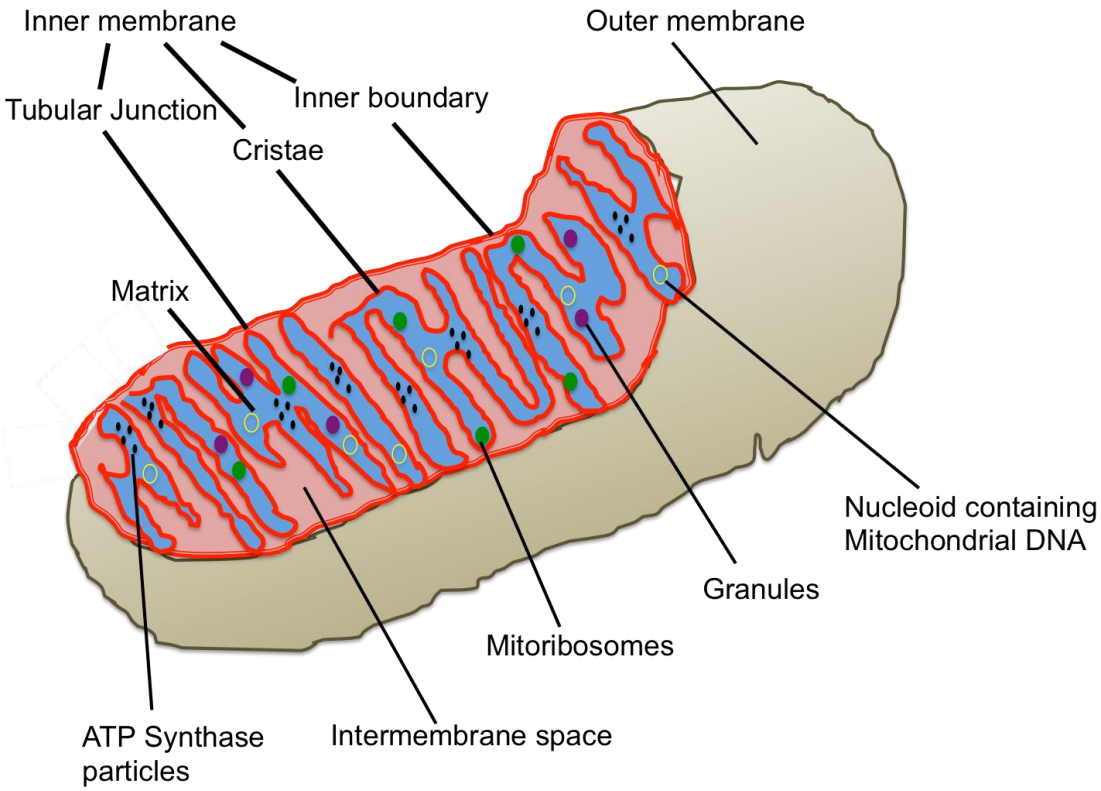


**Figure 1.6: The Structure of Mitochondria**
The semi-autonomous organelle encased by a double phospho-lipid membrane, the inner membrane forms the inner boundary and is convoluted into cristae connected together by thin tubular junctions, the space in between the membranes is the intermembrane space and the internal space is the matrix. Mitochondria contain their own mtDNA contained in nucleoids, mitoribosomes for replication and translation, ATP synthase or complex V of the ETC, and iron containing granules. Image adapted from (250).

to intricate networks. Two opposing processes control this process of mitochondrial morphology; fusion and fission (239, 245, 251) and the balance between these is necessary to maintain cellular and mitochondrial functions described above (239, 252). The shape of mitochondria is linked to $Ca^{2+}$ signalling, the generation of ROS, movement and the cells energy requirements (239, 249, 252). It has been shown that slowly proliferating or quiescent cells have lower energy requirements and will, often, form larger mitochondrial networks whereas, where there is a demand for higher energy production within the cell, smaller mitochondria will move along microtubules of the cytoskeleton and accumulate where needed (239, 244, 249, 252). However, during the process of mitochondrial dynamics, the basic architecture of a mitochondria remains constant (244). The two membranes encapsulating the mitochondria are functionally different (242). The outer mitochondrial membrane (OMM) is a phospholipid bilayer that contains porins such as the voltage-dependent anion channel (VDAC), these are channels spanning the membrane that allow the passage of metabolites (253). Whereas, larger proteins pass through the membrane via translocase of the outer membrane (TOM) complexes (254). The inner mitochondrial membrane (IMM) is also a phospholipid bilayer that, not only forms the inner boundary but, also is convoluted to form cristae that are connected to the inner boundary by small tubular junctions (249, 255). The IMM has a much higher protein:lipid mass ratio than a traditional phospholipid membrane at 75:25% (256). There are transport ports through the IMM called the translocase of the inner membrane (TIM) complexes that allow the transport of proteins into the inner space of the cristae to the mitochondrial matrix, the site of the TCA cycle, which is described in detail in section 1.3.3.2 (254). The space in between the two membranes is the intermembrane space which, along with the electron transport chain (ETC) within the IMM, is the site of OXPHOS, also described in section 1.3.3.4 (242, 257). The mitochondrial cristae are dynamic structures, changing shape to adapt to different cellular processes, as the ETC is integrated into the IMM. One of these processes is mitochondrial respiration (256). Identified in isolated mitochondria, the cristae become condensed during ADP stimulated respiration, thereby decreasing the mitochondrial matrix volume. This is referred to as State III Respiration (258).

Whereas during state IV, following the phosphorylation of ADP to ATP or in ADP limiting conditions, the mitochondria are in the orthodox formation as shown in Figure 1.6 where the matrix is larger and the intermembrane space is small (256). The mitochondrial cristae will fluctuate between these states as the availability of metabolites changes (259). Another change in the cristae shape occurs during apoptosis when the cristae become disorganised, enabling the release of cytochrome *c* (256, 260).

#### 1.3.1.1. Organisation and Production of Mitochondrial DNA

As stated previously, mitochondria are semi-autonomous, contain their own circular DNA and have their own transcription, translation and protein assembly machinery (240). Mitochondrial DNA (mtDNA) is maternally inherited, with paternal mtDNA destroyed after fertilisation (240, 242). The mtDNA is organised into nucleoids located within the mitochondrial matrix (242). The supercoiled, doubled-stranded, circular, molecule encodes for 37 genes (see Table 1.4) within 16.6 kbp of DNA (240, 261, 262). mtDNA contains no introns, genes are encoded back-to-back and, therefore, render the mtDNA more vulnerable to mutations than nuclear DNA and, as they are in the coding region, these mutations tend to cause mitochondrial diseases, as discussed in section 1.3.4 (240). The number of mtDNA mutations are accentuated by the nearby production of DNA-damaging ROS from the ETC (discussed in section 1.3.4.1) and the lack of histone protection or DNA repair mechanisms in the mitochondria (240). mtDNA encodes for 13 of the proteins necessary for OXPHOS, with the remaining 74 proteins being encoded by nuclear DNA and actively imported into the mitochondria and sorted into compartments (240, 242, 261, 262). In addition, mtDNA encodes the 12S, and 16S rRNAs and 22 tRNAs necessary for protein synthesis within the mitochondria (240, 261-263). The replication of mtDNA is independent of nuclear DNA replication and is not synced to the cell cycle (240, 261). Factors unique to mtDNA replication include a DNA polymerase (POLG), helicase (Twinkle) and mitochondrial-specific single-stranded DNA binding protein (mtSSB) but, as with nuclear DNA replication, the process involves RNase H1 and DNA ligase III (261, 262). mtDNA has two strands, the light

**Table 1.4: List of 37 Genes Encoded for by mtDNA**

Mitochondrial DNA encodes 37 genes, these include 13 polypeptide proteins, 22 tRNAs and the two subunits of rRNA. 28 genes are encoded by the heavy strand and 9 genes are encoded by the light strand. Table adapted from (240).

| Gene | Encodes |
|---|---|
| MT-ND1 | NADH Dehydrogenase Complex I |
| MT-ND2 | NADH Dehydrogenase Complex I |
| MT-ND3 | NADH Dehydrogenase Complex I |
| MT-ND4 | NADH Dehydrogenase Complex I |
| MT-ND4L | NADH Dehydrogenase Complex I |
| MT-ND5 | NADH Dehydrogenase Complex I |
| MT-ND6 | NADH Dehydrogenase Complex I |
| MT-CYB | Coenzyme Q - Cytochrome c reductase/ Cytochrome b Complex III |
| MT-CO1 | Cytochrome c oxidase Complex IV |
| MT-CO2 | Cytochrome c oxidase Complex IV |
| MT-CO3 | Cytochrome c oxidase Complex IV |
| MT-ATP6 | ATP synthase Complex V |
| MT-ATP8 | ATP synthase Complex V |
| MT-RNR1 | rRNA 12S |
| MT-RNR2 | rRNA 16S/Humanin |
| MT-TA | Alanine |
| MT-TR | Arginine |
| MT-TN | Asparagine |
| MT-TD | Aspartic Acid |
| MT-TC | Cystine |
| MT-TE | Glutamic acid |
| MT-TQ | Glutamine |
| MT-TG | Glycine |
| MT-TH | Histidine |
| MT-TI | Isoleucine |
| MT-TL1 | Leucine |
| MT-TL2 | Leucine |
| MT-TK | Lysine |
| MT-TM | Methionine |
| MT-TF | Phenylalanine |
| MT-TP | Proline |
| MT-TS1 | Serine |
| MT-TS2 | Serine |
| MT-TT | Threonine |
| MT-TW | Tryptophan |
| MT-TY | Tyrosine |
| MT-TV | Valine |

strand with low guanine levels with a single promoter region (LSP) and the heavy strand, which has high guanine levels and two promoter regions (HSP1 and HSP2) that are responsible for the production of specific transcripts (240, 262). The HSP1 promoter leads to the production of rRNAs for mitochondrial ribosomes (mitoribosomes), HSP2 produces 10 mRNAs and 14 tRNAs and the LSP leads to 8 tRNAs and the transcript to encode the ND6 protein (261). Fully processed mRNAs are produced from the tRNAs following cleavage of their 5' and 3' ends by RNase P and RNase Z respectively and the subsequent polyadenylation and stabilisation by PPR-containing proteins (261, 262). Following this, mRNAs are translated in the mitoribosomes. Mitochondrial translation requires a number of components encoded by nuclear DNA and imported into the mitochondria, including ribosomal proteins, and initiation, elongation and termination factors (261). During initiation, the mitoribosome is separated by an initiation factor ($IF3_{mt}$) into its 39S and 28S subunits. The 28S subunit then forms a complex with the initiation factor and, following the presence of a 5' start codon, adds the first residue (formylmethionyl-tRNA) to the mitochondrial polypeptide chain (264). The 39S subunit then binds to the complex along with a second initiation factor ($IF2_{mt}$). This hydrolyses GTP to GDP and releases the reformed mitoribosome from the initiation factors, allowing elongation to start (261, 264). During elongation, a complex forms, consisting of a GTP bound, active elongation factor Tu ($EF\text{-}Tu_{mt}$) and aminoacyl-tRNAs. This complex enters the A site of the mitoribosome and coordinates codon:anti-codon-specific paring which, if successful, leads to GTP hydrolysis. Ribosomal enzymes then drive the transfer of residues from the P site to the A site of the mitoribosome, extending the polypeptide chain. This process repeats until a stop codon is reached (261, 264). Mitochondrial termination release factor (mtRF1a) recognises the stop codon and binds to the GTP bound ribosome inducing hydrolysis and causing the release of the mature polypeptide. Mitochondrial recycling factors then coordinate the release of the tRNA, mRNA and the mitoribosomal subunits ready for another round of synthesis (261, 264).

### 1.3.2. Mitochondrial Function

The mitochondria are the site of energy sensing and production in the cell. However, they also function in a number of other processes in the cell, including apoptosis, (discussed further in section 4.5.2) through the release of cytochrome *c*, $Ca^{2+}$ homeostasis (discussed in section 6.1.1) through the proximity to the ER and iron metabolism through the synthesis of iron-sulphur clusters. At the start of the apoptosis process, the outer mitochondrial membrane will depolarise, regulated by the Bcl-2 family members, Bax and Bak, causing the release of cytochrome *c* from the inter-mitochondrial-membrane space (265-267). However, at this stage a cell can still overcome this and survive. If full apoptosis occurs there is a conformational change of the mitochondrial cristae regulated by other Bcl-2 family members Bid and Bim, which causes the release of cytochrome *c* from within their convoluted structure (268-271). For the process of calcium homeostasis, the mitochondria are situated near to the ER where $Ca^{2+}$ is produced. The mitochondria regulate levels, through a uniporter, by taking up calcium from intra-mitochondrial ER stores (242, 249) and releasing it when necessary. This process, that is also linked to the mitochondrial shape (249) as the juxtapositioning of the ER to the mitochondria, is also, a site of mitochondrial fission and, again, the Bcl-2 family member, Bak plays an important role in the initiation of this process (272, 273). The mitochondria are responsible for the synthesis of iron-sulphur clusters which are used by proteins, in many areas of the cell, to support enzymatic and structural functions (274). As explained in section 1.3.4 neurological diseases are often associated with dysfunctional mitochondria, and an accumulation of iron. It is still unknown if the iron accumulation is a symptom or a cause, as dysregulated iron metabolism will, subsequently, cause mitochondrial dysfunction (274).

### 1.3.3. Energy Metabolism

As stated previously, mitochondria are responsible for the sensing and production of cellular energy through the process of cellular respiration, a combination of three processes; glycolysis, the TCA cycle and OXPHOS. These processes combine to break down calorie intake into cellular energy in the form of ATP, discarding carbon dioxide

and water as waste. A schematic of how these processes combine with each other is shown in Figure 1.7.

#### 1.3.3.1. Glycolysis

Glycolysis is the first process in cellular respiration and, in brief, it is the conversion of glucose to pyruvate (see Figure 1.8) which, subsequently, enters the mitochondrial-localised TCA cycle, as discussed in section 1.3.3.2. In detail, glycolysis is a series of 10 reactions (as shown in Figure 1.9) that break down glucose and other organic molecules to produce two molecules of ATP, two molecules of pyruvate and two molecules of NADH. This process is not dependent on the presence of oxygen. The first reaction is the phosphorylation of glucose by hexokinase. The phosphate is taken from an ATP molecule and results in the formation of α-glucose 6-phosphate, which is then converted into its isomer β-fructose 6-phosphate by phosphoglucose isomerase in the second reaction (275). The third reaction of glycolysis uses a phosphate from ATP to phosphorylate β-fructose 6-phosphate into β-fructose 1,6-bisphosphate, using the enzyme phosphofructokinase. This is subsequently broken down into two isomers; dihydroxyacetone phosphate and glyceraldehyde 3-phosphate, using the enzyme fructose bisphosphate aldolase in reaction four. These compounds are rapidly turned over by triosephosphate isomerase in reaction five and the glyceraldehyde 3-phosphate is then used in reaction six (275). As there have been two molecules of glyceraldehyde 3-phosphate formed, from this stage onwards there are two molecules at each step. In reaction six, glyceraldehyde phosphate dehydrogenase adds a hydrogen, converting $NAD^+$ to form NADH and adds a phosphate to each glyceraldehyde 3-phosphate to form 1,3-bisphosphoglycerate (275). In reaction seven, phosphoglycerate kinase removes the phosphate from both 1,3-bisphosphoglycerate and uses them in the conversion of ADP to ATP generating two molecules of ATP and two molecules of 3-phosphoglycerate (275). Reaction eight uses the enzyme phosphoglycerate mutase to transfer a phosphate group from the third carbon of 3-phosphoglycerate to the second carbon, forming 2-phosphoglycerate from which water is removed by enolase to form phosphoenolpryuvate in reaction nine (275). In the final, tenth, reaction pyruvate

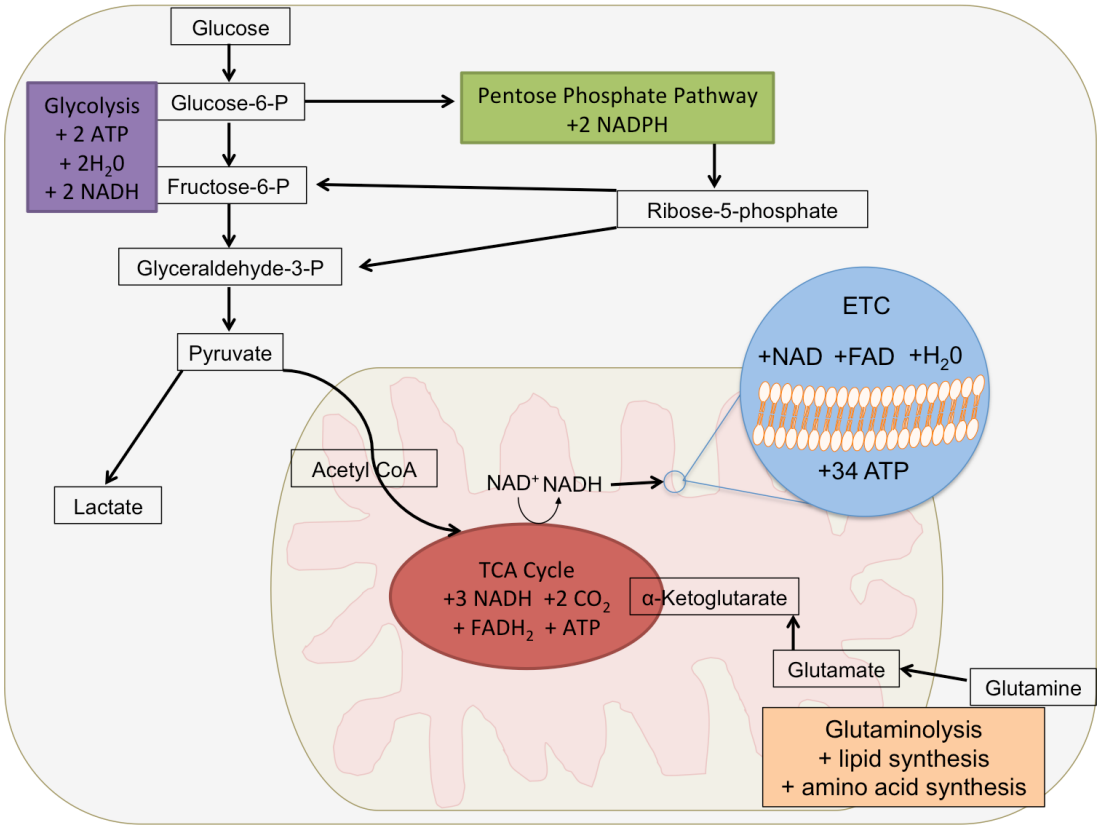


**Figure 1.7: Cellular Respiration**
The combination of glycolysis, the TCA cycle and the ETC make up the processes of normal cellular respiration to produce 36 molecules of ATP. Cancer cells rely on glycolysis for ATP production leading to increased lactate secretion. Connecting into glycolysis, the pentose phosphate pathway produces NADPH and Ribose-5-phosphate. Connecting into the TCA cycle, glutaminolysis can drive the TCA cycle from α-ketoglutarate to drive amino acid synthesis or reverse the TCA cycle for lipid synthesis. Image adapted from (276).

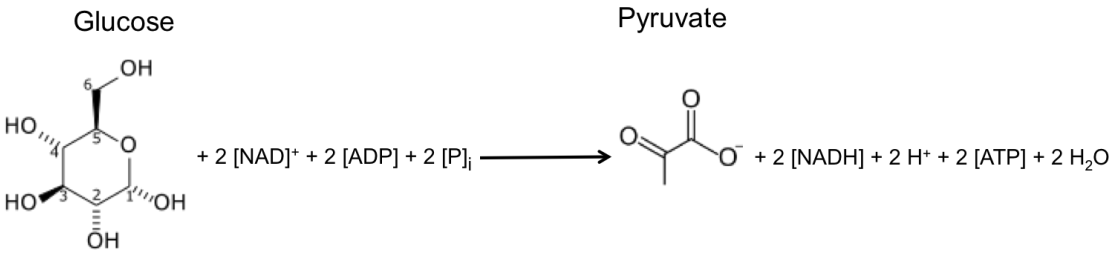


**Figure 1.8: Simplified Model of Glycolysis**
The overall reaction of glycolysis converts glucose to pyruvate also produces two molecules of ATP, two molecules of water, two molecules of NADH and two molecules of Hydrogen.

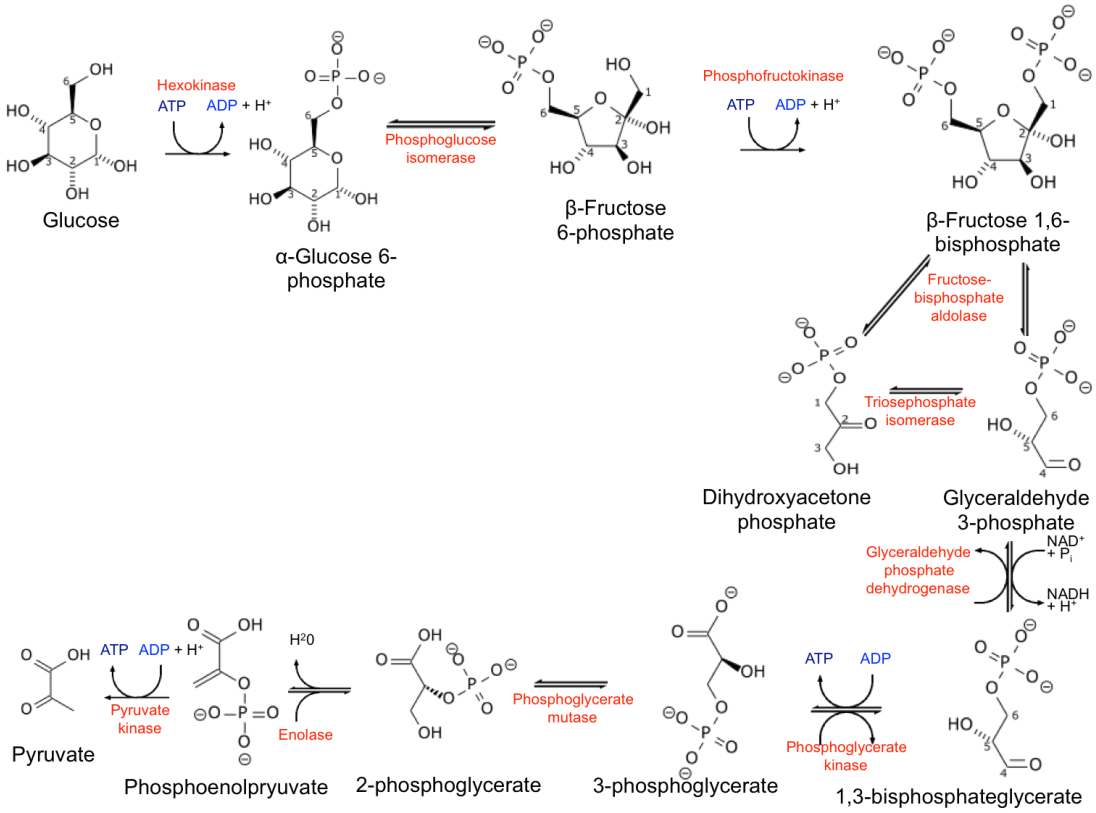


**Figure 1.9: Detailed schematic of Glycolysis**
Glycolysis is a series of 10 reactions that break down glucose to pyruvate and produces 2 molecules of ATP, 2 molecules of $H_20$ and 2 molecules of NADH. All of the reactions take place in the cytosol of cells and are independent of Oxygen. The reactions are driven by the break down of ATP and each reaction uses a different enzyme. The end product of pyruvate is subsequently used in the TCA cycle in the mitochondria. The image is adapted from (277), the black labels indicate the compound formed, red labels indicate the enzyme utilised at each stage. Further details are found in the text.

kinase takes a phosphate from phosphoenolpryuvate and uses it in the conversion of ADP to ATP, resulting in pyruvate as the end product which, subsequently, enters the mitochondria to be processed in the TCA cycle (275).

When oxygen is not present, pyruvate does not enter the TCA cycle and is, instead, converted to lactate by LDH (278). In total, the reaction produces four molecules of ATP but it uses two of these and, therefore, yields a total of 2 molecules of ATP for every molecule of glucose. Consequently, it is an inefficient form of energy production, compared to OXPHOS. However, if OXPHOS is impaired, it is a compensatory mechanism that cells can employ (240).

A second pathway links into glycolysis called the Pentose Phosphate Pathway (PPP) as shown in detail in Figure 1.10. The anabolic PPP pathway initiates from glucose 6-phosphate, from glycolysis, and produces NADPH, the metabolite ribose-5-phosphate, which makes nucleic acids and glyceraldehyde-3-phosphate, which feed back into glycolysis (279). Glucose 6-phosphate is oxidised by the enzyme glucose 6-phosphate dehydrogenase and NADP+ to produce 6-phosphogluconolactone and NADPH. 6-phosphogluconolactone is very unstable and glutconolactonase catalyses the hydrolysis of the ester link, opening the ring resulting in 6-phosphogluconate. This is subsequently oxidized by $NADP^+$ with the enzyme 6-phosphogluconate dehydrogenase producing ribose-5-phosphate and NADPH (275, 279). Ribulose-5-phosphate can then, either be converted to ribose-5-phosphate by isomerase or, once the cells requirements are reached, is instead converted to xylulose-5-phosphate by ribulose 5-phosphate 3-epimerase (275, 279). These two products can then be converted to many different length carbon chains, depending on the enzyme. Transketolase cleaves a two-carbon unit from xylulose-5-phosphate creating glyceraldehyde-3-phosphate and adds it onto either ribose-5-phosphate resulting in the formation of sedoheptulose-7-phosphate, or on to erythrose-4-phosphate resulting in fructose-6-phosphate (275, 279). Transaldolase then transfers a three-carbon unit from sedoheptulose-7-phosphate on to glyceraldehyde-3-phosophate resulting in erythrose-4-phosphate and fructose-6- phosphate, which leads back into the glycolysis process, along with any excess glyceraldehyde-3-phosphate (275, 279).

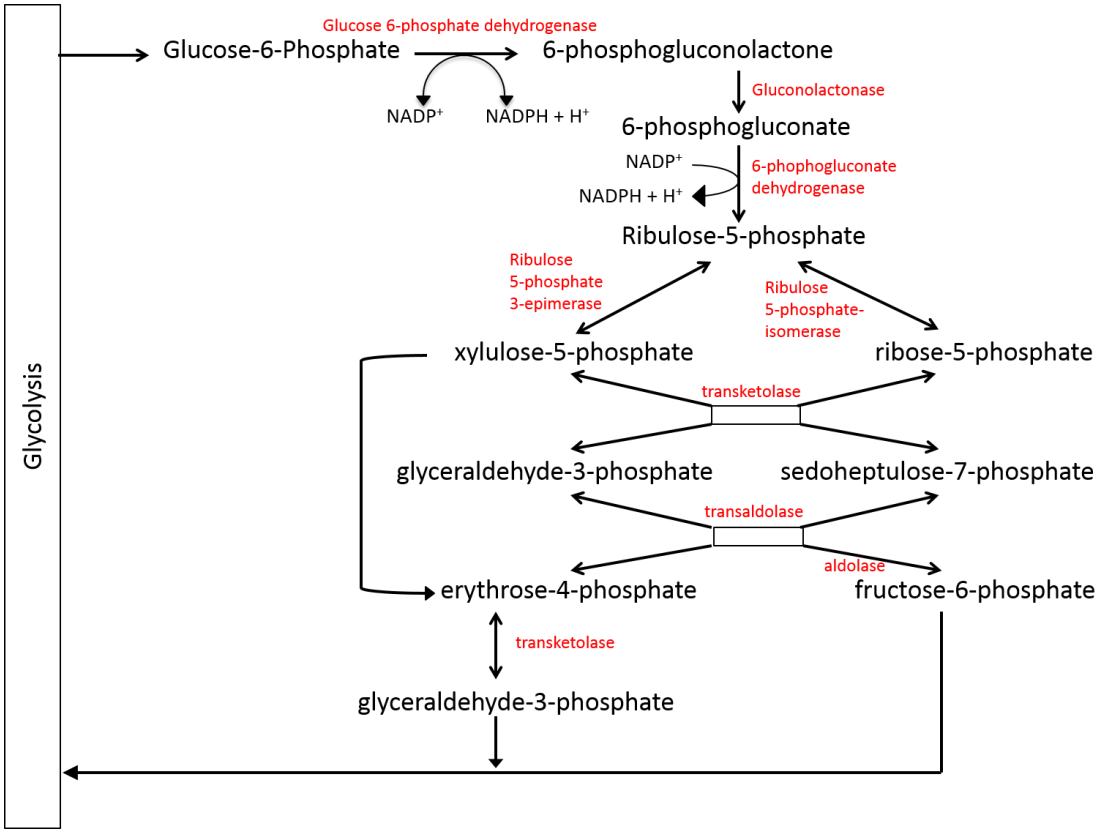


**Figure 1.10: Pentose Phosphate Pathway**

The pentose phosphate pathway takes place in the cytosol and initiates from Glucose-6-phosphate from glycolysis. It is a series of reactions that produces NADPH for fatty acid synthesis and ribose-5-phosphate for nucleic acid synthesis and also feeds back into glycolysis. Black labels indicate the compound formed, red labels indicate the enzyme utilised at each stage. Schematic adapted from (279), further details can be found in the main text.

### 1.3.3.2. The TCA Cycle

The TCA cycle is a series of 8 chemical reactions that occurs in the mitochondrial matrix following the conversion of glucose to pyruvate in glycolysis (see section 1.3.3.1, Figures 1.7 and 1.11). The TCA cycle produces three molecules of NADH, one (flavin adenine dinucleotide) $FADH_2$ and one molecule of ATP for every molecule of acetyl-CoA (277). Before entering the TCA cycle, pyruvate is transformed by pyruvate dehydrogenase with the help of coenzyme A and NAD into acetyl-coenzyme A (acetyl-CoA), the starting product of the TCA cycle (275). Acetyl Co-A is formed of an acetyl group attached to a coenzyme A molecule, which contains an ADP molecule so when it is broken down, large amounts of energy are released to drive the TCA cycle. The first reaction joins acetyl-CoA with oxaloacetate to form citric acid using the enzyme citrate synthase; water then breaks the bonds connecting the acetyl and coenzyme A releasing it from the complex (275). Acontinase then transfers the -OH group from position 3' to 4' of citric acid forming isocitrate. Step three of the TCA cycle has two reactions, firstly isocitrate dehydrogenase and $NAD^+$ drive the oxidation of the –OH group in the 4' position of isocitate, the second reaction then removes $CO_2$ to produce α-ketoglutarate (275). Step four removes another $CO_2$ molecule from α-ketoglutarate and replaces it with coenzyme A to produce succinyl-coA, this reaction uses $NAD^+$ and α-ketoglutarate dehydrogenase. The fifth reaction of the TCA cycle is catalysed by succinyl-CoA synthase, it drives the release of CoA from succinyl-CoA to produce succinate and phosphorylation of GDP to GTP, molecules very similar in structure and function to ADP and ATP. In reaction six, $FAD^+$ is reduced to $FADH_2$ by removing two hydrogen ions from succinate to produce fumarate under the enzyme of succinate dehydrogenase (275). The penultimate reaction uses fumarase to change fumarate to malate with the addition of water. In the final reaction, oxaloacetate is generated by the oxidation of malate using malate dehydrogenase and $NAD^+$ as an oxidizing agent, this is now available to be used in the first stage of the next cycle (275).

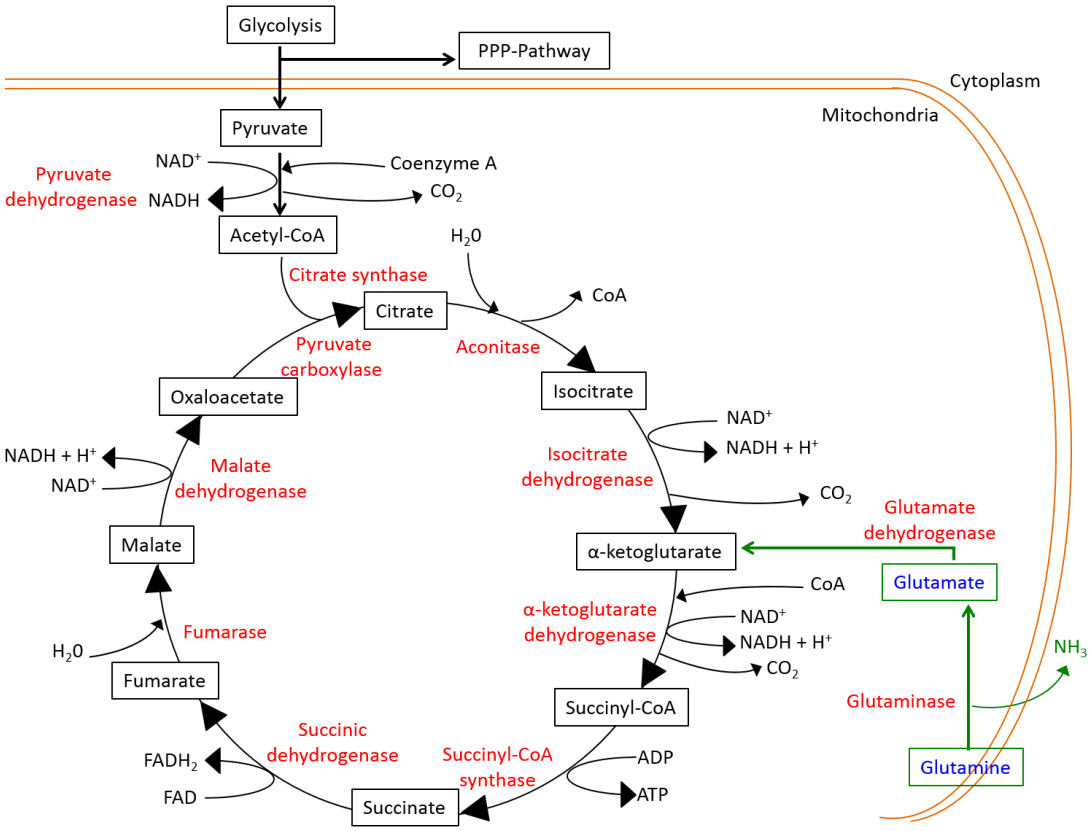


**Figure 1.11: The TCA cycle**

The tricarboxylic acid cycle is driven by the energy from broken down coenzyme A, it is a series of 10 reactions from pyruvate (as a product of glycolysis) to citrate. It produces $CO_2$, ATP, NADH and $FADH_2$, which subsequently feeds into the electron transport chain. The process starts with the conversion pyruvate to acetyl-CoA, this occurs outside of the mitochondria and acetyl-CoA is shuttled into the mitochondria using a transport protein. The cycle can be driven by glutamine from α-ketoglutarate to citrate in a process called glutaminolysis. Alternatively glutamine can drive the cycle in reverse to increase fatty acid synthesis. Image adapted from (277, 280), further details can be found in the main text.

#### 1.3.3.3. Glutaminolysis

Glutaminolysis is an alternative pathway that can drive the TCA cycle from α-ketoglutarate to citrate. Driven by glutamine instead of glucose, cells will undertake glutaminolysis when levels of glucose are low or when levels of enzymes in the TCA cycle are sparse halting its progression. During this process, glutamine is taken into the cells and hydrolysed by glutaminase to produce glutamate and ammonium as a waste product. Glutamate dehydrogenase then converts glutamate to α-ketoglutarate (281, 282). It has also been shown in some cancers, that glutamine can cause a reversal in the TCA cycle to drive fatty acid synthesis using isocitrate dehydrogenase to carboxylate oxoglutarate to isocitrate (241, 281, 283, 284).

#### 1.3.3.4. Oxidative Phosphorylation (OXPHOS)

OXPHOS is a series of redox reactions via five complexes situated in the IMM known as the ETC as shown in Figures 1.7 and 1.12. The reaction catalyses the oxidation of ingested calories into energy in the form of ATP and as a result produces water from the reduction of oxygen (261). The generation of NADH and $FADH_2$ from the TCA cycle (described in section 1.3.3.2) provides the electrons to drive the ETC (242, 276). As previously explained the complexes in the ETC are encoded for by a mixture of both nuclear and mtDNA (240, 242, 261, 262). Specifically, the mtDNA encodes 7 NADH dehydrogenase units of complex I, the largest complex comprising of 45 subunits (242). mtDNA also encodes for 1 cytochrome b in complex III, 3 cytochrome c oxidase subunits in complex IV and 2 ATPase in complex V (240). Nuclear DNA encodes for 36 subunits of complex I, the whole of complex II, which comprises of 4 subunits, 10 subunits of complex III and complex IV and 14 subunits of complex V (240). In Complex I two electrons are taken from NADH and transferred to ubiquinone (285). Complex II does not contribute to the proton gradient as it does not span the whole IMM, it connects the TCA cycle and the ETC as it is the oxidation of succinate to fumarate (see section 1.3.3.2) via $FAD^+$ producing electrons that contribute to the quinone pool (286). Complex III acts in the Q cycle, oxidising ubiquinol and reducing two molecules of cytochrome *c* and subsequently produces four hydrogens that are pumped across the IMM adding to the proton gradient (287).

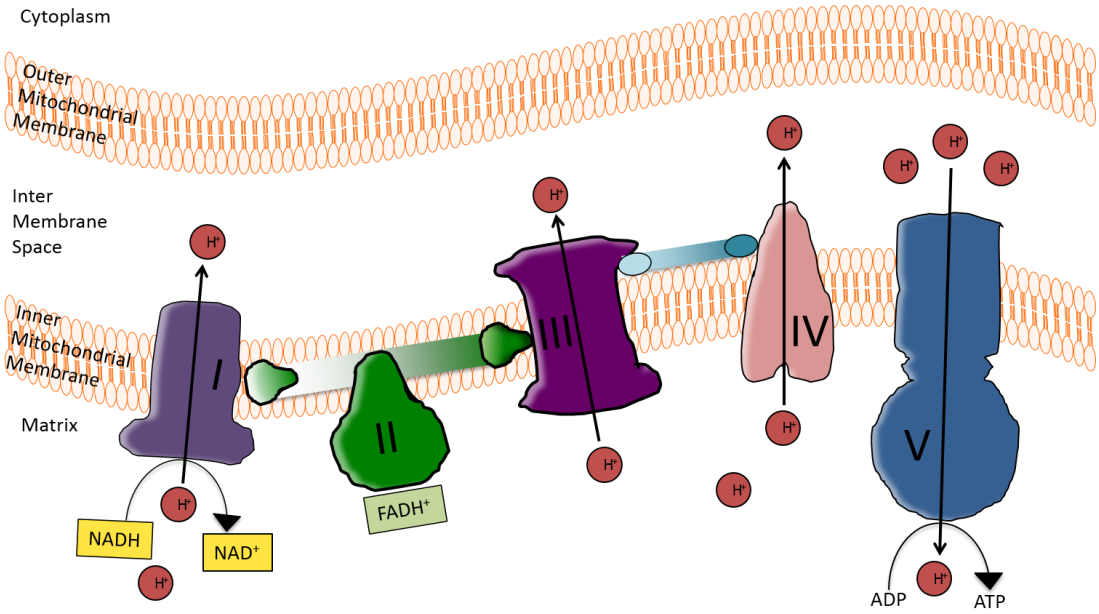


**Figure 1.12: ETC**

The electron transport chain consists of five complexes (288) situated in the inner mitochondrial membrane of the mitochondria. Driven by the oxidation of NAD the ions pass through the complexes creating a membrane potential and eventually are used in the conversion of ADP to ATP by complex V also known as ATP synthase. Image adapted from (240, 275).

Complex IV produces two molecules of water by taking four molecules of hydrogen from cytochrome *c* and transferring them to molecular oxygen, in this process four protons are transferred across the IMM (289). The functions of Complex I, III and IV results in protons being pumped across the IMM creating a proton gradient otherwise known as the mitochondrial membrane potential (261). The proton gradient subsequently drives the conversion of ADP to ATP through the rotary turbine-like complex V also called ATP synthase, generating 34 molecules of ATP per molecule of glucose (242). Complex V is formed of two subunits, the lower $F_o$ subunit, called such due to its interaction with oligomycin, which is located within the IMM. The larger $F_1$ subunit is located in the intermembrane space (as seen in Figure 1.6 labelled ATP synthase particles); it is comprised of 5 subunits named alpha, beta, gamma, delta and epsilon (175, 290).

As the proton gradient drives the activity of ATP synthase, converting ADP to ATP (175, 290), it is essential for efficient OXPHOS but is also vital for other mitochondrial functions including mitochondrial protein import (242) and mitochondrial fusion which can still occur in the absence of ATP or a functional respiratory chain but cannot occur if the membrane potential is removed (245, 291).

Reactive oxygen species (ROS) in the form of oxygen radicals and hydrogen peroxide are generated by complexes I and III of the ETC (242) this is due to electron that leak from the ETC and react with molecular oxygen. ROS can be used as secondary messengers in the cell and can help cells to adapt to stress such as hypoxia (242). However, ROS can also be toxic causing apoptosis (249) and due to their close proximity to the mtDNA replication machinery, are a common cause of mutations in mtDNA (292), as well as nuclear DNA. Mutations within mtDNA can also change the formation of ETC complexes and increase the escape of electrons (240). This is specifically linked to various cancer types as discussed in section 1.3.4.2.

### 1.3.4. Mitochondrial Diseases

Mitochondrial diseases are defined as disorders caused by alterations in mitochondrial proteins encoded for by either, mtDNA, or the nuclear DNA that cause

mitochondrial dysfunction (293). However, as will be explained further in section 1.3.4.3, cancer has an altered metabolism and, therefore, can be defined as a mitochondrial disease (294, 295).

#### 1.3.4.1. Mutations in Mitochondrial DNA

As explained previously (see section 1.3.1.1), mutations within mtDNA are frequent, due to their lack of introns (240). However, as there are between 2-10 copies of the genome in each mitochondrion and multiple mitochondria within each cell, this results in hundreds to thousands of copies of mtDNA in each cell. Therefore, a certain number of mutations can be tolerated until a threshold is reached and the mutations have causative effects (240, 261-263, 293). This can vary, depending on the mutation and the cell type (296). In addition to this, during mitosis, the division of mtDNA is not necessarily equal and, therefore, the amount of mutant mtDNA can accumulate in certain cells, changing their phenotype in a process called mitotic segregation (240, 293, 296, 297). There are currently no curative treatments of mitochondrial diseases (261). Mitochondrial DNA mutations can occur in tRNA, rRNA, or within the factors of mtDNA translation. Some examples of mitochondrial diseases are; mitochondrial encephalopathy, lactic acidosis and stroke-like episode (MELAS) syndrome, caused by a tRNA mutation, non-syndromic sensorineural hearing loss (SNHL), caused by an rRNA mutation incited following treatment with aminoglycoside antibiotics and Leber's hereditary optic neuropathy (LHON), an inherited disease affecting Complex I of the ETC (293, 296, 297). Neurological disorders, including Parkinson's and Alzheimer's disease, are also linked to mitochondrial dysfunction (298-300).

#### 1.3.4.2. Mitochondrial and Cancer

There are also multiple cases of cancer caused by somatic mutations within mtDNA. These include breast, ovarian, colorectal, gastric, hepatic, eosphageal, and pancreatic cancers where the common sites, containing mutations are the non-coding D-loop regions, the NADH dehydrogenase (ND) genes and the cytochrome *b* gene (240). Mutations, within the mtDNA encoding the metabolism machinery, are also known to cause various types of cancer. Mutations within Complex I have been shown to

cause thyroid, colorectal, head and neck, medulloblastoma, bladder and prostate cancers (240, 301). Mutations found within Complex III have been shown to cause thyroid, breast, colorectal, bladder and ovarian cancers (301) whereas, mutations with Complex IV are less common and are only seen in ovarian and prostate cancer (301). Complex V mutations are seen in renal, prostate, thyroid and pancreatic cancers (240, 301). There are also mutations within the enzymes of the TCA cycle linked to various types of cancer. The TCA cycle is encoded by nuclear DNA but, as explained in section 1.3.2.2, is a vital aspect of cellular respiration and, therefore, mutations can have metabolic and oncogenic effects. Citrate synthase has been linked to pancreatic, cervical and renal cancers (302-304). Mutations within aconitase have been found in gastric and prostate cancers (305, 306). Isocitrate dehydrogenase mutations are found in a number of cancers including, AML, prostate, and glioblastoma (307-309). Hereditary forms of renal, breast and GI cancers have been found to have mutations within succinate dehydrogenase (310-312). Alterations in fumarase are linked to glioblastoma and neuroblastoma, as well as hereditary renal cancers (313-315). Mutations within the final enzyme of the TCA cycle, malate dehydrogenase, have been linked to cases of hematologic malignancies (316, 317).

#### 1.3.4.3. Cancer Cell Metabolism

It was stated previously that mitochondrial diseases are those that cause mitochondrial dysfunction, changes to metabolism that lead to, or progress, cancer are becoming better understood and, therefore, cancer is considered as a mitochondrial diseases (294, 295). In 1924, Otto Warburg found that cancer cells had altered metabolism and would preferentially metabolise glucose, even in the presence of oxygen, a process termed the Warburg effect (9, 276, 318). This effect was wrongly attributed to dysfunctional mitochondria (seen in only rare cases; (241) but, now, there are generally two accepted phenotypes of cellular metabolism, the respiratory phenotype and the glycolytic phenotype (257, 319, 320). In the respiratory phenotype (described in sections 1.3.3.1-1.3.3.4), glucose is taken into the cell and converted to pyruvate by the process of glycolysis. Pyruvate then enters

the mitochondria and initiates the TCA cycle where it produces free ions. These pass though the ETC, creating a membrane potential, which is used to convert ADP to ATP, creating 34 molecules per glucose molecule (276). The mitochondria in this phenotype are described as being elongated with well-formed cristae for good gas exchange (265, 318). The glycolytic phenotype, that is typical of cancer cells, has a larger intake of glucose (321). Any ATP produced is through the process of glycolysis, producing just 2 molecules of ATP per molecule of glucose (276). Glycolysis is the primary production of ATP in malignant cells, therefore requiring a high level of glucose intake to keep up with the demand for cellular energy of highly proliferative cells (240). The pyruvate created from glycolysis does not enter the TCA cycle but, instead, is converted to lactic acid by LDH, creating an acidic environment around the cells, even in the presence of oxygen and, therefore, is termed aerobic glycolysis (276, 318). The TCA cycle is still often active in the glycolytic phenotype but, instead of being driven by glucose, it is driven by glutamine (277). Tumour cells often use glutaminolysis preferentially as glutamine tends to be in excess in tumour cells and it leads to an increase in amino acid synthesis (277, 322, 323). The mitochondria in the glycolytic phenotype are described as small, rounded, structures where the cristae are poorly defined (265).

The PPP pathway and the subsequent fatty acid synthesis are also altered in cancer cells. In cancer cells with altered PI3K/Akt signalling, mTOR can upregulate the oxidative portion of the PPP pathway to increase NAHPH for fatty acid synthesis (324, 325). In addition, levels of the enzyme G6PDH are often upregulated in cancer. This enzyme is responsible for the production of the first molecule of NADPH in the pathway, as cancer cells require large levels of NADPH and, therefore, the activity of the enzyme is upregulated (324). It has also been shown that the increased NADPH has been linked to the ability of cancer cells to resist oxidative stress and some therapeutic agents (318). Conversely, RAS activated cancers increase the non-oxidative portion of the PPP pathway by upregulating the enzymes ribulose-5-phosphate isomerase and ribulose-5-phosphate epimerase (326). This requires a large increase in glucose and, subsequently, increases the amount of 5-carbon sugars available for nucleotide synthesis (324). Likewise, there is a substantial increase in

lipid metabolism in cancer and it has been shown that the PI3K/Akt pathway and oncogenic RAS are, once again, involved in the regulation of this process (327). Fatty acids and phosphoglycerides are required for energy storage and the production of new biological membrane and, therefore, are required for the increased proliferation of cancer cells.

It would now appear that the definitions of a respiratory and glycolytic phenotype are too strict, and that cellular metabolism can alter and adapt to meet the specific requirements of the cells or tissues, as necessary (276). These more recent findings indicate that targeting the altered metabolism of cancer cells could provide potential new treatments for cancer but it is necessary to understand the differences between normal and malignant cells (295, 328, 329).

## 1.4. Aims

The purpose of this study is to investigate a panel of 29 melanoma cell lines. The cell lines will be characterised in terms of their 3D Matrigel growth, proliferation, apoptosis, their ability to grow in a non-adherent environment, and the expression of markers associated with models of melanoma progression and tumour initiation. Using a selection of melanoma backgrounds, the effects of Wnt/β-catenin signalling on cancer cell characteristics will then be investigated, measuring cell migration, invasion and the afore-mentioned proliferation and apoptosis. This will help determine if there are any distinct phenotypes that can be identified within different melanoma cells.

I will then investigate the effects of Wnt/β-catenin signalling on the mitochondria of melanoma cells and any subsequent effects on melanoma cell metabolism. It has previously been shown that Wnt/β-catenin signalling plays a vital role in melanoma and that the dysregulated metabolism of cancer cells has been well established. New data is emerging to suggest that Wnt can play a role in the alterations of melanoma cell metabolism. However, the mechanism by which this occurs is not well understood. This research aims to investigate these mechanisms and bridge the knowledge gap that currently exists.

# 2. MATERIALS and METHODS

## 2.1. Materials

| Product | Supplier | Catalog No. |
|---|---|---|
| 0.4% Trypan Blue in PBS | Fisher | HYC-044-010D |
| 10 cm dishes Tissue Culture (TC) Grade | Fisher | 10508921 |
| 10 ml strippette | Fisher | FB55484 |
| 10 µl tips | Fisher | FB78000 |
| 12-well plates TC Grade | Fisher | TKT-190-070N |
| 15 ml falcon tubes | Fisher | FB55951 |
| 1 ml tips | Fisher | FB78076 |
| 200 µl tips | Fisher | FB78036 |
| 24-well companion plate | BD | 734-0067 |
| 25 cm flasks TC Grade | Fisher | TKT-130-250H |
| 50 ml falcon tubes | Fisher | FB55959 |
| 5 ml strippette | Fisher | FB55483 |
| 6 well plates TC Grade | Fisher | TKT-190-110E |
| 8.0 µm pore Cell Culture Inserts | BD | 353097 |
| 96 well plates TC Grade | Fisher | 1056-7131 |
| Acrylamide/bis-aceylamide 40% | Sigma | A7168-100ml |
| Agarose | Fisher | BPE1356-100 |
| Ampicillin | Sigma | A5354 |
| Apop-TRACE | Sigma | Cs1110 |
| APS Ammonium Persulfate | Sigma | A3678 |
| ATP determination Kit | Invitrogen | A22066 |
| BCA Protein Assay Kit | Pierce | 23225 |
| BSA | Fisher | BPE9702-100 |
| Cell Scrapers | Fisher | 11597692 |
| Cell Strainers | VWR | 734-0003 |
| Citrate Synthase Assay Kit | Sigma | CS0720-1KT |
| Competent E.coli Top10 cells | Fisher | FH01006A |
| cOmplete mini Tablets protease inhibitor cocktail | Roche | 4693124001 |
| ConA Sepharose 4B | BioWorld | 20182001-1 |
| Crystal Violet | Fisher | SDS102-2 |
| DCFDA Cellular Ros Detection Assay Kit | abcam | ab113851 |
| DMSO | Fisher | D/4121/PB08 |
| DNA polymerase | NEB | M0530G |
| dNTPs | Sigma | DNTP10 |
| Dual Luciferase Reporter assay | Promega | E1910 |
| Dynabeads Protein G | Novex | 10003D |
| ECL Prime Western Blotting Detection | GE Healthcare | RPN2232 |
| EDTA | Sigma | E9884 |

| | | |
|---|---|---|
| Eppendorfs | Fisher | FB74031 |
| EZ-PCR Mycoplasma Test Kit | GeneFlow | K1-0210 |
| FBS (Lot # RVJ35882) | Hyclone | SV30160 |
| Fermentas spectra multicolour broad range protein ladder | Fisher | SM1841 |
| Filter paper | Fisher | CJF-500-150K |
| Gel Red nucleic acid stain | VWR | BT41003 |
| GeneJet RNA purification Kit | Thermo Scientific | K0731 |
| GFP-Parkin Construct pEGFP-parkin WT | Addgene | 45875 |
| Glucose (HK) Assay Kit | Sigma | GAHK20-1KT |
| Lactate Assay | BioVision | K607-100 |
| LC3 construct pQCXI Neo DsRed-LC3-GFP | Addgene | 31183 |
| L-Glutamine TC Grade | Sigma | G7513 |
| LightCycler FastStart DNA Master SYBR Green I | Roche | 3515869001 |
| LightCycler® 480 Multiwell Plate 96 | Roche | 04729692001 |
| LightCycler® 480 sealing foil | Roche | 04729757001 |
| Lipofectamine 2000 | Invitrogen | 11668-027 |
| Lipofectamine RNAi Max | Invitrogen | 13778-075 |
| Loading buffer 3X | BioLabs | B7703s |
| Magic Marker | Novex | LC5602 |
| Marvel Milk Powder | Marvel | 00183932773 |
| Matrigel basement membrane matrix | BD | 356234 |
| Melanocyte media | Fisher | M-254-500 |
| Mitochondrial isolation Kit for Mammalian Cells | Thermo Scientific | 89874 |
| Nitrocellulose 0.45um 300mmx3.5m | Fisher | 1077-3485 |
| NovaQUANT Human mitochondrial to nuclear DNA Ratio Kit | Novagen | 72620-1KIT |
| Parafilm | Fisher | SEL-400-060G |
| Paraformaldehyde | Sigma | 158127 |
| PBS tablets | Fisher | BPE9739-1 |
| Pen/Strep TC Grade | Sigma | P0781-100ml |
| PhosSTOP phosphatase inhibitor cocktail tablet | Roche | 4906837001 |
| Propidium Iodide (PI)/RNase Staining solution | Cell signalling | 4087s |
| Poly-D-Lysine | Sigma | P7280 |
| PolyHEMA | Sigma | P3932-10G |
| Protein G Sepharose Fast Flow Beads | Sigma | P3296-5ML |
| Proteinase K | Sigma | P6556 |
| PVDF | Thermo Scientific | 88518 |

| | | |
|---|---|---|
| Qiaquick gel purification | Qiagen | 28704 |
| Quick load 100bp DNA ladder | NEB | H04675 |
| Quick load 1Kb DNA ladder | NEB | N0468 |
| Rat Tail Collagen Type I | BD Bioscience | 354236 |
| Recombinant Human DKK-1 (rDKK1) | R&D | 5439-DK-010 |
| Recombinant Human Wnt3a protein (rWnt3a) | R&D | 5036-wn |
| RPMI-1640 | Hyclone | SH30096.01 |
| SeeBlue Pre-stained standard | Novex | LC5625 |
| Sequence Grade Modified Trypsin | Promega | V511c |
| Silencer Select Validated siRNA CTNNB1 | Ambion | 4390824 #s437 |
| Silencer Select validated siRNA negative control #1 | Ambion | 4390843 |
| Silencer Validated siRNA PTEN | Ambion | 114050 |
| Silencer validated siRNA negative control #1 | Ambion | AM4611 |
| Taq DNA polymerase | Bioline | BIO-21085 |
| TEMED NNNN-Tetramethylethylenediamine | Sigma | T9281-50ML |
| Trizma HCl | Sigma | T5941-500g |
| Trypsin-EDTA 0.5% | Fisher | FF01058J |
| Vectashield | Vector laboratories | H1000 |
| Waters Sep Pack Vac 1cc (50mg) c18 cartridge | Waters | Wat054955 |
| Wizard Genomic DNA extraction Kit | Promega | A1120 |
| XF Cell Mito Stress Test Kit | Seahorse Bioscience | 102308-400 |

| **Antibodies and Cell Stains** | | |
|---|---|---|
| ABCB5 PAb | Abgent | AP6122a |
| AF488 phalloidin | Invitrogen | A12379 |
| AF633 anti-mouse | Invitrogen | A21050 |
| Akt (pan) (C67E7) Rabbit mAb | Cell Signalling | 4691P |
| Anti p75 NGF receptor Ab | Abcam | ab8874 |
| Anti Rabbit IgG HRP | NEB | 7074s |
| Anti-CD146 rabbit mAb | Abcam | ab75769 |
| Anti-CD44 rabbit mAb | Abcam | ab51037 |
| Anti-Drp1 | Abcam | ab56788 |
| Anti-LEF Rabbit Mab | NEB | 2230s |
| Anti-Mitofusin 1 | Abcam | ab57602 |
| Anti-Mitofusin 2 | Abcam | ab56889 |
| Anti-mouse IgG HRP | Cell Signalling | 7076s |
| Anti-Nanog rabbit pAb | Abcam | ab80892 |

| | | |
|---|---|---|
| Anti-OPA1 | Abcam | ab55772 |
| Anti-Parkin (PRK8) Mouse mAb | Abcam | ab15954 |
| Anti-Sox2 rabbit pAb | Abcam | ab97959 |
| Anti-TCF4 Rabbit Mab | NEB | 2569s |
| Anti-TOMM20 | Sigma | HPA011562 |
| β-catenin Antibody rabbit | Cell signalling | 9562 |
| CD20 mAB | Abgent | AJ1155a |
| Chicken anti-goat IgG HRP | R&D Systems | HAF019 |
| Cytochrome C | AbD Serotec | MCA2740 |
| Donkey anti-rabbit AF488 | Invitrogen | A-21206 |
| E-cadherin (32A8) | Cell Signalling | 5296s |
| GFP (4B10) Mouse mAb | Cell signalling | 2955 |
| Goat anti-Rat IgG HRP | R&D Systems | HAF005 |
| Hoechst 33342 | Invitrogen | H1399 |
| Human MITF Pab | R&D Systems | AF5769 |
| Human/Mouse Wnt5a Mab | R&D Systems | MAB645 |
| JC-1 | ebioscience | 65-0851-38 |
| Lamin A/C Rabbit Ab | Cell Signalling | 2032 |
| LC3 | Sigma | L7543 |
| MitoTracker Deep Red FM | Invitrogen | M22426 |
| MitoTracker Green FM | Invitrogen | 7514 |
| MitoTracker Red Fm | Invitrogen | M22425 |
| N-cadherin | Cell Signalling | 4061s |
| P-Akt (s473) (D9E) XE Rabbit mAb | Cell Signalling | 4060P |
| p62 | Abcam | ab91526 |
| pAb anti-PINK1 | Novus Biologicals | BC100-494 |
| Parkin (Prk8) mouse Mab | Cell Signalling | 4211 |
| Phopho-DRP1 (Ser616) Antibody rabbit | cell signalling | 3455 |
| PROM1 Pab | Abnova | PAB12663 |
| PTEN (A2B1) | Santa Cruz Biotechnology | sc-7974 |
| Rhodamine 123 | Invitrogen | R302 |
| Snail (C15D3) Rabbit mAb | Cell Signalling | 3879P |
| TMRM | Fisher | VXT668 |
| Vimentin (D21H3) XP Rabbit mAb | Cell Signalling | 5741 |
| Wnt3a Mouse mAb | R&D Systems | MAB1324 |
| α-tubulin mouse Mab | Cell Signalling | 3873s |

## 2.2. Recipes

### 2.2.1. PBS 1X

1 Tablet in 100 mls $dH_2O$
Autoclave

Formation:
Sodium Chloride 137 mM
Phosphate Buffer 10 mM
Potassium Chloride 2.7 mM
(pH 7.4)

### 2.2.2. TE buffer

10 mM Tris-HCL
1 mM EDTA
(pH 8.0)

### 2.2.3. 50X TAE

121 g Tris Base
28.55 mls acetic acid
50 mls 0.5M EDTA (9.3 g in 50mls)
(pH 8.0)
$H_20$ to 500mls

### 2.2.4. 4% PFA

150 mls PBS
8 g PFA (in fume hood)

Stir in a beaker of water heated to 60°C to disolve
pH 7.3 with NaOH
Fill to total volume of 200 mls with PBS

Cool to room temperature
Store at 4°C

### 2.2.5. Lysis Buffer

50 mM Tris-HCL
1% Triton-X
10 mM $MgCl_2$
20% Glycerol
(pH 7.4)
Store at 4°C

### 2.2.6. 0.5M Tris-HCL pH 6.8

0.5 M TrisHCL (19.7 g)
(pH 6.8)
200 mls $H_20$

### 2.2.7. 1.5M Tris-HCL pH 8.8

1.5 M Tris HCL (36.4 g)
(pH 8.8)
200 mls $H_20$

### 2.2.8. 10% SDS 200 mls

20 g SDS
up to 200 mL water

### 2.2.9. 10X Running Buffer 1 L

25 mM TrisBase (30.2 g)
190 mM Glycine (144 g)
0.1% SDS
(pH 8.3)

### 2.2.10. 10X Transfer Buffer 1 L

25 mM TrisBase (30.2 g)
192 mM Glycine (144 g)
(20% methanol to be added to 1X solution)
Store at 4°C

### 2.2.11. Ponceau S Stain 100 mls

5ml glacial acetic acid
0.2 g Ponceau S
up to 100 ml with water
Store at 4°C

### 2.2.12. Stripping Buffer 100 mls

1.5 g Glycine
0.1 g SDS
1 ml Tween 20
(pH 2.2)
Store at 4°C

### 2.2.13. 10X TBS 1 L

24.23 g TrisHCL
80.6 g NaCl
800 mls $ddH_2O$
(pH 7.6)
$ddH_2O$ to 1 L
(Tween to be added to 1X solution to make TBST)

### 2.2.14. 2.5% PolyHEMA

Sigma P3932-10G, Poly(2-hydroxyethyl methacrylate). Make a 2.5% solution in 95% ethanol dissolve by heating to 95°C.

### 2.2.15. EDTA 40 mM

0.5 g EDTA
150 mls H20
pH 8.9 with NaOH
Total volume 250 mls
Autoclave

### 2.2.16. PBS-EDTA (Cell dissociation Buffer for Flow)

50 ml PBS
0.5 ml EDTA (40mM)

### 2.2.17. FACS Buffer

0.5% FBS in PBS
Store at 4°C

### 2.2.18. Seahorse Media

1X Sodium Pryuvate
DMEM + Glucose

### 2.2.19. Hoechst Stain

4 ml 1 M NaCl
40 µl 1 M Tris-HCL pH7.4
40 µl 0.1 M EDTA
1.6 µl Hoechst 33342 10 mg/ml in $H_20$

### 2.2.20. Fixative for Immunofluorescence

5% formaldehyde at 37% = 26.8 ml
2% sucrose at 50% = 8 ml
40 mg of sodium azide
165.2 ml PBS

### 2.2.21. Wash Buffer for Immunofluorescence

198 ml PBS
2 ml serum
40 mg sodium azide

### 2.2.22. Permeabilization Buffer for Immunofluorescence

1 ml Triton-X
20 g sucrose
2 ml serum
40 mg sodium azide
197 ml PBS

### 2.2.23. Antibody Diluent for Immunofluorescence

198 ml PBS
2 ml serum
4 g sucrose
40 mg sodium azide

## 2.3. Methods

### 2.3.1. Routine Culture of Cell Lines

All cell culture methods are adapted from protocols outlined in a manual of basic technique for the culture of animal cells (330), unless otherwise stated. Human cells were cultured in sterile, tissue culture grade plastic flasks of 25 or 175 $cm^2$ in surface area, or dishes 100 mm in diameter. All manipulations were carried out in a class II safety cabinet (LabGard). Unless otherwise stated, cells were grown in RPMI-1640, supplemented with 10% heat-inactivated foetal bovine serum (FBS), 2 mM L-Glutamine, 100 U/ml penicillin and 100 ug/ml streptomycin. This media is referred to as growth media throughout the text. Incubation was carried out in a humidified incubator at 37°C with 5% $CO_2$. Once opened, all medium was used within 1 month and all cultures checked visually using an inverted microscope at least three times a week. FBS (HyClone), batch number RVJ35882 was used throughout the project to limit variability. Cells were subcultured every 4 days. For a 100 mm diameter Petri dish, the medium was removed and discarded; cells were washed once with 3 ml 1X PBS (see section 2.2.1) and incubated with 1 ml 0.05% trypsin (Gibco) at 37°C for 1-5 minutes depending on the cell line. Once cells had become unattached they were resuspended in 5 ml of medium containing 10% FBS and centrifuged at 180*g* for 5 minutes to remove the trypsin. Cells were then diluted as desired and plated in new tissue culture flasks/dishes, with appropriate reagent volumes.

#### 2.3.1.1. Melanoma Cell Line Panel

The melanoma cells were gifted by Prof. A. Ribas (UCLA; M285, M296 and M375) and Prof. A. Chien and Prof. R. T. Moon (University of Washington; A2058, A375, Colo829, HMB2, HTB63, M202, M207, M229, M308, Malme3M, Mel501, Mel624, SkMel5, Skmel24, SkMel28 and UACC1273).

#### 2.3.1.2. Melanocytes

Human Epidermal Melanocytes Neonatal (HEMa-LP; Invitrogen) are primary human melanocytes that are a mixed population, extracted from lightly pigmented forskins.

These cells were cultured in Medium 254 (Invitrogen) supplemented with Human Melanocyte Growth Supplement (HMGS; Invitrogen) in the absence of antibiotics and antimycotics. The media was changed every 2-3 days. Subculturing of these cells was carried out at $5X10^3$ cell/$cm^2$. 4 ml of Trypsin/EDTA solution was added to the flask and immediately 3 ml was removed. The flask was incubated at room temperature for approximately 1-3 minutes until the cells have become nearly completely round with a few small processes remaining. The flask was then gently knocked to dislodge the cells and 3 mls of Trypsin Neutralizer solution was added to the flask, the cell suspension was then transferred to a sterile 15 ml conical tube. An additional 3 mls of Trypsin Neutralizer solution was added to the flask and pipetted over the flask surface several times to remove any remaining cells. This solution was also added to the 15 ml conical tube and it was centrifuged at 180*g* for 7 minutes. The cell pellet was resuspended in 4 mls supplemented Medium 254 and the cell concentration determined by trypan blue exclusion count (see section 2.3.5). The cells were diluted in supplemented Medium 254 to $5X10^3$ cells/$cm^2$ and added to a new culture flask.

#### 2.3.1.3. Wnt3a Overexpression Cell lines

The Moon group at the University of Washington have developed cell lines to overexpress Wnt3a as well as encode GFP expression. The sequences for human *WNT3A* was amplified by PCR and cloned into third-generation lentiviral vectors. The Wnt3a and control cells were sorted by FACS to obtain populations expressing equal levels of GFP (203). Cells were cultured in the same media as described in section 2.3.1 with the exception that 5% FBS was used (203). Cells were serum starved for 48 hours prior to all assays unless otherwise stated.

### 2.3.2. Seed Stock Preparation of Cell Lines

Seed stocks of all cell lines were stored in sterile cryovials in liquid $N_2$. Cells were frozen at a concentration of approximately $0.75X10^6$ cells/ml in a solution of FBS with 10% dimethyl sulfoxide (DMSO). Freezing was carried out at a controlled rate of 1°C per minute using a Mr Frosty (Nalgene) apparatus containing 100% Isopropanol. At

-70°C the cells were placed in liquid $N_2$ for long-term storage. Resuscitation of the cells was carried out rapidly by thawing in a 37°C water bath, and the cell stock resuspended gently in 5 ml of the appropriate growth medium, to dilute the DMSO concentration. Once all the seeded cells had adhered to the tissue culture flask, approximately 12-24 hours after resuscitation, the growth media was changed. Alternatively, in hypersensitive DMSO cells (M375, M296, Malme3M and Mel624) cells were thawed as described above and after were centrifuged at 180*g* for 5 minutes to remove the DMSO and the cell pellet was resuspended and seeded.

### 2.3.3. PCR Detection of Mycoplasma

Mycoplasmas are a potential source of tissue culture contamination that do not reveal themselves by alterations to the cells growth medium. Many mycoplasma species grow slowly in continuous cell lines and do not destroy the host cells. Therefore, it was essential to routinely screen for Mycoplasma contamination. Testing for Mycoplasma was carried out using the EZ-PCR Mycoplasma Test Kit according to the manufacture's instructions. Analysis of the PCR results was done using a 2% agarose gel (see section 2.3.4). Screening was also carried out using the PCR primers and method shown below (331, 332):

Forward Primer (GPO-3): 5'-gggagcaaacaggattagataccct -3'

Reverse Primer (MGSO): 5'-tgcaccatctgtcactctgttaacctc -3'

The sample preparation and PCR protocol was adapted from (332), briefly, the cells were centrifuged in the media they had grown in, at 180*g*. 1 ml of supernatant was removed from the cells; this had to have been on the cells for a minimum of 48 hours with the cells at least 50% confluent. A positive control (*Mycoplasma hominis* DNA) was included in the PCR reaction. A positive result produces a band of 270 bp when resolved on a 2% agarose gel (see section 2.3.4).

### 2.3.4. Agarose Gel

Unless otherwise stated a 1% (w/v) agarose solution was made up in 1X TAE (see section 2.2.3) and boiled to dissolve the powder. The solution was cooled down to touch and 2 µl of Gel-Red was added. A gel-casting tray was prepared by sealing the

edges with tape and inserting a comb. The agarose solution was poured into the casting tray and left to set at room temperature. Before use, the tape and comb were removed and the samples loaded with 5 µl Quick load 100 bp DNA ladder. A 50 ml gel was run at 90 V for 30 minutes and visualised under UV light on the BioRad Molecular Imager ChemiDoc XRS.

### 2.3.5. Viable Cell Counts

Cell suspension concentrations were determined using an Improved Neubauer cell counter (Marienfeld). Cells were diluted 1:1 in 0.4% trypan blue solution (333) before transferring to the counting chamber. Viable cells excluded the dye, while dead cells stained blue. Viable cell concentration could then be calculated using the defined area of known depth within the counting chamber.

### 2.3.6. Stimulation of Cells

Cells were counted, seeded and left to adhere overnight. The growth media was removed and 1X PBS (see section 2.2.1) was added to wash the cells and then discarded. Stimulants or a carrier control were then added to the cells in serum free media for a period of 48 hours, unless otherwise stated. Recombinant Human Wnt3a (rWnt3a) and Recombinant Human DKK1 (rDKK1) were used at 50 ng/ml unless stated otherwise.

### 2.3.7. 3D Cell Culture

The protocol was adapted from (334) briefly, matrigel basement membrane matrix was pre-aliquoted in 1 ml vials and kept at -20°C, vials were defrosted on ice overnight before use. Matrigel was coated at a volume of 100 µl/cm$^2$ in a 48-well plate ensuring no air bubbles remained and left to solidify at 37°C until use. Plates could be pre-coated and re-frozen but were not freeze-thawed more than once. 4X10$^4$ cells were seeded (see section 2.3.5) per well in 400 µl of growth media and left at 37°C for 48 hours before analysis. Analysis was done at 10X magnification on an inverted light microscope. For stimulated experiments (see section 2.3.6) cells were counted and seeded onto Matrigel following 48 hours of stimulation.

### 2.3.8. Population Doubling Assay

Cells were counted as previously described (see section 2.3.5), and seeded in triplicate onto 12-well plates at a concentration of $4X10^4$ cells/well. After 24, 48 and 72 hours a viable cell count was carried out (333, 335). For stimulated experiments, the cells were stimulated as previously described (see section 2.3.6), for 48 hours before being seeded into the assay plates. They were then analysed after 48 and 96 hours of growth.

Population doublings of overexpression cells were calculated over a longer period of time (336). Cells were seeded in triplicate into a 6-well plate at a concentration of $2X10^4$ cells/well and left to proliferate to confluency. They were then counted and passaged at an appropriate ratio and seeded back into the same plate and left to proliferate. The number of cells counted, the number of days taken to reach confluency and ratio of the split were all recorded. The number of population doublings that had occurred was calculated using the following LOG2 formula:

Number of population doublings = Log (average cell count/number of cells seeded, 2)

Using the above results, the population doubling times were then calculated:

Time taken for population doubling = ((Day of count - Day of seeding)*24hours)/number of population doublings

The average population doubling time for the cells could then be calculated over the course of the experiment.

### 2.3.9. Invasion Assay

Cells were serum starved for 48 hours before the assay. Matrigel basement membrane matrix was treated according to the manufacturer's instructions and coated onto cell culture inserts with 8.0 µm pores placed inside a 24-well companion plate. Matrigel was coated at a volume of 50 µl/$cm^2$ of growth surface making sure no air bubbles remained and left to solidify (30 minutes) at 37°C until use. The coating was thin enough so that the cells, when seeded, were in the same plane of vision as the pores of the insert. Cells were seeded onto the matrigel coated inserts

(see section 2.3.5) at $4X10^4$ cells/well in 0.4 ml of serum free media. Complete growth media was then added to the bottom of the well and the cells were left for 48 hours at 37°C. After 48 hours the invaded cells were fixed, stained and counted as previously described (337). For stimulated experiments (see section 2.3.6) the cells were seeded on to Matrigel following 48 hours of stimulation and the assay carried out as described above.

### 2.3.10. Protein Extraction

Cells were lysed in protein lysis buffer (222) centrifuged at 10,000*g* for 10 minutes at 4°C and the supernatant transferred to a fresh tube unless otherwise stated. A BCA assay (see section 2.3.11) was carried out to calculate total protein to allow for equal loading on the gel.

### 2.3.11. BCA protein Assay

The assay was carried out according to the manufacturer's protocol (ThermoScientific #23225 Pierce BCA Protein Assay Kit). Briefly, a standard curve was diluted according to the method for a microplate procedure and total protein was calculated from the standard curve. If necessary, samples were diluted in lysis buffer to fit them into the standard curve (this dilution was then taken into account when protein concentrations were calculated). The assay was analysed using the POLARstar Optima microplate reader (BMG Labtech).

### 2.3.12. SDS-Polyacrylamide gel preparation and electrophoresis

The gel-casting apparatus was set up according to the manufacturer's instructions (Bio-Rad, mini PROTEAN II, 165-2940). A 12% resolving polyacrylamide gel solution was prepared (see Table 2.1), poured and overlaid with a 5% stacking gel (see Table 2.1). Once the gels were set, the gel-tank was filled with 1X running buffer (see section 2.2.9) and equal amounts of protein were loaded in each well. 10 µl of pre-stained SDS-PAGE standard low or high range protein marker were run simultaneously with the samples to determine protein size. Gel electrophoresis was carried out at 90 V until stacking of the samples had occurred and then increased to 120 V until the samples had reached the bottom of the gel.

**Table 2.1: Formulation of Resolving and Stacking Gel for SDS-Polyacrylamide Gel Electrophoresis**

| | **Resolving Gel** | **Stacking Gel** |
|---|---|---|
| | 12% | 5% |
| **$dH_2O$** | 3.45 ml | 2.9 ml |
| **40% acrylamide mix** | 2.4 ml | 0.75 ml |
| **1.5M tris pH 8.8** | 2 ml | - |
| **0.5M Tris pH 6.8** | - | 1.75 ml |
| **10% SDS** | 0.08 ml | 0.05 ml |
| **10% APS** | 0.08 ml | 0.05 ml |
| **TEMED** | 0.008ml | 0.005ml |
| **Total** | 8ml | 5.5ml |

### 2.3.13. Western Blotting

The following apparatus was set up as shown in Figure 2.1. The transfer tank (Bio-Rad Mini PROTEAN II) was filled to the brim with 1X transfer buffer (see section 2.2.10). The transfer was carried out at room temperature with an ice pack at 250 mA for 2 hours. Transfer efficiency was checked with Ponceau S (see section 2.2.11) stain before being rinsed in $dH_2O$ and the membrane was imaged on the BioRad Molecular Imager ChemiDoc XRS.

The following steps were undertaken in a falcon tube on a roller (338). The membrane was blocked for at least 1 hour in 5% blocking buffer at room temperature. The blocking buffer used was dependant on the antibody, either 5% BSA or 5% Marvel milk. It was then incubated for overnight at 4°C in the primary antibody diluted accordingly in 5% blocking buffer. The membrane was washed 3 x 10 minutes in TBST (see section 2.2.13) followed by a 1 hour incubation in the secondary antibody conjugated to horseradish peroxidase in a 1:10,000 dilution for the mouse IgG or a 1:5,000 dilution for rabbit IgG. The blot was then washed 3 x 10 minutes in TBST. The ECL (Enhanced Chemi-Luminescence) method was used to detect the antibody. The blot was incubated with the ECL solution for 5 minutes, before imaging on the BioRad Molecular Imager ChemiDoc XRS.

### 2.3.14. Melanosphere Assay

Protocol adapted from (339, 340), briefly 12-well plates were coated 3 times in Poly(2-hydroxyethyl methacrylate), this is referred to as polyHEMA throughout the text (see section 2.2.14). After each coating the plates were put onto a rocker for 5 minutes and then left to dry in a sterile hood. Before cells were seeded the wells were washed twice with 1X PBS, if the PBS turned cloudy the polyHEMA had degraded and the plate discarded. Cells were counted as previously described (see section 2.3.5). $1X10^4$ cells were seeded/well in 1 ml growth media. Cells were left for 7 days at 37°C with a very gentle top-up of media every three days. Images were captured using an inverted light microscope, Zeiss camera and AxioVision software at 10X magnification. The first 20 objects to be seen in the images were measured

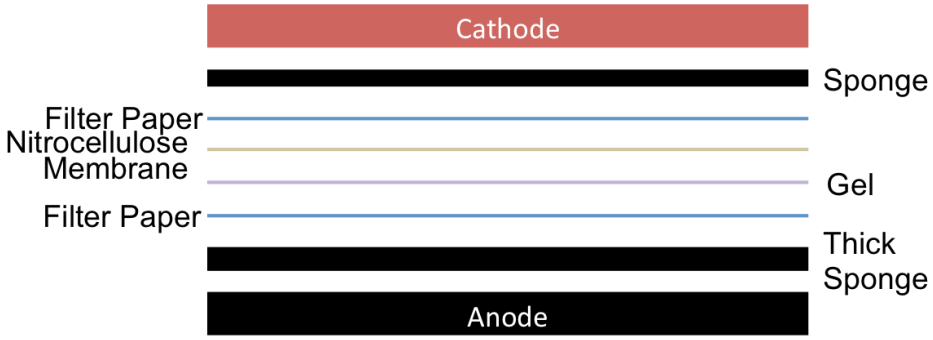


**Figure 2.1: Set up of Protein Transfer Equipment**
Set-up of the BioRad Mini PROTEAN II transfer system, to transfer proteins from SDS-Polyacrylamide gel onto nitrocellulose membrane.

whether they were single cells or clusters. Melanospheres were measured in µm using Image J software. For stimulated experiments the cells were stimulated as previously described (see section 2.3.6) for 48 hours before seeding into the polyHEMA coated plates.

### 2.3.15. Flow Cytometry

#### 2.3.15.1. Stem Cell Markers

Cells were washed once in PBS, and detached using PBS-EDTA (see section 2.2.16). Cells were counted (see section 2.3.5) and $2X10^5$ cells were centrifuged at 180*g* for 5 minutes and resuspended in FACS buffer (see section 2.2.17). Samples were incubated at 4°C for 1 hour as a blocking step. Cells were centrifuged at 180*g* for 5 minutes, and the supernatant removed. Primary antibodies were added directly to cell pellets (Table 2.2) and to the unstained control and secondary antibody only samples, 300 µl of FACS buffer was added. Samples were incubated at 4°C for 1 hour.

1 ml FACS buffer was added to each sample and centrifuged at 180*g* for 5 minutes; the supernatant was tipped off the pellet. The same secondary antibody was used for each of the samples, Donkey anti-rabbit AF488 (Invitrogen). This was added directly to the cell pellet at 1:400 (40 µl per sample). Samples were incubated in the dark at 4°C for 1 hour. 1 ml FACS buffer was added to each sample and centrifuged at 180*g* for 5 minutes and the supernatant was removed. 350 µl of FACS buffer was added to all samples and analysed using an Accuri C6 bench top flow cytometer and C-Flow Plus software (BD). Mean levels of the FL2 channel were recorded and compared to unstained and secondary antibody only staining.

#### 2.3.15.1. Fixed Cell Antibody Staining for Flow Cytometry

The cells were cultured and stimulated as normal in cell culture plates; they were then trypsinized and put into an eppendorfs before the fixation step. Cells were centrifuged at 180*g* for 3 minutes between each stage. Cells were fixed and permeablised as described (see section 2.3.26.1) before primary antibodies were added at a working concentration for 1 hour (337). Species relevant secondary

**Table 2.2: Antibodies used in Flow Cytometry of cell Surface markers.**

| Antibody | Catalogue Number | Recommended Dilution |
|---|---|---|
| CD271 | Abcam #ab8874 | 1:100 from stock in 1X PBS |
| CD133 | Abnova #PAB12663 | 15 µg per $10^6$ cells, stock is 0.5 µg/µl |
| CD20 | Abgent #AJ1155a | 1:20 from stock in 1X PBS |
| ABCB5 | Abgent #AP6122a | 10 µg/ml per $10^6$ cells, stock 250 µg/ml |

antibodies conjugated to fluorophores were diluted 1:400 to 5 µg/ml and 100 µl put onto the cells for 1 hour in the dark. Cells were resuspended in FACS buffer (see section 2.2.17) and analysed immediately on a BD Accuri C6.

#### 2.3.15.2. Cell Cycle Analysis

Protocol adapted from (341), briefly cells were pelleted and resuspended in ice cold 70% ethanol. The cell suspension was stored at 4°C for at least 24 hours. Pellet the cells by centrifugation at 180*g* for 5 minutes and wash once in PBS. Resuspend the pellet in 300 µl of PI/RNase A solution and incubated for 30-45 minutes. Analysis was carried out on the accuri C6 flow cytometer firstly gating on the live population in a forward scatter/side scatter plot and then exclude any doublets in a forward scatter-area/forward scatter-height plot. Following this gating, analysis of the FL2 channel on a linear scale was carried out.

#### 2.3.15.3. Live Cell Staining for Flow Cytometry

Live cells were stained with Mitotracker Green diluted in phenol-red free media to 10 nM (Invitrogen) as previously described (342), JC1 at 2 µM or TMRM at 20 µM. Following staining, the cells were washed with phenol-red free media, trypsinized and put into eppendorfs. Cells were resuspended in FACS buffer (see section 2.2.17) and analysed immediately on a BD Accuri C6.

### 2.3.16. TOPFlash Assay

Protocol adapted from (203), briefly cells were counted as previously described (see section 2.3.5), and seeded on to 24-well plates at a concentration of $4X10^4$ cells/well. The following day, cells were transfected with the Super8TOPFlash or Super8FOPFlash reporter constructs (343, 344). DNA was mixed in eppendorfs for 5 minutes as described below:

Positive Control: 300 ng PGL3, 150 ng Renilla

TOPFlash: 300 ng TopFlash, 150 ng Renilla

FOPFlash Negative control: 300 ng Fop Flash, 150 ng Renilla

1 µl/per well of Lipofectamine was mixed with 100 µl transfection media (RPMI with no FBS, no antibiotics and no L-Glutamine) for 5 minutes. The DNA and the lipofectamine were then combined for 30 minutes. The cells were washed twice in the transfection media before 100 µl of the lipofectamine/DNA mixture was added to the cells and incubated at 37°C for 6 hours. The transfection media was then replaced with normal growth media. For melanocytes the transfection process was carried out in normal melanocyte growth media and the transfection mix was only incubated on the cells for three hours. The following day the melanoma cells were stimulated as described in section 2.3.6. Melanocytes were stimulated with rWnt3a at the same concentration (see section 2.3.6) in melanocyte growth media. Wnt3a-overexpression cells were not stimulated with rWnt3a but fresh media was added to the cells following the transfection.

The dual luciferase kit (Promega #E1910) was used according to the manufacturer's instructions and the luciferase readings were carried out on PerkinElmer Envision plate reader. The LaII and Stop&Glow readings were calculated as a ratio to analyse the Wnt3a stimulated response.

### 2.3.17. Apoptosis

Protocol adapted from (345), briefly overexpression cells were counted as previously described (see section 2.3.5), and seeded on to 24-well plates at $6X10^4$ cells/well. After 48 hours of serum starvation the assay was carried out according to the manufacturer's instructions (Sigma #CS1110). Fluorescent readings were normalised to protein concentration analysed by BCA from the two wells left without Apo-TRACE.

### 2.3.18. Migration Assay

Protocol adapted from (337), briefly cells were counted as previously described (see section 2.3.5), and seeded on to 6-well plates at a concentration of $4X10^5$ cells/well. After the cells had adhered overnight the monolayer was scratched three times with a pipette tip in a long strip, the media was changed and 10X images were taken of the scratch. The media was then changed and images taken at 24 and 48 hours in the same region along the scratch. The images were analysed using Image J to

measure the open area of cells and the data represented as fold-change compared to control.

### 2.3.19. Tail Vein Metastasis Assay

Protocol adapted from (346), this work was carried out at the University of Washington by Peggy Yang (all mouse work), Rima Kulikauskas (cell preparation). All animal studies were performed using Institutional Animal Care and Use Committee protocols as approved by a review board at the University of Washington.

Cultured control and Wnt3a overexpression cells were removed from the culture surface using PBS-EDTA (see section 2.2.16) and were washed in 1X PBS three times before $1X10^6$ cells were counted and resuspended in 1 ml sterile saline. The cells were injected using a 26 G needle into the tail vein of NOD-SCID mice, 6 mice per cell line. The mice were monitored for 4 weeks checking for any significant weight loss, change in behaviour or death. After 4 weeks the mice were sacrificed and the lungs removed, these were initially imaged under fluorescent light on a Nikon SMZ1500 microscope. The samples were then fixed in 10% neutral buffered formalin (Thermo Scientific).

#### 2.3.19.1. Tissue Immunohistochemistry

This work was carried out at the University of Washington by Brian Johnson (HIC/Comparative Pathology Program). Paraffin embedded tissue is hydrated on an ice bath for 30 minutes and placed on a Rotary Microtome (Leica RM2265, Leica Microsystems Inc.) for sectioning. The paraffin block is cut to approximately 100 µm to "face in" and ensure maximum tissue area per section. The block is then cut at 4 µm and sections are placed on a glass slide. The first section is stained for H&E, 30 serial sections are cut (4 µm) and the $30^{th}$ section is again stained for H&E.

Immunohistochemical staining was performed on the Leica Bond Automated Immunostainer. Sections were deparaffinized in Leica Bond Dewax Solution (Leica) and rehydrated through 100% ETOH. After antigen retrieval with EDTA buffer pH 9.0 (Lieca Bond Epitope Retrieval Solution 2) at 100°C for 20 minutes and blocking

endogenous peroxidase activity with 3.0 % $H_2O_2$ for 5 minutes and blocking with 10% Normal Goat Serum in TBS for 20 minutes the sections were incubated with Rabbit polyclonal S-100 antibody, (Invitrogen) 46.8 mg/mL or Normal Rabbit IgG, isotype control, (Invitrogen) at (1:1000 dilution, 1 µg/ml) both in Bond Primary Antibody Diluent (Leica) for 30 minutes at room temperature. Sections were then incubated with Goat anti Rabbit Poly-HRP polymer secondary detection (Leica) for 8 minutes at room temperature. Sections were then incubated with Leica Bond Mixed Refine DAB substrate detection for 10 minutes at room temperature. (Leica). After washing with $DIH_2O$ the sections were counter stained with Hematoxylin solution (Leica Bond Refine Kit) dehydrated through 100% ETOH, cleared in Xylene and mounted with synthetic resin mounting medium and 1.5 coverslip.

Slides were scanned in Brightfield at 20X objective using a Nanozoomer Digital Pathology slide scanner (Olympus America). The digital images were then imported into Visiopharm software (Hoersholm, Denmark) for analysis. Using the Visiomorph Digital Pathology module, regions of interest (ROIs) were applied around relevant areas using a tissue detect protocol and manual clean-up. The software was then programmed to label positively stained areas versus normal tissue areas, using project-specific configurations created for each staining set. Images were processed in batch using these configurations to generate the desired output calculations.

### 2.3.20. XF96 Seahorse Bioanalyzer Analysis – Cell Mito Stress Test

Seahorse XF96 Cell Culture Plates were coated in Poly-D-Lysine (347) at 0.1 mg/ml for 1 hour in a cell culture hood. The plate was then washed twice in 1X PBS and left to dry in the hood for an hour. Overexpression cells were counted as before (see section 2.3.5) and seeded on to the plates at $8X10^3$ cells/well in 80 µl culture media (see section 2.2.18). The plate preparation and running of the Mito Stress Assay was carried out according to manufacturer's instructions (Seahorse Bioscience) (348). The compounds were diluted in seahorse media as stated below (349); please note the concentrations are adjusted to allow for the change in volume after each injection as shown in Table 2.3:

Port A: Media

Port B: Oligomycin 2.5 µM

Port C: FCCP 1 µM

Port D: Antimycin and Rotenone both at 2.5 µM

To normalise the Seahorse data to cell number a Hoechst stain assay was carried out on each plate. Ensuring the Seahorse XF96 Cell Culture Plate was at room temperature; 40 µl/well of 0.01% SDS (diluted in water) was added and the plate stored at -80°C for 30 minutes. The plate was then thawed and 40 µl/well of staining solution (see section 2.2.19) was added, the plate was then incubated at 37°C for 1 hour on a nutator before the fluorescence was read at excitation 355, emission 460 (349).

### 2.3.21. XF96 Seahorse Bioanalyzer Analysis – Glycolysis Stress Test

The seahorse Gylcolysis Stress test was carried out according to manufacturer's instructions (Seahorse Bioscience). All other aspects of the assay were kept the same as for the Mito Stress Assay (see section 2.3.20). The compounds were diluted in seahorse media as shown in Table 2.4, please note the concentrations are adjusted to allow for the change in volume after each injection, Table 2.4 shows the highest concentration of Glucose, the dose range was 0, 2.5, 5, 7.5 and 10 mM:

Port A: Glucose 0-10 mM

Port B: Glucose 0-10 mM

Port C: Oligomycin 2.5 µM

Port D: 2-DG 100 mM

The plates were stored at -20 °C until cell number normalisation could be carried out as explained in section 2.3.20.

### 2.3.22. Citrate Synthase

The Citrate Synthase Assay Kit (Sigma) was used according to the manufacturer's instructions and a positive control was used at 1 µl. Briefly, cells were seeded on to 6-well plates at $2X10^5$ cells/well. After 48 hours of stimulation as previously

**Table 2.3: Mito Stress Test Compound Dilutions**

| Compound | Stock Conc. | Preparation Conc. | Final Conc. | Volume needed for 1.7mls |
|---|---|---|---|---|
| Oligomycin | 5 mM | 15 µM | 2.5 µM | 5.1 µl |
| FCCP | 2.5 mM | 7 µM | 1 µM | 4.76 µl |
| Antimycin and Rotenone | 2.5 mM | 20 µM | 2.5 µM | 13.6 µl each |

**Table 2.4: Glucose Stress Test Compound Dilutions**

| Compound | Stock Conc. | Preparation Conc. | Final Conc. | Volume needed for 1.7mls |
|---|---|---|---|---|
| Glucose | 350 mM | 50 mM | 10 mM | 242.86 µl |
| Glucose | 350 mM | 60 mM | 10 mM | 291.60 µl |
| Oligomycin | 5 mM | 17.5 µM | 2.5 µM | 4 µl |
| 2-DG | 1 M | 800 mM | 100mM | 800 µl |

described (see section 2.3.6), the cells were lysed in 100 µl lysis buffer (see section 2.2.5) and centrifuged at 20,000*g* for 15 minutes at 4°C. A BCA was carried out (see section 2.3.11) and the volume of lysate required for 8 µg of protein was calculated. The absorbance was read at 412 nm before and after addition of Oxaloacetate (OAA) using the POLARstar Optima microplate reader (BMG Labtech). Citrate Synthase Activity was then calculated using the manufacturer's guidelines and represented as the fold change compared to control.

### 2.3.23. Lactate Assay

The lactate Assay was carried out according to the manufacture's (BioVision) protocol for the colorimetric assay. Briefly, cells were seeded onto 6-well plates at $2X10^5$ cells/well. After 48 hours of stimulation, as previously described (see section 2.3.6). The cell supernatant was removed and stored at -80°C for at least 24 hours, to stop Lactate dehydrogenase activity. The cells were lysed and the total protein measured using a Peirce BCA assay Kit (see section 2.3.11). The standard curve of lactate was extended to include a 12 and 14 nmol/well measurement and 1 µl of sample was used. The absorbance was analysed using the POLARstar Optima microplate reader (BMG Labtech) and the results were calculated as the fold change compared to control.

### 2.3.24. ROS Assay

The ROS Assay was carried out according to the manufacturer's instructions (Abcam). 96-well plates were coated for 1 hour in 50 µg/ml collagen in 0.02 M acetic acid. Wnt3a overexpression cells were seeded at $1X10^4$ cells/well and serum starved for 48 hours. A positive control of 0.01% Triton X and a negative control of serum free media only were included. DCFDA was used at 25 µM, for 45 minutes. The plate was read on a POLARstar Optima microplate reader (BMG Labtech) at ex 485nm em 535nm, results were analysed after the subtraction of background from the negative control.

### 2.3.25. Glucose Assay

The Glucose assay was carried out according to the manufacturer's instructions (Sigma). Briefly, Wnt3a-overexpression cells were seeded on to 6-well plates at $2X10^5$ cells/well. After 48 hours of serum starvation, the cells were lysed in 100 µl of lysis buffer (supplied with assay kit) and centrifuged at 20,000*g* for 15 minutes at 4°C. Three controls were used, a sample blank which contained sample but no reagent, a reagent blank that contained regent and no sample and a positive standard sample. Equal volumes of each sample were used and the assay was measured using the POLARstar Optima microplate reader (BMG Labtech) and results normalised back to protein concentration determined by BCA analysis (see section 2.3.11).

### 2.3.26. Cell Staining

#### 2.3.26.1. Mitotracker Staining For Fixed Cell Confocal Imaging

Sterile cover slips were placed into 12-well plates. Cells were counted as previously described (see section 2.3.5) and $2X10^4$ cells seeded into the wells ensuring no air bubbles were under the cover slips. The cells were left to adhere and stimulated with rWnt3a or serum starved as required.

Live cells were stained with Mitotracker Deep Red, diluted in phenol-red free media to 250 nM (Invitrogen) as previously described (342). Cells were the fixed and stained with counter-stains; Phalloidin 488 (6nM) and Hoechst 33342 (10 nM). Briefly, cells were fixed (see section 2.2.20) using PBS with 5% formaldehyde, 2% sucrose and permeabilized (see section 2.2.22) with 1% Triton-X, 10% sucrose and 1% calf serum. Cells were incubated for 20 minutes with Phalloidin 488 and counterstained with Hoechst before being mounted onto slides with mounting medium (337). They were left at 4°C overnight before the edges were sealed with nail varnish. Slides were then imaged on a Zeiss LSM510 confocal microscope.

#### 2.3.26.2. Antibody staining for Confocal Imaging

Sterile cover slips were placed into 12-well plates. Cells were counted as previously described (see section 2.3.5) and $2X10^4$ cells seeded into the wells making sure no air

bubbles were under the cover slips. The cells were left to adhere and stimulated or serum starved as required.

Cells were fixed and permeablised as previously described (see section 2.3.29.1) before primary antibodies were added at working concentration for 1 hour in a damp environment (337). Secondary antibodies conjugated to fluorophores were diluted (see section 2.2.23) 1:400 to 5 µg/ml and 100 µl put onto the cells for 1 hour in a dark, damp environment, followed by counterstaining with Phalloidin and Hoechst stains and mounting as previously described (see section 2.3.26.1). Slides were imaged on a Zeiss LSM510 confocal microscope.

### 2.3.27. Quantitative Analysis of mRNA expression

#### 2.3.27.1. NovaQUANT Human Mitochondrial to Nuclear DNA Ratio Kit

The protocol was carried out according to the manufacturer's instructions (NovaQUANT) for whole cell lysis. Briefly, cells were counted and diluted to allow for 50 cells per well, and resuspended in DNase/RNase free water to a volume of 10 µl per well. 2X RT2 Fast SYBR Green Mastermix was added to the cells and mixed gently by pipetting. Three controls were used in each run, a no template control (NTC) was included by replacing the cell suspension with PCR grade water. A positive and negative control for mitochondrial targets were used; human wildtype and human rho zero DNA controls were provided in the kit, these are used to verify the primers work effectively and the plate run was successful. A fast SYBR protocol was run with an extended denaturing step at 95 °C for 10 minutes. Data analysis was carried out using the relative copy number method. The Ct values for each of the four genes are used to determine mtDNA copy numbers as described in the manufacturer's protocol.

#### 2.3.27.2. RNA purification

RNA was extracted from cells using the GeneJet RNA purification kit, according to the manufactuer's instructions for the Mammalian Cultured Cells Total RNA Purification Protocol. RNA was eluted in 50 µl of nuclease free water and the elution was

repeated to increase RNA concentration. RNA samples were then quantified on a NanoDrop ND-100 Spectrophotometer.

#### 2.3.27.3. Reverse Transcription PCR

2 µg of RNA was diluted with DEPC-$H_2O$ to total volume of 10 µl this was then converted to cDNA by adding; 1 µl oligo(dT)18 primer (0.5 µg/µl), 1 µl random hexamer primer (0.2 µg/µl), 4 µl 5X reaction buffer, 2 µl 10 mM dNTPs, 1 µl RiboLock Ribonuclease Inhibitor (20 U/µl), 1 µl RevertAid M-MuLV Reverse Transcriptase (200 U/µl). The 20 µl reaction mix was then put into a PTC-100 thermocycler (BioRad) and incubated for 25°C for 10 minutes, 42°C for 60 minutes, 70°C for 10 minutes, samples were then held at 4°C until use in qRT-PCR reactions (350).

#### 2.3.27.4. PCR

10 µM primer pairs (see Table 2.5) were checked for their specificity using a standard Tm melting point assay following the manufacturer's instructions (Roche), good primer pairs are seen as one single peak on the melting curve. PCR was carried out using 1× of 10×*Taq* Buffer, 1 mM MgCl, 0.1 mM dNTPs, 0.3 µM primers, 1 unit Taq DNA polymerase enzyme and 5 µl cDNA in 50 µl reactions for 35 cycles. PCR products were run on a 1.5% agarose gel (see section 2.3.4), and purified using QIAquick gel extraction kit according to the manufactures protocol (Qiagen). DNA was eluted in 30 µl 10 mM Tris and quantified on a NanoDrop ND-100 Spectrophotometer. The DNA copy number was then calculated using the equation below:

1 mol = MW x g

1 mol = $6X10^{23}$ molecules = copies

$$\text{Copies/µl} = \frac{(6x10^{23}\ \text{copies/mol}) \times (\text{concentration g/µl})}{(\text{MW g/mol})}$$

Using the value of copies/µl a standard curve was generated starting at $1X10^{10}$ down to $1X10^{1}$, for experimental use only use 6 points of the curve, usually starting at $1X10^{6}$.

**Table 2.5: qRT-PCR Primer Sequences**

| Gene | Forward Primer | Reverse Primer | Reference |
|---|---|---|---|
| AXIN2 | CTCCCACCTTGAATGAAGA | TGGCTGGTGCAAAGACATAG | (350) |
| MFN1 | CTCTCCGCCTTTACTTCTC | TCTGCCATTATGCTAAGTCTCC | Self Designed |
| MNF2 | CTCAAGACTATAAGCTGCGA | TCAAGCCATCTATCATGTCC | Self Designed |
| OPA1 | TATGACAGAACCGAAAGGGA | GAATAACCCTCAAGCTGTCCT | Self Designed |
| DRP1 | GAAATGCTACTGGTCCTCGT | ACGAAGAAGACAAGTCACCA | Self Designed |
| UBC | CTGCTCATAAGACTCGGCCT | AAGATCTGCATTGTCAAGTGACG | (337) |
| β-actin | AGAGCAAGAGAGGCATCCTC | CTCAAACATGATCTGGGTCA | (351) |
| YWHAZ | ACTTTTGGTACATTGTGGCTTCAA | CCGCCAGGACAAACCAGTAT | (337) |

#### 2.3.27.5. Quantitative Real-Time PCR

cDNA from samples and standards were diluted 1:10 in $H_20$ and 2 µl were added to a 8 µl reaction mix including 5 µl SYBR Green, 1 µl primer pair mix at 10 mM, 2 µl $H_20$. Samples were loaded into 96-well qPCR plate, sealed with qPCR plate sealer and centrifuged to ensure all contents are at the bottom of the well. A standard TM meting point assay was then run and the Δct values of the samples compared to that of the standard curve (352).

### 2.3.28. Knockdown of Gene Expression

A reverse transfection protocol was used (203). The following siRNA mixes were made:

- Lipofectamine RNAi Max: 3 µl/well in 100 µl/well of optimum media.
- Gene of interest siRNA: 20 nM in 100 µl/well of optimum media.
- Negative control: 20 nM in 100 µl/well of optimum media.

These were incubated for 5 minutes at room temperature before the lipofectamine mix was added to each of the siRNA mixes and incubated for 30 minutes at room temperature. The cells were then prepared to be 30% confluent in a 12 well plate. 1 ml of cell suspension was put into the plate with 200 µl siRNA/lipofectamine mixture. The cells were then incubated for 72 hours before analysis of the knockdown. The following siRNAs were used:

β-catenin siRNA 5'-3': GGAUGUUCACAACCGAAUUtt (353)

PTEN siRNA 5'-3': CGAACUGGUGUAAUGAUAUtt (Ambion, Validated)

### 2.3.29. Mitochondrial Isolation

The protocol was carried out according to the manufacturer's instructions (ThermoScientific) for the Mitochondrial Isolation Kit from Cultured Cells using Reagent Based Method. The samples were centrifuged at 12,000*g*. If multiple samples preps were carried out for one sample they were combined to increase the overall protein yield. The pellets were resuspended in 1X loading buffer consisting of 3X SDS, 30X DTT and lysis buffer (+ protease and phosphatase inhibitors). An

appropriate volume was used according to how many samples preps had been carried out per sample and how many western blot samples were subsequently needed.

### 2.3.30. Immunoprecipitation

Protocol adapted from (354-356). Cells were lysed for 30 minutes on ice in lysis buffer with added protease and phosphatase inhibitors (see section 2.2.5), and a BCA carried out (see section 2.3.11). 20 µl of Con-A beads per sample were washed twice in lysis buffer and centrifugation was used to remove the supernatant at 90*g* for 2 minutes. 2 mg of cell lysate was diluted to 1 ml in lysis buffer added to the beads (ensuring to keep some total cell lysate for western blotting) and incubated at 4°C on a rotator. 50 µl of Dynabeads G were used per sample and washed twice in PBS using a magnetic rack for separation. 200 µl of Rabbit IgG was diluted to 1 µg/ml in PSBT (0.02% Tween), 200 µl and incubated with the beads at room temperature for 30 minutes, vortexing every 5 minutes. IgG was removed, and lysates previously incubated with the Con-A beads were added and incubated at 4°C on a rotator for 30 minutes.

A second washed aliquot of Dynabeads G were resuspended using β-catenin antibody diluted in PBST 1:100, and incubated at room temperature for 30 minutes, vortexing every 5 minutes. The antibody was removed and the beads resuspended in the cell lysate samples from the IgG coated beads, and incubated at 4°C overnight on a rotator. The IgG coated beads were washed 3X in PBS and resuspended in 20 µl 1X SDS sample buffer with 0.1 M DTT, heated to 98°C for 10 minutes. The pre-cleared fraction sample was removed from the beads and stored at -20°C until the western blot was performed.

The unbound cell lysates were transferred from the β-catenin coated beads to a fresh eppendorf. The beads were washed 5X in PBS and resuspended in 30 µl 1X SDS sample buffer with 0.1 M DTT, heated to 98°C for 10 minutes. Then the IP sample was removed to a fresh tube and stored until analysis. Samples were analysed either

by western blot (see section 2.3.13) or prepared for mass spectrometry (MS) analysis as described below.

#### 2.3.30.1. Sample preparation for mass spectrometry

Immunoprecipitated proteins were solubilized in 1 M urea, 50 mM ammonium bicarbonate, pH 7.8, and heated to 50°C for 20 minutes. Proteins were reduced with 2mM DTT, alkylated with 15 mM iodoacetamide, and digested overnight with a 1:50 ratio of trypsin to total protein. The resulting peptides were desalted on Waters Sep-Pak C18 cartridges.

#### 2.3.30.2. Nano-LC-MS/MS measurements

The running of the MS samples was carried out at The University of Washington by Dr Aaron Robitaille. Peptides were measured by nano-LC-MS/MS on a Thermo Scientific Q Exactive (QE). Peptides were separated online by reverse phase chromatography using a heated 50°C 30cm C18 columns (75 mm ID packed with Magic C18 AQ 3 μM /100 Å beads) in a 180 minute gradient (1% to 45% acetonitrile with 0.1% formic acid) separated at 250 nL/min. The QE was operated in data-dependent mode with the following settings: 70000 resolution, 400-1600 m/z full scan, Top 10, and an 1.8 m/z isolation window.

#### 2.3.30.3. Data Processing and Analysis

Identification and label free quantification of peptides was done with MaxQuant 1.5 (355), using a 1% false discovery rate (FDR) against the human Swiss-Prot/TrEMB database. The databases contained forward and reverse mouse sequences as well as common contaminants. Three replicates per condition were analysed. Peptides were searched using a 5 ppm mass error and a match between run window of 2 minutes. Proteins that were significantly regulated between conditions were identified using a permutation-based t-test (S1, FDR 5%) in Perseus 1.4.1.3. GO-terms were analyzed using Protein ANalysis THrough Evolutionary Relationships (PANTHER) 9.0.

### 2.3.31. Statistical Analysis

All data was normalised to control and analysed using a student's two-tailed paired t-test unless otherwise stated. Imaris data was analysed from the whole data set (not data represented as % of a whole) and analysed using a two-way ANOVA test. Seahorse data was analysed using an unpaired t-test with Welch's correction. S100 staining on mouse lung tissue was analysed using an unpaired t-test with Welch's correction. Significance was defined as a *P* value of ns (not significant) = >0.05. * = <0.05, ** = <0.01, *** = <0.001, **** = <0.0001.

# 3. PHENOTYPIC CHARACTERISATION OF A GENETICALLY DIVERSE MELANOMA CELL LINE PANEL

## 3.1. Introduction

Metastatic melanoma is one of the most aggressive malignancies in humans and is responsible for 60% of all deaths associated with skin cancer (49). As explained in detail in Chapter 1, there are a number of different genetic backgrounds associated with metastatic melanoma, most noteably the $BRAF^{V600E}$ mutation (123, 132-136). Less common, but having the same subsequent effect of hyperactive MAPK signalling, are mutations within NRAS (134, 135, 137) and other mutations also known in melanoma, such as PTEN (142-145), Akt (148-150), CDKN2A (3, 49, 152, 153) and C-kit (154, 155). These muations likely infer differing effects on melanoma progression (142, 150, 163). Due to this diversity, it is important to compare how different mutational backgrounds affect the various characteristics of tumour cells, such as the alterations between wildtype (WT)C and $BRAF^{V600E}$. It is also important for us to understand the cellular mechanisms that result in tumour heterogeneity, forming distinct subpopulations of cells capable of different levels of proliferation, invasion and therapeutic resistance (357, 358).

### 3.1.1. Melanoma Phenotypes

There are two current theories that exist within the field to explain establishment of the rapid and, typically, lethal metastasis that occur as the disease progresses (121, 334, 359-370). The first is the phenotype switching model that defines two phenotypes, proliferative and invasive. The model suggests that microenvironmental factors cause the phenotypes of melanoma cells to switch, driving progression between a tumour expansion phase with highly proliferative cells and a metastatic phase where the cells are more invasive (365) see Figure 3.1. This model can lead to drug resistance by creating subpopulations with variable levels of chemo-resistance (359) and has recently been shown to act as a treatment itself by forcing the cells towards one phenotype and targeting them specifically in a lineage-specific therapy (371). The second theory is that of a ‘stem-like’, or tumour initiating, cell population capable of disseminating and are responsible for initiating secondary tumours, which may also be responsible for the high levels of

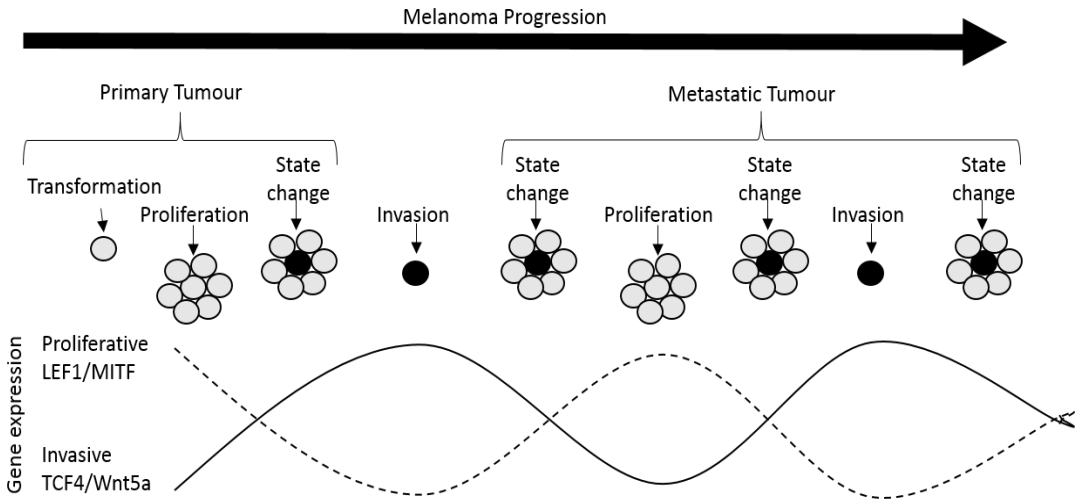


**Figure 3.1: Schematic of the phenotype switching model**
Model schematic adapted from (365) Hoek, K. S., O. M. Eichhoff, et al. (2008). "In vivo Switching of Human Melanoma Cells between Proliferative and Invasive States." Cancer Research 68(3): 650-656. Melanoma cells initially proliferate into the primary tumour. Changes in microenvironmental conditions alter the gene expression prolife from high LEF1 and MITF to high TCF4 and WNT5A causing the cells to switch and become more invasive, breaking away from the primary tumour and initiating metastasis. Expression profiles switch again turning the cells back to a proliferative phenotype and the process continues to progress tumour formation.

drug resistance in melanoma (359). These cells can sit dormant and, therefore, avoid traditional chemotherapeutic treatments that target dividing cells (372) and after, many years, can initiate growth of genetically resistant tumours. Cancer stem cells were first identified in acute myeloid leukaemia (373) but have now been identified in a number of other solid tumours, including breast cancer (374, 375) and some would argue, also, in malignant melanoma (364). Cancer stem cells are defined as self-sustaining cancer cells that are able to divide and expand the cancer stem cell pool, as well as differentiate into heterogeneous non-tumourigenic cancer cells that constitute the bulk of the tumour (376). Therefore, they have the properties of a stem cell in their ability to self-renew and give rise to other cell types but with the underlying tumourigenic properties of a cancer cell. It is possible that the phenotype switching model and the cancer stem cell model could be linked and that it is the cancer stem cell's tumourigenic properties that could be responsible for the switching between the two cell phenotypes.

### 3.1.2. The Phenotype Switching Model

The phenotype switching model in melanoma has been described as two phenotypes - proliferative and invasive which switch back and forth to drive melanoma progression (359). The phenotypes draw on two of the original hallmarks of cancer (377), limitless replicative potential and increased invasiveness and can be distinguished by a number of factors. These factors include their growth in 2D cell culture and 3D culture, the expression patterns of certain molecular markers and by comparisons in proliferation and invasion assays (334, 361, 365). In 2D cell culture on untreated tissue culture plastic, proliferative phenotype cells appear smaller, more rounded and have dendritic processes, whereas the invasive phenotype cells are flatter, larger and fibroblastic in shape (361). When grown on a 3D growth medium such as Matrigel basement membrane matrix, proliferative phenotype cells form small individual clusters. However, invasive cells form connected networks within the matrix as shown in Figure 3.2 (334). The phenotypes also differ in their molecular expression profiles; proliferative cells show higher expression of the transcription factors, MITF and LEF1, whereas

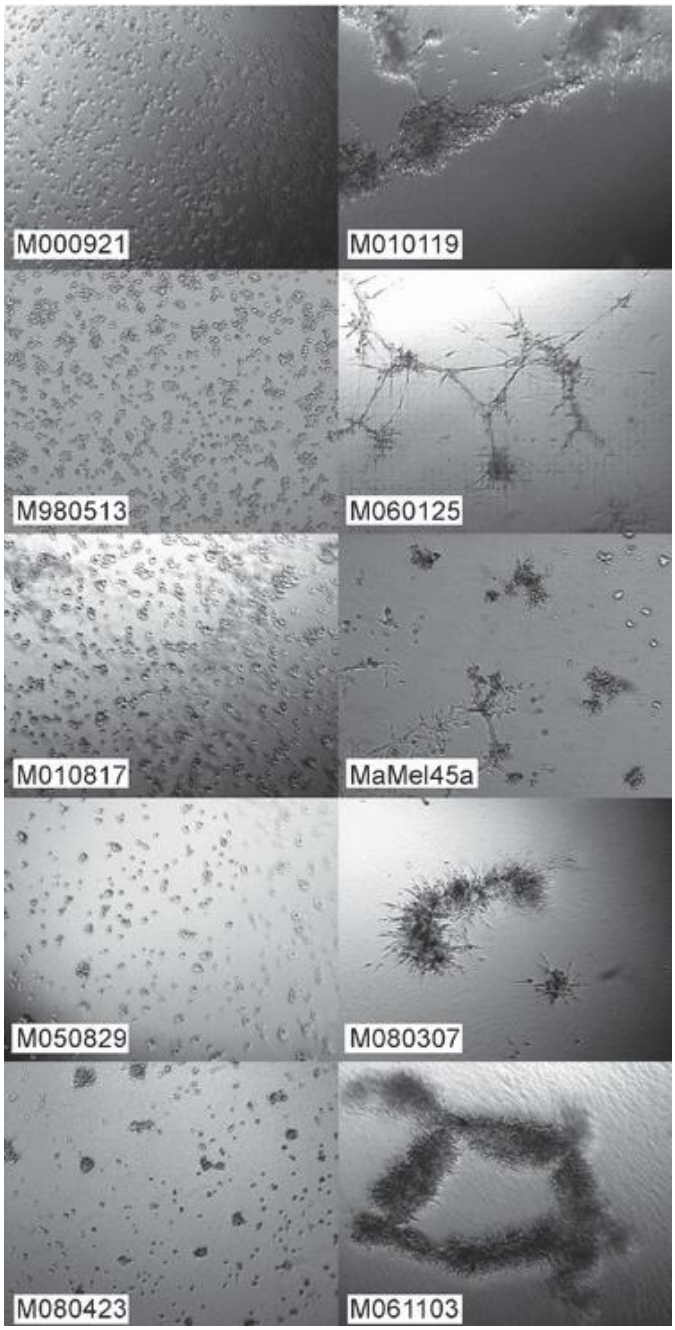


**Figure 3.2: 3D Matrigel growth defines melanoma phenotype**
Image taken from (334) Zipser, M. C., O. M. Eichhoff, et al. (378). "A proliferative melanoma cell phenotype is responsive to RAF/MEK inhibition independent of BRAF mutation status." Pigment Cell & Melanoma Research 24(2): 326-333. Melanoma cells grown on Matrigel form different patterns. Proliferative (175) form small, individual colonies whereas Invasive cells (right) form connected networks with in the Matrigel.

invasive cells have higher expression of Wnt5a and TCF4 (361). Finally, the phenotypes differ in their proliferative and invasive potentials, giving the phenotypes their respective names. The proliferative cell lines have a much faster population doubling time and the invasive phenotypes have higher levels of cellular invasion (361). Characterising melanoma cells in their 2D and 3D growth patterns, molecular expression markers of proliferative and invasive phenotypes, along with their proliferative and invasive potentials helps to verify this model.

### 3.1.3. The Cancer Stem Cell Model

As stated previously, there is a second theory to explain establishment of metastasis in melanoma which is the 'stem-cell' or tumour initiating model. The topic of cancer stem cells has been widely discussed by references (121, 360, 366, 376, 379, 380). The idea of cancer stem cells is controversial, with many arguments for and against their existance. This is especially true in melanoma, whereas in other cancers, such as hematopoietic-derived tumours, they have been very well defined (374). It has been shown that tumours are heterogeneous in their formation. They consist of distinct genotypes and phenotypes and many believe that cancer stem cells are responsible for giving rise to this heterogeneity. However, it has yet to be indisputably proven that these cells exist in melanoma. It has been hypothesised that, as part of the phenotype switching model, it is the invasive phenotype stage that is responsible for metastasis and, therefore, it is within the invasive cell population when they arise, that a sub-population of tumour initiating cells could exist (121, 359). Various groups have tried to distinguish a distinct 'stem-like' population using cell surface markers due to this and a number of potential markers have been suggested, including ABCB5, CD271 and CD133. A more recent suggestion is that expression of multiple markers might be required in combination to distinguish the cancer stem cells from the general bulk tumour cell population (381). There are a number of techniques used to detect tumour initiating populations of cells. Most commonly, cells are detected and isolated using flow cytometry using defined markers. These cells are then often tested for their tumour initiating capabilities in growth assays such as soft agar colony formation, the growth of non-

adherent spheroids and in immunodeficient mouse xenotransplantation experiments. It has been argued that the use of traditional cell culture methods creates an unnatural environment to investigate solid tumours and, instead, 3D culture techniques provide a more appropriate *in vitro* model for investigations (382). As quiescent cancer stem cells are thought to be resistant to current therapeutic treatments, identifying and isolating cells with tumour initiating potential could lead to new targeted therapies for treating melanoma and preventing metastatic spread. This could be especially effective if they are found to have characteristics that can be specifically targeted, without effecting normal cells such has been identified in leukemia (383).

### 3.1.4. Wnt is Implicated in Models of Melanoma

As explained in detail in Chapter 1, Wnt plays an important role in melanoma and the basis of this research is to understand those effects. Understanding more about the models of melanoma can help in such investigations. Wnt has been shown to have an effect on both the proliferation and invasion of melanoma cells (203, 384), therefore potentially implicating it in the phenotype switching model. This model also highlights that there are changes in the expression levels of different Wnt signalling genes that can be used to define the phenotypes; Proliferative lines highly express MITF and TCF4 whereas invasive lines express higher levels of LEF1 and WNT5A (361, 385). The expression of these genes and the inter-play between them in the two phenotypes implicate Wnt as being heavily involved in the establishment of melanoma cell phenotype switching.

Proliferative cells highly express genes associated with the differentiation of melanocytes, such as MITF and MLANA which are controlled in a β-catenin-dependent manner through LEF1 (20). MITF-M isoform controls the development and function of melanocytes and subsequent melanin production (29). Therefore, MITF is inherently linked to melanoma but, also, to Wnt signalling as Wnt has been shown to up-regulate the expression of MITF-M by increasing recruitment of β-catenin and LEF-1 to the MITF promoter to drive transcription (386). LEF1 and TCF4 are a vital part of the Wnt/β-catenin signalling pathway. They are located in the

nucleus and, when a Wnt ligand binds, β-catenin will translocate to the nucleus and bind to LEF1 and TCF4 transcription factors, displacing Groucho and activating transcription of Wnt target genes (387). Independently of β-catenin, LEF1 down-regulates TCF4 and WNT5A expression. Changes in the microenvironment, such as hypoxia, induce the expression of genes, such as TGFβ, causing the increased expression of WNT5A (388). This, in turn, acts in an autocrine manner, binding to Frizzled or ROR2 receptors, and causes the phosphorylation of PKC and subsequent suppression of the melanocytic markers LEF1 and MITF. With lower expression of LEF1, the down-regulation of TCF4 and WNT5A is relieved and, therefore, drives invasion (361). This is represented in Figure 3.3.

Wnt has also been implicated in the stem cell/tumour initiating model. Wnt signalling has been highly conserved throughout evolution, as a part of the embryonic development process and is vital for the regulation of somatic stem cell production (389). It has, also, been shown to be involved in regulation of haematopoietic stem cells in both an autocrine and paracrine manner, along with Hedgehog and Notch signalling, which are also often dysregulated in cancer (357, 390-392). The Wnt pathway is linked to tumour initiating cells as many markers associated with identifying cancer stem cells are direct targets of activated Wnt such as CD44 or CD24 (389, 393). Expression levels of MITF and DKK1 have also been linked to the ability of melanoma cells to form melanospheres and self-renewing capacity (394). Activation of the Wnt/β-catenin pathway could, therefore, control cancer stem cell formation and, therefore, change tumour progression in melanoma models.

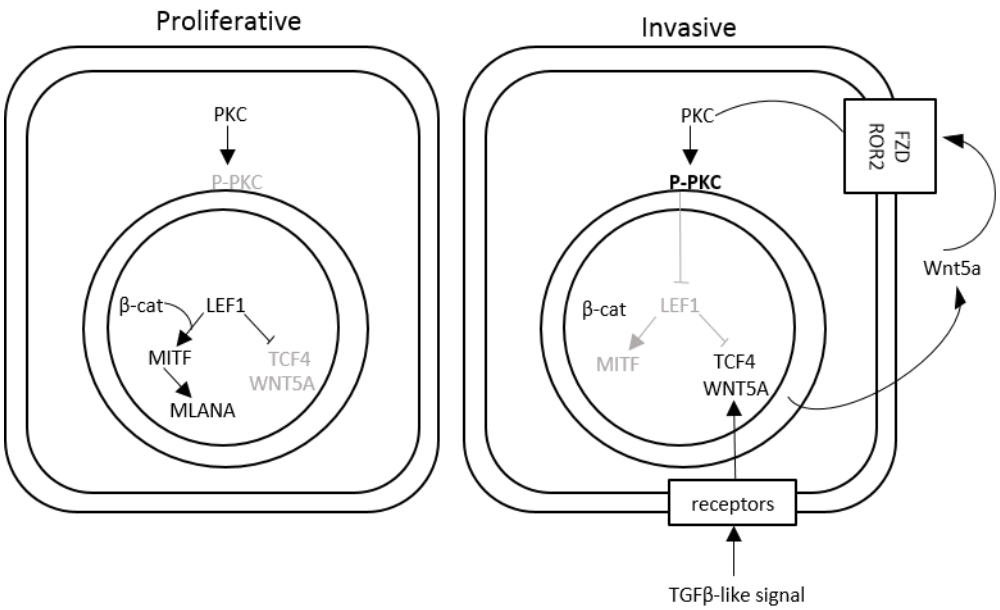


**Figure 3.3: Gene expression patterns in melanoma phenotype switching model**
Model schematic adapted from (361) Eichhoff, O. M., A. Weeraratna, et al. (378). "Differential LEF1 and TCF4 expression is involved in melanoma cell phenotype switching." Pigment Cell & Melanoma Research **24**(4): 631-642. Proliferative cells express high levels of LEF1 and MITF driven by the Wnt/LEF1/β-catenin signalling pathway and supress TCF4 and WNT5A in a β-catenin independent manner. Changes to external signals such as TGFβ cause increases in TCF4 and WNT5A which in turn signals through frizzled to phosphorylate PKC and supress LEF1 therefore removing its suppressive effects on TCF4 and WNT5A increasing their expression further to drive the invasive phenotype.

### 3.1.5. Aims

The aim of this first chapter is to characterise a panel of 19 human melanoma cell lines. Firstly, the cells will be defined in terms of their phenotype according to their growth in 3D Matrigel, looking for individual cells as a proliferative phenotype and connected networks as an invasive phenotype comparing them to Figure 1 (334). A selection of cells will then be further characterised with respect to their melanoma and cancer cell properties by measuring their proliferative and invasive potentials and their expression of markers associated with the different melanoma phenotypes. The cells will also be analysed in terms of their tumour initiating properties and cancer stem cell populations by assessing their ability to form melanospheres and the expression of selected cell surface markers. This data will provide an understanding of the basic characteristics of these cells, including how they grow and behave in these assays. This will then allow effective comparison, in future work, of the effects of activating the Wnt/β-catenin signalling pathway.

## 3.2. Characterizing growth in 2D and 3D Culture

### 3.2.1. Phenotype Analysis

We had access to a large cohort of genetically-diverse melanoma that we wanted to characterise, prior to our future work investigating the role of the Wnt/β-catenin signalling pathway in melanoma. These lines were gifted from Prof. R. Moon and Dr. A. Chien (University of Washington) and Prof. A. Ribas (UCLA). Firstly, we wanted to characterize them as either proliferative or invasive according to the phenotype switching model. To do this, we grew the lines in a 3D cell culture system. It has previously been described that 3D growth on Matrigel basement membrane matrix (see section 2.3.10), can define melanoma cells into two different phenotypes, proliferative and invasive (365). Proliferative phenotype cells will form small individual clusters in 3D, whereas invasive cells will form connected networks within the matrix (334). The panel could be divided into the two phenotypes (proliferative and invasive) according to their growth characteristics in 3D, as shown in Table 3.1. 7 cell lines (A375, HMB2, M285, M296, M308, Mel501, and SkMel28) produced inter-connected networks within the matrigel. This formation has previoulsy been described as being indicative of the invasive cell phenotype. 12 cell lines (A2058, Colo829, HTB63, M202, M207, M229, M375, Malme3M, Mel624, SkMel5, SkMel24 and UACC1273) formed either small clusters of cells or stayed individual. This formation was previoulsy described as representing the proliferative phenotype (334). From the initial 19 cell lines, 4 of each phenotype were chosen to carry through for further characterisation where their mutation status was well understood.

In total, 8 cell lines (shown in Table 3.2), representing a mix of wildtype BRAF or a V600E mutation and wildtype or mutant N-Ras (395), were characterised in more depth. There is both an invasive and a proliferative cell line with a PTEN mutation (146) and one line each with MITF amplification (29, 396), as well as a variety of other mutations including Akt, CCND1 and EGFR amplification, deletions of CDKN2A and mutations of MC1R. These mutations have previoulsy all shown to cross talk with Wnt signalling pathways and are important in the progression of malignant

**Table 3.1:The Molecular Characterisation of 19 Melanoma Cell Lines:**

3D growth on matrigel over 48 hours was captured at 10X magnification. 7 cell lines produced connected networks within the matrigel, this formation has previoulsy been described as being indicative of an invasive cell phenotype. 12 cell lines formed either small clusters of cells or remained individual, this formation was previously described as representing a proliferative phenotype

WT – Wildtype, Amp – Amplification, Het – Heterozygous, Homo – Homozygous, Pro – Proliferative, Inv – Invasive.

| Cell Line | BRAF Status | N-Ras | PTEN | PI3K | MITF Amp | AKT Amp | EGFR Amp | CDKN2A | MC1R | PRO/ INV | 3D growth |
|---|---|---|---|---|---|---|---|---|---|---|---|
| A2058 (144) | Het V600E | WT | Het Del | | | | | Homo del | | PRO | 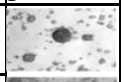 |
| A375 (163, 397) | Homo V600E | WT | INTACT | WT | No | No | | Homo del | R151C=R | INV | 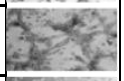 |
| Colo829 (223, 397) | Het V600E | WT | NULL | WT | No | No | No | Homo del | V92M=r | PRO |  |
| HMB2 (398) | V600E | WT | | | | | | | | INV | 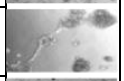 |
| HTB63 (163) | V600E | WT | | | | | | | | PRO | 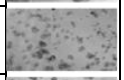 |
| M202 (397, 399) | WT | Q61L | INTACT | WT | No | No | Yes | Homo del | WT | PRO | 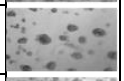 |
| M207 (397, 399) | WT | Q61L | Het Del | WT | Yes | No | L747_P 753>s | WT | V60L=r | PRO | 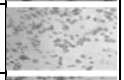 |
| M229 (397, 399) | Homo V600E | WT | Het Del | WT | No | AKT 1 | No | WT | R151C=R | PRO | 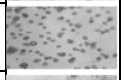 |
| M285 (400) | WT | WT | INTACT | WT | No | No | No | | | INV |  |
| M296 (397, 400) | WT | Q61R | INTACT | WT | No | No | No | | WT | INV | 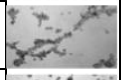 |
| M375 (400) | WT | WT | INTACT | WT | No | No | No | | | PRO | 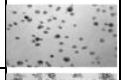 |
| M308 (397, 399) | Het V600E | WT | INTACT | WT | Yes | AKT 2 | Yes | Het del | WT | INV | 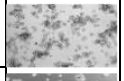 |
| Malme3M (397, 401) | Het V600E | WT | INTACT | WT | Yes | | | Homo del | WT | PRO | 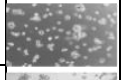 |
| Mel501 (402) | V600E | WT | Null | | | | | | | INV | 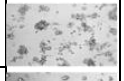 |
| Mel624 (223) | V600E | WT | | | | | | | | PRO | 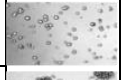 |
| SKmel5 (397, 403) | Het V600E | WT | INTACT | WT | No | No | | WT | V92M=r | PRO | 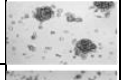 |
| SKmel24 (144, 397) | Het V600E | WT | NULL | WT | No | | | Homo del | R163Q=r | PRO | 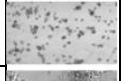 |
| SKmel28 (397, 399) | Homo V600E | WT | Het Del | WT | Yes | No | P753s | Het del | I155T=r | INV | 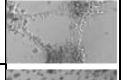 |
| UACC 1273 (223) | V600E | WT | | | | | | | | PRO |  |

melanoma (20, 165, 173, 404). Therefore, these mutations could play an important role in the way cells respond to Wnt signalling later in our investigations. The chosen 8 lines were; A375, M285, M296 and SkMel28 representing the invasive phenotype, and M202, M229, M375 and SkMel5 representing the proliferative phenotype (see Table 3.2 and Figure 3.4). Using the 3D matrigel, defines melanoma cells into two different cohorts, those that form connected networks and those that do not. The selected panel of 8 cell lines will now be further analysed in terms of their melanoma and cancer cell characteristics.

### 3.2.2. Cell Culture Growth Patterns of Melanoma Lines

Following the initial 3D Matrigel growth assay we decided to test the time the cells took to form their respective patterns in a time trial with images taken at 1, 2, 4, 6, 24, 48, 72 and 96 hours, Figure 3.5. It is noteworthy that there is variation in the time different cell lines took to form their respective clusters or networks. Some lines (M296 and M375) formed networks within the first hour following seeding, whereas the A375 and M285 cells took over 24 hours before the phenotype was distinguishable. The reason for this is unknown but could potentially be due many factors such as age of the cells, proliferation rate or strength of the specific phenotype. In 3D culture, the A375, M296, M285 and SkMel28 cells all formed connected networks with the Matrigel typical of the invasive phenotype (Figures 3.5a-d). Likewise, the proliferative lines M202, M229 and Skmel5 (Figures 3.5e-g) all remain as individual clusters in 3D culture. However, not all cell lines behaved as expected. The M375 cells (Figure 3.5f) formed an invasive phenotype pattern within the first hour of the time course; this is the different phenotype to that which was observed in the initial 3D growth assay, indicating that phenotypes could switch spontaneously.

It has also been previously noted that the two phenotypes (proliferative and invasive) can be distinguished by their appearance in 2D cell culture as well as in 3D (334, 361). In 2D cell culture on untreated tissue culture plastic, proliferative phenotype cells are smaller, more rounded and have dendritic processes, whereas the invasive phenotype cells are flatter, larger and fibroblastic in shape (361).

**Table 3.2: 8 cell lines chosen for further characterisation with 3D growth images**
Invasive cell lines A375, M285, M296 and SkMel28 form connected networks in a 3D Matrigel growth assay and proliferative cell lines M202, M229, M375 and SkMel5 stay individual or form small clusters. Scale bar, 200 μm.

| Cell Line | BRAF Status | N-Ras | PTEN | PI3K | MITF Amp | AKT Amp | EGFR Amp | CDKN2A | MC1R | PRO /INV |
|---|---|---|---|---|---|---|---|---|---|---|
| A375 | Homo V600E | WT | INTACT | WT | No | No | | Homo del | R151C=R | INV |
| M202 | WT | Q61L | INTACT | WT | No | No | Yes | Homo del | WT | PRO |
| M229 | Homo V600E | WT | Het Del | WT | No | AKT 1 | No | WT | R151C=R | PRO |
| M285 | WT | WT | INTACT | WT | No | No | No | | | INV |
| M296 | WT | Q61R | INTACT | WT | No | No | No | | WT | INV |
| M375 | WT | WT | INTACT | WT | No | No | No | | | PRO |
| SkMel5 | Het V600E | WT | INTACT | WT | No | No | | WT | V92M=r | PRO |
| SkMel28 | Homo V600E | WT | Het Del | WT | Yes | No | P753s | Het del | I155T=r | INV |

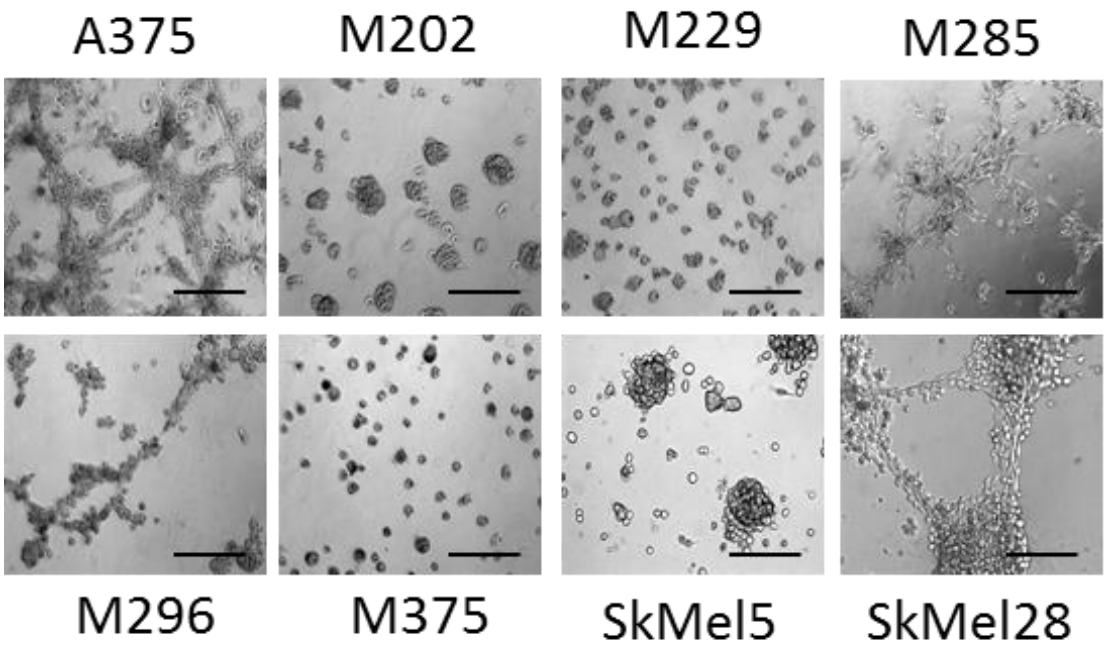


**Figure 3.4: 3D Matrigel growth of 8 selected cell lines**
3D culture growth, eight cell lines seeded onto matrigel basement membrane at $4x10^4$ cells/well and images were captured at 48 hours at 10X magnification.

Therefore, images were captured of the cells under normal 2D cell culture conditions to see if differences could be identified as shown in Figure 3.5i. The A375, M296, M375, M202, M229, and SkMel5 appear in 2D culture as expected, defined by their previous appearance in 3D phenotypes. However, not all cells are as uniform. The M285 cells appear invasive in 3D culture but have the appearance of a proliferative phenotype in 2D culture, looking small and rounded while the SkMel28 cells had a mixture of large, flat, fibroblastic cells and small rounded cells, therefore making it hard to define phenotype through this method.

It is clear that there are distinctions between the cells in the patterns that they form within the Matrigel membrane and their appearance in 2D culture, but not all cell lines tested correlated to the previous description in both assays. It also appears that cells are capable of switching without any pre-emptive signals, an observation that has not previously been reported before, making phenotype analysis hard to interpret consistently.

## 3.3. Investigation of the Proliferative and Invasive Potential of the Melanoma Cell Line Panel

### 3.3.1. Proliferation

It was expected that the proliferation of melanoma cells would represent the distinct phenotype observed in the 3D cell culture conditions, according to previous findings (361). This was investigated and 3D cell culture assays were set up, at the same time as cell proliferation and invasion analysis, to verify the 3D cell culture phenotype at the time of seeding (See Figure 3.6a). The proliferation assays were carried out as population doubling times (see section 2.3.11) over a time period of 72 hours (Figure 3.6b). The cell lines Skmel28 and M202 appeared to have mixed phenotypes, areas of connected networks and areas of individual cells as shown in Figure 3.6a. There were areas of joined up matrix associated with invasive phenotypes and areas of smaller individual clusters, which is commonly associated with a proliferative phenotype. The other cell lines produced uniform patterns in the 3D Matrigel growth.

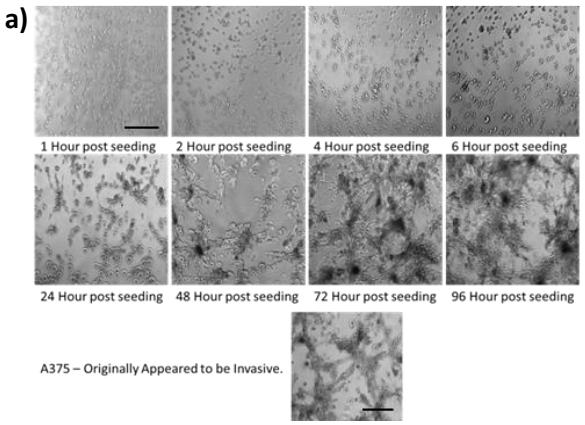
a)
1 Hour post seeding
2 Hour post seeding
4 Hour post seeding
6 Hour post seeding
24 Hour post seeding
48 Hour post seeding
72 Hour post seeding
96 Hour post seeding
A375 – Originally Appeared to be Invasive.

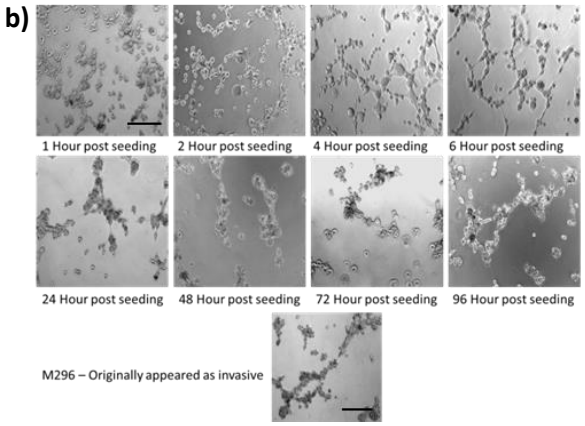
b)
1 Hour post seeding
2 Hour post seeding
4 Hour post seeding
6 Hour post seeding
24 Hour post seeding
48 Hour post seeding
72 Hour post seeding
96 Hour post seeding
M296 – Originally appeared as invasive

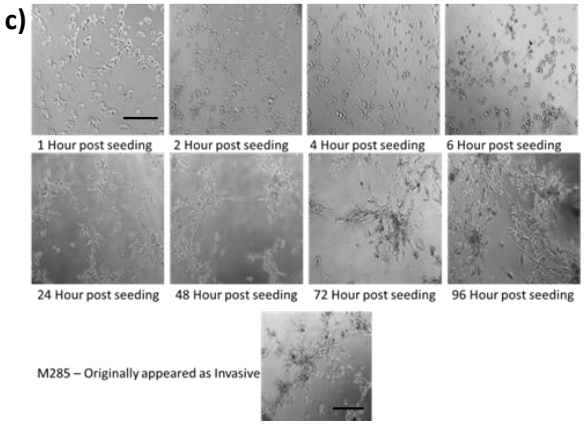
c)
1 Hour post seeding
2 Hour post seeding
4 Hour post seeding
6 Hour post seeding
24 Hour post seeding
48 Hour post seeding
72 Hour post seeding
96 Hour post seeding
M285 – Originally appeared as Invasive

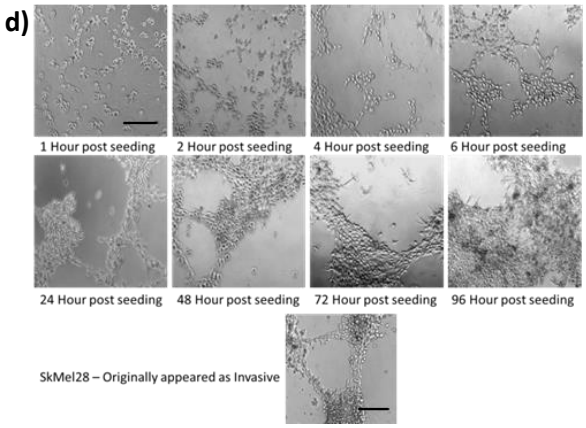
d)
1 Hour post seeding
2 Hour post seeding
4 Hour post seeding
6 Hour post seeding
24 Hour post seeding
48 Hour post seeding
72 Hour post seeding
96 Hour post seeding
SkMel28 – Originally appeared as Invasive

e)

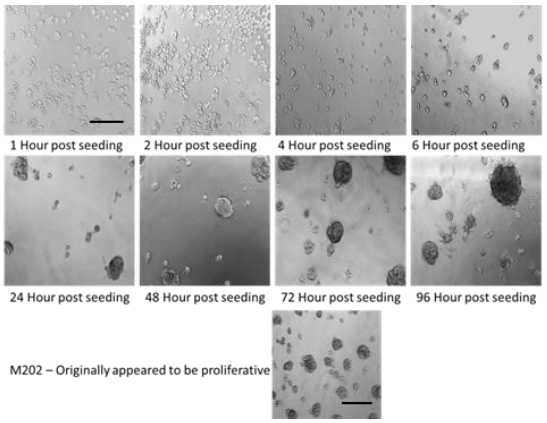
1 Hour post seeding
2 Hour post seeding
4 Hour post seeding
6 Hour post seeding
24 Hour post seeding
48 Hour post seeding
72 Hour post seeding
96 Hour post seeding
M202 – Originally appeared to be proliferative

f)

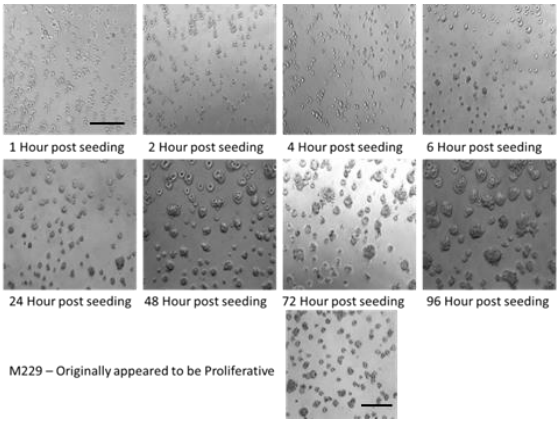
1 Hour post seeding
2 Hour post seeding
4 Hour post seeding
6 Hour post seeding
24 Hour post seeding
48 Hour post seeding
72 Hour post seeding
96 Hour post seeding
M229 – Originally appeared to be Proliferative

g)

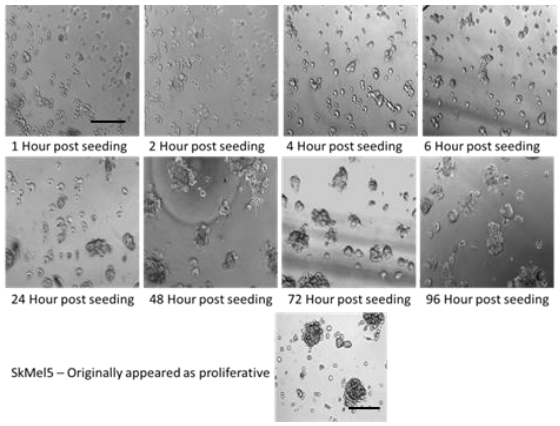
1 Hour post seeding
2 Hour post seeding
4 Hour post seeding
6 Hour post seeding
24 Hour post seeding
48 Hour post seeding
72 Hour post seeding
96 Hour post seeding
SkMel5 – Originally appeared as proliferative

f)

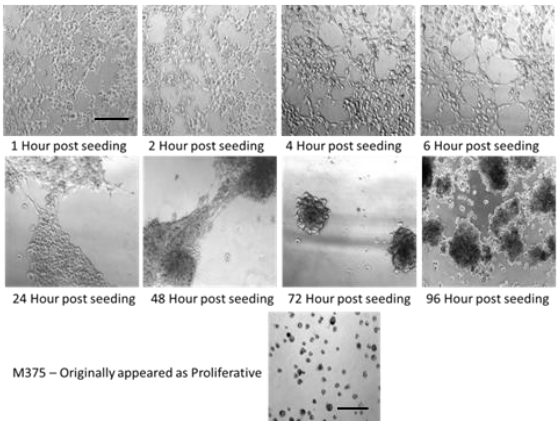
1 Hour post seeding
2 Hour post seeding
4 Hour post seeding
6 Hour post seeding
24 Hour post seeding
48 Hour post seeding
72 Hour post seeding
96 Hour post seeding
M375 – Originally appeared as Proliferative

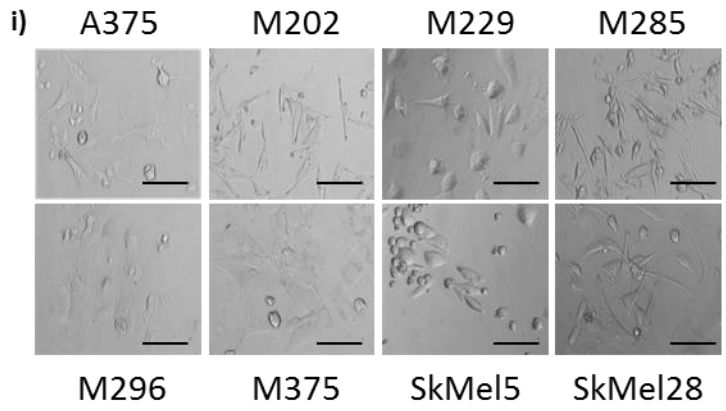


**Figure 3.5: Time Course Analysis of Melanoma Cell Lines Panel Growth in 3D with 2D Cell Culture Conditions:**
3D culture growth, eight cell lines seeded onto matrigel basement membrane at $4x10^4$ cells/well and images were captured at 1, 2, 4, 6, 24, 48, 72 and 96 hours at 10X magnification. Images were captured at the same XY location for each image and compared to the original 3D growth assay as shown in Table 2, **a)** A375, **b)** M296, **c)** M285, **d)** SkMel28, **e**) M202, **f)** M229, **g)** SkMel5, **h)** M375. All cells were cultured on non-treated tissue culture plastic under normal culture conditions to capture 2D cell growth at 10X magnification, **i)** 2D culture. Scale bar, 200 µm.

The population doubling shown in Figure 3.6b does not seem to follow the expected patterns of the phenotypes. All lines show a steady rate of growth over the course of the assay. The A375 cell line is the fastest growing line, doubling nearly 25 times in 72 hours. M202 is the next fastest at 22 population doublings in 72 hours. M285 doubled 16 times while SkMel28 carried out 11 population doublings in 72 hours. SkMel5 doubled 9 times and the remaining lines M2296, M375 and M229 doubled around 5 times over 72 hours. Therefore, these population doubling times varied irrespective of the phenotypes indicated in 3D cell culture conditions. Thus, the melanoma panel cannot be distinguished, based on population doublings between high and low proliferative cell types.

### 3.3.2. Invasion

It was also expected that the invasion of melanoma cells would represent the distinct phenotype observed in the 3D cell culture conditions, according to previous findings (361). The invasion assay (see section 2.3.12) was adapted from a previously published method, which involves coating a membrane based insert with a thin layer of Matrigel. Due to the method of this assay studying the invasion of the cells through a Matrigel layer, it is possible to simultaneously use this assay to analyse the cell lines 3D Matrigel growth patterns for phenotype analysis. Cells are serum starved and seeded into the top of the insert and complete media is used in the lower well as a chemoattractant to draw the cells through the membrane. Cells were then fixed, stained and counted (361). The cells were seeded at ($4x10^4$) equal cell numbers across the lines, rather than adjusted for growth rates and the assay was left to run for 48 hours. Figure 3.6c shows the results of the invasion assay. On average, over 500 cells were seen for the A375 cell line and around 200 cells moved through the membrane for both M285 and M296 cell lines. These are the lines that appear invasive in 3D culture. The fourth invasive line, SkMel28 had an average of 50 cells. Approximately 100 cells for the M202 cells were stained with Crystal Violet, the M229 and SkMel5 cells had around 50 cells pass through the membrane and M375 had around 10 cells in each assay. These were previously tested to be proliferative lines by the 3D culture assay. The overall trend for each phenotype

**a)**

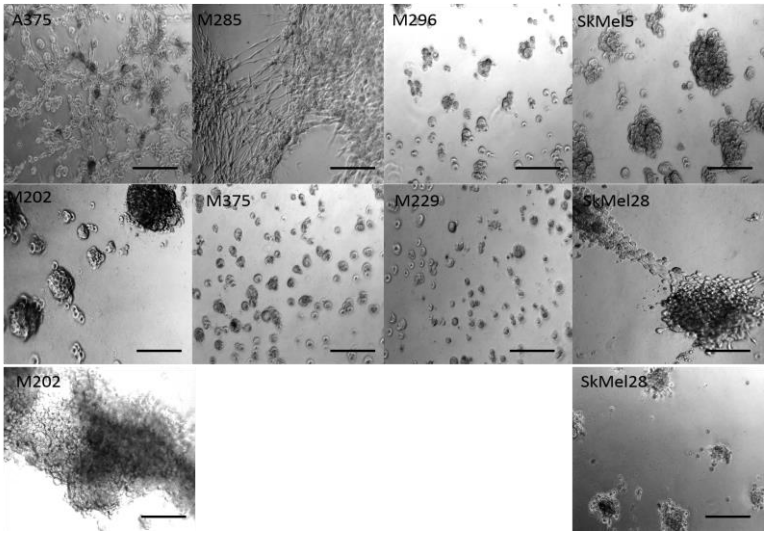


**b)**

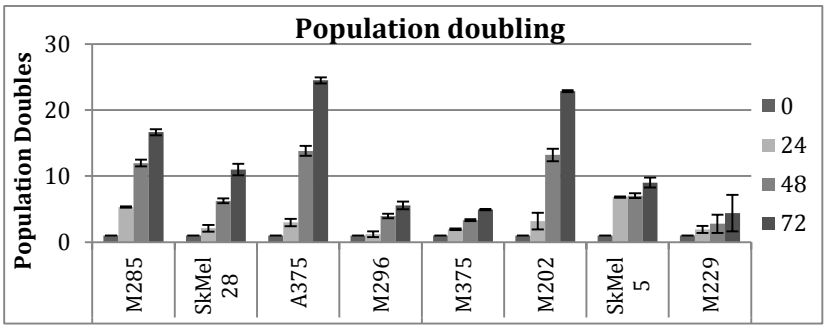


**c)**

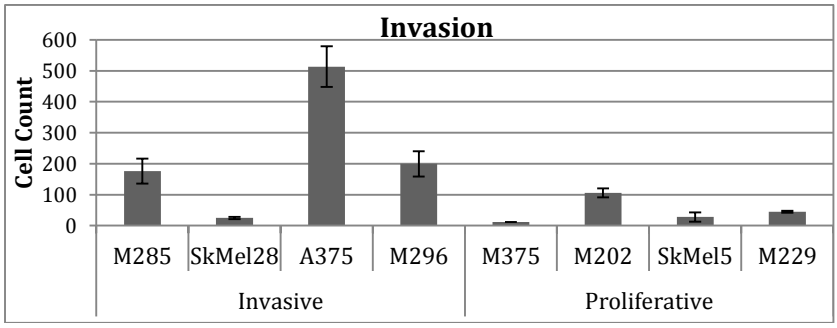


**Figure 3.6: Proliferation and Invasion with Matched 3D matrigel Growth Assay**
**a)** Matrigel 3D growth assay at 10X magnification seeded simultaneously using same method as previously described. Two images were captured for M202 and SkMel28 as they had areas of individual clusters and areas of joined up matrix, all other cell lines produced a uniform pattern. Scale bar, 200 µm. **b)** $4x10^4$ cells seeded and population doubling counts carried out at 24, 48 and 72 hours using trypan blue exclusion. N=3. 3D growth in figure a shows two lines (M202 and SkMel28) are both proliferative and invasive, so the distinction is based on earlier data (figure 3.4) **c)** Average (n=2) number of cells invaded through matrigel coated membrane after 48 hours plotted with SEM. $4x10^4$ cells were serum starved in 3% serum for 48 hours before seeding into serum free media. 10% serum media was used as an attractant to draw the cells through the membrane. Matrigel was coated onto 8 µm pore inserts at 50 µl/$cm^2$. Cells that had passed though the membrane after 48 hours were stained with Crystal Violet and counted.

shows increased invasion in the invasive phenotype and lower levels of invasion for the proliferative phenotype. However, this is not true for all cells lines as the SkMel28 cells had particularly low invasion compared to that of the other 'invasive' cell lines. Therefore, like the proliferation assay (Figure 3.5b), the invasion assay also corresponded poorly to 3D phenotype analysis.

### 3.3.3. Phenotype Gene Expression Analysis

As shown in section 3.1.4 and Figure 3.3, the phenotypes switching model suggests that the expression of particular markers can also be used to identify the different phenotypes. Higher expression of MITF and LEF1 have been described as defining the proliferative phenotype and higher expression of TCF4 and Wnt5a are associated with an invasive phenotype (361). Therefore, using western blotting (see sections 2.3.13 – 2.3.16), the expression of these markers were analysed in the eight cell lines and the results shown in Figure 3.7. It is clear that the pattern of expression does not fit the previously published data (361). All samples have very different levels of expression of all four markers. For example, M375 (a proliferative cell line) has particularly high expression of TCF4, a marker associated with the invasive phenotype, yet it has low expression of Wnt5a another marker of invasion. Whereas, the proliferative line M229 has very high expression of LEF1 but low expression of MITF, the two markers of the proliferative phenotype (361). The panel of four invasive lines all have higher expression of MITF, a marker of the proliferation phenotype, but their expression levels of LEF1 are lower. Overall, these markers do not correlate with the phenotypes as analysed by 3D cell growth in these cell lines. Nor do the proliferative and invasive assays correlate with each other. The A375 cell line has the highest rate of proliferation and invasion. Likewise, the M375 cell line has the lowest rate in both assays. Therefore, it is hard to use these assays to define distinctive phenotype characteristics.

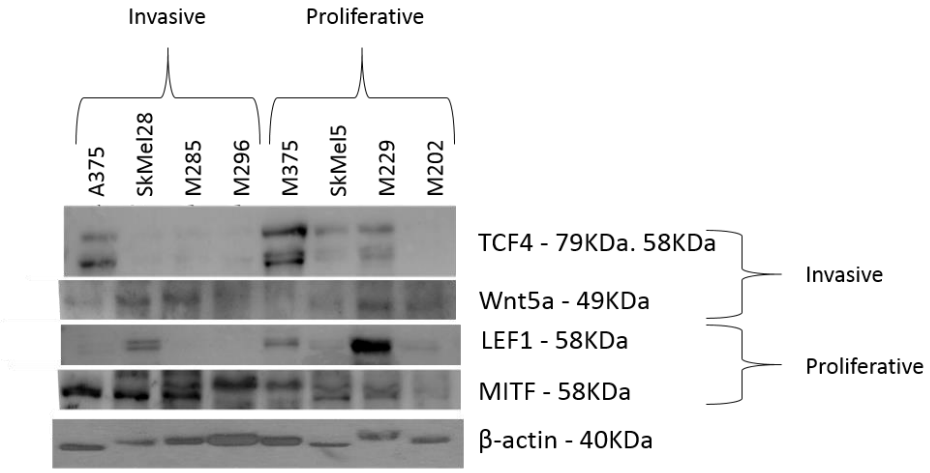


**Figure 3.7: Expression of proteins associated with different phenotypes**
Cell lysates were separated by SDS-PAGE and transferred onto nitrocellulose membrane. Expression of markers TCF4 and Wnt5a, described as markers of the invasive phenotype and MITF and LEF1 as markers of the proliferative phenotype were analysed and β-actin was used as a loading control. The cell line phenotypes were defined using the 3D culture assay shown in Figure 3.4.

## 3.4. Identification of Tumour Initiating Cells in the Melanoma Cell Line Panel

### 3.4.1. Melanosphere Formation

Now the growth patterns have been analysed and it was found that the proliferative and invasive potential correlate poorly with markers of the phenotype switching model, it was decided to assess if, instead, it correlated with the other model of melanoma, the tumour initiating potential/cancer stem cell model (359). The ability to form spheroids (see section 2.3.17) has been suggested to be indicative of tumour initiating properties, such as self-renewing ability and surface marker expressions (120, 382, 405). In order to allow melanospheres to form, the cells were seeded on plates coated with polyHEMA which produces a non-adherent surface (336). Cells were seeded on polyHEMA coated plates and images captured after 1 week of culture. The first 20 objects in the images were measured using Image J software. Figure 3.8a shows the typical formations seen in invasive and proliferative cell lines and Figure 3.8b shows the average and the range of sizes of melanospheres seen in the eight cell lines. The invasive phenotype (as defined by their growth in 3D culture) form large, rounded, solid clusters of cells called melanospheres. In contrast, the proliferative cell lines are only able to form smaller spheres, but the majority of the cells remained individual. This ability may be indicative of tumour initiating properties within the invasive phenotype. All of the 'invasive' lines formed spheroids. A375 formed the largest spheres at 900 µm. Of the 'proliferative' lines, M229 and SkMel5 did not form any spheroids and remained as individual cells. However, M375 and M202 cells did form smaller spheres but were all less than 400 µm. The overall trends shown in Figures 3.8a and 3.8b indicate that, on average, the invasive phenotypes have the ability to form much larger spheroids and, therefore, may have potential tumour initiating properties.

### 3.4.2. Tumour Initiating Cell Surface Marker Expression Analysis

It has been suggested that the expression of various cell surface markers could allow for the detection of cancer stem cells or tumour initiating cells in cancer and,

**a)**

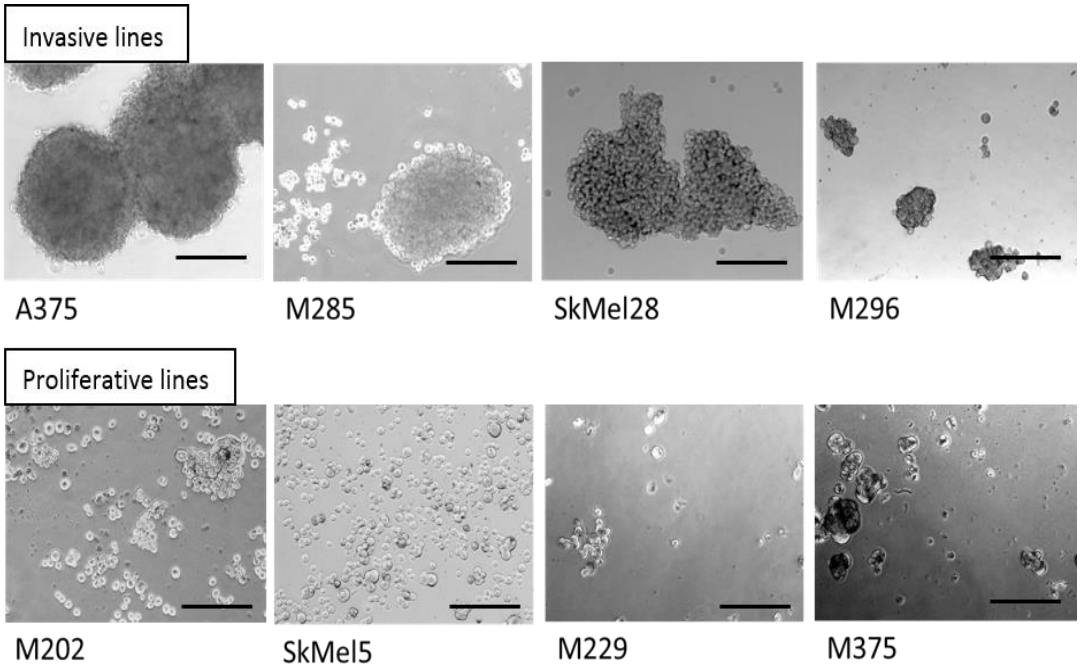


**b)**

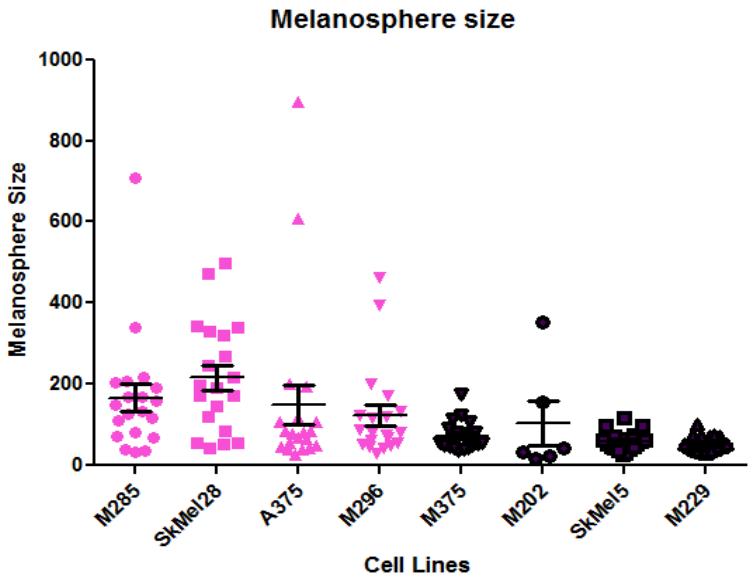


**Figure 3.8: Non-adherent melanosphere formation**

**a)** Images of Melanospheres in culture after 7 days on polyHEMA coated plates at 10X magnification. Scale Bar, 200 µm. The phenotypes were defined using the 3D culture assay shown in Figure 3.4. **b)** Analysis of the size distribution of melanospheres formed by eight different cell lines with SEM plotted. Pink indicated invasive phenotypes and purple represents proliferative phenotypes as determined by the matrigel 3D growth patterns. N=3.

therefore, enable the isolation of these cells from a heterogeneous multicellular tumour (362, 364, 367-370, 406-417). Table 3.3 shows some of the previously suggested markers able to identify melanoma initiating cells. Based on the previously published literature using patient derived tumour cells in xenotransplatation experiments, the expression of cell surface markers; ABCB5, CD271, CD20 and CD133 were analysed by flow cytometry (see section 2.3.18.1). Marker CD133, currently, has unknown function but has been found to be expressed on both normal and cancer stem cells, especially breast cancer stem cells (406, 407, 417). Marker CD271 is expressed on neural crest stem cells and is involved in development, survival and differentiation of cells (408, 409). Marker CD20 is typically associated with B-cell immune response but has also been found to be expressed on cancer stem cells (409). Finally, marker ABCB5 regulates skin progenitor cell fusion and mediates chemotherapeutic drug resistance in stem-like tumour cell subpopulations in human malignant melanoma and is over-expressed on circulating melanoma tumour cells in patients, suggesting potential role in metastasis (364, 407). The initial analysis was done individually, in order to determine expression levels of each of the markers in the cell line panel. All antibodies were designed to be compatible with the same secondary conjugated antibody; this would allow relative intensities to be estimated. Figure 3.9a shows an example of the live cell gating for cell line M285. Figure 3.9b shows an example of the expression of CD271 (red) and secondary only control (418) in M285 cells. Figure 3.9c summarises the flow cytometry data for all cell lines, which was consistent across multiple experiments. The unstained results show that there are high levels of autofluorescence in these cells and high variability between the cell lines. For example, the fluorescence of M296 is especially high compared to the other cell lines. This could be due to high levels of the autofluorescent polymer melanin in these cells (419). The secondary antibody alone, shows that there are also high levels of non-specific binding in all the cell lines. In five out of the eight cell lines, ABCB5 showed high expression levels and CD20 was expressed above background in four of the eight lines. Overall, four of the lines showed above background expression of all four of the markers. These were SkMel28, A375,

**Table 3.3: Melanoma Tumour Initiating Cell Surface Expression Markers:**
All markers have previously been identified in melanoma cell lines and have a variety of secondary assays carried out to confirm the stem-like phenotypes of the cells.

| Marker | Cancer Stem Cell Assays |
|---|---|
| ABCB5 (364) | Primary-patient-derived tumour cells in serial human-to-NOD/SCID mouse xenotransplantation experiments |
| CD133 (406) | Primary-patient-derived tumour cells in serial human-to-NOD/SCID mouse xenotransplantation experiments |
| CD271 (408) | Intradermal injection in 30% matrigel into B-, T- and NK cell deficient Rag2−/− γc−/− (130) mice |
| ALDH (410) | Cell suspensions were xenografted subcutaneously into NOD/SCID mice and NSG mice |
| CD20 (370) | Sphere formation followed by s.c. injection in SCID mice |
| CD146 (MCAM/ MUC18) (411) | Male athymic nude mice (BALB/c background<br>Melanosphere formation |
| CD40 (412) | Tumour cell proliferation |
| CD44 (368) | S.c. flank injection into C57BL/6 mice<br>Soft agar colony formation |
| MDR1 (414) | Melanosphere formation |
| ABCG2 (406) | Primary-patient-derived tumour cells in serial human-to-NOD/SCID mouse xenotransplantation experiments |
| JARID1B (369) | Melanosphere and soft agar formation, Single cell growth assays<br>s.c. injection into NOD/LtSscidIL2Rγ null mice |
| CD49F (362) | Single cell tumour formation<br>NOD/SCID mouse xenotransplantation experiments |
| CD166 (367) | None carried out, expression analysis only. |

SkMel5 and M229 cells. To verify these results, two proliferative and two invasive lines were chosen. These were; A375 (I), M285 (I), SkMel5 (P) and M229 (P), for their relatively low background autofluorescence levels. The antibodies were tested again using their respective isotype controls to remove any background from non-specific binding. Figure 3.9d shows an example of M285 cells with CD271 expression shown in red and the isotype control shown in blue. As each antibody is different in terms of the species that it was produced in and the immunoglobulin type, it was important that each antibody was compared to its cognate isotype. Figure 3.9e summarises the data from the four cell lines and shows the isotype controls abated any previously seen differences. In only four of the sixteen samples was the antibody intensity higher than that of the isotype control. Three of these were with the CD20 antibody in the A375, M285 and M229 cell lines. The SkMel5 cells only showed increased expression over the isotype control with the ABCB5 antibody. The increases seen were very small and the results were inconsistent. In repeated experiments, the expression levels shown here could not be matched and there was variation between cell lines and antibodies (data not shown). There was no consistency to the expression levels, no pattern in expression levels to identify proliferative verses invasive phenotypes and no outstanding marker of melanoma cells. Therefore, in this panel of melanoma lines with the markers tested, it is not possible to identify a cancer stem cell marker that can delineate proliferative against invasive melanoma cell types.

a)

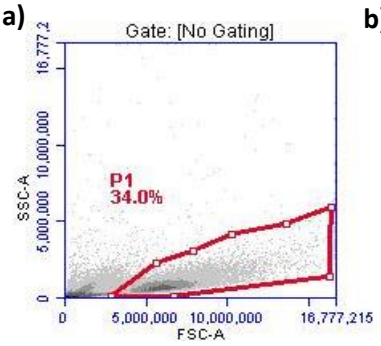


b)

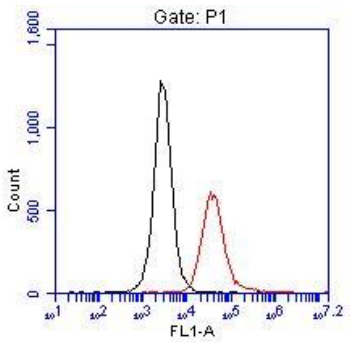


c)

| | M285 (I) | SkMel28 (I) | A375 (I) | M296 (I) | M375 (P) | M202 (P) | SkMel5 (P) | M229 (P) |
|---|---|---|---|---|---|---|---|---|
| un-stained | 3356 | 7139 | 3718 | 13079 | 7508 | 4665 | 4707 | 3848 |
| 2° only | 21313 | 9742 | 8551 | 27433 | 31680 | 30131 | 6737 | 23395 |
| CD271 | 72397 | 37833 | 17113 | 37845 | 32725 | 40836 | 22932 | 45465 |
| CD20 | 11808 | 12392 | 9865 | 25091 | 9145 | 19642 | 8648 | 23578 |
| CD133 | 30463 | 18304 | 19877 | 40372 | 31873 | 32500 | 11396 | 70032 |
| ABCB5 | 22393 | 10006 | 12562 | 23861 | 22257 | 10411 | 10692 | 37434 |

d)

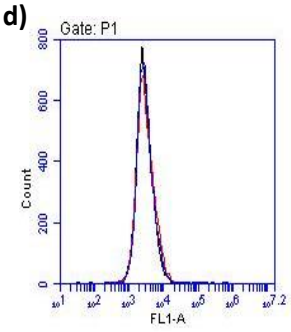


e)

| | A375 (I) | M285 (I) | SkMel5 (P) | M229 (P) |
|---|---|---|---|---|
| Unstained | 3,655.27 | 3,161.68 | 4,747.92 | 3,724.02 |
| CD133 | 3,580.12 | 3,269.30 | 5,321.75 | 3,936.07 |
| Isotype control | 4,568.00 | 3,370.51 | 5,848.87 | 4,211.24 |
| CD20 | 3,386.38 | 3,371.09 | 4,875.95 | 4,158.94 |
| Isotype control | 2,927.13 | 3,207.35 | 4,931.30 | 3,941.93 |
| CD271 | 2,753.19 | 3,552.54 | 5,162.81 | 3,702.72 |
| Isotype control | 3,007.34 | 5,315.87 | 6,603.56 | 4,073.05 |
| ABCB5 | 2,890.36 | 3,456.14 | 6,159.24 | 3,787.71 |
| Isotype control | 4,181.56 | 4,084.78 | 5,135.84 | 3,856.05 |

**Figure 3.9: Flow Cytometry of Cell Surface Marker Expression:**
**a)** Example of live gating on flow cytometry analysis for M285 cell line. **b)** expression of CD271 (red) and secondary only antibody staining (418), **c)** expression of CD271 (red) and isotype control (333), **c)** Mean FL1-A fluorescence values for each sample. Shading (red) represents fluorescence levels seen above background of secondary antibody only. **d)** expression of CD271 (red) in the M285 cell line with isotype control (333) **e)** Mean FL1-A fluorescence values for each sample. Shading (red) represents fluorescence levels seen above isotype control. (I)-Invasive Line, (P)-Proliferative Line.

## 3.5. Discussion

In order to help further investigations into the effects of Wnt/β-catenin signalling on melanoma cells, a selection of cell lines have been characterised in terms of the phenotypic switching model (334, 361, 365) and the cancer stem cell model (121, 360, 366). However, the melanoma lines tested did not fit either of the published models. In an attempt to distinguish different types of melanoma cells based on their phenotypes, the basal rates of proliferation and invasion were measured. The cells also did not express the suggested markers to define phenotypes, thereby not providing any significant features with which to delineate different phenotypes. The cells were distinctive in their 3D Matrigel growth, but spontaneous switching provides an unstable characteristic upon which to base future investigations. Finally, the cells were assessed for their cell surface markers and tumour initiating properties. No cell surface marker could be identified in this group of cells that could isolate potential cancer stem cells. However, some lines did show tumour initiating potential through the formation of melanospheres. Given that Wnt has been implicated in both of these models of melanoma, future work will go on to investigate if activating the Wnt/β-catenin signalling pathway changes any of these findings.

Deciding to choose eight cell lines based on their 3D Matrigel growth and previously described mutations (397) has limited the cell lines available for further characterisation. However, it was necessary to match cell lines based on their mutational background in case these differences affected how the cells behave in these assays and in future assays, in response to Wnt/β-catenin signalling. It is worthy to note that the data previously published on the phenotype switching model was on 6 lines chosen from an original panel of 86 (385). Generally, the data produced that was able to match to the published phenotype descriptions was all measured by visual interpretation as shown by 3D and 2D cell culture growth patterns, shown in Table 3.1 and Figure 3.5. As this is qualitative and not quantitative it is obviously left open to a degree of subjectivity. However, the 3D Matrigel does represent a difference between the two phenotypes but, given the additional data, it is difficult to conclude that it corresponds to proliferative verses invasive

phenotypes. The 3D Matrigel time course assay showed that the different cell lines not only produce very different patterns within the Matrigel, but they also vary hugely in the time taken to do so. The most interesting observation was the M375 cells, as they appeared to switch phenotypes from proliferative, in the initial analysis, to invasive throughout the time course - an observation that was again later seen in SkMel28 and M202 cells. In contrary to Hoek's published statement that; '*in vitro*, spontaneous phenotypes changes are not observed because intra-tumoural microenvironmental changes are absent, and their differences are maintained by epigenetic mechanisms (361)', we have seen a number of these cell lines change in their 3D growth patterns, suggesting phenotype switching is potentially capable in these melanoma cells. The fact that the cells can switch in culture could cause problems interpreting data from our assays. This also raises questions as to the differences in our cell culture methods and the culture environment, compared to that of Hoek's laboratory that enable us to observe spontaneous switches in melanoma cell phenotypes, *in vitro.* It has previously been suggested that it is changes to cellular conditions during inflammation or hypoxia that can induce these switches in tumours (365, 385, 388). The final characteristic analysed to determine phenotype was expression molecular markers (361, 385). All cell lines tested showed expression of MITF, TCF4, LEF1 and WNT5A. However, none of the cells showed distinct patterns that could help define their phenotype. Despite this, all of these markers are components of the Wnt signalling network and investigating if activation of the Wnt/β-catenin signalling pathway induces any changes could give insight into Wnt driven melanoma progression.

It has been suggested that there are tumour initiating cells within the heterogeneous cell population of melanomas (363, 364, 393, 408). It has also been suggested that these tumour initiating cells would be defined within the invasive cell phenotype population (121, 359). The best method to test if a population of cells are capable of initiating tumour formation would be to inject these cells into immunocompromised mice (362, 364, 368-370, 406, 408, 410), as this gives an accurate representation of the size and number of tumours formed from patient derived cells *in vivo*. In the interest of the 3R's (340), an *in vitro* method seemed more appropriate, initially, to

explore if there was a difference between the phenotype's abilities to form tumours. Following a week of culture in a non-adherent environment, the invasive cells produce melanospheres more easily. This ability may be indicative of tumour initiating properties within the invasive phenotype. The invasive phenotype form large, rounded melanospheres and it appears that they not only recruit cells to these structures but, also, continue to grow in this formation. It would be interesting to stain these clusters for proliferative markers such as PI or EdU to test if the melanospheres are actively proliferating or, simply recruiting cells to the outside of the sphere, as previously suggested for other cancer spheroid models (420, 421). In contrast, the proliferative cell lines seem unable to form these structures, although they can form smaller clusters, the majority of the cells remain individual. If Wnt/β-catenin signalling can change the size or formation of the melanospheres, it could again have implications in melanoma initiation and metastasis.

The cancer stem cell topic in melanoma is highly debated in the literature and there are many experiments that could be carried out to further assess tumour initiating ability and cancer stem cells marker expression, such as assays looking at tumour formation in soft agar and the cell autonomous ability to form spheroids from individual cells (408).

It has been suggested by others that individual markers could be used to identify the tumour initiating cells from the rest of the population (362, 364, 367-370, 406, 408, 410-412, 414). Using flow cytometry, cell surface markers that have previously been shown in the literature to have tumour initiating properties were assessed. Initial findings showed that CD133 and CD271 are expressed on all of the cell lines. CD20 and ABCB5 are expressed on half of the lines. However, upon further investigation with more stringent controls, it seemed unlikely that any of these markers were expressed above the isotype control on these cell lines and, therefore, none were able to identify and isolate tumour initiating cells. However, it is possible that it would take a combination of these markers to identify subpopulations responsible for tumour initiation and it is tempting to speculate that when looking at multiple markers, cells would show a comprehensive spectrum of expression combinations

(381). It has also been debated as to how large the population of cancer stem cells would be in the total cell population of the tumour. This seem to vary not only between tumour type but, also, within tumours of the same type (357). For example, in melanoma, ABCB5 expression has been shown to vary between 2-20% of the total tumour cell population (357, 360, 364). Likewise, CD133 expression has also been shown to vary to as low as 1% of the melanoma cell population (360, 364, 370, 406, 417). Therefore, it is likely that if such low populations of these cancer stem cells exist in these melanoma cell lines, they could have easily have been missed in the flow cytometry analysis. To overcome such problems, it is possible to enrich for the cancer stem cells expressing particular markers (409). It is also likely that growing cells in 3D melanospheres could produce differences in the expression of cell surface markers, compared to expression levels of cells grown in 2D (394) and the use of a stem cell media to generate the spheroid population, rather than an engineered polymer, may also alter any expression results (422, 423). It has also been suggested that cancer stem cells could, instead, express markers associated with normal stem cells (120-122, 417, 422), such as nestin, E-cadherin, N-cadherin, NANOG and SOX2, as a number of these markers stem from the neural crest, they have merit as potential markers in melanoma which, again, could have their expression changed by Wnt/β-catenin signalling. Such markers should be investigated in future studies.

### 3.5.1. Summary

It has been hard to define specific melanoma phenotypes using these cells with high levels of proliferation and invasion seen in all cell lines. However, the cells do differ in their 3D Matrigel growth patterns and investigating which factors determine these differences could give important information about melanoma progression. The tumour initiating properties to facilitate melanosphere formation also vary across the panel of cells but, as yet, an expression pattern capable of identifying and isolating them has not been found. This work has given important information about the growth of these cells and it will now be interesting to investigate if the activation of the Wnt/β-catenin signalling pathway has any effect on the features that have been analysed within this chapter.

# 4. THE EFFECTS OF WNT/β-CATENIN SIGNALLING IN MELANOMA

## Acknowledgements

Rima Kulikauskas, a Research Scientist from Prof. Chien's laboratory (University of Washington Department of Dermatology), performed the cell preparation for the in vivo study. Dr. Peggy Yang, a post-doc from Prof. Moon's laboratory (University of Washington School of Medicine) carried out the in vivo study. Brian Johnson, Research Scientist from The Histology and Imaging Core (University of Washington School of Medicine) carried out all IHC staining and scoring.

## 4.1. Introduction

The roles of Wnt signalling in cancer are complex given that there are different Wnt pathways that are often antagonistic of each other (167, 424), their function is commonly context dependent (425-427) and Wnts are morphogens (170). The β-catenin-dependent (canonical) and -independent (non-canonical) pathways are already known to have opposing effects in different cancer types, including melanoma (165, 428, 429). It is generally accepted that β-catenin-dependent Wnt signalling promotes melanocyte differentiation and tumour development, whereas β-catenin-independent Wnts are responsible for melanoma progression and induction of melanoma metastasis (165). This research focuses on the β-catenin-dependent pathway but, as the data shows, it is not necessarily as simple as which Wnt pathway is activated but, rather, that the mutational background of melanoma plays an important role in how the cells respond to Wnt.

### 4.1.1. Wnt Signalling in Melanoma

Melanoma is a cancer of melanocyte cells - melanin-producing cells derived from the neural crest (17, 19, 25). As explained in Chapter 1, Wnt signalling is highly involved in embryogenesis and the formation of the neural crest (22) but Wnt signalling also controls neural crest cell fate and melanocyte specification (22, 430). Neural crest cells gradually lose their pluripotency during development as cells differentiate into their specific cell types. This is usually determined by their anatomical location in the neural crest (19). Melanocytes are formed and migrate along the dorso-lateral pathway (20). Initially lineage specification forms melanoblasts which proliferate, migrate and eventually differentiate into melanocytes (17). Wnt-1 and Wnt-3 (β-catenin-dependent Wnts) are implicated in the neural crest cell specification, as double knockout mice do not have any melanoblasts (19, 20, 25). Overexpression of Wnt-1 caused an increase in melanoblast number and differentiation into pigmented melanocytes (25) and Wnt3a conditioned media caused differentiation of neural crest cells into melanoblasts (431). MITF, a known transcriptional target of the Wnt signalling pathway, is expressed in melanoblasts and regulates melanogenesis (production of pigment) in melanocytes (22). This is upregulated by Wnt3a and

removal of MITF results in the development of no melanocytes (432). β-catenin also has control over melanoblast differentiation, overexpression in the neural crest cells of zebrafish, increased pigmented melanocytes and a loss of β-catenin in mice removed all melanoblasts (19, 20, 25). It was also found that melanoblasts have very low levels of the Wnt signalling inhibitor Frzb-1, a finding not common to all neural crest derived cells, as neuroblasts and glioblasts have higher levels (431). Another Wnt signalling inhibitor DKK1, inhibits melanocyte differentiation and melanogenesis (433), also implicated in melanocyte differentiation, are Trpm1, Met, SOX9 and Kit, all known to interact with the Wnt/β-catenin signalling pathway (203). This data shows that canonical Wnt signalling is very important in the location and differentiation of melanoblasts.

As described by Larue *et al.* as well as others, β-catenin leads to the immortalisation of melanocytes, bypassing senescence due to the inactivation of p16 (20, 165, 430, 434, 435) therefore, leading to melanomagenesis but its continued expression inhibits metastasis formation and promotes differentiation. Therefore, the roles of β-catenin and the β-catenin-dependent-Wnts in melanoma are controversial. Some groups show nuclear accumulation of β-catenin in over 30% of melanoma cell lines (164, 436), leading to increased melanoma proliferation (177, 437) and reduced patient survival (436). Likewise, other groups show increased transcriptional activity of β-catenin during melanoma progression and downregulation of β-catenin increased apoptosis in melanoma cell lines (430). Linking the increase of β-catenin to the reduction in E-cadherin expression (438), it is suggested that reduced cell adhesion can lead to the increased cell migration and invasion that has been recorded (404, 430, 439-441). These studies have also shown that, in mouse models of melanoma, Wnt-β-catenin increased proliferation and tumour growth through MITF (437) and Ras signalling (435).

However, there are alternative views on the effects of Wnt/β-catenin pathway in melanoma and, in contrast, to some of the studies described above, several other groups report that higher levels of nuclear β-catenin in patient samples prolongs survival (20, 166, 203, 442-444). In addition to this data, it is known that most benign

nevi are positive for nuclear β-catenin which is subsequently lost in melanoma progression (443). Chien *et al.* show that activation of the Wnt/β-catenin pathway decreased proliferation in both patient samples and a murine model of melanoma (203). An increase in β-catenin caused by inhibiting GSK3β, which normally degrades β-catenin, has been seen to also cause reduction in proliferation in mouse B16 cells and melanocytes (445). Whereas, downregulation of β-catenin has been shown to cause poor survival rates in melanoma patients (442, 443) and, in B16 cells, caused increased metastasis (446). Likewise, other studies have shown stabilisation of β-catenin reduced cellular invasion (384) and increased apoptosis (350). Genome Wide Association Studies have shown transcriptional upregulation of genes such as Trpm1 and MelanA in B16–F1 melanoma cells treated with Wnt3a (203). These genes are associated with melanocyte differentiation, but are shown to be lost in melanoma progression (154).

In support of this view of the effects of Wnt/β-catenin signalling in melanoma is the knowledge that β-catenin independent Wnts are known to be antagonistic of the Wnt/β-catenin-dependent pathway (167, 424). The β-catenin-independent signalling pathway is also implicated in the development of melanocytes, driving EMT from the neural plate and migration of neural crest cells (22). It has been shown that blocking the Wnt inhibitor DKK1, the FZD7 receptor, or activity of β-catenin-independent Wnt11 or Wnt5a will halt neural crest cell migration, proliferation and melanogenesis (26, 447). As described in Chapter 1, β-catenin independent Wnts can be divided into two separate pathways - the Wnt/planar cell polarity (PCP) and the Wnt/$Ca^{2+}$ pathway. The PCP pathway is activated by non-canonical Wnt ligands and signals through the small GTPases, Rho and Rac to promote changes in the actin cytoskeleton but has not yet been shown to play a role in melanoma (22, 165).

The Wnt/$Ca^{2+}$ pathway promotes intracellular $Ca^{2+}$ signalling and negatively regulates the Wnt/β-catenin pathway (22, 404, 448). Wnt5a can antagonise β-catenin signalling and increase metastasis but is not involved in tumour formation (165). Wnt5a expression is not measured in melanocytes, nor in benign nevi, but is highly expressed in advanced, aggressive melanoma, indicating that it is turned on during

melanoma progression (449). This is correlated with decreased patient survival (450). Once melanocytes transform, Wnt5a activation can decrease β-catenin signalling through activation of SIAH2 (451, 452) but has also been shown to signal through FZD receptors 2 and 5 and increase β-catenin signalling in the presence of LRP6 (221, 453). More commonly, Wnt5a can interact with the ROR2 receptor (453-456) which is highly expressed in melanoma and this interaction mediates downstream signalling to alter melanoma metastasis and degrade β-catenin (25, 165, 454). Therefore, Wnt5a signalling is context and receptor-dependent. Wnt5a has also been shown to increase cell motility and invasion (228, 449, 450, 453, 457-461) through its upregulation of the transcriptional repressor Snail and Vimentin and downregulation of E-cadherin (228), thereby changing cell shape, increasing motility and progressing melanoma (462). Wnt5a can also increase cell adhesion (453) which is known to be less favourable for melanoma patient outcome (463).

Therefore, it is clear that depending on the stage of development from melanocyte to benign nevi to advanced melanoma, Wnt signalling can vary and it is important to look at the context of the cells and the receptors available to understand the oncogenic and tumour suppressor roles of Wnt signalling in cancer (22, 165, 166, 173, 404).

### 4.1.2. Aims

Having previously analysed the merits of the melanoma models of phenotype switching and cancer stem cells and found that they correlate poorly with the behaviour of our panel of melanoma cell lines, the question was raised if any of these parameters would be affected by the activation of the Wnt/β-catenin signalling pathway? The aim of this chapter was to use a selection of melanoma cell lines to assess the effects of active Wnt/β-catenin signalling on the previously investigated models of melanoma progression. Four cell lines of each phenotype (invasive and proliferative) have had their growth in 3D Matrigel assessed following activation of the Wnt/β-catenin pathway with recombinant Wnt3a protein (rWnt3a), to assess if Wnt/β-catenin signalling could force the cell lines to switch their phenotype. The same panel of cells was also analysed for changes in the growth of melanospheres as

an indication of Wnt/β-catenin signalling in being able to regulate tumour-initiating properties. Following this, both short and long term growth was assessed, as well as changes to apoptosis, cell cycle, invasion, migration and metastatic burden, all with the use of either rWnt3a or stably transfected overexpression cells that secrete Wnt3a to activate the Wnt/β-catenin signalling pathway.

## 4.2. Recombinant Wnt3a Activates the Wnt/β-catenin Signalling Pathway

It was necessary to ensure that the cell lines used had the ability to respond to recombinant Wnt3a (rWnt3a) protein stimulation by checking for activated β-catenin induced transcription. The binding of a Wnt ligand to the frizzled receptor and co-recptor LRP5/6 activates a series of signalling events that eventually lead to the the stabilisation of β-catenin (see Chapter 1 for details), allowing it to translocate to the nucleus and activate transcription of Wnt target genes (20, 169, 207). The SuperTOPFlash dual reporter assay (see section 2.3.19) was developed in order to do this (429). Adapted from the TOPFlash transcription-based luciferase designed by Korinek *et al.* (344), the SuperTOPFlash reporter contains eight TCF response elements (CCTTTGATC) upstream of Clontech's minimal TA promoter (464). A control construct has also been developed called SuperFOPFlash which, instead, contains eight mutant TCF response elements with the sequence CCTTTGGCC (343).

The cells were co-transfected with a Renilla control and stimulated with rWnt3a at 50 ng/ml or carrier control for 24 hours before the dual luciferase assay was carried out. To analyse the results, the TOP and FOPFlash readings were first normalised to Renilla transfection levels. FOPFlash was then subtracted from the TOPFlash to give the final results. Figure 4.1 shows the normalised data for 10 cell lines stimulated with rWnt3a protein or carrier control. All cells show a higher response to rWnt3a compared to their respective controls. The A375 have the highest response at over 50,000 ALU. Other cell lines, such as Mel501 and SkMel28, also have high responses at over 15,000 ALU. However they also have the highest control responses, indicating that the cell lines A2058, M202, M229 and SkMel5 may have a higher response as their relative background levels are lower. However, not all cell lines have such a high luciferase response. M285, M296 and M375 all show a response above their controls but are much lower with under 200 ALU. All cells respond to rWnt3a stimulation, leading to active β-catenin transcription.

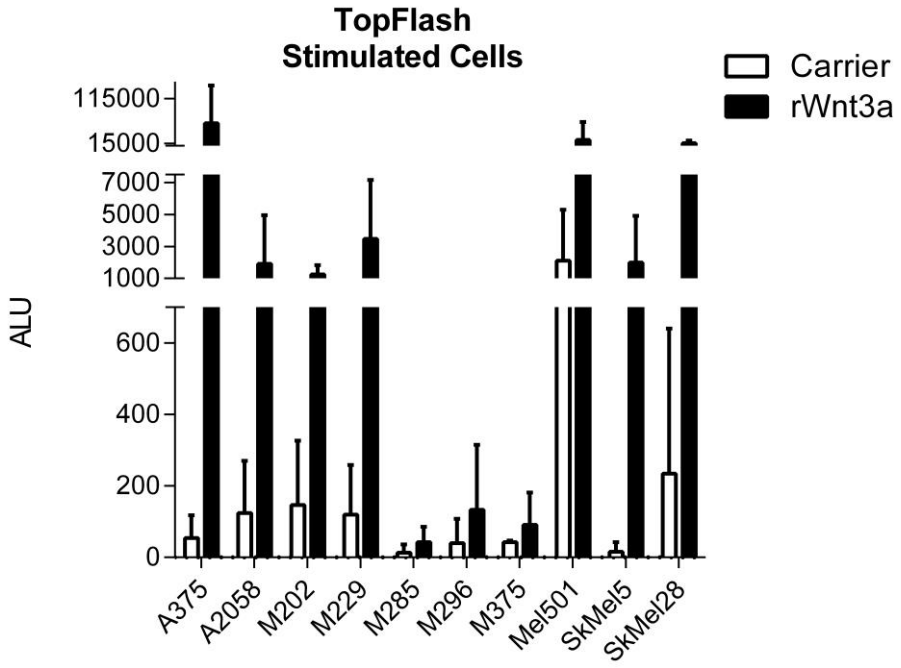


**Figure 4.1: Analysis of Wnt/β-catenin signalling using the TOPFlash reporter assay.**
Cell lines were co-transfected with Renilla and either TOPFlash or FOPFlash for 6 hours. Following this, cells were stimulated with either carrier control or rWnt3a (50 ng/ml) for 24 hours. Dual luciferase reporter analysis was carried out and results were firstly normalised to Renilla as a transfection control and then to FOPFlash. 10 melanoma cell lines were used and show all lines respond to rWnt3a stimulation. N=4.

## 4.3. rWnt3a has no Effect of the Phenotype Switching Model

The cell lines have already had their growth in 3D matrigel basement membrane assessed (see section 3.2.1), allowing their phenotypes to be defined. Cells that form connected networks within the matrigel are defined as the invasive phenotype and those that remain individual are defined as the proliferative phenotype (334). As explained in detail in section 3.1.4 Wnt signalling is intrinsically linked to the phenotype switching model through the expression of MITF, LEF1, TCF4 and WNT5A (364, 385). Figure 3.3 shows the interaction of these genes and, if, the Wnt/β-catenin signalling pathway was to be activated, this should drive the proliferative pathway, as it would stabilise β-catenin, driving the expression of the proliferative genes MITF and LEF1 which would, in turn, inhibit the expression of the invasive genes TCF4 and Wnt5a. Therefore, in order to see if the 3D growth patterns within the matrigel were affected by the activation of Wnt/β-catenin signalling, the panel of eight cell lines were treated as described in section 2.3.6 and seeded into the assay, as previoulsy described (see section 2.3.10). Images were captured after 48 hours and Figure 4.2 shows representative images which demonstrate that there were no changes to the 3D matrigel phenotype growth patterns of these cells following rWnt3a treatment. The A375 and SkMel28 cell lines form connected networks within Matrigel and the M202 and M229 cell lines are small, individual, clusters (see Figure 4.2). The upper panel shows cells treated with control and the lower panel are the cells treated with rWnt3a. There are no differences in the 3D Matrigel growth patterns of these cells in response to rWnt3a treatment.

## 4.4. rWnt3a Has no Effect on Melanosphere Formation

As previoulsy described in section 3.1.4, the cancer stem cell model/tumour-initating model is also linked to Wnt/β-catenin signalling (389-393). The formation of melanospheres is an indication of tumour initating properties (120, 382) and, therefore, to determine if the sizes of the melanospheres formed were affected by the activation of Wnt/β-catenin signalling, the cells were treated for 48 hours with

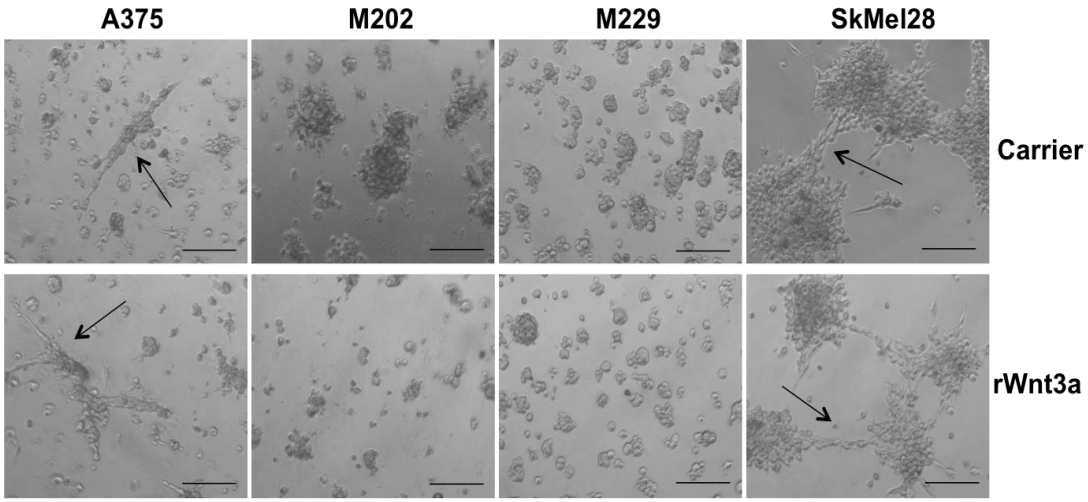


**Figure 4.2: The Effects of rWnt3a on 3D Melanoma Cell Culture**
Cells were stimulated for 48 hours with either carrier control or rWnt3a (50 ng/ml), they were then seeded onto matrigel coated plates at $4x10^4$ cells/well for 48 hours. Images were captured at 10X magnification. Arrows highlight connected cell clusters typical of an invasive phenotype. Scale bar = 200µm.

rWnt3a before being counted and seeded into the polyHEMA plates, as previously described in section 2.3.14 (339, 340). Figure 4.3a shows representative images of the melanospheres with, and without, treatment with rWnt3a and Figure 4.3b shows the size of melanospheres (above 50 µm in diameter) formed after one week, cultured in media treated with either carrier control or rWnt3a. As stated previously in section 3.5.1, the different cell lines showed differing abilities to form melanospheres under general growth conditions (Figure 3.4a), but there was no affect of Wnt/β-catenin signalling on melanosphere size.

## 4.5. Wnt/β-catenin Signalling Reduces Proliferation and Increased Apoptosis of Melanoma Cells

### 4.5.1. Wnt/β-catenin Increases Short-Term Proliferation, but Reduces Long Term Melanoma Cell Growth

#### 4.5.1.1. Short Term Proliferation is Increased using rWnt3a Stimulation

It has already been shown that Wnt/β-catenin signalling can affect melanoma cell proliferation (203). To check this, a selection of melanoma cells were stimulated (see section 2.3.6) with rWnt3a for 48 hours, then proliferation measured over 48 (Figure 4.4a) and 96 (Figure 4.4b) hours (see section 2.3.11). All three cell lines used (A375, M202 and SkMel28) showed a small, yet significant, increase in proliferation at 48 hours post-treatment. This is contrary to what has previously been published, where a reduction in proliferation was measured over 3 and 6 days in stable overexpression B16-F1 mouse melnaoma cells (203). Not all data was measured to a significant level for the 96-hour data. M202 show a small, but significant, increase, but the increase seen in A375 and SkMel28 cells are not significant. These results suggest that there may be an initital signalling event activated by Wnt3a that increases melanoma cell proliferation which, for some lines may be transient.

**a)**

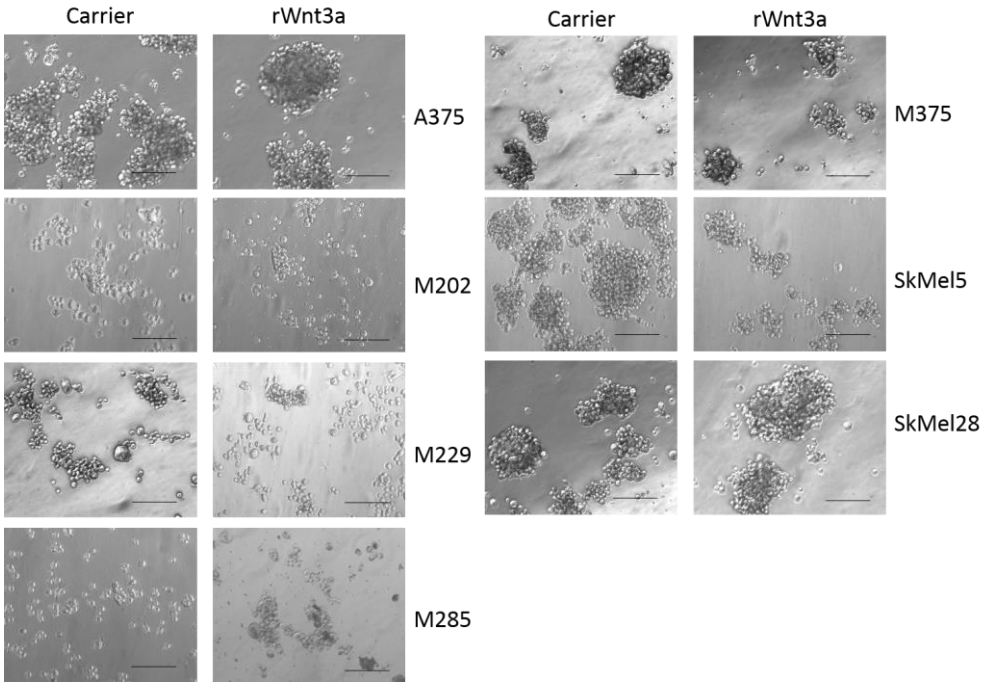


**b)**

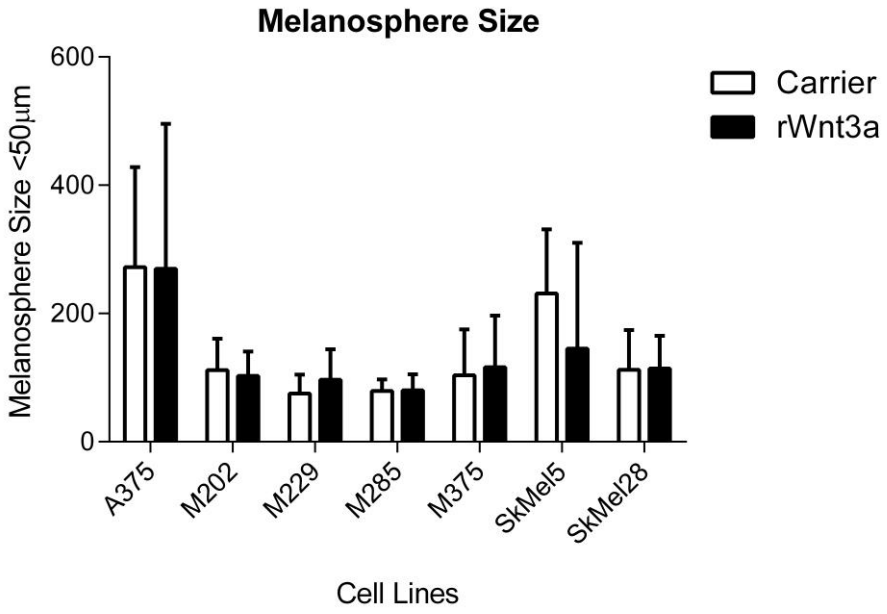


**Figure 4.3: The Effects of rWnt3a on Melanosphere Growth.**
**a)** Cells were stimulated for 48 hours with either rWnt3a at 50 ng/ml or carrier control, they were then seeded onto polyHEMA coated plates at $4x10^4$ cells/well for 7 days before images were captured at 10X magnification. **b)** Image J was used to measure melanosphere size, anything smaller than 50 µm was discounted. Ns.

**a)**

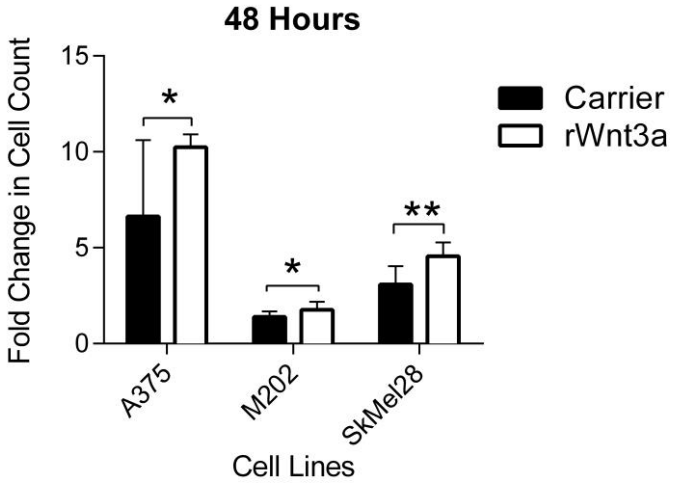


**b)**

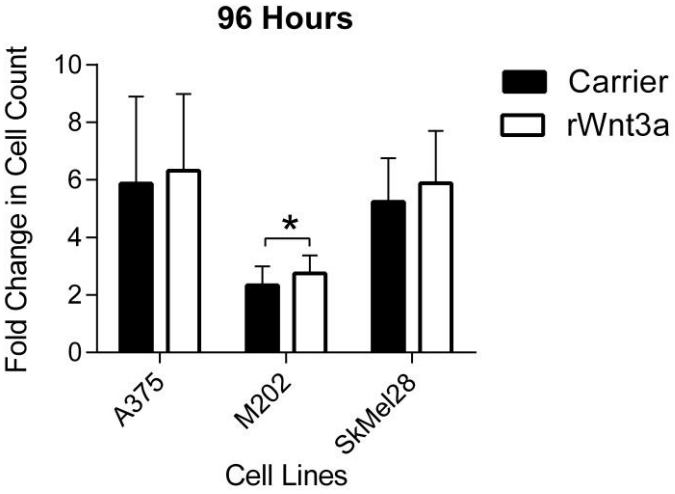


**Figure 4.4: rWnt3a increases melanoma cell population doublings over 48 and 96 hours.** A375, M202 and SkMel28 cells were stimulated for 48 hours with either rWnt3a at 50 ng/ml or carrier control, they were then seeded in triplicate at $4x10^4$ cells/well and viable cell counts carried out after 48 (**a**) and 96 (**b**) hours. N=3. Mean shown ± SD. $p$ = <0.05* or <0.01**.

#### 4.5.1.2. Wnt/β-catenin Signalling Reduces Long Term Cellular Growth

A375 and A2058 cells have been transfected to overexpress a Wnt3a or control backbone vector (see section 2.3.1.3). These cells were chosen as they are well-characterised melanoma lines and differ in their genetic backgrounds. Figure 4.5a shows western blot analysis of Wnt3a overexpression and Figure 4.5b the normalised TOPFlash analysis (see section 2.3.19) of the β-catenin stabilisation, compared to controls. These results suggest that the cells can secrete Wnt3a and activate the Wnt/β-catenin pathway. Using the overexpression cell lines (see section 2.3.4), it is possible to monitor the growth of the cells for longer periods of time without the use of recombinant protein. rWnt3a stimulation is carried out in serum free media, making long-term assays hard to carry out using this method. The overexpression cells were kept in culture for 36 (A375) and 21 (A2058) days to monitor their growth patterns. The A2058 cells were only cultured for 21 days as the difference in population doubling time between the cells was bigger and, therefore, a significant difference in total cell number could be detected more quickly. This allowed the calculation of the average population doubling times shown in Table 4.1 (see section 2.3.11). A375 cells take an average of 21.9 hours to double their population. This is increased in the Wnt overexpression cells to 22.4 hours. The A2058 cells proliferate a little quicker, taking 18.7 hours to double their population but this is, again, reduced in the Wnt3a overexpression cells to 19.7 hours. The longer time taken for the Wnt3a overexpressing cells to double their population, compared to the control cells, is represented in their overall lower total cell counts as shown in Figures 4.6a and 4.6b. This long-term data is supported by the previoulsy published study (203), which showed that activation of the Wnt/β-catenin signalling pathway reduces melanoma cell proliferation.

### 4.5.2. Wnt/β-catenin Signalling Increases Cellular Death

As a reduction in cell number was seen in these cells and one of the hallmarks of cancer cells is their ability to evade programmed cell death or apoptosis (377, 465), it was necessary to analyse the effects of Wnt/β-catenin signalling on apoptosis. ApoTRACE (see section 2.3.20) was used to measure alterations in plasma

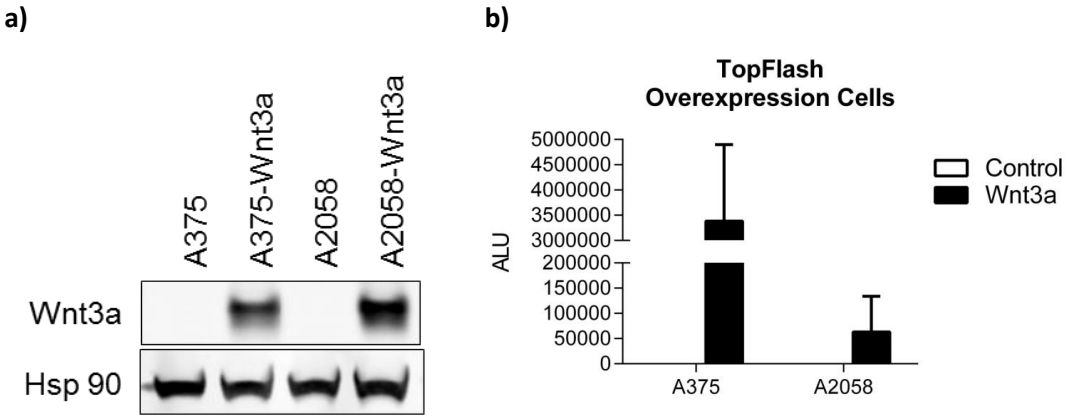


**Figure 4.5: Overexpression of Wnt3a in melanoma lines A375 and A2058 with control.**
**a)** 10 µg of cell lysates were separated by SDS-PAGE and transferred on to nitrocellulose membrane. The Odyssey system was used for blocking, antibody dilution, washing and developing. Antibody dilutions used were 1:2000 for anti-Wnt3a and 1:10,000 for anti-Hsp90. Carried out by R. Kulikauskas at UW. **b)** TOPFlash analysis of stabilised β-catenin. A375 and A2058 Wnt3a overexpression cells secret Wnt3a activating the β-catenin pathway, the GFP control cells show no activation. N=4. ALU = Arbitrary Light Unit, measurement of luminescence.

**Table 4.1: Cell population doubling times, A375 and A2058-Wnt3a overexpression cells and controls**

Cells were cultured over 36 (A375) and 21 (A2058) days, the average time taken for the cell population to double was calculated in hours.

| Cell Line | Population Doubling Time (hours) |
|---|---|
| A375 | 21.9 |
| A375-Wnt3a | 22.4 |
| A2058 | 18.7 |
| A2058-Wnt3a | 19.7 |

**a)**

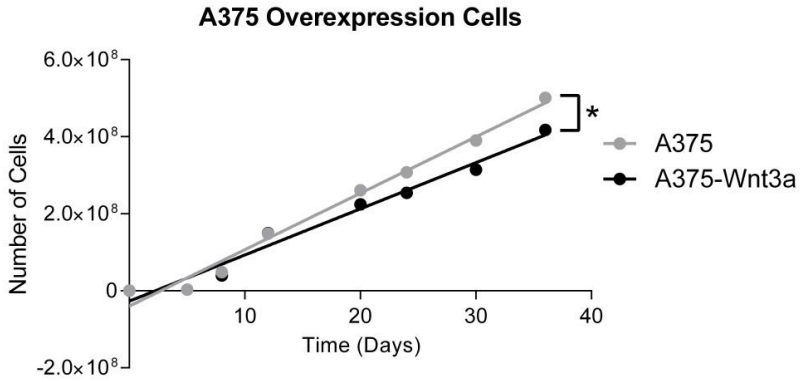


**b)**

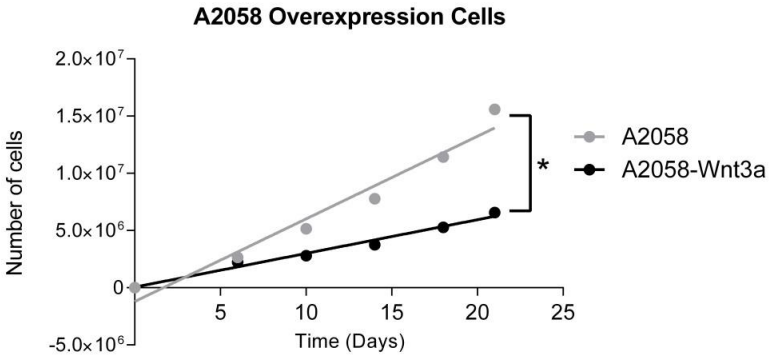


**Figure 4.6: Long-term proliferation of Overexpression Cells**

Wnt3a Overexpression cells and control cells were seeded in triplicate at $2x10^4$ cells/well. When confluent a viable cell count was carried out, the population was split at a known ratio and reseeded, this continued for 36 days (A375) and 21 days (A2058). From this a total cell number could be plotted and a population doubling time calculated. **a)** A375 **b)** A2058. N=3. Mean shown ± SD. T-test of total cell number over entire time course $p$ = <0.05*.

membrane potential and phospholipid scrambling (466). The levels of fluorescence measured was normalized to total protein concentration and the data shown in Figure 4.7 shows both cell types (A375 and A2058) having a significant 1.4 fold increase in apoptosis in response to Wnt/β-catenin signalling.

Cytochrome *c* is an essential component of the electron transport chain (ETC). A protein found loosely associated to the inner mitochondrial membrane, it transfers electrons between complexes III and IV (268). It is also a component of the apoptosis pathway being released from the mitochondria during apoptosis. Therefore, levels can be measured as an indication of apoptosis in the cell (269-271). Using flow cytometry (see section 2.3.18.2), the levels of cytochrome *c* in the Wnt3a overexpressing cells was measured. Figure 4.8 shows that both the A375 and the A2058 cells have a significant 1.3 fold increase in cytochrome *c* levels, again indicating an increase in apoptosis in response to Wnt-β-catenin signalling and confirming the results from the apoTRACE assay in Figure 4.7.

As increases in apoptosis (Figure 4.7 and 4.8) and a reduction in cell proliferation (Figure 4.6) are often a result of cell cycle arrest and often observed in cancer cells (467), it is necessary to check if Wnt/β-catenin signalling caused cell cycle arrest in melanoma cells (see section 2.3.18.3). By measuring the amount of propidium iodide (PI) staining it is possible to measure the DNA content of cells, making sure that no RNA will be stained with the use of RNase A and cell doublets excluded. A typical cell cycle will produce a pattern where cells in the $G_0/G_1$ phase of the cell cycle will be diploid (2n DNA). Cells in S phase are in the process of duplicating their DNA so will be a mixture of diploid and tetraploid and cells in $G_2$/M will be tetraploid (4n DNA). The relative fluorescence of cells in $G_2$/M will, therefore, be twice as high as those in $G_0/G_1$ (468). Figure 4.9 shows the cell cycles of the A375 and A2058 cells. There is no difference between them nor any difference from a standard cell cycle pattern, suggesting that Wnt/β-catenin signalling does not cause a cell cycle arrest in melanoma cells.

The increase in apoptosis that has already be shown in Figures 4.7 and 4.8 can also be seen in the cell cycle profiles (See Figure 4.9). The cell cycles of the Wnt3a

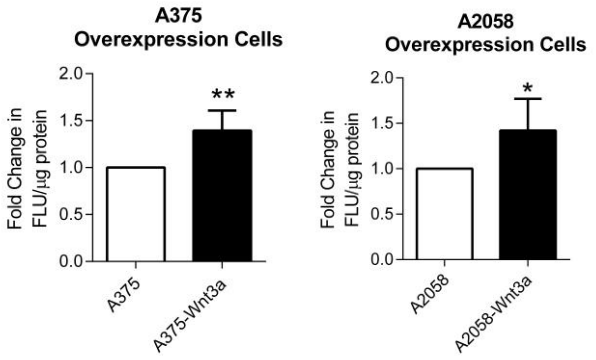


**Figure 4.7: Increase in fold change in apoTRACE (FLU/µg of protein) in A375 and A2058 Wnt3a overexpression cells.**

Cells were seeded at 6x10$^4$ cells/well then stimulated for 48 hours with serum free media. ApoTRACE was added to the cells for 1 hour in the dark before the cells were lysed and analysed for fluorescence at ex 328 nm em 563 nm. A BCA was carried out to determine total protein concentration for normalisation and fold change over control was then calculated. N=3 Mean shown ± SD. *p* = <0.05* or <0.01**. FLU = Fluorescence Light Unit.

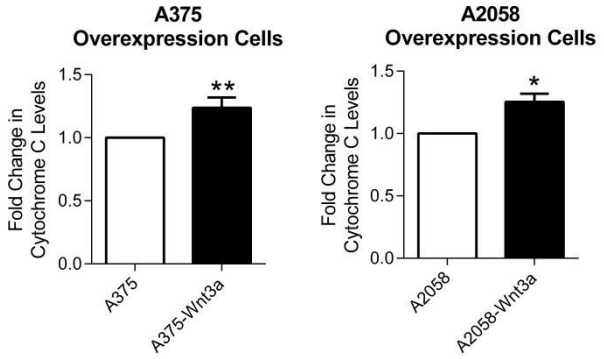


**Figure 4.8: Increase in fold change in Cytochrome C measured by flow cytometry in A375 and A2058 Wnt3a overexpression cells.**

Cells were fixed, permeablised and incubated with cytochrome c antibody at 20 µg/ml for 1 hour. An anti-mouse secondary antibody conjugated to AF633 was used and live events were measured on the C6 Accuri flow analyser in far-red channel FL4. Fold change in FLU was calculated. N=3. Mean shown ± SD. *p* = <0.05* or <0.01**.

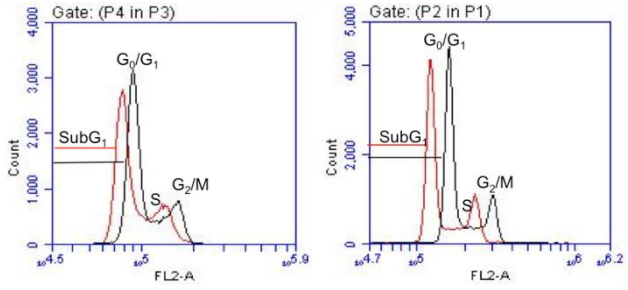


| | A375 | A375-Wnt3a |
|---|---|---|
| $SubG_1$ | 0.6% | 2.07%* |
| $G_0/G_1$ | 66.02% | 65.54% |
| S | 14.14% | 16.32% |
| $G_2/M$ | 16.12% | 14.68% |

| | A2058 | A2058-Wnt3a |
|---|---|---|
| $SubG_1$ | 0.6% | 2.87%* |
| $G_0/G_1$ | 66.58% | 68.72% |
| S | 13.00% | 12.69% |
| $G_2/M$ | 19.16% | 17.22% |

**Figure 4.9: Cell cycle analysis of Wnt3a overexpression cell lines.**

Cells were fixed overnight in 70% EtOH before incubation for 45 minutes with PI/RNase. Live events were measured, excluding doublets on the C6 Accuri flow analyser in channel FL2. Representative % of cells in different stages of the cell cycle are displayed. N=3. Mean shown. *p* = <0.05*.

samples shift to the right of their controls, thereby showing a significant increase in the sub $G_1$ measurement which is a sign of DNA fragmentation associated with apoptosis (469). Taken together, this data showed that activation of Wnt/β-catenin signalling increase apoptosis in melanoma cells.

## 4.6. Wnt/β-catenin Signalling Alters Invasion, Migration and Metastasis in a PTEN Context-Dependent Manner

### 4.6.1. Wnt/β-catenin Signalling Alters Melanoma Cell Invasion in a PTEN Context-Dependent Manner

The effects of Wnt/β-catenin signalling on reducing melanoma cell invasion has already been published (384) and it is known that Wnt5a signalling in a non-canonical manner increases invasion in melanoma cells (453). Therefore, it was expected that Wnt3a would inhibit melanoma cell invasion. To confirm this in our panel of cells, the invasion through a Matrigel coated transwell was analysed over 48 hours (see section 2.3.12). Across a panel of 6 cell lines stimulated with rWnt3a and the two sets of overexpression cells we observed a significant difference in invasion. As shown in Figure 4.10a, the cell lines A375, M202 and Mel501 showed up to a 0.3 fold reduction in invasion in response to rWnt3a, whereas the A2058, M229 and SkMel28 cells showed up to a 10 fold increase. This pattern was replicated in the A375 and A2058 Wnt3a overexpression cells where A375 cells showed a 0.4 fold significant decrease in invasion, whereas the A2058 cells measured nearly a 2 fold increase in cell invasion. The difference in the number of cells stained on the transwell chamber was clearly visable as shown by representative images in Figure 4.10b.

Upon further investigation of Table 3.1 (chapter 3), it was noted that the cells with reduced invasion had wild-type PTEN ($PTEN^{WT}$) and those that showed increased invasion had a mutation within PTEN ($PTEN^{Mut}$). PTEN expression was confirmed by western blot analysis in the panel of 6 lines in Figure 4.11, where lower or no PTEN expression is seen in the cells with $PTEN^{Mut}$ status depending on their homozygous

**a)**

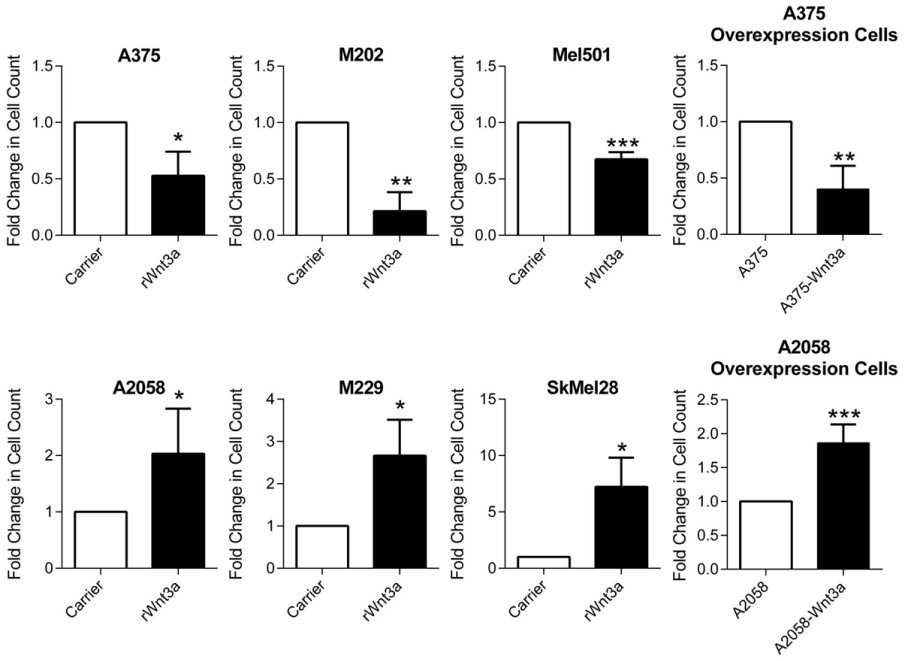


**b)**

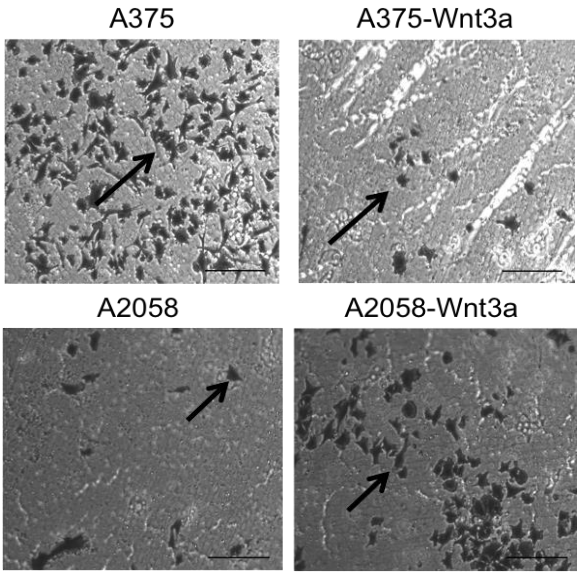


**Figure 4.10: Reduced invasion in PTEN intact melanoma cells and increased invasion in PTEN null melanoma cells in response to Wnt3a signalling.**

**a)** Cells were stimulated for 48 hours with either rWnt3a (50 ng/ml), carrier control or just serum free media for the overexpression cells, and then seeded on to matrigel coated transwells at $4x10^4$ cells/well in serum free media, using 10% media as a chemoattractant in the lower well. After 48 hours the cells that had invaded through the membrane were fixed, stained and counted with fold change compared to control calculated. **b)** Representative images of stained cells on transwell membranes for the Wnt3a overexpression cells. Arrows indicate cells fixed to the membrane following invasion. 10X magnification. N=4. Mean shown ± SD. *p* = <0.05*, <0.01** or <0.001***. Scale bar = 200µm.

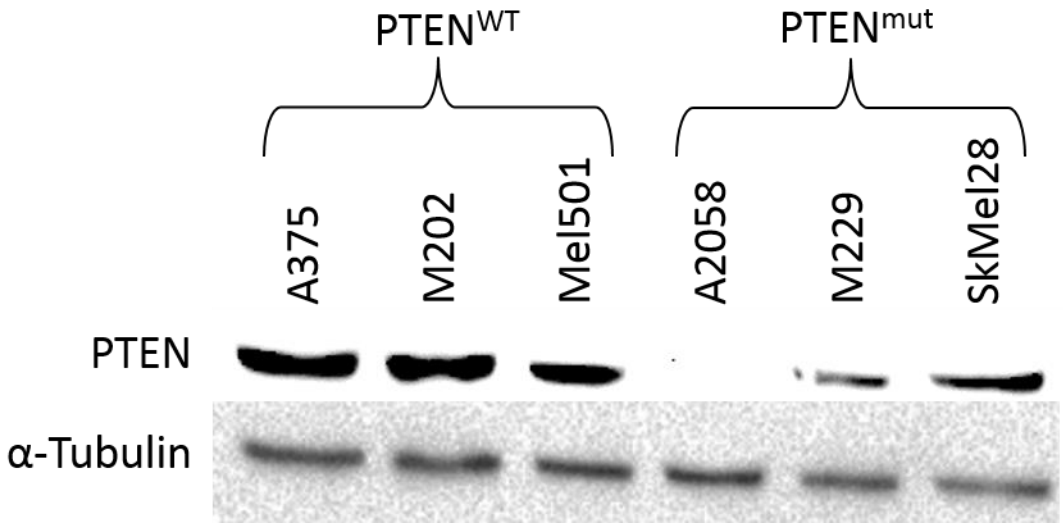


**Figure 4.11: PTEN Expression analysis by Western Blot**
10 µg of cell lysates were separated by SDS-PAGE and transferred on to nitrocellulose membrane. Antibody dilutions used were 1:500 for anti-PTEN and 1:10,000 for anti-α-tubulin. Cell lines A375, M202 and Mel501 are $PTEN^{WT}$. A2058 have a homozygous deletion of PTEN, lines M229 and SkMel28 have a heterozygous deletion for PTEN.

(A2058) or heterozygous (M229 and SkMel28) mutation. Interestingly, these data show that hyper-activated Wnt/β-catenin signalling increases invasion in $PTEN^{Mut}$ cells but reduces invasion in $PTEN^{WT}$ cells.

### 4.6.2. Wnt/β-catenin Signalling Reduces Cellular Migration in $PTEN^{WT}$ cells

It was predicted that, given the previous result in cellular invasion, a similar effect would be seen in cellular migration as the two are often indicative of each other (470). Using a standard scratch assay (471), the monolayer of the Wnt3a overexpression and control melanoma cells was disturbed and an image of the scratch was captured. After 24 hours, the same site was imaged again and the difference in area calculated (see section 2.3.21). Figure 4.12a shows the results were as predicted and match the invasion assay data. The $PTEN^{WT}$ cells show a 0.5 fold reduction in migration and the $PTEN^{Mut}$ cells measure a 0.5 fold increase in response to hyper active Wnt/β-catenin signalling. Figure 4.12b shows representative images of the wound 24 hours after insult. The A375 ($PTEN^{WT}$) overexpression cells showed a reduced migratory effect after 24 hours and the A2058 ($PTEN^{Mut}$) overexpression cells showed the opposite in response to Wnt3a. This matches the invasion capacity of these cells, indicating that activation of the Wnt/β-catenin pathway affects how melanoma cells migrate, which is dependent on PTEN expression to determine whether this effect is promoted or inhibited. This shows that in melanoma cells, activated Wnt/β-catenin signalling increases migration in $PTEN^{Mut}$ cells but reduces migration in $PTEN^{WT}$ cells.

## 4.7. Wnt/β-catenin Signalling Reduces Metastasis of $PTEN^{WT}$ Melanoma Cells in an *In Vivo* Model

*In vitro*, the $PTEN^{WT}$ cells showed a reduction in cellular invasion and the $PTEN^{Mut}$ cells showed an increase (see Figure 4.10). To see if this is translated in an *in vivo* model of metastasis, a tail vein injection study was carried out (see section 2.3.22). This model analyses if the cells form tumours in organs as an indication of

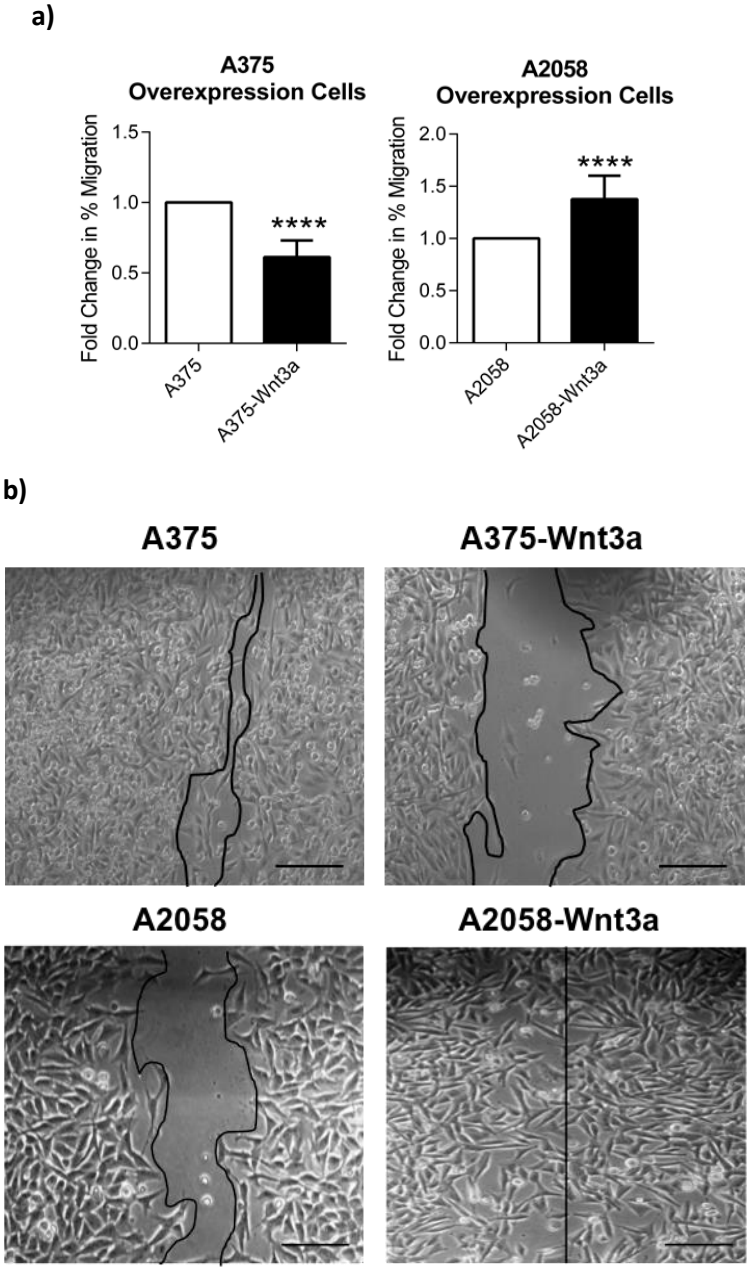


**Figure 4.12 Reduced migration in PTEN intact melanoma cells and increased migration in PTEN null melanoma cells.**

**a)** Cells were stimulated for 48 hours with serum free media, and then seeded at $4x10^5$ cells/well. After 24 hours the monolayer of cells was disturbed with a pipette tip and the assault was marked and imaged. The cells were left for 24 hours when the damaged area was imaged again and the area calculated as a % of the original was calculated, fold change over control was then calculated. **b)** Representative images of migration assay 24 hours after assault. 10X magnification. N=3. Mean shown ± SD. *p* = <0.0001****. Scale bar = 100µm.

metastasis and if there are differences in the size and number of tumours formed by the different cell types (472). The Wnt3a overexpression cells and their respective control lines were injected into the tail vein of NOD-SCID mice and left for four weeks. The cells were prepared and labelled as groups A-D by one researcher before injection by another, to allow for the analysis to be unbiased. This work was carried out at the University of Washingon with help from Dr. Peggy Yang and Rima Kulikauskas. The groups were as follows:

A = A2058-Wnt3a

B = A2058

C = A375-Wnt3a

D = A375

Each group consisted of 6 mice, one mouse from group C and D died at week three, the remaining mice were culled at week four and the lungs were extracted for further analysis. In addition to Wnt3a, the overexpression cells encode GFP allowing them to be easily visualised under a fluorescent microscope (203).

The images shown in Figure 4.13a and 4.13b show a reduction in metastasis between the A375 control and Wnt3a overexpression cells through the reduction of fluorescent tissue in the A375-Wnt3a samples. However, initial analysis showed the same is true for the A2058 cells shown in Figure 4.13c and 4.13d. The *in vitro* invasion assay would have predicted an increase in metastasis but the images show a reduction in the A2058-Wnt3a samples, compared to control.

Further analysis was carried out on the extracted lung tissue samples. Representative images are shown in Figure 4.14 of S100 staining, a commonly used marker for melanoma cells *in vivo* (473). The reduction in metastasis in the Wnt3a samples is clear in both cell lines A375 (Figure 4.14a) and A2058 (Figure 4.14b). This staining was scored independently and the reduction is shown to be significant in both the A375 cells (Figure 4.15a) and the A2058 cells (Figure 4.15b) However, it is clear from the IHC images in Figure 4.14 that the types of tumours formed by the

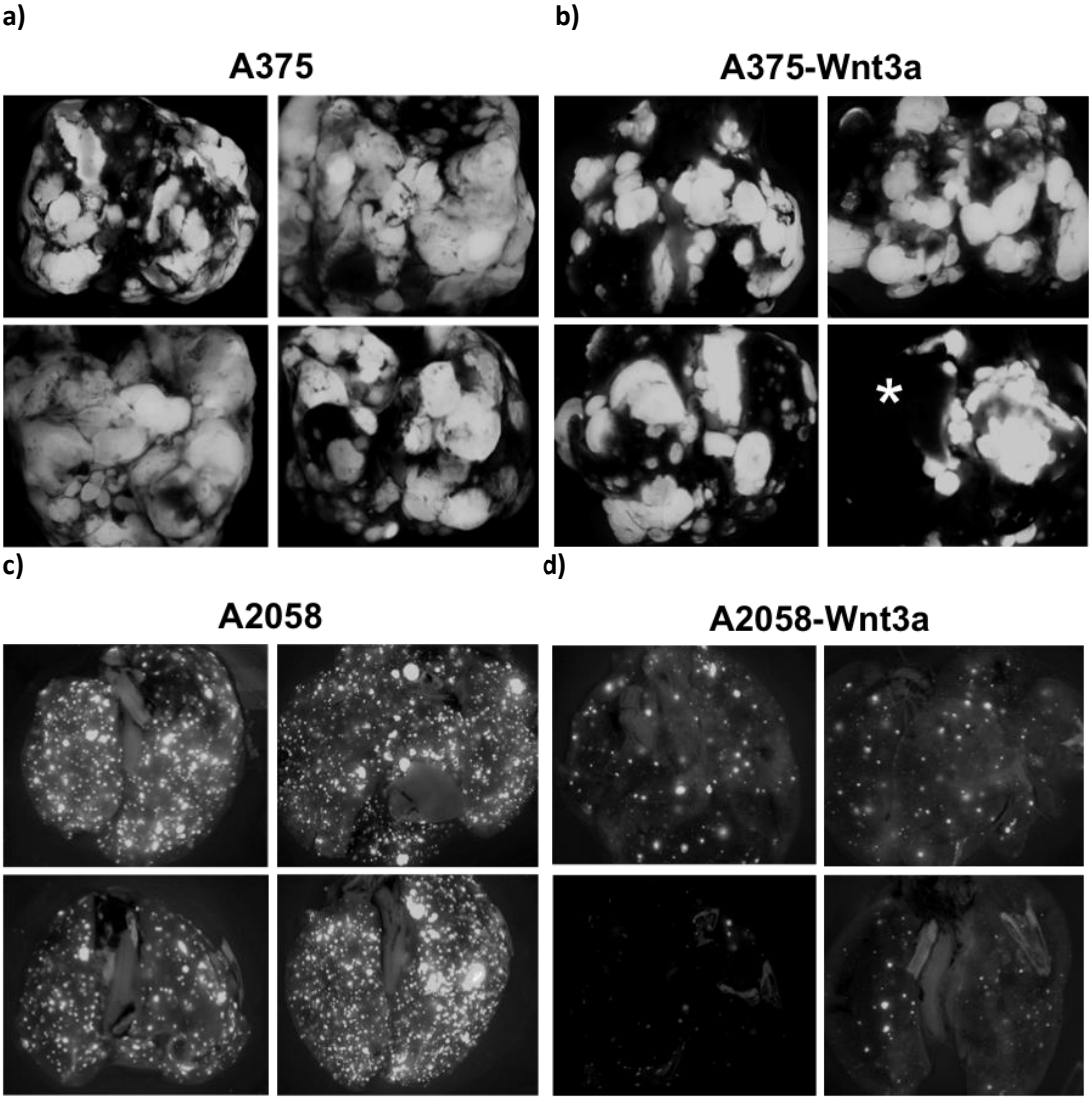


**Figure 4.13: Fluorescent images of Mouse Lungs Following In Vivo Tail Vein Model of Metastasis**

0.75X GFP fluorescence images of mouse lungs following tail vein metastasis model, **a)** A375 **b)** A375-Wnt3a **c)** A2058 d) A2058-Wnt3a. Star indicates a metastasis free lobe.

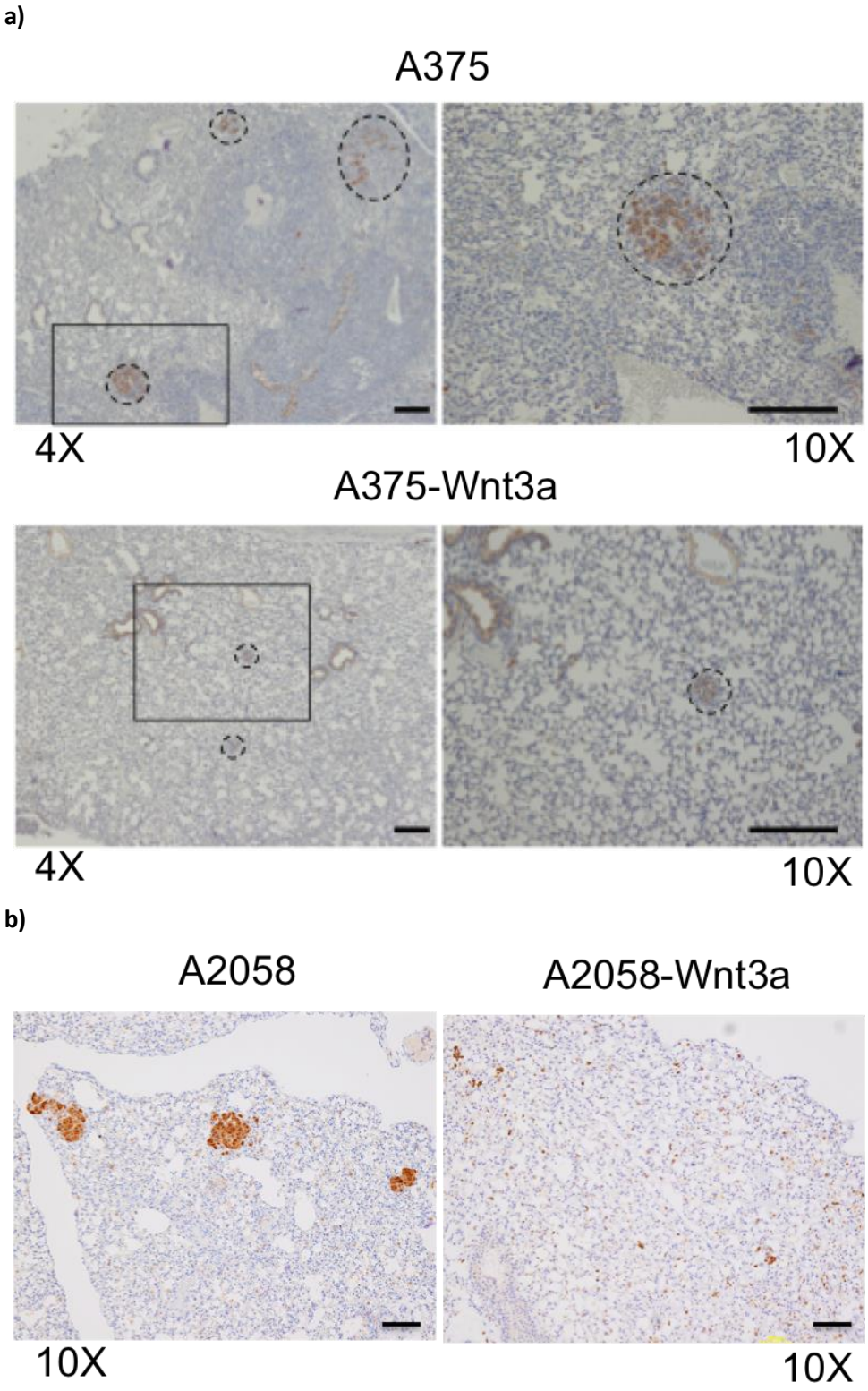


**Figure 4.14: S100 staining of Lung samples**
Representitive images of IHC S100 staining **a)** 4X and 10X images A375 and A375-Wnt3a sections **b)** 10X images of A2058 and A2058-Wnt3a sections. Metastasis and lung boundary are circled by dash lines. Magnified areas are marked by squares. Scale bar = 100 µM.

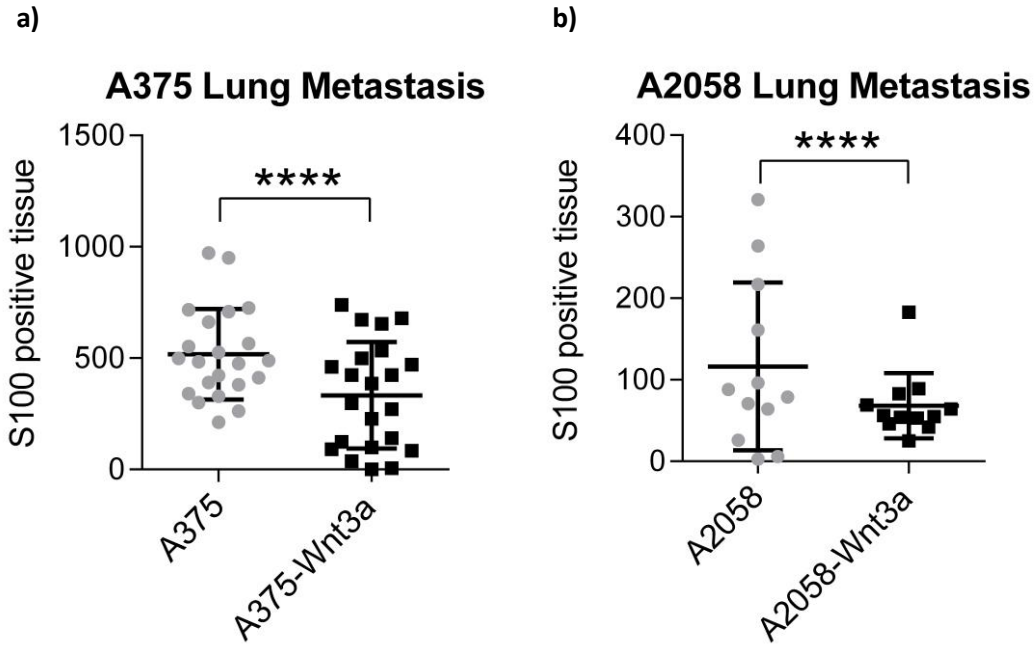


**Figure 4.15: In Vivo model of metastasis.**
Statistical analysis of IHC staining of S100 melanoma specific marker on mouse lung sections n=15 **a)** A375 cells **b)** A2058 cells. Mean shown ± SD. *p* = <0.0001****.

A375 cells are very different to those formed by the A2058 cells. In the A2058 samples, there appears to be a considerable number micro-metastasis, rather than fewer large metastatic tumours. Using the Image J point selector tool, the number of micro-metastasis in the A2058 samples were counted. There were roughly three times more micro-metastasis in the A2058-Wnt3a samples, compared to the control. Figure 4.16 shows a 40X zoomed section of the IHC staining with crosses marking each micro-metastasis. The A2058 control sample has 28, whereas the A2058-Wnt3a sample has 78. This indicated that, although, the S100 scoring showed a decrease, the number of micro-metastasis increased in the A2058-Wnt3a samples and could indicate increased in metastatic burden. *In Vivo*, Wnt/β-catenin signalling causes a reduction in metastasis to the lungs in $PTEN^{WT}$ cells but an increase in $PTEN^{Mut}$ cells.

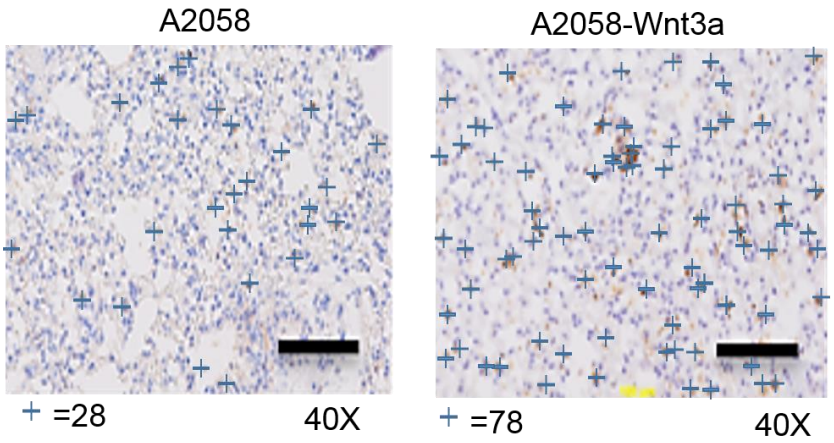


**Figure 4.16: 40X zoomed IHC**

Image J analysis of micro-metastasis in A2058 IHC samples, crosses represent visible micro-metastasis with S100 staining A2058 has 28 micro-metastasis, A2058-Wnt3a has 78 micro-metastasis. Scale bar = 400 µM.

## 4.8. Discussion

Despite the fact that the cell line panel used within this research did not correlate well with either the phenotype switching model nor the tumour initiation model, as shown in Chapter 3, it was interesting to investigate if Wnt/β-catenin signalling had any effects on these models of melanoma progression. As has already been explained, Wnt/β-catenin signalling has been implicated in both models of melanoma progression and therefore it was reasonable to assume it might change the cellular characteristics associated with the two models. However, no effects were seen in either the 3D Matrigel growth nor melanosphere formation with active Wnt/β-catenin signalling. Conversely, other melanoma characteristics such as proliferation, invasion and metastasis were significantly affected by activation of the Wnt/β-catenin pathway. Wnt/β-catenin signalling has been implicated in both the progression (164, 177, 404, 430, 436, 437, 439-441) and regression of melanoma (20, 165, 166, 203, 350, 384, 442-444). This research shows that the effect of Wnt/β-catenin signalling in melanoma is context dependent and that the mutational status of PTEN is playing an important role in dictating the cellular response to active canonical Wnt signalling.

The growth of melanoma cells in 3D Matrigel basement membrane (see Figure 3.1) provided the best distinction of different melanoma cells but it was hard to link these findings to the previously described melanoma phenotypes (334). Despite Wnt/β-catenin signalling being highly relevant in this model of melanoma (364, 385), there was no effect of hyperactive Wnt/β-catenin signalling on switching the invasive/proliferative phenotypes on any of the cell lines tested (see Figure 4.2). Previously, Wnt/β-catenin signalling was linked to this model of melanoma through the phenotype specific expression of genes involved in Wnt signalling which switched between the proliferative expression of MITF and TCF4 and the invasive expression of LEF1 and Wnt5a in a process driven by microenvironmental factors, such as hypoxia and inflammation (361, 365, 385). However, as no switching was seen here (see Figure 4.2), Wnt/β-catenin signalling is not capable of inducing a switch in

melanoma cell phenotype as described by the phenotype switching model (334, 361, 365).

Wnt signalling has also been linked to cancer stem cells with tumour initiation properties (394) but there was no effect of Wnt/β-catenin signalling on the cells' ability to form melanospheres (see Figure 4.4) contrary to previous work (435). It has been suggested that melanosphere formation is an indication of a cancer stem cells' ability to regenerate a growing tumour (474). As stated in Chapter 3, the identification of cancer stem cells from their expression profiles could offer another way of isolating them. However, as yet, a distinct set of markers for melanoma has not been found (367, 392, 415, 416) and we were unable to find consistent data using the previously described markers (see Figure 3.7). It is currently viewed that the most reliable indication of cancer stem cell presence is the ability to form tumours in a xenotransplantation assay, followed by serial *in vivo* xenotransplantation assays (474). Using such models will identify tumour initiating properties within cancer cells. It has previously been suggested that using cells isolated from melanosphere cultures will enhance *in vivo* tumour formation (370, 406, 414) but it has, in fact, been shown by Perego *et al.* that the ability to form tumours in xenotransplantation assays showed no difference in cells from melanospheres or adherent cultures (363). Instead, this assay showed that both cultures contained cells with tumour forming abilities and, therefore, contained cancer stem cells. As there was no effect of Wnt signalling on the formation of melanospheres in these cells, it was unnecessary to continue with serial passages in immunocompromised mice. In summary, Wnt/β-catenin signalling does not increase the growth of melanospheres and does not appear to enhance the number of melanoma cancer stem cells within the cell lines tested.

When testing the effects of the Wnt/β-catenin pathway on cellular characteristics, it was possible to validate a number of already published findings. We also found a distinct pattern in the cells' ability to move and invade, based on their PTEN status. It has previously been shown that Wnt/β-catenin signalling can reduce melanoma cell proliferation and increase melanoma cell apoptosis (203, 344, 353), effects that we were able to replicate (see Figures 4.6 - 4.9). The proliferation was measured

over long periods of growth, gradually decreasing the population doubling rate in cells with active Wnt/β-catenin signalling, over time confirming work by Chien *et al* (203). An increase in apoptosis was measured by an increase in cytochrome *c* release and by an increase in apoTRACE indicating changes to the plasma membrane, a finding supported by other groups (353). As it is known that the Wnt signalling pathways can be opposing of each other (167, 424), the increase in apoptosis in response to Wnt3a is supported by the reduction in apoptosis seen in response to Wnt5a in melanoma and other cancers (42, 223). However, these results are in contrary to previous studies showing that inhibition of Wnt/β-catenin signalling can induce apoptosis in lung, breast and colorectal cancers (475-477). An increase in apoptosis could be explained by a cell cycle arrest (467). Cells that have damaged DNA will sense that they are no longer functional and target themselves for destruction, a process that is often perturbed in cancer (478). However, as was clear from our analysis, there is no cell cycle arrest in these cells (see Figure 4.10) as there is no expansion of any individual phase of the cell cycle in response to active Wnt/β-catenin, nor are there any differences between the two cells types with the percentages of cells at each stage remaining consistent. Thus Wnt/β-catenin signalling decreases proliferation and initiates apoptosis in melanoma cells.

Throughout the proliferation, apoptosis and cell cycle analysis, all melanoma cells were responding to rWnt3a stimulation or Wnt3a overexpression in the same way. However, it was when the cells were assessed on their ability to migrate and invade that we detected significant differences between them, based on PTEN expression. In a standard scratch assay and a transwell invasion assay through Matrigel, the same pattern was seen across the whole panel of cells, with the $PTEN^{WT}$ cells showing significant decreases in cell motility and $PTEN^{Mut}$ lines measuring significant increases in response to active Wnt/β-catenin signalling. A reduction in migration and invasion could be due to changes in cell adhesion (463). This seems especially possible as Wnt5a has been shown to increase cell adhesion and subsequent invasion and metastasis in melanoma (222, 460). Decreased melanoma cell invasion and metastasis due to active Wnt/β-catenin signalling has been published by other groups (142, 143, 165, 384). Bosenberg's genetically engineered mouse model uses

a variety of genetic backgrounds common to human melanoma to investigate the role of Wnt/β-catenin signalling in melanoma initiation and progression. When β-catenin signalling was constitutively active in a model of mutated Braf and PTEN (PTEN/Braf/βcat-STA), there were high levels of metastasis to the lungs, spleen and bowel, the mice had shorter life expectancy and tumours were large and pigmented (143). Linking this to the fact that the majority of melanoma related deaths are due to distant metastasis (479), these findings indicate that this genetic phenotype (PTEN/Braf/βcat-STA) exhibits poor prognosis and led to the lowest survival rate in these animals. This is comparable to the increased invasion we observed in the A2058-Wnt3a cells (see Figure 4.10). It has previously been shown that the aggressiveness of breast cancers can be determined by its PTEN status (480) and that the role of β-catenin is highly context dependent (481). This research corroborates these previous findings in a melanoma model. However, this study focused on the increased aggressiveness of tumours with a PTEN/Braf background. PTEN mutations are seen in 30-50% of melanoma patients (146), whereas Braf mutations are seen in nearly 70% of melanomas (142), indicating that there are other models of aggressive melanoma still to be studied. Bosenberg's model also only focused on Braf mutations but there are other mutations of the MAPK pathway, including those of Nras seen in the M202 cells, and up to 29% of melanoma patients (137). Therefore this too has clinical relevance and models of Nras interaction with β-catenin (435) and PTEN (145) also show high rates of melanoma formation in transgenic mouse models. Based on this, it is important to see if the differences measured *in vitro* were also seen *in vivo*.

In order to investigate if the $PTEN^{WT}$ and $PTEN^{Mut}$ cells responded to activated Wnt/β-catenin signalling *in vivo* in the same manner as *in vitro*, the Wnt3a overexpression cells and their controls were injected into the tail vein of NOD-SCID mice and the lung metastasis were analysed after 4 weeks growth (see Figure 4.13-4.16). *In vivo*, the $PTEN^{WT}$ A375 cells match the *in vitro* cell invasion assay; Wnt3a causes a reduction in metastasis to the lungs compared to the control cells. However, the $PTEN^{Mut}$ A2058 cells did not initially produce the expected result with the Wnt3a cells also causing reduced metastasis to the lungs as measured by S100 staining, contradicting the *in vitro* invasion assay results. However, upon further analysis, the tumour formation

between the two cell lines was vastly different. The $PTEN^{WT}$ cells form large tumours that are clearly visible, whereas the $PTEN^{Mut}$ cells form much smaller punctate tumours. Due to this, an alternative form of analysis was undertaken and the number of micrometastasis in the tumour samples was recorded. The $PTEN^{Mut}$ cells with activated Wnt/β-catenin showed substantial increase in the number of micrometastasis, potentially indicating an increase in tumour burden.

The differences in tumour formation between the two cell types could be due to the changes in relative cell growth and apoptosis. The $PTEN^{Mut}$ cells have a lower population doubling rate that the $PTEN^{WT}$ cells (see Table 4.1) and this could suggest the smaller tumour size. An alternative reason for this could be described by Paget's theory of Seed and Soil (482, 483) as they are different cells from different patients and, therefore, differences between them should be expected. Using Paget's theory, it is possible the $PTEN^{Mut}$ cells metastasise to different organs better than the lungs, due to other factors such as the environment or genetics. Therefore, comparing metastasis of both cell lines to just the lungs might not be sufficient. As shown by Bosenberg's model, metastasis was seen to the lymph nodes, lungs, spleen and bowel at varying levels (143), indicating other organs should be considered in future analysis. One future possible approach in order to investigate the effects of the genetic background on melanoma metastasis, would be ideal to alter the PTEN status of the cells. To do this, a PTEN knockout would be needed in the A375 cells and to knock-in PTEN in the A2058 cells, comparing each to their own controls. This would strongly confirm that the effects of canonical Wnt signalling on metastasis were dependent on PTEN.

These findings show that, in advanced melanoma, the activation of the Wnt/β-catenin pathway can have both beneficial and detrimental effects on the progression of the disease. If patients could be stratified, based on their PTEN status, potentially those patients with both an activating BRAF mutation and an inactivating PTEN mutation could be treated with Wnt inhibitors to reduce invasion and metastasis. Currently, in clinical trials for prostate cancer (484), small molecular inhibitors targeting Porcupine blocking the palmitoylation of Wnt ligands and their subsequent

secretion have proved beneficial in breast and head and neck cancer (485-487) and, in this specific genetic context, could be beneficial for melanoma patients.

### 4.8.1. Summary

Activation of the Wnt/β-catenin pathway had little effect on the phenotype switching or tumour-initiation models of melanoma. However, there were significant effects on cell growth and cell death, which were similar across the cell lines tested. The cells differed dramatically in their ability to migrate, invade and metastasise, which was dependent upon their PTEN status. $PTEN^{WT}$ cell lines showed reduced invasion, migration and metastasis, whereas $PTEN^{Mut}$ cell lines showed an increase in response to active Wnt/β-catenin signalling. This novel finding could be exploitable in the treatment of metastatic melanoma. It would now be interesting to investigate how these genetic differences affect other aspects of cancer cell behaviour, such as tumour metabolism and the mechanism that controls the changes in cellular invasion.

# 5. THE EFFECTS OF THE WNT/β-CATENIN SIGNALLING PATHWAY ON THE METABOLISM AND MITOCHONDRIA OF MELANOMA CELLS

## 5.1. Introduction

Altered cellular metabolism in cancer cells has been known since it was first described by Otto Warburg in 1924, when he showed the switch to aerobic glycolysis from aerobic respiration, where the production of ATP occurs through glycolysis rather than the TCA cycle (9). However, initially this was wrongly attributed to the dysfunction of the mitochondria. The study of cellular metabolism has since discovered that the mitochondria of cancer cells are not non-functioning but, instead, have altered metabolism to increase fatty acid synthesis and glutamine driven metabolism (242, 281, 318). Using the findings from Chapter 4 showing Wnt3a has differing effects on genetically diverse melanoma cell types, the hypothesis was suggested that; Wnt3a would have differing effects on melanoma metabolism, depending on their specific mutational backgrounds.

### 5.1.1. The effects of Wnt signalling on Cell Metabolism

In cells, processes such as proliferation, apoptosis, differentiation and growth arrest are intrinsically linked to changes in metabolism. Increased proliferation associated with cancer growth requires a shift in metabolism to produce the extra energy required for rapid cell division (319). This shift, typically seen in cancer cells, is termed the Warburg effect and involves metabolism changes from oxidative phosphorylation (OXPHOS) to glycolysis, even in the presence of oxygen known as aerobic glycolysis (276). This shifts the way energy is produced by the cells, but also increases the amount of macromolecules and lipid biosynthesis which is needed for biomass production for accelerated cell proliferation (488). Many oncoproteins not only activate proliferative and anti-apoptotic pathways, but also trigger metabolic changes in order to transform cells (489). For example, changes in cancer metabolism cause increased lipogenesis of signalling lipids such as phosphatidylinositol, phosphatidylserine or phosphatidylcholine, which subsequently regulate proliferation and apoptosis through signalling pathways such as PI3K/Akt, RAS and Wnt (490). In addition to this, the structure of Wnt proteins themselves can also be modified by fatty acids from increased lipogenesis and

therefore, Wnt oncogene properties can be activated in response to changes in fatty acid metabolism (489-491).

There are a number of different pathways that connect apoptosis to metabolism and the mitochondria (492) and many of these have links to the Wnt/β-catenin signalling pathway. Section 4.5.2 showed the Wnt/β-catenin pathway increased cell death in melanoma cells. This included increases to cytochrome *c*, a component of the apoptosis pathway (269-271), and metabolism via the ETC (268). It has been shown that both Wnt3a (193) and Wnt1 (493), another commonly β-catenin-dependent Wnt ligand, suppress cytochrome *c* oxidase in breast cancer. Other connections of the Wnt pathway to the mitochondria include mutated APC proteins accumulating at the mitochondria preventing apoptosis (494). APC mutations are common in colorectal cancer (428, 429), it is known that the Wnt/β-catenin pathway often has opposing effects in both colorectal and breast cancer compared to those seen in melanoma.

It has already been shown that Wnt ligands alter cancer metabolism (191, 195, 495). Wnt5a, a commonly non-canonical Wnt ligand, effects both melanoma and breast cancer cell metabolism (448) where, unsurprisingly, given its known role as either a tumour suppressor, as in breast cancer tumours or oncogene, as in melanocytic tumours (496), its effects on metabolism vary between tumour types. Specifically, β-catenin-independent Wnt signalling increased aerobic glycolysis in malignant melanoma cells through elevated Akt signalling and lactate dehydrogenase (LDH) activity whereas, in breast cancer cells, Wnt5a increased OXPHOS (448). As it is already well established that the canonical and non-canonical pathways oppose each other (428), it suggests that Wnt3a, a predominantly canonical Wnt ligand, could also affect melanoma cell metabolism (potentially in an opposite way to that of Wnt5a). It has been shown that C2C12 cells, a murine muscle cell line, responded to Wnt3a signalling with an increase in OXPHOS and mitochondrial mass. Increased oxygen consumption was also seen in adipocytes, along with enhanced mitochondrial gene expression in response to active β-catenin signalling (235). It has also been shown in hepatocytes that activation of the Wnt/β-catenin pathway up-regulated genes

involved in glutamine metabolism (190). Interestingly, the Wnt/β-catenin pathway is further implicated in the control of metabolism as a number of metabolism genes contain TCF/LEF response elements in their promoters (497). Collectively this research suggests that the Wnt signalling network is a regulator of cancer cell metabolism.

### 5.1.2. The Roles of Wnt Signalling on the Mitochondria

The function and structure of mitochondria are described in detail in Chapter 1 but, briefly, they are the main source of energy for eukaryotic cells. A cell's mitochondrial content is directly regulated by the metabolic requirements of the cell (498). As highly dynamic organelles, they are capable of changing size, shape and location. Typically described as rod shaped structures, they can range in size from 1-10 µm in length, depending on the processes of fusion and fission which occur primarily to regulate the health of cells (499). In 2010, Yoon *et al.* showed that Wnt3a could affect mitochondrial shape and function in C2C12 cells (495). Wnt5a signalling in a $Ca^{2+}$-dependent manner has also been shown to play a role in mitochondrial fusion and fission in rat neurons (500) and, through the Wnt/PKC pathway, has been shown to regulate mitochondrial distribution and dynamics by degradation of Alex3 protein, part of the KIF5/Miro/Trak2 protein complex (501). It is known that the shape of the mitochondria is linked to cell death (249, 502) and, as explained, above (see section 5.1.1) the Wnt pathway can directly affect apoptosis in cells, cancer and specifically, in melanoma (350, 503), therefore potentially linking Wnt to mitochondrial shape. For example, the Bcl-2 family are regarded as regulators of apoptosis but have recently been linked to mitochondrial dynamics (504). This family of genes are intrinsically linked to the Wnt pathway (494, 505, 506) and provide a direct link between the processes. Currently, we do not know how the Wnt/β-catenin pathway regulates mitochondrial shape and whether this is controlled through manipulations of mitochondrial dynamics. Furthermore, it is currently unknown if the Wnt/β-catenin pathway regulates mitochondrial shape and function in cancer cells. These are all important questions that require further investigation.

### 5.1.3. Aims

The aims of this chapter are to assess the effects of active Wnt/β-catenin signalling on melanoma cell metabolism and their mitochondria, specifically comparing the effects upon melanoma cells with $PTEN^{WT}$ to those with a deletion within the PTEN gene ($PTEN^{Mut}$). Cellular metabolism will be investigated through live cell flux analysis as well as biochemical analysis of the cells. This will include analysis of basal metabolism, the response to Wnt/β-catenin signalling and their function in low glucose. Confocal imaging with the use of a mitochondrial specific dye will be used to carry out investigations into the mitochondrial structure and any changes due to Wnt/β-catenin signalling. Comparisons will also be made between mitochondria of melanoma cells and non-cancerous melanocytes. To assess if there is any effect on the mitochondrial content of the cells, qPCR and flow cytometry will analyse mitochondrial number. Finally, this chapter will determine if any effects are dependent on activation of the Wnt/β-catenin signalling pathway or on β-catenin itself and if the differences seen can be reversed with the PTEN status of the cells.

## 5.2. Wnt/β-catenin Signalling Changes Melanoma Cell Metabolism

### 5.2.1. Melanoma Cell Metabolism is Affected by Wnt/β-catenin Signalling

In order to analyse the cellular metabolism of the melanoma cells including their aerobic respiration and glycolytic capacity the $PTEN^{WT}$ and $PTEN^{Mut}$ cells were analysed on the Seahorse $XF^e96$ Extracellular Flux Analyzer. This 96-well plate-reader is capable of analysing the Oxygen Consumption Rate (507) and Extracellular Acidification Rate (507) of live cells, thereby analysing mitochondrial respiration and glycolysis simultaneously. Following the standard protocol for the Mito Stress Test Kit (see section 2.3.23), at known time points, compounds are injected on to the cells and the changes in OCR and ECAR can be measured, allowing the calculation of a number of different metabolic parameters. Indicated in Figure 5.1a, the following compounds are injected through the built-in compound injection ports, A = Oligomycin, B= FCCP, C = Antimycin A and Rotenone. Oligomycin is an ATP synthesis inhibitor. It blocks the proton channel necessary for oxidative phosphorylation of ADP to ATP and will cause a reduction in the flow of electrons through the electron transport chain (ETC) (508). Carbonyl cyanide-*4*-(trifluoromethoxy)phenylhydrazone (509) is a mitochondrial uncoupler that causes ETC acceleration by dissipating the proton gradient and causing an increase in the flux of electrons (510), leading to a subsequent depolarisation of the mitochondrial membrane and inhibition of OXPHOS (511). Antimycin A and Rotenone are inhibitors of complex III and complex I of the ETC, respectively. Antimycin A binds to the quinone reduction site of the cytochrome bc1 complex, whereas Rotenone inhibits the transfer of electrons from iron-sulfur centers in complex I to ubiquinone. This prevents NADH from being converted into ATP (508, 512). Following the assay, the data was normalised to cell number calculated from a Hoechst stain (see section 2.2.23) and the following readings were calculated (511) - Basal Respiration is the steady OCR reading before any injections; ATP Production was calculated as the change in OCR before and after oligomycin injection (injection A). Maximal Respiratory Capacity is the OCR reading following FCCP injection (injection B) subtracting non-mitochondrial respiration. Non-mitochondrial respiration is the final OCR reading following injection of

Antimycin A and Rotenone (injection C). Protein leak is the OCR reading following Oligomycin injection (injection A), subtracting non-mitochondrial respiration. Basal ECAR is the steady ECAR reading before any injections. This is shown in graphical form in Figure 5.1a.

The raw data shown in Figure 5.1b+c are representative traces of OCR and ECAR readings using the A375 and A2058 Wnt3a overexpression and control cells. It is clear that the A375 cells (Figure 5.1b) show the opposite pattern to the A2058 cells (Figure 5.1c) in response to increased Wnt3a expression. Wnt3a overexpression in A375 cells causes lower OCR and ECAR readings, compared to their cognate control cells. This is in contrast to the higher OCR and ECAR levels observed in the A2058 cells in response to Wnt3a overexpression. Figure 5.2 shows the data following these calculations. The A375 Wnt3a overexpression cells showed a significant reduction, compared to control cells, in every metabolism parameter measured; basal respiration, ATP production, maximal respiratory capacity, non-mitochondrial respiration, proton leak and basal ECAR. Conversely, the results from the A2058 cells indicated that every parameter was possibly increased in the Wnt3a overexpression cells compared to control cells, but not significantly. Thus, activating the Wnt/β-catenin signalling pathway causes a global downregulation of cellular metabolism in $PTEN^{WT}$ melanoma cells, which is not observed in $PTEN^{Mut}$ melanoma lines.

The Seahorse $XF^{e}96$ Extracellular Flux Analyzer is also capable of analysing ECAR response in no glucose conditions using the Glycolysis Stress Test Kit (see section 2.3.24). Using media with added L-Glutamine, instead of glucose, the basal ECAR shows the minimum glycolysis activity, gradually increasing the amount of glucose in the media through two subsequent injections will increase the glycolysis levels. The injection of oligomycin will have the same effect, as seen in the cell mito stress test kit, inhibiting ATP synthesis and causing the ECAR to increase. Finally 2-DG, a glycolysis inhibitor (348), is injected, causing the ECAR reading to fall back to their minimum levels, allowing any non-glycolytic ECAR to be analysed. 2-DG does this by competitively inhibiting the production of glucose-6-PO4 from glucose at the

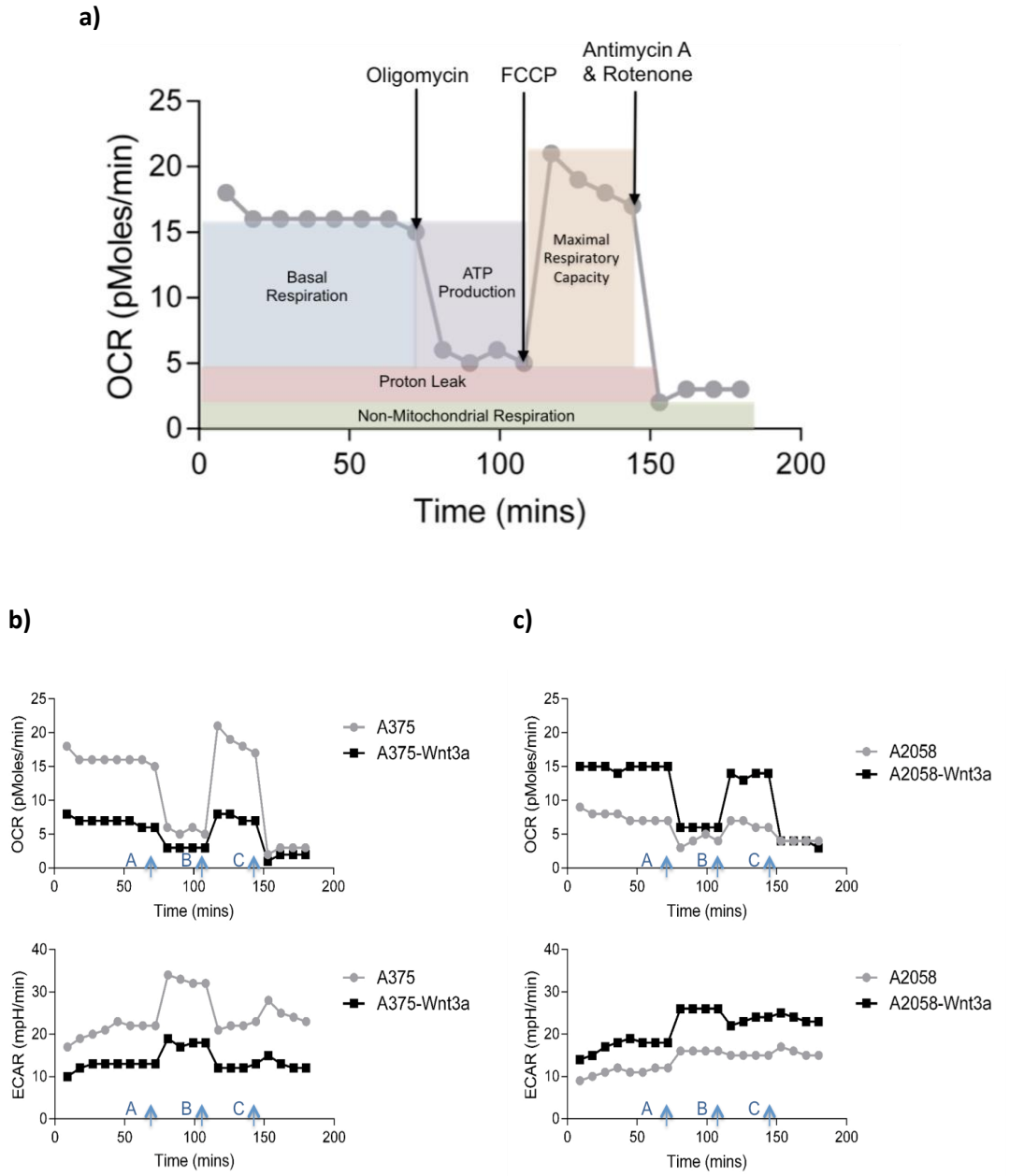


**Figure 5.1: Seahorse Mito Stress analysis of A375 and A2058 cells**.
**a)** Using the changes in OCR readings due to compound injections various metabolic parameters can be calculated. Image Adapted from http://www.seahorsebio.com **b)** Representative traces of OCR and ECAR from $PTEN^{WT}$ A375 overexpression cells. **c)** Representative traces of OCR and ECAR from $PTEN^{Mut}$ A2058 Wnt3a overexpression cells. Arrows indicate point of compound injections; A=oligomycin, B=FCCP, C=Antimycin A and Rotenone.

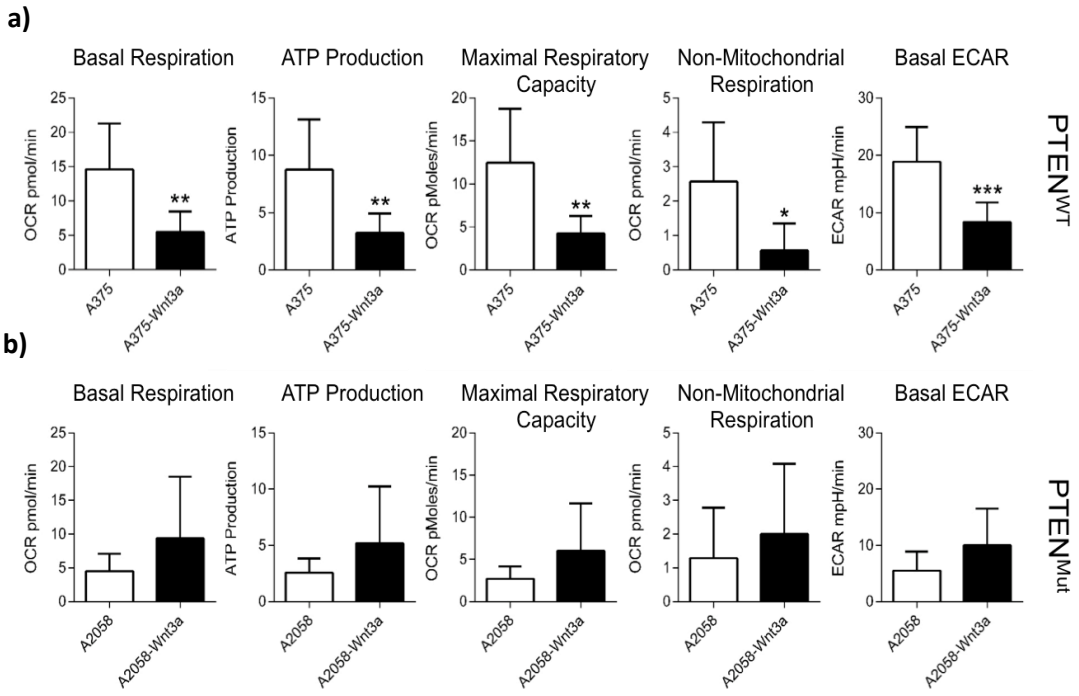


**Figure 5.2**: **Seahorse Mito Stress Analysis of A375 and A2058 cells**.
**a)** A375 and **b)** A5058 Wnt3a overexpression and control cells were seeded at $8x10^3$ cells/well into PDL coated Seahorse 96 well plates. Compounds were diluted as described and loaded into the companion plate. The assay was run as described (section 2.3.23) and data was normalised to cell number before the following calculations were done: Basal Respiration is the steady OCR reading before any injections. ATP Production was calculated as the change in OCR before and after oligomycin injection (injection A). Maximal Respiratory Capacity is the OCR reading following FCCP injection (injection B) subtracting non-mitochondrial respiration. Non-mitochondrial respiration is the final OCR reading following injection of Antimycin A and Rotenone (injection C). Protein leak is the OCR reading following Oligomycin injection (injection A) subtracting non-mitochondrial respiration. Basal ECAR is the steady ECAR reading before any injections. N=8. Mean shown ± SD. $p$ = <0.05*, <0.01** or <0.001***. Not significant (Ns).

phosphoglucoisomerase level as it is the same as a glucose molecule with a hydrogen in place of the 2-hydroxyl group (513). An initial dose response assay was set up to gather the optimum amount of glucose to use in a Glycolysis Stress Test, the results are shown in Figure 5.3. Both the A375 and the A2058 cells responded to the addition of compounds. However, what was apparent was that the concentration of glucose did not seem to have an effect on the A375 cells with the reaction across the different doses seemingly having no effect (see Figure 5.3a+b), nor was there any difference between the control and the Wnt3a overexpression cells. In the A2058 cells, however, there was an effect of the dose response in the control and the Wnt3a overexpression cells (see Figure 5.3c+d). In both cell lines, the patterns of ECAR seen in the Cell Mito Stress Test are seen here; in the A375 cells, the control cells have higher ECAR than the Wnt3a and the reverse is seen in the A2058. In both, the 5 mM concentration of glucose (which is the concentration in the standard growth media) gave the highest readings, implying that excessive glucose does not increase glycolysis in the A2058 cells. Figure 5.4 shows that the A2058-Wnt3a cells respond to a statistically higher level than the A375-Wnt3a cells in the Glucose Stress Test at 5 mM glucose. This could indicate a preference for glutaminolysis in A375 cells, whereas the A2058 cells are more reliant on glycolysis. This shows that glycolysis in A375 cells is not necessarily dependent on the amount of glucose present, but that the A2058 cells are potentially more reliant on glucose. This data highlights that basal metabolism of melanoma cells in culture varies, as would be expected. Importantly however, regardless of differences in basal metabolism our data shows that Wnt3a expression is able to dramatically alter basal metabolism of melanoma cells.

### 5.2.2. TCA Cycle Activity is Reduced in PTEN$^{WT}$ Cells

Next we wanted to confirm the Seahorse OCR data. So we decided to use biochemical analysis of citrate synthase levels. As the first enzyme of the TCA cycle, levels of citrate synthase are a measurement of TCA cycle activity (304). Citrate synthase catalyses the condensation reaction of the two-carbon acetate residue from acetyl coenzyme A, and a molecule of four-carbon oxaloacetate, to form the six-

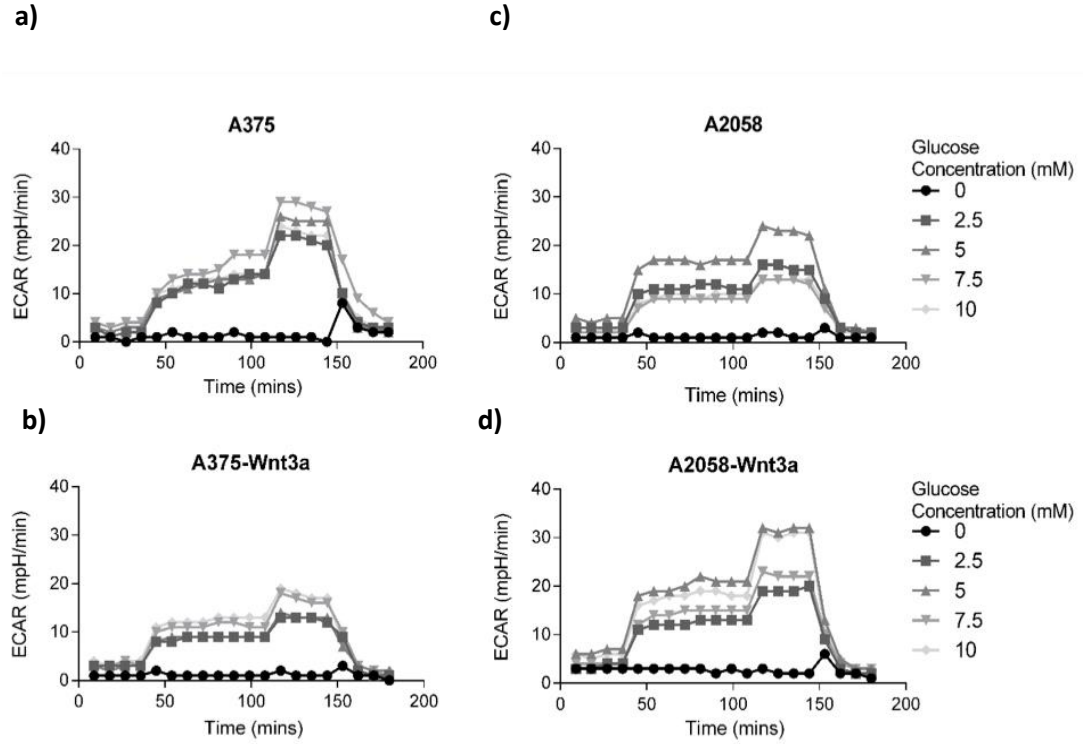


**Figure 5.3: Seahorse Glycolysis Analysis of A375 and A2058 Cells.**
Representative traces of ECAR from A375 and A2058 Wnt3a overexpression cells following the Glycolysis Stress Test. **a)** A375, **b)** A375-Wnt3a, **c)** A2058, **d)** A2058-Wnt3a. Cells were seeded at $8x10^3$ cells/well into PDL coated Seahorse 96 well plates. Glucose was added to the cells at various concentrations, followed by the injection of Oligomycin and 2-DG. The assay was run as described and data was normalised to cell number. N=4.

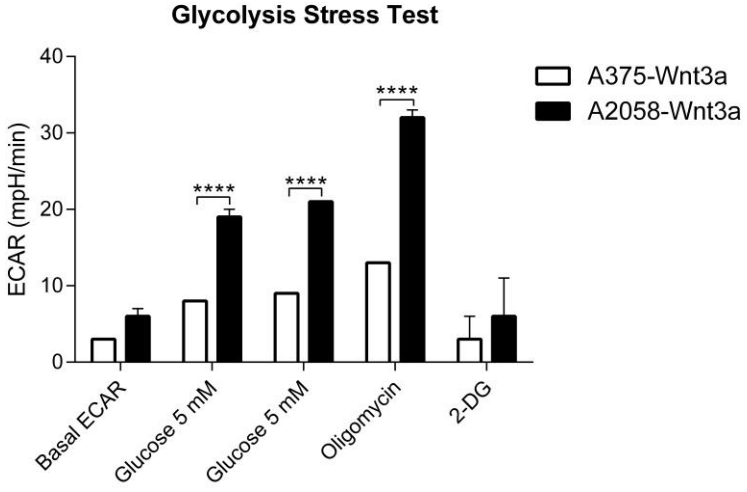


**Figure 5.4: A2058-Wnt3a Cells have Higher ECAR in a Glycolysis Stress Test at 5 mM Glucose compared to A375-Wnt3a Cells**
Data extrapolated from the Glycolysis Stress Test in Figure 5.3. The average ECAR values from A375-Wnt3a and A2058-Wnt3a overexpression cells were calculated following each compound injection. The data was taken from the 5 mM glucose level. N=4.

carbon citrate (514). Citrate synthase levels (see section 2.3.25) were measured in the whole panel of melanoma cells, normalised to total protein levels and can be represented as fold change compared to the control cells (see Figure 5.5). The $PTEN^{WT}$ cells (A375, M202, Mel501 and A375-Wnt3a overexpression cells) all showed a significant decrease (between 0.7 fold and 0.2 fold, in citrate synthase activity), verifying the results that OXPHOS in these cells is decreased as previously indicated by the Seahorse Flux analysis. The $PTEN^{Mut}$ cells, however, showed mixed results; two cell lines, A2058 and M229, showed a significant 1.3 and 1.6 fold increase respectively, whereas SkMel28 and the A2058-Wnt3a overexpression cells showed a 0.5 and 0.7 fold decrease to significant levels. This suggests that in $PTEN^{Mut}$ melanoma cells, hyperactive Wnt3a signalling produces inconsistent effects on citrate synthase activity, which could be representative of differences in basal metabolism between the $PTEN^{Mut}$ cell lines. Taken together, this data suggests that on $PTEN^{WT}$ cells, Wnt/β-catenin activity reduces oxidative metabolism but has less predictable effects in $PTEN^{WT}$ cells.

### 5.2.3. Lactate Secretion in $PTEN^{WT}$ Melanoma Cells is Reduced

In order to confirm the Seahorse ECAR data, we wanted to use biochemical analysis of LDH activity by measuring lactate secretion from the cells. Lactate is secreted by cells following the conversion of pyruvate to lactate by lactate dehydrogenase (515). Measurement of lactate (see section 2.3.26) can provide an indication of the glycolytic activity of cells. Cancer cells tend to have increased glycolytic respiration and, therefore, the lactate secretion is expected to be high (9). Figure 5.6 shows total lactate secretion that was normalised to protein concentration and represented as fold change compared control cells.

The panel of four $PTEN^{WT}$ cells all showed between 0.5 and 0.8 fold significant decreases in lactate secretion. The ECAR results seen in Figure 5.2 indicated a reduction in cellular acidification in A375 cells in response to Wnt3a overexpression cells so the lactate secretion data corroborates these findings (Figure 5.6). Lactic acid will be one of the main components of this measurement and, therefore, supports the lactate secretion results shown here. The $PTEN^{Mut}$ cells all showed between a 1.1

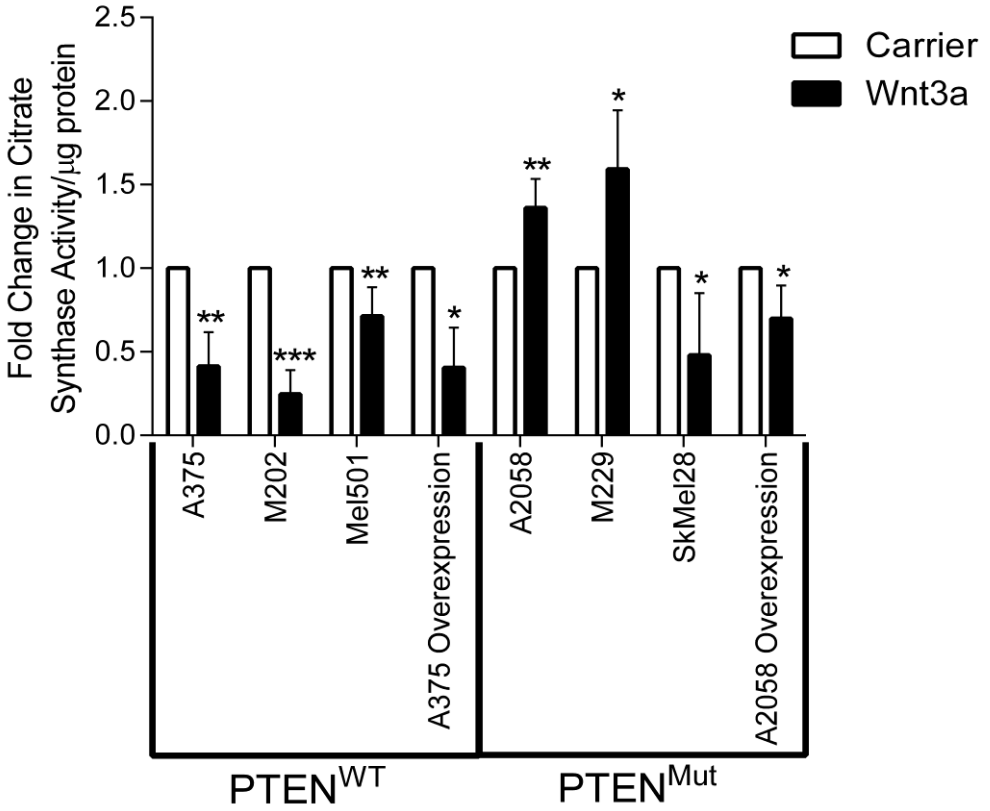


**Figure 5.5: Citrate Synthase Activity is Reduced in PTEN$^{WT}$ Cells in Response to Wnt/β-catenin**

Melanoma cells were seeded at 2x10$^5$ cells/well before being stimulated for 48 hours with either rWnt3a at 50 ng/ml, carrier control or (for the overexpression cells) serum free media. A BCA was carried out to normalise data to total protein concentration and fold change in citrate synthase activity compared to control was calculated. N=4. Mean shown ± SD. *p* = <0.05*, <0.01** or <0.001***.

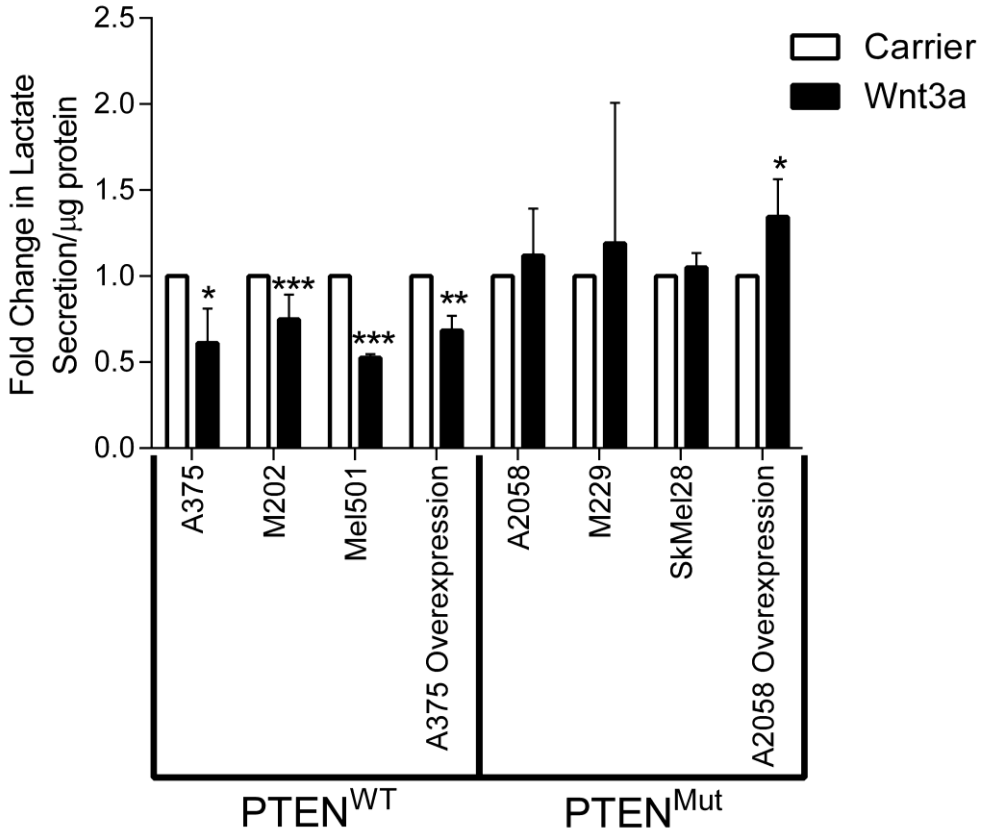


**Figure 5.6: Lactate Secretion is Reduced in PTEN$^{WT}$ Cells in Response to Wnt/β-catenin**
Melanoma cells were seeded at 2x10$^5$ cells/well before being stimulated for 48 hours with either rWnt3a at 50 ng/ml, carrier control or (for the overexpression cells) serum free media. Cell supernatants were stored at -80°C overnight before the assay was carried out. A BCA allowed for normalisation of data to total protein concentration and fold change compared to control was calculated. N=4. Mean shown ± SD. *p* = <0.05*, <0.01** or <0.001***.

and 1.3 fold increase in lactate secretion, but only the A2058 Wnt3a overexpression cells were measured to a significant level. Wnt/β-catenin signalling reduces glycolysis in PTEN$^{WT}$ melanoma cells and has no effect in the PTEN$^{Mut}$ cells, albeit the trend indicates it may increase lactate secretion from PTEN$^{Mut}$ cells.

### 5.2.4. Wnt/β-catenin Signalling Reduces ROS Production in PTEN$^{WT}$ Cells

Reactive Oxygen Species (ROS) are involved in the regulation of many different physiological processes and the production of ROS, to a certain level, is required for normal cellular homeostasis (516). In melanoma, high ROS levels have been linked to increased melanin production and apoptosis via Bax, but lower levels have been seen to increase proliferation and reduce apoptosis (241). One of the main sources of ROS is the mitochondrion. Using the Wnt3a overexpression cells, total cellular ROS was measured (see section 2.3.27) and represented as fold change, compared to control cells. In Figure 5.7, the A375-Wnt3a cells showed a 0.8 fold significant reduction in cellular ROS, whilst the A2058-Wnt3a cells showed a 1.1 fold increase, which was not however significant. Taken together, these results shown that Wnt/β-catenin signalling reduces ROS production in PTEN$^{WT}$ melanoma cells, but has no significant effect on PTEN$^{Mut}$ cells.

### 5.2.5. Glucose Consumption is Increased in Melanoma Cells

Glucose is animal cells' main source of energy. It is taken into the cells and used in the process of glycolysis in both aerobic and anaerobic respiration. Cancer cells typically have higher glucose intake, as the glycolytic phenotype only produces 2 molecules of ATP per molecule of glucose through glycolysis, but they need more energy to keep up with the demand for higher proliferation rates (277). This enzymatic, glucose determination assay (see section 2.3.28) allows the amount of total cellular glucose to be measured by assessing the amount of NAD reduced to NADH. NADH is fluorescent and NAD is not. The change in the fluorescence is proportional to the concentration of glucose as the reaction is equal to the phosphorylation of Glucose to Glucose-6-phosphate and the oxidation of Glucose-6-phosphate to 6-phospho-gluconate (517).

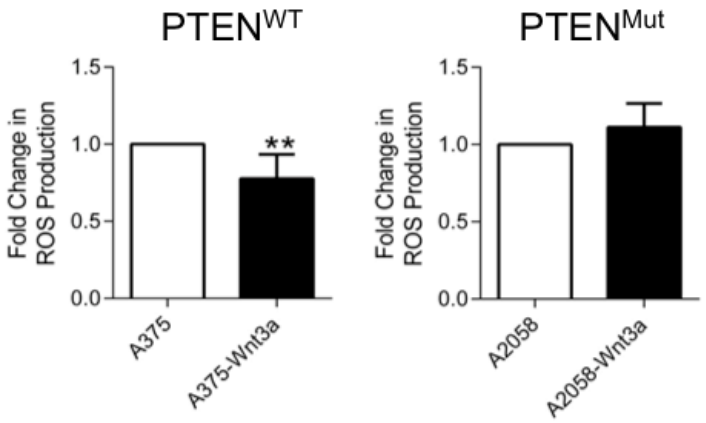


**Figure 5.7: Total cellular ROS is Reduced in PTEN$^{WT}$ Cells in Response to Wnt/β-catenin**
A375 and A5058 Wnt3a overexpression and control cells were seeded at 1x10$^4$ cells/well onto collagen coated plates. They were serum starved for 48 hours before the assay was carried out. Results were calculated as fold change over control. N=5. Mean shown ± SD. *p* = <0.01**.

Using the Wnt3a overexpression cells, total cellular glucose was measured and represented as fold change over the control cells. Figure 5.8 shows glucose consumption for both the A375 and A2058-Wnt3a cells. Both lines show a 2.1 fold increase in cellular glucose. However, only the A375 cells were measured to significant levels, indicating that, despite a reduction in glycolysis in the A375-Wnt3a cells, there is a paradoxical increase in glucose consumption. This might potentially be a compensatory mechanism to provide additional energy that is not produced do to the low metabolism.

## 5.3. Wnt/β-catenin Changes the Mitochondria of PTEN$^{WT}$ Melanoma Cells

The mitochondria are the bioenergetic and metabolic centres of eukaryotic cells. In order to study the metabolism of these cells, investigation of the mitochondria was necessary and may reveal differences in cell lines upon activation of the Wnt/β-catenin pathway.

### 5.3.1. Wnt/β-catenin Changes the Shape and Location of Mitochondria in PTEN$^{WT}$ Cells

To investigate the mitochondria of melanoma cells in response to Wnt/β-catenin signalling we first stained the cells with Mitotracker Deep Red organelle, specific stain. Mitotracker dyes are mitochondrial selective stains that contain a mild thiol-reactive chloromethyl moiety, allowing it to be retained by the cell following fixation (518, 519). Mitotracker Deep Red is also retained after cell permeabilization, therefore making it the best option for multi-colour immunocytochemistry. The stain passively diffuses across the plasma membrane, accumulating in active mitochondria. It is not, however, dependant on the mitochondrial membrane potential. All the cells were imaged in a three colour set up; mitochondria stained with Mitotracker Deep Red, cell nucleus stained with Hoechst and the cytoskeleton labelled with Phalloidin for F-actin (see section 2.3.29.1). The laser power and gain settings for each cell type are shown in Table 5.1. These remained consistent between the carrier control and Wnt3a treated samples for each cell type.

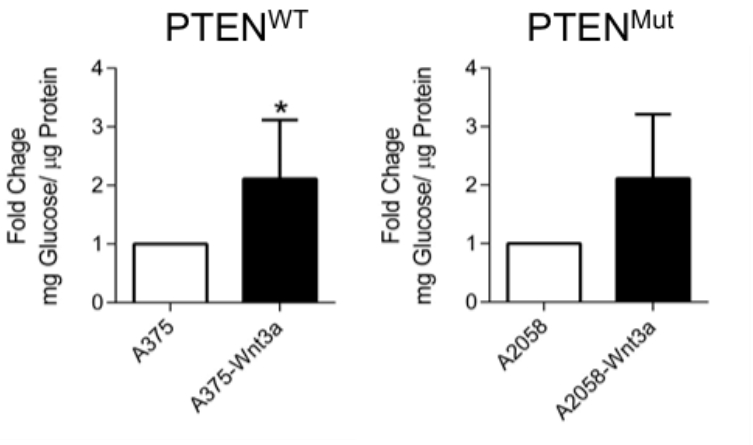


**Figure 5.8: Total Cellular Glucose is Increased in Response to Wnt/β-catenin**
A375 and A5058 Wnt3a overexpression and control cells were seeded at $2x10^5$ cells/well. They were serum starved for 48 hours before the assay was carried out and a BCA was used to normalise results. The results were then calculated as fold change over control. N=5. Mean shown ± SD. *p* = <0.05*.

**Table 5.1: Laser Power Settings And Gain Adjustments For Mitotracker Tri-Colour Images**
All samples were analysed on a Zeiss 510 LSM 63X oil/1.4 DIC objective, unless otherwise stated.
They all have a voxel size of 0.08 x 0.08 x 0.45 µm with 8 bits per pixel.
The microscope was set to HFT UV/488/543/633 with the following filters:
1 – BP385-470
2 – LP650
3 – BP505-550
Each sample was analysed using 4X track sampling using two tracks, 1st for Hoechst and Deep Red and 2nd track for Phalloidin.
The channels used were:
Ch1 – 633 pinhole 124
Ch2 – 364 pinhole 122
Ch3 – 488 pinhole 119.9

| Cell Type | Channel Power % | Gain settings ABU |
|---|---|---|
| **A375** | **9** | **638.9** |
| | **6** | **632** |
| | **0.5** | **681** |
| **M202** | **10** | **873.93** |
| | **2** | **737.00** |
| | **0.5** | **681.45** |
| **Mel501** | **12** | **644** |
| | **2** | **614** |
| | **0.5** | **686.5** |
| **A375 overexpression cells** | **3** | **585.9** |
| | **3** | **772.1** |
| | **0.5** | **566.5** |
| **A2058** | **18** | **525** |
| | **2** | **604** |
| | **0.5** | **656.5** |
| **M229** | **12** | **599** |
| | **2** | **569** |
| | **0.5** | **591.5** |
| **SkMel28** | **10** | **873** |
| | **2** | **737** |
| | **0.5** | **681** |
| **A2058 overexpression cells** | **12** | **529** |
| | **2** | **554** |
| | **0.5** | **646.5** |

The panel of PTEN$^{WT}$ cells lines Figure 5.9a all show a relocation of the mitochondria (red) towards the nucleus (333) of the cell, as indicated by the arrows. In the majority of the cells, a few mitochondria were still seen in the very tips of the cells but there were large areas of cytoplasm left with no mitochondria. The panel of PTEN$^{Mut}$ cells Figure 5.9b showed no differences between carrier control and rWnt3a treated cells or any differences between the control or Wnt3a overexpression cells. The mitochondria do not change location or shape. It was observed that, when treated with or when Wnt3a is overexpressed, the mitochondria of the PTEN$^{WT}$ cells not only move towards the nucleus but also appear clustered together and looked very elongated. When the images were zoomed to 150X magnification, the elongation of the Wnt3a overexpression cells is very clearly seen Figure 5.10. The mitochondria of the control cells are small, round and appear individual; the Wnt3a cells are much longer and thinner in shape with intense punctate staining indicating areas of overlap or joining. Activating the Wnt/β-catenin signalling pathway appears to cause the mitochondria of PTEN$^{WT}$ cells are located nearer towards the nucleus, become elongated and potentially fused into networks.

### 5.3.2. Wnt/β-catenin Signalling Increases Mitochondrial Networks in PTEN$^{WT}$ Melanoma Cells

In order to quantify the changes in mitochondrial shape seen in Figures 5.9-10, we used Imaris (Bitplane), a software package capable of visualising cells in 3D and analysing the interaction of subcellular structures. Therefore, it can quantify if the mitochondria of the PTEN$^{WT}$ cells are, in fact, connected in larger networks. Using immunofluorescence images taken as Z-stacks to create a 3D image in Mitotracker stained cells, the software derives a surface, based on the fluorescent channel of the users' choice. In the case of this data, the red channel is selected to study the mitochondria stained with Mitotracker Deep Red. The surface created is a computer-generated representation of the specified region of interest. This surface object is visualised as an artificial solid object and allows the user to verify the accuracy of segmentation against the original data, in an interactive manner, by

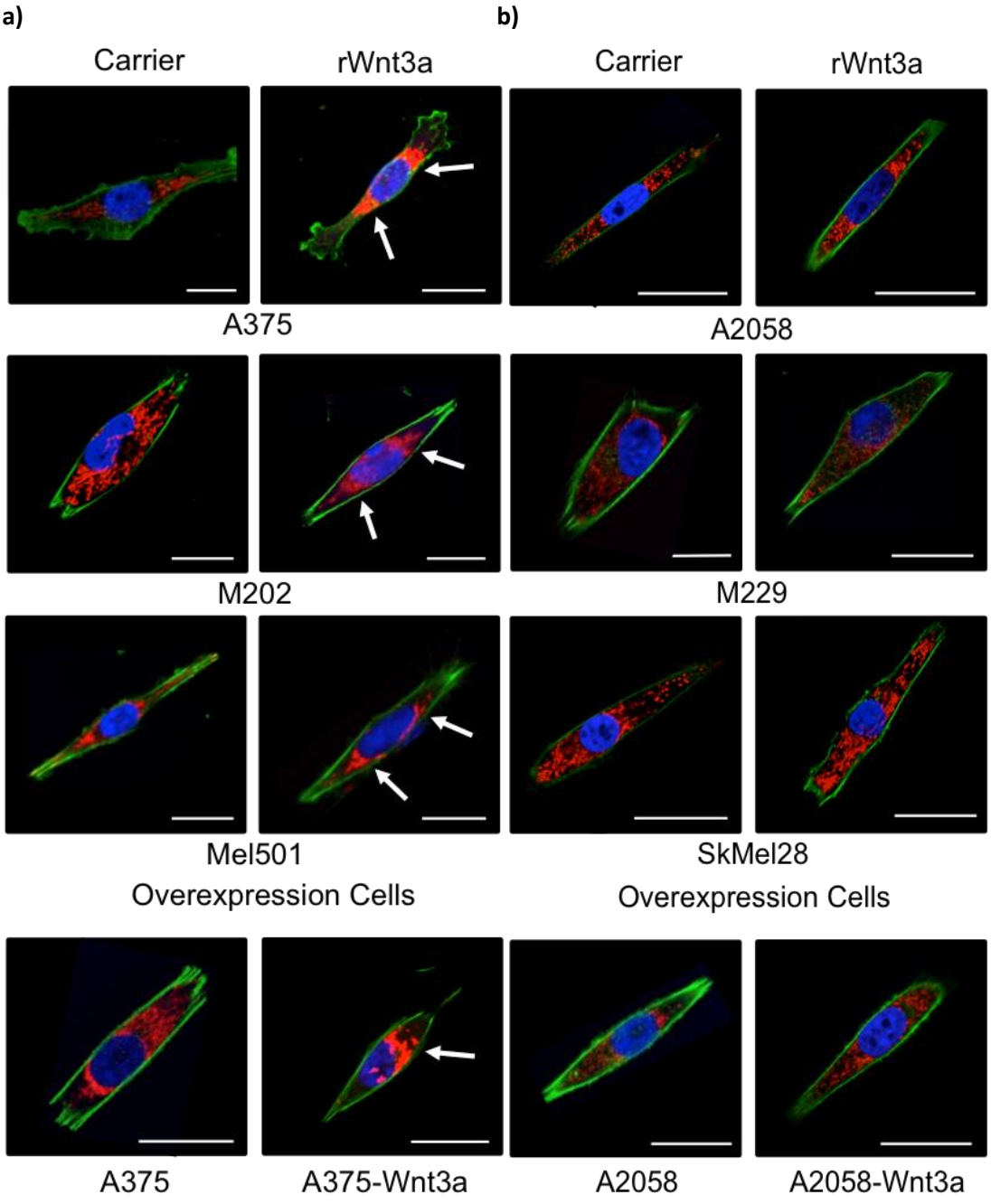


**Figure 5.9: Representative Mitotracker Images of the Whole Cell Panel**
Cells were seeded at $2x10^4$ cells/well onto sterile coverslips, before stimulation for 48 hours with either rWnt3a at 50 ng/ml, carrier control or just serum free media for overexpression cells. Cells were incubated with mitotracker deep red before fixation and counter staining with Hoechst and Phalloidin. Cells were imaged on a Zeiss LSM510 META with a 63X oil objective. Laser power and gain settings remained constant between carrier and stimulated but were adjusted between cell types. **a)** Panel of PTEN intact cell lines treated with carrier control or Wnt3a. Scale bar = 50µm. Arrows highlight areas of perinuclear mitochondria. **b)** Panel of PTEN null cell lines treated with carrier control or Wnt3a. Scale bar = 50µm.

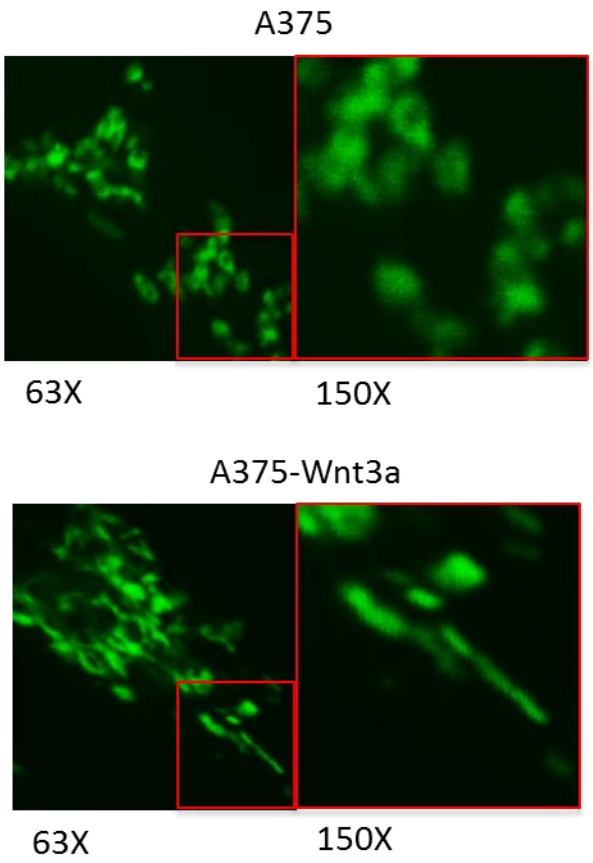


**Figure 5.10: Representative Mitotracker Images of the Whole Cell Panel**
A375 overexpression cells were seeded at $2x10^4$ cells/well onto sterile coverslips, before 48 hours in serum free media. Cells were incubated with mitotracker deep red before fixation. Cells were imaged on a Zeiss LSM510 META with a 63X oil objective, with the nucleolus in focus. Laser power and gain settings remained constant between carrier and stimulated but were adjusted between cell types. A375 and A375-Wnt3a overexpression cells shown in 150X magnification. Images were falsely coloured green during analysis.

sliding a scale bar, revealing the original image beneath. It is possible to set a background level and, knowing the average size of a mitochondria can vary between 0.5 – 1 µm, the background was set in these samples to 0.5 µm for all the cells in the interest of 'fair' experimentation. Imaris is capable of measuring various aspects of the surface including voxel size, number of structures, and volume of structures, but the data presented here is a measurement of the area of the structures. The data produced by the software shows that the area of all structures measured are within the parameters set. The total area of all mitochondrial surfaces was calculated and then the area of those within defined ranges was represented as a percentage of the total (see Figure 5.11). Representative images from the M202 cell line with carrier or rWnt3a are shown in Figure 5.11a with either individual or large networks highlighted in yellow.

After analysis was carried out on the whole panel of cells it was clear that the changes seen in the confocal images in Figure 5.9 were quantifiable by the Imaris software. The $PTEN^{WT}$ cells treated with rWnt3a or overexpressing Wnt3a all show very large networks of mitochondria. They all have an additional section on their graphs above their respective carrier controls. A375 control cells have a maximum network size of 1000 $\mu m^2$, whereas the A375 treated with rWnt3a have networks in the region of 1000-10000 $\mu m^2$. The same pattern is seen in Mel501 and A375 overexpression cells. The M202 control cells have networks in the region of 1000-10000 $\mu m^2$, but the M202 cells stimulated with rWnt3a have increased network sizes as large as 10,000+ $\mu m^2$. These shifts are all shown to be significant by a two-way ANOVA, as shown in Figure 5.11b. In addition to this, the percentages shown at the bottom of each graph represent the percentage of structures measured with the smallest group of 0-10 $\mu m^2$. The $PTEN^{WT}$ Wnt3a treated or overexpression cells have a reduction in this group showing that they have less fragmented individual mitochondria. A375 cells reduce the percentage in this category from 11.5 to 7.9%, M202 reduce from 12.1 to 6.7%, Mel501 show a decrease from 26.2 to 8.1% and the overexpression cells show the biggest reduction from 64.3 to 45.3%. As expected from their confocal images, the $PTEN^{Mut}$ cells do not show any differences in the quantified data from Imaris shown Figure 5.11c. None of the $PTEN^{Mut}$ cell

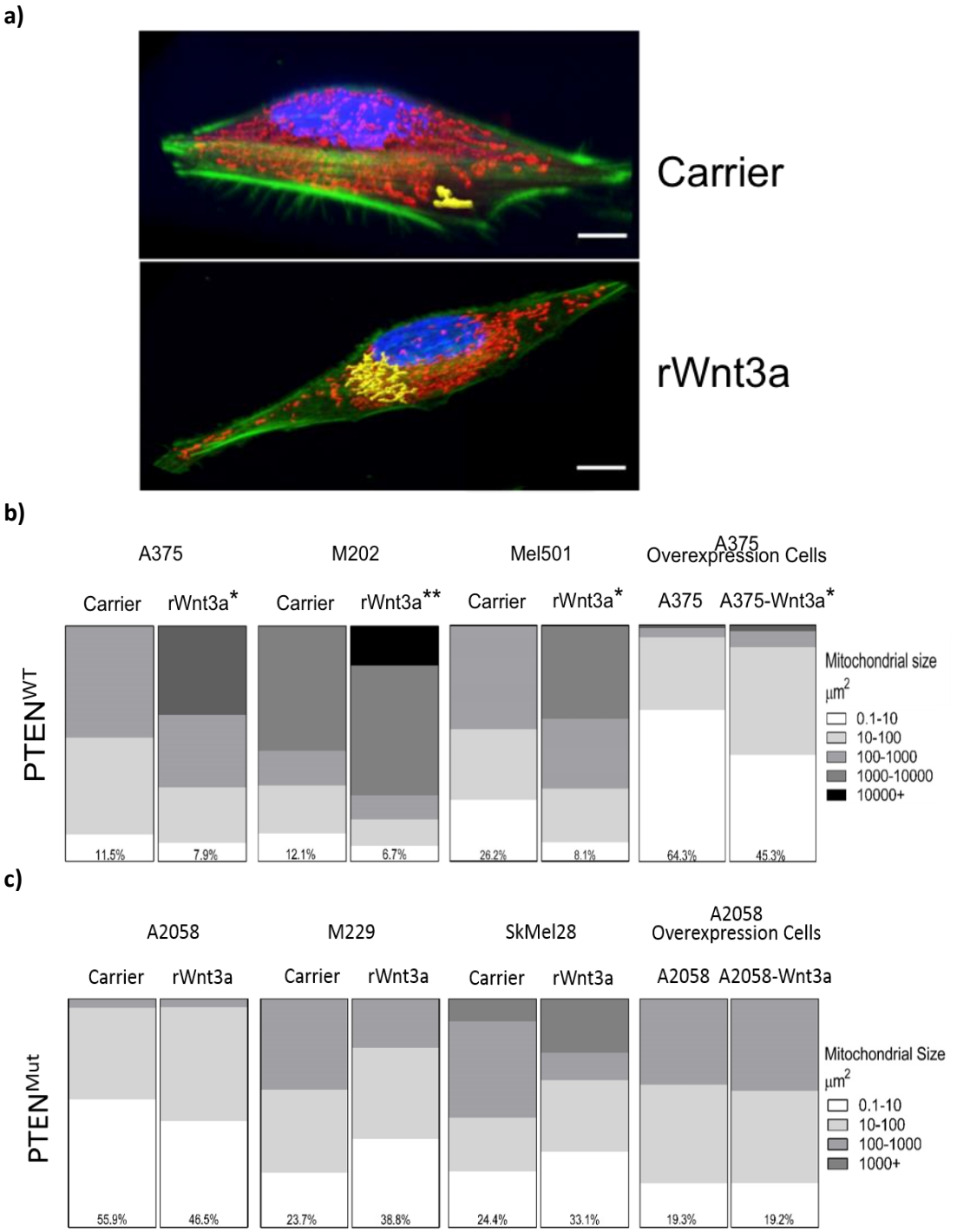


**Figure 5.11: Representative 3D Images of Whole Cell Panel using Imaris Software**
Z-slices of confocal images were carried out at the optimum depth for each sample. **a)** Representative images of 3D reconstructions for M202 cells following Carrier or Wnt3a stimulation, isolated mitochondrial network are highlighted in yellow, nucleus is shown in blue, cytoskeleton is shown in green and mitochondria are shown in red. Data was collated from multiple cell images for each data set. The area of every 'Red channel' object was calculated by the software and a total area calculated. Scale bar = 10 µm. The total areas of all objects within the defined ranges were then represented as a percentage of the total. **b)** $PTEN^{WT}$ cell lines. $p$ = <0.05* or <0.01**. **c)** $PTEN^{Mut}$ cell lines. Ns. A two-way ANOVA was used to compare each data set compared to carrier treated cells.

lines produce a network above 1000+ $\mu m^2$. Only in the SkMel28 cells is there an increase in the percentage of cells in the largest range seen and only in the A2058 cells did we find a reduction in the smallest range by 0.1%. This matches the images captured by confocal microscopy and confirms that there is increased networking of mitochondria in the panel of $PTEN^{WT}$ cells when the Wnt/β-catenin signalling pathway is activated, but there is no effect on the panel of $PTEN^{Mut}$ cells.

### 5.3.3. Wnt/β-catenin Does Not Change Mitochondrial Content in the $PTEN^{WT}$ Melanoma Cells

A potential explanation of the changes to the mitochondria seen in the $PTEN^{WT}$ Figure 5.9a could be an increase in mitochondrial mass upon stimulation with Wnt3a. In order to determine if there were changes to the number of mitochondria between the samples two different methods were utilised.

#### 5.3.3.1. There is no Increase in Mitochondrial Mass in Response to Wnt/β-catenin Signalling

In order to determine if there was an increase in mitochondrial number in the Wnt activated $PTEN^{WT}$ cells, Mitotracker Green was used in live cell flow cytometry (see section 2.3.15.4). Mitotracker Green has the advantage over the Mitotracker Deep Red in that it is non-fluorescent in aqueous solutions and only becomes fluorescent once in the lipid environment of the mitochondria. It also has relatively low background levels making it the ideal stain for live cell imaging or flow analysis (509). As with Mitotracker Deep Red, the stain passively diffuses across the plasma membrane, accumulating in active mitochondria and, again, is not dependant on the mitochondrial membrane potential, therefore making it a tool for mitochondrial mass analysis (509). However, as the overexpression cells also encode GFP (203), this does pose an additional problem of false results. Due to this, for these cells an unstained sample was used to gate on the natural fluorescence and allow compensation to be added accordingly. Figure 5.12 shows the flow cytometry data with controls shown in red and Wnt3a shown in black. The mean FL1 readings are shown below each graph indicating the average intensity of Mitotracker green. The

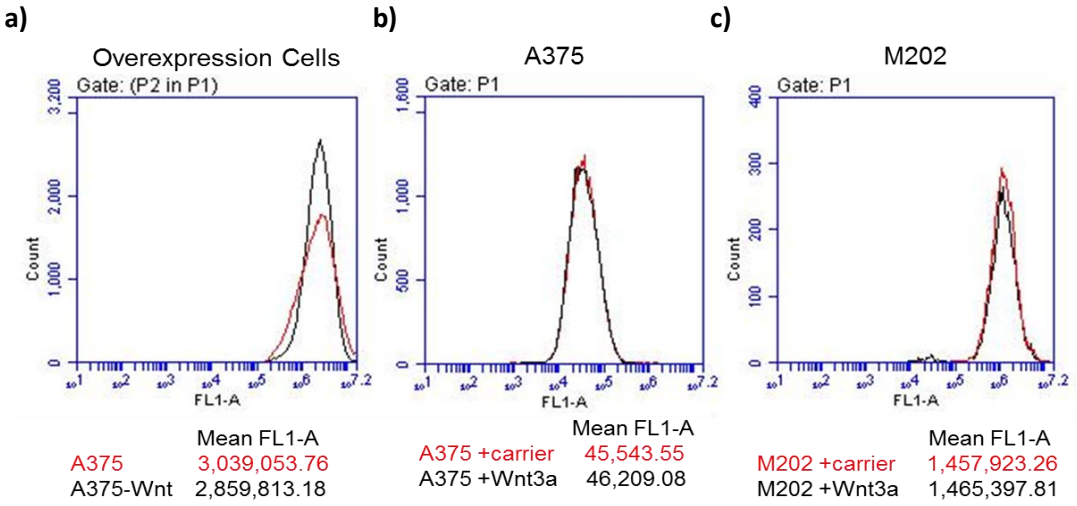


**Figure 5.12: Mitochondrial Mass by Flow Cytometry for Mitotracker in PTEN$^{WT}$ Cell Lines.** Cells were seeded at 2x10$^4$ cells/well before stimulation for 48 hours with either rWnt3a at 50 ng/ml, carrier control or just serum free media for overexpression cells. Cells were incubated with mitotracker green at 10nM before being washed and analysed immediately on the Accuri C6 analyser. Cells were gated on live cell population on a FFC/SSC plot before analysis of the FL1 channel. **a)** Overexpression cells were also gated against an unstained control to allow for the auto-florescence of the GFP construct. **b)** A375 **c)** M202. N=3. Ns.

differences are very small for all three cell lines used and inconsistent, as the FL1 reading decreased for the Wnt3a overexpression cells but increased for the A375 and M202 treated cells. This data show that there is no increase in mitochondrial mass as measured by this method.

#### 5.3.3.2. Wnt/β-catenin Does Not Increase DNA Content in PTEN$^{WT}$ Cells

An alternative method to determine if there are more mitochondria in the PTEN$^{WT}$ Wnt3a treated cells is to analyse the amount of mitochondrial DNA, compared to the amount of nuclear DNA. Using the NovaQUANT Human Mitochondrial to Nuclear DNA ratio kit (see section 2.3.30.1), whole cells were lysed directly in the qPCR plate during the reaction. The pre-designed plate houses four sets of primers, two genes encoded by mitochondrial DNA (ND1 and ND6) and two nuclear encoded genes (BECN1 and NEB). ND1 encodes NADH dehydrogenase I, ND6 encodes NADH dehydrogenase 6, and these are both mitochondrial DNA encoded genes. BECN1 encodes Beclin-1 and NEB encodes Nebulin, and these are the two nuclear DNA encoded genes. ND1 is paired with BECN1 and ND6 is paired to NEB. These provide the ratios between mitochondrial and nuclear and then the average between the two is calculated for each sample, providing a relative copy number (RCN). Figure 5.13 shows that neither the A375 (Figure 5.13a) overexpression cells, nor the A2058 (Figure 5.13b) overexpression cells are there significant increases in relative copy number of mitochondrial DNA in the Wnt3a samples. This data show that there is no effect of Wnt/β-catenin on mitochondrial DNA content.

## 5.4. Increased Mitochondrial Networking and Reduced Metabolism Are Dependent on the Wnt/β-catenin Pathway

The effects reported so far in this chapter 5 were all as a result of Wnt3a stimulation or overexpression, presumably by activating the Wnt-β-catenin signalling pathway. Therefore, the question was posed; do these effects of reduced cellular metabolism and increased mitochondrial networking depend on activation of β-catenin signalling?

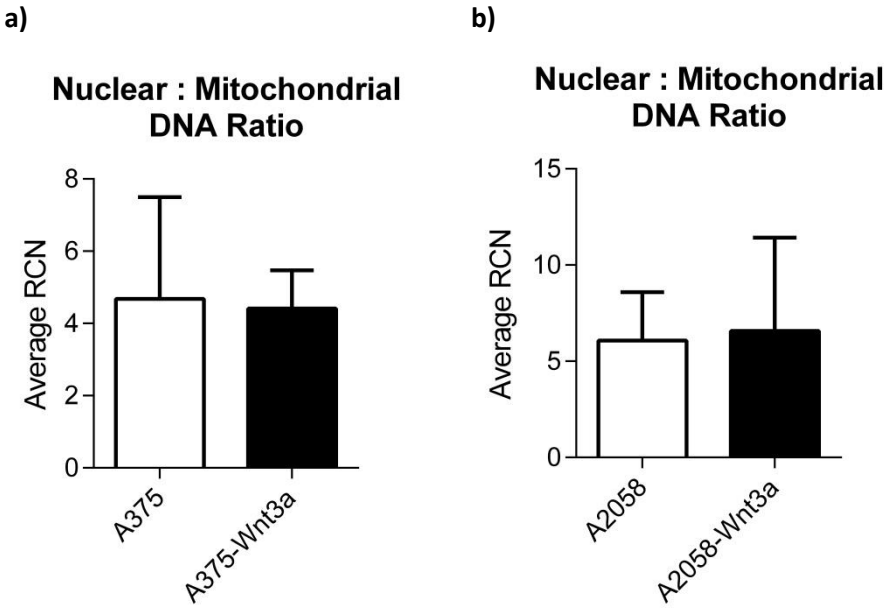


**Figure 5.13: Nuclear to Mitochondrial DNA Ratio in Wnt3a Overexpression Cells.**
Using the whole cell lysis method described by the manufacturer, the NovaQUANT Human Mitochondrial to Nuclear DNA ratio kit was used with 50 cells per well. A Fast SYBR green programme was run with an extended 10 minute denature at 95°C. Data was analysed according to the manufactures instructions for (RCN) relative copy number. **a)** A375 cells **b)** A2058 cells. N=3. Ns.

### 5.4.1. DKK1 Blocks the Wnt/β-catenin Signalling Pathway

Dickkopf related protein 1 (DKK1) is a member of the Dickkopf family of genes composed of two cysteine rich domains. It is a secreted protein that is known to be involved in embryonic development and is a specific inhibitor of the Wnt/β-catenin signalling pathway (520). By forming a complex with the transmembrane protein Kremen, it causes internalisation of LRP6 therefore, blocking its co-receptor activity in Wnt ligand binding (521). We wanted to see if DKK1 could block mitochondrial fusion, but before this, we first needed to check it could block the canonical Wnt pathway.

To check the efficiency of the recombinant DKK1 protein at blocking the Wnt/β-catenin signalling pathway, the TOPFlash dual reporter assay was used (see section 2.3.19). A375 cells were transfected with the dual luciferase reporter constructs and treated with carrier control or Wnt3a. In addition, some cells were treated with DKK1 alone or DKK1 in combination with Wnt3a. The results shown in Figure 5.14 were as expected showing DKK1 could inhibit Wnt/β-catenin signalling. Carrier control and rDKK1 protein have no effect on activation of the Wnt/β-catenin pathway. rWnt3a protein activates the Wnt/β-catenin pathway and this effect is significantly reduced by the rDKK1 protein. This confirms that rDKK1 has the expected effect of blocking the Wnt/β-catenin pathway.

#### 5.4.1.1. Blocking the Wnt/β-catenin Pathway with DKK1 Removes the Mitochondrial Fusion Effect

Next we investigated the effects of blocking the Wnt/β-catenin pathway by DKK1 on mitochondrial fusion. The A375 cells were treated using the same conditions as for the TOPFlash assay described above and they were stained, as previously described, for the initial analysis of the mitochondria using Mitotracker (see section 2.3.29.1). Cells were treated with carrier, rWnt3a or rWnt3a in combination with rDKK1, as shown in Figure 5.15 for the TOPFlash assay, which showed that rDKK1 alone had no effect on the Wnt/β-catenin pathway. The carrier control and the rWnt3a affected the mitochondria as previously seen in Figure 5.9a. The carrier has

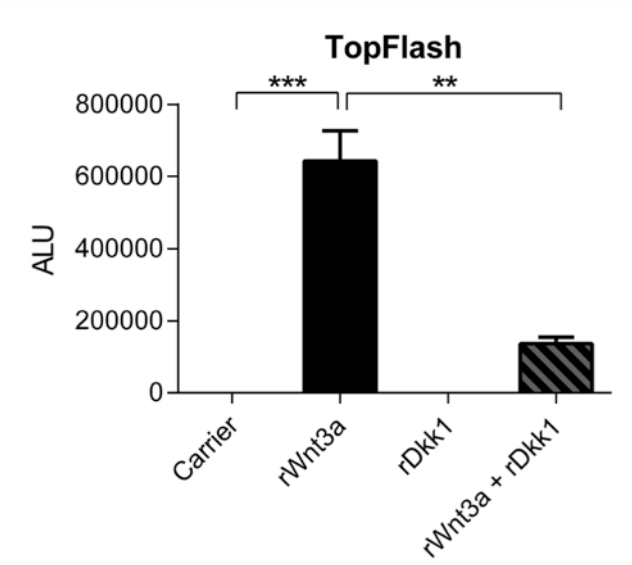


**Figure 5.14: TOPFlash Analysis of DKK1 Treatment in A375 cells**
A375 cells were seeded at $4x10^4$ cells/well and co-transfected with Renilla and either TOPFlash or FOPFlash for 6 hours. Following this, cells were stimulated with carrier control, rWnt3a at 50 ng/ml, rDKK1 at 50 ng/ml or rWnt3a and rDKK1 both at 50 ng/ml for 24 hours. Dual luciferase reporter assay was carried out and luminescence (ALU = Arbitrary Light Units) results were normalised to Renilla as a transfection control and then to FOPFlash. N=3. Mean shown ± SD. *p* = <0.01** or <0.001***.

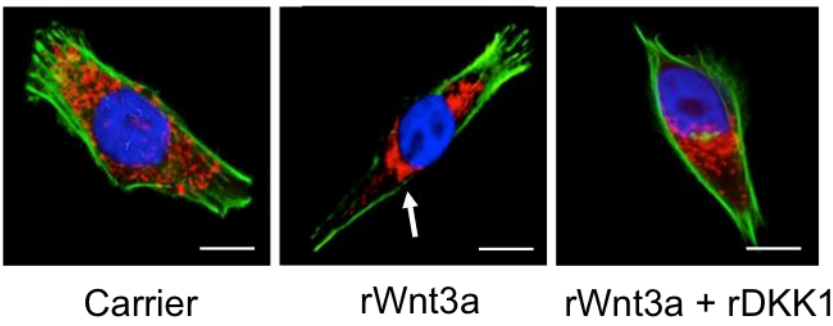


**Figure 5.15: Confocal images of A375 with rDKK1 Treatment**
A375 cells were seeded at $2x10^4$ cells/well onto sterile coverslips, before stimulation for 48 hours with either carrier control, rWnt3a at 50 ng/ml, rDKK1 at 50 ng/ml or rWnt3a and rDKK1 both at 50 ng/ml. Cells were incubated with Mitotracker deep red before fixation and counter staining with Hoechst and Phalloidin. Cells were imaged on a Zeiss LSM510 META with a 63X oil objective. Laser power and gain settings remained constant between carrier and stimulated cells. Arrows highlight areas of perinuclear mitochondria. Scale bar = 20 µm. Representative images shown.

the mitochondria spread out throughout the cytoplasm, they are small and individual, but the rWnt3a treated cells have highly networked, perinuclear mitochondria. When the cells are treated with rWnt3a and rDKK1 in combination, DKK1 inhibits the effects of the rWnt3a already described above. The mitochondria are still located near the nucleus, although they are starting to spread out into the cytoplasm. They are smaller in shape and size, and are very small and round and appear to have lost the high levels of networking.

Imaris software was utilised to measure the amount of mitochondrial networking. Representative images of the 3D reconstructions are shown in Figure 5.16a, with representative mitochondria from the data highlighted in yellow. The data generated by the software was analysed as a percentage of the whole mitochondrial area. The results of the rDKK1 effect on Wnt3a-induced mitochondrial networking are shown in Figure 5.16b. The control cells and the rWnt3a cells have a distribution similar to that previously seen in Figure 5.11a, while the rWnt3a samples have a higher percentage of larger networks. In cells co-stimulated with rWnt3a and rDKK1, 75% of the mitochondria switch from a size range of 100-1000 $\mu m^2$ down to 10-100 $\mu m^2$. This is even smaller than the networks seen in the control cells. The data shows that DKK1 antagonises the Wnt/β-catenin pathway and appears to block the networking of mitochondria in A375 melanoma cells.

### 5.4.2. Mitochondrial Fusion in Melanoma Cells is Dependent on β-catenin

To confirm these findings further, we next decided to reduce the expression of β-catenin using siRNA transiently knocked down.

#### 5.4.2.1. β-catenin can be Successfully Knocked Down in A375 Cells

To check the efficiency of the β-catenin siRNA knockdown (see section 2.3.31), two methods were used. Firstly, qPCR was used to check the expression levels of Axin2 (see section 2.3.30.2). Axin2 plays an important role in the Wnt/β-catenin signalling pathway. It causes a negative feedback loop as it is a part of the destruction complex responsible for the proteasomal degradation of β-catenin but, it is, itself,

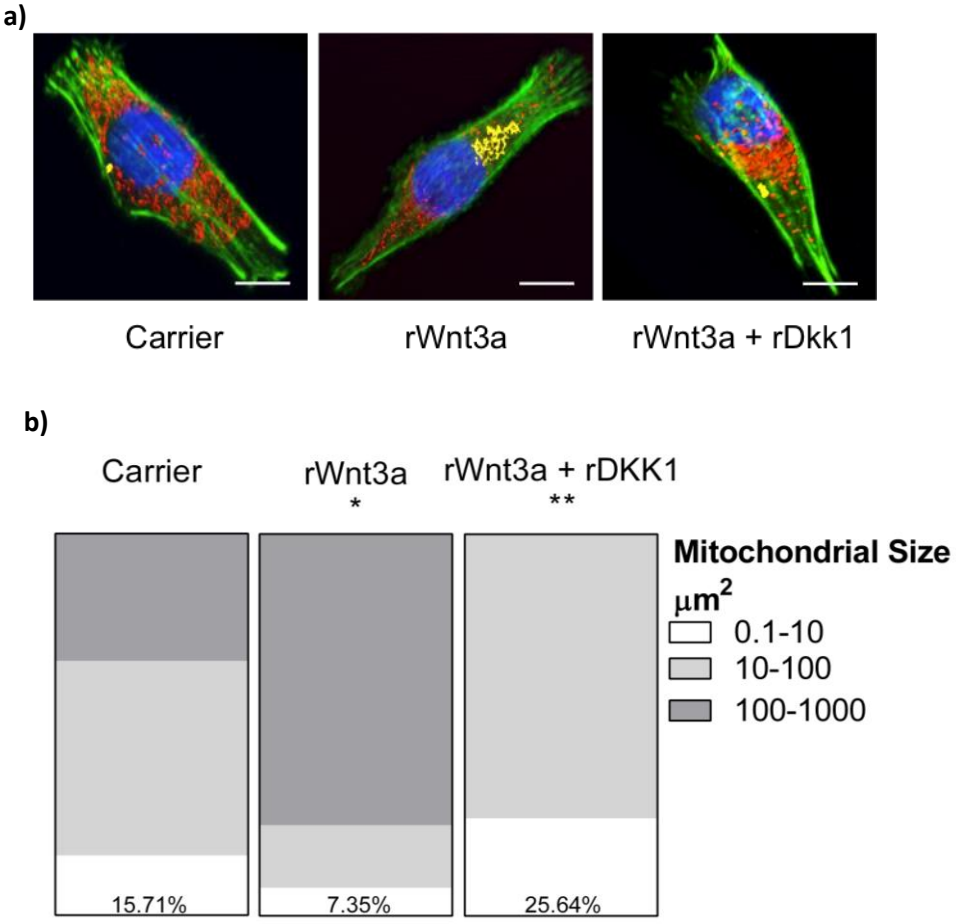


**Figure 5.16: Imaris Images and Data from rDKK1 Treated A375 cells**
**a)** Z-slices were carried out at the optimum depth for each sample. Representative images of 3D reconstructions for each cell type following Carrier, Wnt3a or Wnt3a+DKK1 stimulation, isolated mitochondrial network is highlighted in yellow. Scale bar = 20 µm. **b)** Data was collated from multiple cell images for each data set. The area of every 'Red channel' object was calculated by the software and a total area calculated. The total areas of all objects within the defined ranges were then represented as a percentage of the total. A two way ANOVA was carried out to compare variance of the data compared to carrier treated cells. $p$ = <0.05* or <0.01**.

regulated by activation of the TCF promoter transcription by activation of Wnt/β-catenin signalling (201). Therefore if β-catenin is successfully knocked down, there will be reduced expression of Axin2 mRNA (351). A control siRNA was also used as a negative control. The control siRNA is a non-targeting siRNA with the same chemical modifications for enhanced transfection efficacy as in the siRNA of choice. Figure 5.17a shows that the β-catenin knockdown significantly reduces the expression of Axin2 in both the A375 control cells and the Wnt3a overexpression cells. As expected, there are higher levels of Axin2 produced by the Wnt3a overexpression cells as these have constitutively active Wnt/β-catenin signalling as shown in Figure 4.5a.

The second method utilised to measure knockdown of β-catenin was western blot analysis (see section 2.3.13-16) for β-catenin protein expression, shown in Figure 5.17b. The protein expression of the A375-Wnt3a overexpression cells with either scrambled or β-catenin siRNA, were probed with an anti-β-catenin antibody and an α-tubulin antibody, the latter of which was used as a loading control. The blot shows that β-catenin expression is knocked down using siRNA technology.

#### 5.4.2.2. Knocking Down β-catenin Reduces Mitochondrial Fusion

The A375 and the A375-Wnt3a cells were treated with both scrambled control and β-catenin siRNA for 72 hours before the cells were stained as previously described (see section 2.3.29.1). The cells shown in Figure 5.18a were imaged on a Nikon A1R confocal with a 60X oil objective. The images show there is no effect on the mitochondria of cells treated with scrambled siRNA. In the control cells, they look small and individual throughout the cytoplasm and in the Wnt3a overexpression cells, they are highly networked around the nucleus, as expected. The cells treated with the β-catenin siRNA show a significant reduction of mitochondrial networking. In both the control and Wnt3a overexpression cells, the mitochondria are small and individual. The Imaris data in Figure 5.18b quantitatively shows the mitochondrial networking. The Wnt3a overexpression cells had no networks over 100 $\mu m^2$ and the percentage of mitochondria in the smallest size range increased from 44 to 71% in control cells and from 24 to 88% in the Wnt3a overexpression cells upon siRNA

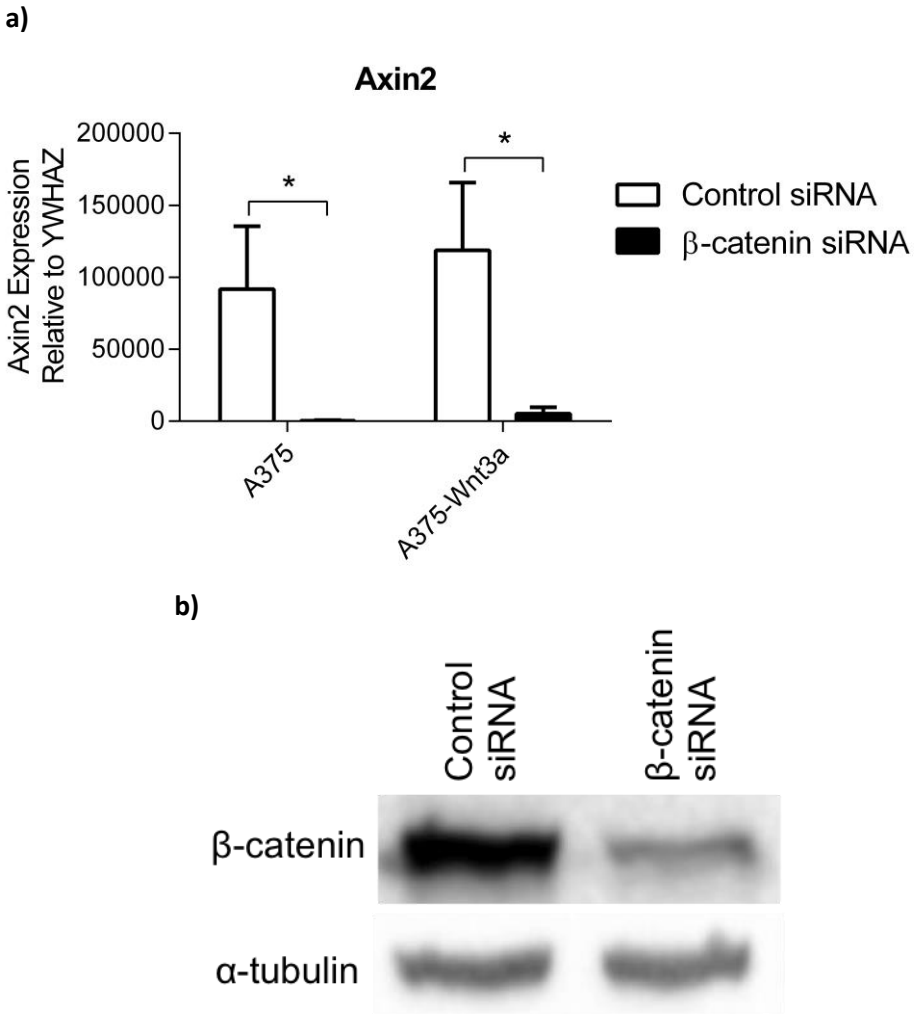


**Figure 5.17: β-catenin siRNA Knockdown Confirmation by qPCR for Axin2 and Western Blot for β-catenin**

A375 cells were reverse transfected with β-catenin siRNA or a scrambled control siRNA for 72 hours. **a)** RNA was extracted using GeneJetRNA purification Kit, 2 µg of RNA was transcribed using a Revertaid First Strand cDNA synthesis Kit. qPCR for Axin2 was run on a LightCycler 480 system, mRNA expression levels were normalised based on the expression of YWHAZ. N=3. **b)** A375 overexpression cells were lysed and BCA for protein concentration was carried out. 10 µg of protein was run on a 12% Bis-Tris gel and transferred onto nitrocellulose membrane. Blocking and antibody dilutions were carried out in a 5% BSA solution, β-catenin antibody was diluted 1:1000 and incubated overnight before anti-rabbit secondary antibody and ECL development. α-tubulin was used as a loading control. Mean shown ± SD. $p$ = <0.05*.

knockdown of β-catenin. The removal of β-catenin in the A375 cells, whether treated with Wnt3a or not, causes mitochondrial networking to be reduced in the cells. This shows that β-catenin is a necessary component of mitochondrial networking.

#### 5.4.2.3. Knocking Down β-catenin also Induces Cellular Metabolism and Migration in PTEN$^{WT}$ Melanoma Cells

As it seems that there are large effects upon the cells treated with β-catenin siRNA, it was easy to hypothesise that the knockdown would also have effect on other parameters previously tested. The A375-Wnt3a cells previously showed a reduction in their ability to migrate, compared to their controls. The Wnt3a overexpression cells treated with siRNA were seeded, as previously described, and the monolayer disturbed (see section 2.3.21). After 24 hours, the ability of the cells to migrate into the wounded area was measured and represented as fold change over the Wnt3a cells treated with scrambled siRNA. Figure 5.19a shows that there was a 1.3 fold increase in the migration ability of the A375-Wnt3a cells with knockdown of β-catenin compared to the siRNA controls.

Biochemical analysis of the Wnt3a overexpression cells showed a reduction in lactate secretion and citrate synthase compared to controls (see Figures 5.4-5.5). When treated with the β-catenin or control siRNA and seeded into the assays (see sections 2.3.25-2.3.26), cells treated with the β-catenin siRNA showed a 1.3 fold increase in lactate secretion compared to those cells treated with the scrambled control siRNA (Figure 5.19b). Citrate synthase activity was also increased by 2.3 fold in β-catenin knockdown cells (Figure 5.19c).

When β-catenin is reduced in the PTEN$^{WT}$ cells the previous reduction in migration, lactate secretion and citrate synthase activity (shown in Figures 4.12, 5.5 and 5.6) were all reversed, indicating that β-catenin plays an important role in cellular migration and metabolism.

**a)**

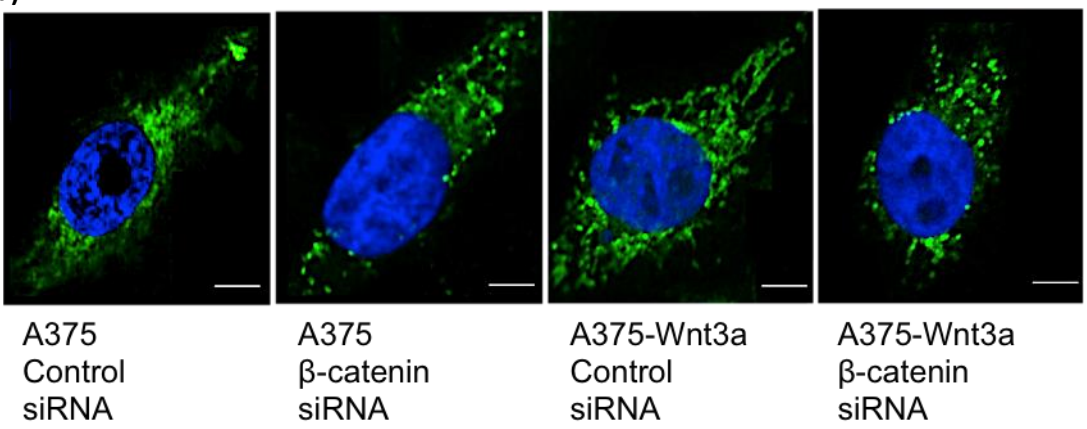


**b)**

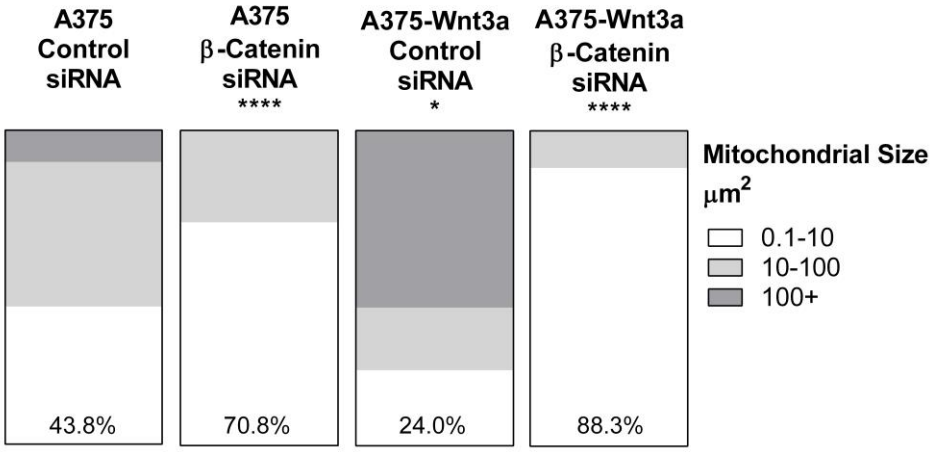


**Figure 5.18: β-catenin siRNA Knockdown Mitotracker Images, Imaris Images, Imaris Data**
**a)** β-catenin or control siRNA transfected cells were seeded at $2x10^4$ cells/well onto sterile coverslips. Cells were incubated with mitotracker green before counter staining with Hoechst. Cells were imaged on a Nikon A1R confocal with a 60X oil objective, with the nucleolus in focus. Laser power and gain settings remained constant between carrier and stimulated cells. Scale bar = 10μm. **b)** Data was collated from multiple cell images for each data set. The area of every 'Red channel' object was calculated by the software and a total area calculated. The total areas of all objects within the defined ranges were then represented as a percentage of the total. A two way ANOVA was carried out to compare variance of the data. $p$ = <0.05* or <0.0001****.

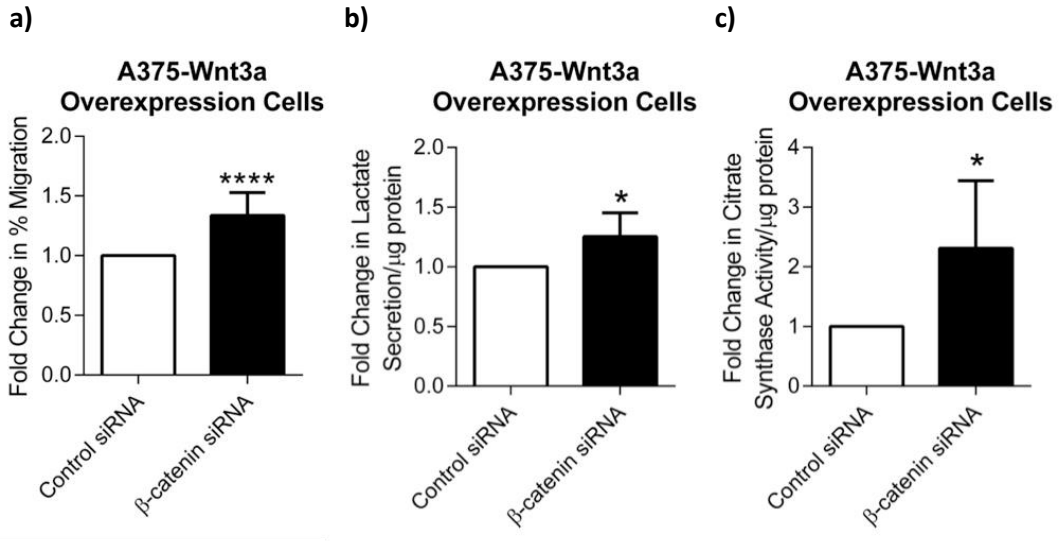


**Figure 5.19: β-catenin siRNA Knockdown Reverses Wnt3a-Mediated Effects on Cell Migration, Lactate Secretion, Citrate Synthase Activity**

**a)** Transfected cells were seeded at $4x10^5$ cells/well. After 24 hours the monolayer of cells was disturbed with a pipette tip and the assault was marked and imaged. The cells were left for 24 hours when the damaged area was imaged again and the area calculated as a % of the original was calculated, fold change over control was then calculated. N=6. **b)** Transfected cells were seeded at $2x10^5$ cells/well before the cell supernatant was removed and stored at -80°C overnight before the assay was carried out. A BCA allowed for normalisation of data to protein concentration and fold change over control was calculated. N=6. **c)** Transfected cells were seeded at $2x10^5$ cells/well before the cells were lysed and the assay carried out according to manufacturer's instructions. A BCA for total protein was carried out to normalise data to protein concentration and fold change over control was calculated. N=6. Mean shown ± SD. $p$ = <0.05* or <0.0001****.

#### 5.4.2.4. PTEN Knock Down in PTEN$^{WT}$ Melanoma Cells Blocks Wnt3a-Mediated Mitochondrial Remodelling

In order to determine if the effects on mitochondrial networking in the PTEN$^{WT}$ cells are dependent on intact PTEN signalling, siRNA was used to transiently knock down PTEN. The PTEN$^{WT}$ A375 cells were treated with scrambled control or PTEN siRNA for 72 hours, followed by a 48-hour stimulation with rWnt3a or carrier control. Figure 5.20a shows the successful but partial knockdown of PTEN expression levels, verified by western blotting (see section 2.3.13-16). Cells were then stained with Mitotracker deep red as previously described (see section 2.3.29.1) and imaged on a Zeiss LSM510 META confocal with a 63X oil objective. Figure 5.20b shows representative images of the Mitotracker staining and the scrambled control samples. These results show that, when treated with carrier control, there is no effect upon the mitochondria of the cells but, when treated with rWnt3a, the mitochondria form large networks around the nucleus, as expected. The cells transfected with PTEN siRNA also show no differences when treated with carrier control. However, when they are treated with rWnt3a the mitochondria do not become perinuclear and have reduced mitochondrial networking. The mitochondria are not as fused together and, also, they are not as focused to the nucleus. Rather they are spread out into the cytoplasm of the cells with individual mitochondria visible.

Imaris data shown in Figure 5.20c quantifies the mitochondrial fusion effect in these cells. It clearly shows the expected result in the scrambled control siRNA samples with networks over 1000 $\mu m^2$ being formed in the rWnt3a treated cells corroborating previous findings (see Figure 5.9a). The reduction in the smallest size range 0-10 $\mu m^2$ is reduced from 32% in the carrier cells to 12% in the rWnt3a cells. The same pattern is seen in the cells transfected with PTEN siRNA. There is an increase in the percentage of cells in the larger size range. However, the rWnt3a treated cells do not form networks larger than their respective controls. There is also a reduction in the percentage in the lower size range but only from 31% to

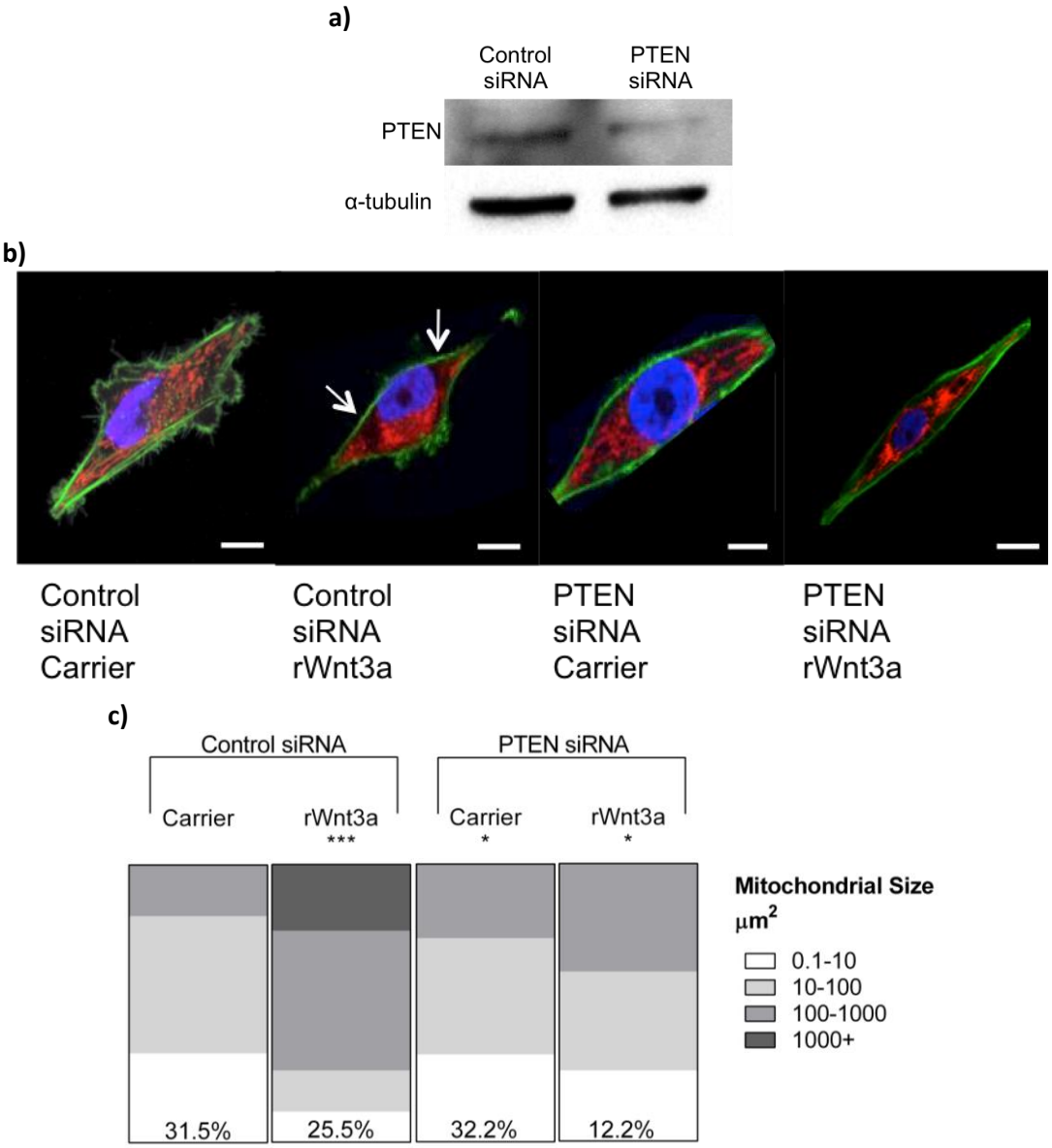


**Figure 5.20 PTEN Knockdown Reduces Mitochondrial Networking**

A375 cells were reverse transfected with PTEN siRNA or a scrambled control siRNA for 72 hours. **a)** Cells were lysed and BCA for protein concentration was carried out. 10 µg of protein was run on a 12% Bis-Tris gel and transferred onto nitrocellulose membrane. Blocking and antibody dilutions were carried out in a 5% BSA solution, Anti-PTEN antibody was diluted 1:200 and incubated overnight before anti-rabbit secondary antibody and ECL development. α-tubulin was used as a loading control. **b)** PTEN or control siRNA transfected cells were seeded at $2x10^4$ cells/well onto sterile coverslips. Cells were incubated with Mitotracker deep red before fixation and counter staining with Hoechst and Phalloidin. Cells were imaged on a Zeiss LSM510 confocal with a 63X oil objective. Laser power and gain settings remained constant between carrier and stimulated cells. Scale bar = 10µm. **c)** Z-slices were carried out at the optimum depth for each sample. Data was collated from multiple cell images for each data set. The area of every 'Red channel' object was calculated by the software and a total area calculated. The total areas of all objects within the defined ranges were then represented as a percentage of the total. A two way ANOVA was carried out to compare variance of the data compared to carrier treated cells. $p$ = <0.05* or <0.001***.

25%. These results show that the knockdown of PTEN significantly reduces the effects of Wnt/β-catenin on mitochondrial networking.

## 5.5. Analysis of Melanocytes Mitochondria in Response to Wnt3a Signalling

Melanocytes are melanin producing primary cells that become mutated and are the basis of melanoma. Therefore, it is interesting to investigate how the cell type of origin responds to Wnt3a in terms of their mitochondria. Initially, it was necessary to make sure melanocytes had the capability to respond to rWnt3a stimulation, using the TOPFlash assay (see section 2.3.19). Stabilised β-catenin and Wnt activated transcription via the TCF response elements was measured to a significant level, when melanocytes were stimulated with rWnt3a (see Figure 5.21a). Following this, confocal imaging of the mitochondria in melanocytes treated with rWnt3a cells showed that there were no differences observed between cells treated with carrier control or rWnt3a (as shown in representative images in Figure 5.21b). However, what is interesting in these findings is the mitochondria of melanocytes are very elongated as previously seen in the Wnt activated $PTEN^{WT}$ cells. This is especially clear in the yellow highlighted mitochondria by Imaris analysis in Figure 5.21c. There is no change in the location of the mitochondria. They remain distributed throughout the cytoplasm of the cells in both carrier control and rWnt3a stimulated samples. When analysed by the Imaris software, the carrier and rWnt3a treated cells have very comparable distribution of mitochondrial sizes, (Figure 5.21d) indicating that there is no obvious effect of activating the Wnt/β-catenin pathway on the mitochondria of melanocytes.

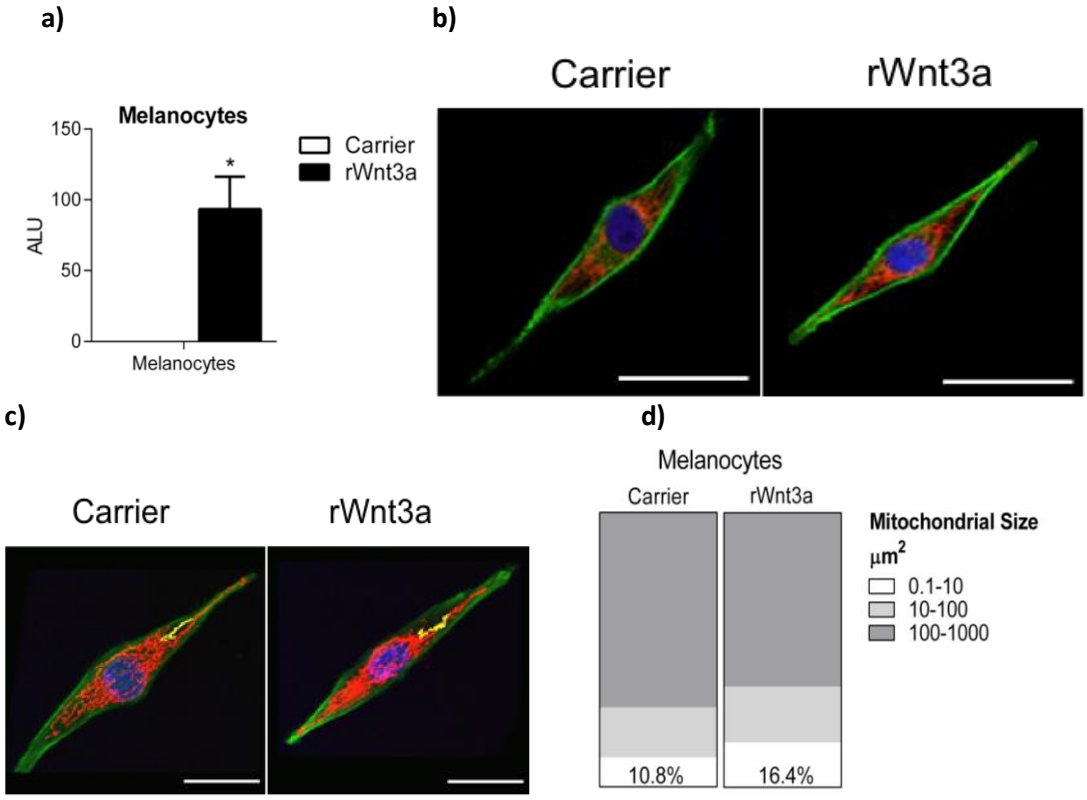


**Figure 5.21: Confocal Images of Melanocytes with Imaris Analysis**
**a)** TOPFlash analysis of Melanocytes stimulated with carrier or rWnt3a normalised to Renilla showing activated Wnt/β-catenin signalling in response to rWnt3a. Cells were seeded at $2x10^4$ cells/well onto sterile coverslips, before stimulation for 48 hours with either rWnt3a at 50 ng/ml or carrier control. Cells were incubated with mitotracker deep red before fixation and counter staining with Hoechst and Phalloidin. Cells were imaged on a Zeiss LSM510 META with a 63X oil objective. Laser power and gain settings remained constant between carrier and stimulated. **b)** Representative confocal images. Scale bar = 20 µm. **c)** Representative screen shots of Imaris analysis, individual mitochondria highlighted in yellow. Scale bar = 20 µm. **d)** Imaris data**,** data was collated from multiple cell images for each data set. The area of every 'Red channel' object was calculated by the software and a total area calculated. The total areas of all objects within the defined ranges were then represented as a percentage of the total. Mean shown ± SD. *p* = <0.05*. Ns.

## 5.6. Discussion

Here we show that activation of Wnt/β-catenin signalling reduces the global metabolism of $PTEN^{WT}$ melanoma cells, shown by reduction in OCR, ECAR, lactate secretion and citrate synthase activity. In the Wnt/β-catenin activated $PTEN^{WT}$ cells, the mitochondria become perinuclear and highly networked. The reduction of PTEN expression in these cells removed the fusion effect, indicating that the expression of PTEN is necessary for Wnt/β-catenin-induced mitochondrial fusion. Reduction of β-catenin also reduced the mitochondrial fusion effect and reversed the Wnt-mediated reduction in migration, lactate secretion and citrate synthase activity. This indicates that β-catenin is vital for mitochondrial dynamics and function, in cells with intact PTEN expression.

The Seahorse Extracellular Flux Analyzer measures two basic parameters of cellular bioenergetics, oxygen consumption and acid secretion. However, from these two readings a number of different metabolic factors can be calculated (511). The readings are measured by small solid state sensor probes that sit 200 μm above the surface of the cells and record the changes in dissolved oxygen and free protons in the media approximately every 9 minutes. This gives an accurate, real-time recording and any changes following the pneumatic injection of the compounds are seen in real time in the readings. The data calculated for the A375 cells showed that there was a global down regulation of metabolism in these cells when the Wnt/β-catenin pathway was activated through the overexpression of Wnt3a. Every aspect of cellular metabolism that can be calculated from these readings was reduced in the Wnt3a samples. The Basal OCR and Basal ECAR are readings taken at the start of the assay before the injection of any compounds and these readings measure how the cells compare in their normal growth conditions. These were both reduced by over 50% of the control cell readings. This shows that there are substantial differences in the cell's metabolic phenotype with reduced cellular respiration and glycolysis levels when Wnt/β-catenin is activated. Following injection of oligomycin (508), ATP synthesis is inhibited and the reduction in OCR can be used to calculate the ATP production from the cells. FCCP is injected to uncouple the mitochondria, forcing the

cells to take in large volumes of oxygen as a compensation mechanism and allowing the maximal respiratory capacity of the cells to be calculated (511). Finally, the inhibition of complex I of the electron transport chain by Rotenone (512) and complex III by Antimycin A (508) inhibits any mitochondrial respiration, allowing the calculation of any non-mitochondrial respiration, i.e. any oxygen consumption by non-mitochondrial sources and the proton leak, which is the re-entering of protons back into the mitochondrial matrix without contributing to ATP synthesis (522). To reiterate, all of these factors were reduced in Wnt activated $PTEN^{WT}$ cells and can possibly explain the reduction in proliferation, apoptosis, invasion and migration that has previously been seen in the $PTEN^{WT}$ cells in response to active Wnt/β-catenin signalling (see Figures 4.6-4.10 and 4.12). The experiments that followed, tested lactate secretion and amount of citrate synthase activity. These, also, were measured as significantly reduced in the whole panel of $PTEN^{WT}$ cell lines with active Wnt/β-catenin signalling. All these measurements suggest that the activation of Wnt/β-catenin signalling reduces the global metabolism of $PTEN^{WT}$ melanoma cells, including both OXPHOS and glycolysis. In published data using mouse melanoma cells, B16 (203) and Figures 4.6, 4.10, 4.12-16 using $PTEN^{WT}$ melanoma cells, activation of the Wnt/β-catenin signalling pathway reduced cell proliferation, invasion, migration and metastasis. With reduced cellular metabolism, the cells will likely have reduced energy production needed for invasion, migration and metastasis (470), or macromolecule and lipid biosynthesis necessary for proliferation (257, 488, 523). In addition, a reduction in OXPHOS could be linked to the increase in apoptosis (see Figures 4.7-4.9), as the release of cytochrome *c* can halt the ETC and inhibit ATP synthesis (276, 524) and caspase 3 will reduce oxygen consumption via complex I and complex II (525).

The results from the Extracellular Flux Analyzer for the $PTEN^{Mut}$ A2058 cells were not as uniform and could not be measured to a significant level. There is a trend in all measurements that the metabolism of the Wnt3a cells is increased in both respiration and glycolysis, albeit this was not significant. These results were somewhat verified by the lactate secretion where insignificant increases were seen in all cell lines and citrate synthase assays, where increases were seen in two lines

and decreases in two lines, showing the results are variable for the $PTEN^{Mut}$ cells but with a trend towards increased metabolism, which could explain the increased migration and invasion of the $PTEN^{Mut}$ cells. The increased lactate secretion creates an acidic environment around the cells and facilitates invasion (318). Although they could not be measured to a significant level the results, especially the basal OCR and ECAR readings, are very interesting as they trend towards the opposite in the A2058 cells to the previously described A375 cells. The activation of Wnt/β-catenin signalling causes a decrease in the metabolism of $PTEN^{WT}$ cells, which was not seen in the $PTEN^{Mut}$ cell lines indicating that the presence of PTEN in melanoma cells has a significant effect on their response to Wnt/β-catenin signalling. It is already known that glycolysis is regulated by PI3K-Akt pathway (194, 526). Therefore, if signalling is disrupted by the lack of PTEN, an increase in glucose uptake, lactate secretion and increased proliferation would be expected (147). These two pathways are linked by GSK3β as it is a downstream target of Akt and an upstream regulator of β-catenin. However, previous data is mixed on whether Akt-inhibition of GSK3β can lead to stabilised nuclear β-catenin (527-529). It has already been shown that Wnt5a can alter melanoma cell metabolism in an Akt-dependent manner in A2058 $PTEN^{Mut}$ cells (196), increasing LDH activity and glycolysis. Therefore, it would be expected that, in a $PTEN^{WT}$ cell line, Wnt3a would reduce glycolysis and lactate secretion, as is seen in this data.

The preliminary results gathered for the Glycolysis Stress Test assay show that the two cell lines also respond very differently in low glucose conditions. The ability of the A375 cells to continue to respond independently of the glucose concentration implies that they are able to run their metabolism via another energy source. As the media contains glutamine, this is probably the energy source in a process termed glutaminolysis (190, 277, 281, 322, 323). Glutaminolysis allows tumour cells to partially run the TCA cycle from α-Ketoglutarate to citrate (277, 281, 323). This alternative energy production is insensitive to high tumour ROS levels and does not use as much acetyl-coA, leaving it available for fatty acid synthesis (530). Glutaminolysis has already been found to be active in melanoma samples (281, 284), and, increases in c-Myc expression, leads to increase glutamine catabolism (284). C-

Myc is upregulated by Wnt/β-catenin signalling (531). Therefore, in these cells, the activation of the Wnt/β-catenin pathway could be driving the $PTEN^{WT}$ cells away from glycolysis and towards increased glutaminolysis, this could be tested by measuring glutamine levels. The A2058 cells respond to different glucose concentrations, thereby indicating that glucose plays a more vital role in driving the metabolism of these cells. It would be interesting to now assess the metabolism of both cell lines in the absence of glutamine.

In the $PTEN^{WT}$ A375 melanoma cells, there is a reduction in cellular ROS production in response to Wnt/β-catenin signalling. As ROS can be associated with many different elements of cell biology, this could be seen as both positive and negative for the cancer cells. ROS are a natural product of oxygen metabolism, but in times of cellular stress ROS can be produced at levels that cause damage to cellular components including DNA and RNA, which can lead to cell death (532). High levels of ROS drive genetic instability as they are capable of diffusing to the nucleus where they damage DNA (533). Therefore, a reduction in ROS could indicate that there is less cellular stress (516, 534-536) and be positive for cancer cells. However, they have also been shown to have protective implications in wound repair mechanisms and immunology. So, a reduction could be seen as detrimental for the cancer cells (535, 537). They have also been implicated in the regulation of cell migration (538, 539) and play a complex role in autophagy via a negative feedback loop (540-545). A reduction in ROS could indicate an increase in autophagy that removes damaged mitochondria that are sources of ROS (543, 544) or a reduction of ROS induced autophagy (546). In metastatic melanoma it is thought that a subset of ROS produced from NADPH oxidase (NOX) are increased and that they interact with reactive nitrogen species to drive melanomagenesis (90), indicating a reduction in total cellular ROS could be beneficial for melanoma prognosis. The trend for the melanoma cells is the same as seen in the Seahorse data and the variations in aerobic glycolysis, and OXPHOS, can explain the relative changes in ROS levels, reduced in the $PTEN^{WT}$ cells and increased in the $PTEN^{Mut}$ cells. The ETC is a major source of ROS, therefore, a reduction in OXPHOS would result in reduced ROS and conversely (242),

higher levels of glycolysis leads to ROS production (547), but as with previous data, it is not significant and therefore could be unsubstantial as the increase is small.

Recently, it has been shown that Wnt/β-catenin is linked to cellular redox via dishevelled (548, 549). Nucleoredoxin (548) can reduce Wnt/β-catenin by binding to dishevelled and a knockdown of Nucleoredoxin activates TCF, increases proliferation, c-Myc and Cyclin D expression and lead to increased Ras-mediated tumourigenesis (548).

The A375 cells overexpressing Wnt3a show a significant increase in total cellular glucose. It has previously been shown that there is reduced glycolysis, reduced OXPHOS and ATP production. Therefore, a significant increase in total cellular glucose poses the questions - are the cells taking in more glucose as a compensation for the low ATP production? Where is this glucose being used if not through glycolysis? In podocytes, Wnt/β-catenin signalling can lead to increased glucose and cellular stress (550). Alternatively, Wnt/β-catenin signalling protects mesangial cells from high glucose induced stress (551). It has also been shown that increased glucose can drive Wnt/β-catenin signalling in some cancers (188). As described previously, the metabolism of melanoma cells has already shown to be dissociated from glucose and, rather, can be driven by glutamine (284). Therefore, the only way to understand the role of glucose in these cells and answer these questions is to do a full metabolomics study, where $^{13}$C-glucose would be used in the culture media of the cells and mass spectrometry would analyse which metabolites contain labelled carbon atoms (552, 553). This would be very useful for future work.

Having previously seen differences between the PTEN$^{WT}$ and PTEN$^{Mut}$ cohorts of melanoma cells in their metabolism, migration and invasion capacity, it was expected that their mitochondria and mitochondrial activity might be affected. The main difference between the two cell cohorts is that there is no effect of Wnt/β-catenin signalling on the PTEN$^{Mut}$ cells. In both the treated and the control cells, the mitochondria are individual and spread out throughout the cytoplasm and this effect is confirmed by the Imaris data. There is no difference between the percentage of mitochondrial networks in any of the size ranges between control and treated cells

(see Figure 5.11c). As there were no significant changes in the extracellular flux analysis either, these results indicate that Wnt/β-catenin signalling has no effect on the mitochondria or metabolism of $PTEN^{Mut}$ melanoma cells. The $PTEN^{WT}$ cells however, show a dramatic change in response to active Wnt/β-catenin signalling. The mitochondria appear perinuclear and the zoomed images show that they are elongated compared to control cells. It has previously been shown that non-canonical-Wnt5a signalling causes mitochondrial fission in rat neurons (500) and, through PKC, regulates mitochondrial distribution and dynamics by degradation of Alex3 protein (501). Yoon *et al.* linked Wnt3a to altered mitochondrial physiology, but no mechanism was suggested for this effect in C2C12 cells (495). Here we show that Wnt3a alters mitochondrial shape in melanoma cells. The Imaris data shows that the mitochondria become highly networked. The $PTEN^{WT}$ cells lose a lot of their small individual mitochondria and the percentage of networks in the largest size range increases. Interestingly, there is no effect of Wnt/β-catenin signalling on the mitochondrial remodelling of melanocytes. The mitochondria of these cells are spread throughout the cytoplasm, but they are elongated. Scott *et al*. have already studied the metabolic profile of melanocytes and shown that they have lower glycolysis levels and respond to hypoxia with a typical Pasture effect, with increased fermentation of glucose to lactate (284). It would be interesting to see if Wnt/β-catenin has an effect on melanocyte metabolism given that it had no effect on the mitochondrial structure (20).

The movement of the mitochondria towards the nucleus in the $PTEN^{WT}$ cells could explain the reduction in invasion and migration previously seen in Figures 4.10 and 4.12. The mitochondria are the site of cellular energy production. Without the mitochondria at the leading edge of the cell, they do not have the energy to migrate and invade (239, 554). This relocation was not seen in the $PTEN^{Mut}$ cells therefore leaving the mitochondria available at the leading edge. Here, they will provide for the higher bioenergetic demands of the migrating cells, and will allow for an increased influx of $Ca^{2+}$ to maintain cellular sensitivity to stimuli, and aid in cellular migration (554). It is noteworthy that this is not the case for all cell types, as it has been shown that migrating lymphocytes have mitochondria to the posterior of the

nucleus and are seen to be pushed by uropods rather than pulled by pseudopods as seen in cancer cells (554). The clustering or fusion of the mitochondria could have been due to increased numbers of mitochondria in the cells. However, through both qPCR and mitochondrial mass, this was shown not to be the case, as there was no change in mitochondrial mass in the $PTEN^{WT}$ cells and no difference in the ratio of nuclear to mitochondrial DNA ratio.

Following these initial findings in the $PTEN^{WT}$ cells, it was subsequently investigated if the changes to the mitochondria were dependent on the Wnt/β-catenin signalling pathway. The same results were seen by blocking the pathway and by knocking down β-catenin. DKK1 inhibits Wnt/β-catenin signalling by binding to the LRP5/6 receptor and blocks it from acting as a c0-receptor to FZD (234, 520). Whereas, small interfering RNA is targeted to specifically disrupt the expression of β-catenin protein. Both of these methods result in incomplete Wnt/β-catenin signalling and the subsequent effect was that the mitochondria, which had previously become highly networked and perinuclear in response to Wnt3a signalling, now became smaller and spread throughout the cytoplasm, even in the presence of Wnt3a stimulation. This was more severe in the β-catenin knock down, especially as a similar effect was seen in the control cells where the mitochondria were already small and individual. Imaris quantified the effects caused by DKK1 blockage of the pathway and β-catenin knockdown. The large networks are not formed and the percentage of small individual mitochondria is significantly increased. This shows that β-catenin is a vital protein in the process of mitochondrial fusion and localisation. Further investigation showed that β-catenin is also important in cell migration and metabolism. The previously seen Wnt-induced reduction in migration, lactate secretion and citrate synthase assays were all reversed by β-catenin siRNA knockdown in the Wnt3a overexpressing A375 $PTEN^{WT}$ cells. However, what must be considered in these results are the wider ranging effects of β-catenin removal. Stabilised β-catenin regulates the transcription of up to 70 genes (20, 168) including, Cyclin D1 and MYC, removal of which would affect progression through the cell cycle (439, 531), as well as CD44 which would change cell adhesion and migration (555). In addition, it would remove the pool of β-catenin from the adherens junctions (439), therefore, altering

the cytoskeleton and subsequently cell shape. However, the experiments blocking the pathway with DKK1 negate this effect. However, despite these considerations, these findings indicated that β-catenin is vital for mitochondrial dynamics and function and activation of the Wnt/β-catenin signalling pathway has significant effects on the metabolism and mitochondria of $PTEN^{WT}$ melanoma cells.

The initial differences seen in invasion and metastasis and the subsequent differences in metabolism and upon the mitochondria were seen in cell cohorts with differences in PTEN. When the PTEN levels are reduced in the $PTEN^{WT}$ cells, the control over PI3K signalling is reduced. It has already been shown that the PI3K/Akt pathway has an effect on cellular metabolism (526) and specifically that Wnt5a can alter melanoma metabolism in an Akt-dependent manner (196). Therefore it would be expected that levels of PTEN would directly affect the mitochondria. In addition, in neuronal cells (556, 557), and recent data in breast cancer cells (558, 559) shows PTEN can play a direct role in cellular metabolism and mitochondrial dynamics. The data from this research supports this and shows that knockdown of PTEN subsequently removes the effects of increased fusion and localisation of mitochondria when the Wnt/β-catenin pathway was activated and, instead, the mitochondria were small and individual as in the $PTEN^{Mut}$ cells where there was no effect of Wnt3a signalling on the mitochondria (See Figure 5.9b). These results confirm that the changes to the mitochondria were dependent on the PTEN status.

These findings now push the investigation to understand why and how mitochondrion move towards the nucleus, forming the large networks and is this as a result of the reduced metabolism or is the cellular metabolism reduced because of the mitochondrial changes?

### 5.6.1. Summary

The effects of the Wnt/β-catenin pathway were altered in melanoma cells based on the PTEN status. $PTEN^{WT}$ cells that previously showed a reduction in invasion, migration and metastasis (Chapter 4), also show a global reduction in cellular metabolism with effects upon both glycolysis and OXPHOS. These changes were

accompanied by a change in mitochondrial shape and location, with the mitochondria becoming highly networked and perinuclear. It was determined that these results were dependent upon the activation of the Wnt/β-catenin pathway and crucially on the presence of β-catenin itself. Such changes to the mitochondria were not seen in the $PTEN^{Mut}$ cells. However, reversing the PTEN status of the $PTEN^{WT}$ cells did block these effects. These results show that the PTEN status of melanoma cells plays a vital role in how the cells respond to Wnt/β-catenin signalling. In addition they show that β-catenin is vital for mitochondrial fusion and cellular metabolism.

# 6. INVESTIGATING THE MECHANISM OF WNT/β-CATENIN-MEDIATED MITOCHONDRIAL NETWORKING AND METABOLISM IN PTEN$^{WT}$ MELANOMA CELLS

**Acknowledgements**

Dr Aaron Robitaille, a post-doc from Prof. Moon's laboratory (University of Washington School of Medicine) carried out the mass spectrometry.

## 6.1. Introduction

Chapter 5 showed that activated Wnt/β-catenin signalling caused changes to mitochondrial shape and location and, also, reduced the metabolism of $PTEN^{WT}$ melanoma cells. The shape and function of the mitochondria has also been discussed in detail in Chapter 1. This chapter will investigate the processes of mitochondrial dynamics, mitochondrial quality control, mitochondrial clearance and any currently known effects of the Wnt/β-catenin signalling pathway. To date, most work investigating mitochondrial dynamics has been carried out in yeast as it is a system very similar to that of mammalian cells. *In vitro* studies have typically used neuronal cells, as defects within these mitochondrial processes often lead to neurological disorders (242, 560). However, the field of mitochondrial dynamics is starting to expand, especially given the realisation that metabolism plays such a vital role in many other disorders, including cancer. Here we investigate how Wnt/β-catenin signalling effects mitochondrial dynamics in melanoma cells.

### 6.1.1. Mitochondrial Dynamics

Mitochondria are dynamic organelles that constantly go through the processes of fusion and fission (245, 499, 561-563), however these two opposing processes do not just control mitochondrial shape, but also play important roles in metabolism (258, 564), cell cycle regulation (565) and apoptosis (238, 249, 504, 566). It has already been shown in the previous chapters that Wnt signalling is highly involved in all of these processes. Mitochondrial fusion and fission occur constantly during the cell cycle, where the biogenesis of mitochondria is dictated by cell proliferation levels (567). Mitochondria have been seen to elongate during $G_1$ phase to increase ATP levels for continued growth (265, 561), but they are seen to fragment during S-phase (265) to make sure each daughter cell has its required allocation of mitochondria (561, 568, 569). The process of fusion allows for the exchange of mitochondrial matrix, proteins but also controls mitochondrial size and morphology (245). There are three genes that control mitochondrial fusion; Mitofusin 1 (*MFN1*) and Mitofusin 2 (*MFN2*) located on the outer mitochondrial membrane (OMM), and Optic Atrophy 1 (*OPA1*) on the inner mitochondrial membrane (570). Mfns are transmembrane

GTPase proteins that share a high percentage of primary sequence homology (560, 564) and have the same functional domains, but it is thought that they play different roles in the fusion process. Mfn1 is known to be involved in tethering of two neighbouring mitochondria together (571, 572). This tethering can be achieved by homotypic or heterotypic activity of the two Mfn proteins; Mfn1-Mfn1 or Mfn1-Mfn2 (560, 564). However, it has been shown that the homotypic Mfn1 tethering is 100-fold more efficient at fusing mitochondria than any other combination (571). Mfn1 directly interacts with Opa1 (249, 251) on the IMM to facilitate the fusion of mitochondrial contents. Mfn2 has a more specific tissue expression pattern than that of Mfn1 (560, 572-574), which could be explained by the fact that as well as its role in fusion, Mfn1 is involved in a number of other processes, such as oxidative metabolism, cell cycle, cell death and in neuronal cells, mitochondrial axonal transport (560, 564). Mfn2 tethers the mitochondria to the endoplasmic reticulum (ER) as part of intracellular calcium flux (560, 564, 575). Mfn2 also binds to apoptosis proteins including Bak, Bcl-x and Bcl-2 in order to aid mitochondrial fission during apoptosis (249, 504, 560).

Opa1 is a dynamin-related GTPase located on the IMM that regulates mitochondrial shape, fusion and cristae remodelling (249, 258, 564). It is known that Opa1 is responsible for the fusion of the inner mitochondrial membrane, allowing the final step in fusing two mitochondria together and the mixing of the mitochondrial DNA (560). Opa1 can form up to eight isoforms following post-transcriptional regulation (560, 564). Dominant isoforms are isoform 1 (containing exon 4) and 7 (containing exon 4 and 5b). Subject to proteolytic cleavage, the longer isoforms are often degraded (564), leaving up to 5 bands visible by western blot analysis (560). Cleavage of Opa1 can also be induced by apoptosis and by loss of membrane potential (418). *OPA1* knockdown experiments resulted in cells having reduced respiratory potential (561, 576), reduced membrane potential, disorganised cristae (258) and mitochondrial fragmentation (249, 564), but surprisingly, overexpression of *OPA1* can also lead to mitochondrial fragmentation and an increased rate of fission (258, 418, 574).

There are two genes involved in the mitochondrial fission process - Dynamin-related protein (*DNM1L*) and Fission protein 1 homolog (*FIS1*) (560). Drp1 is located in the cytoplasm and is recruited to the mitochondria when fission occurs (577). It has has been shown that Drp1 forms a ring of beads around the mitochondria, gradually tightening until the organelle separates into two (520). Fis1 is located on the mitochondria and is thought to be involved in the recruitment of Drp1 (517, 560, 578). Drp1 is also linked to ROS production, but the mechanism to explain this finding is currently unclear (249). As well as in normal mitochondrial maintenance, fission occurs to break up severely damaged mitochondria to allow for more efficient removal of mitochondria from the cell (499, 579).

The roles of these four genes are quite distinct in the fusion and fission processes. However, as stated previously, they are also involved in a number of other cellular processes. Their roles in apoptosis are convoluted, involving Mfn2, Drp1 and Opa1. It was previously stated that Mfn2 tethers the mitochondria to the ER (560, 564, 567) and also binds apoptotic factors such as Bak, Bcl-x and Bcl-2 (249, 504, 560, 580). In normal cells, these Bcl-2 proteins play a role in mitochondrial fusion (242, 266, 504) but, during early apoptotic signals, have the opposite effect to facilitate mitochondrial fission (265-267), to make mitochondria small enough for efficient removal from the cell (499, 581). The juxtapositioning of the ER and the mitochondria is important for the up-take of $Ca^{2+}$ through a uniporter from the intra-mitochondrial ER stores, but it also makes the mitochondria vulnerable to apoptosis (242, 249, 564, 575). The ER has been shown to be present at the site of mitochondrial fission, wrapping itself around the mitochondria in a constrictive manner (242, 561) and, at these sites of fission, Drp1 co-localises with the pro-apoptotic factor Bak (272, 560) which normally regulates Mfn2 complex assembly but, in this situation, inhibits Mfn2 activity (266). These findings indicate that $Ca^{2+}$ influx increases mitochondrial fission via Drp1 and it has been shown in rat neurons that this can be induced specifically by Wnt5a β-catenin-independent signalling (500). This is further justified by the finding that increased $Ca^{2+}$ levels lead to Drp1 related fission via PKC activation (as discussed in Chapter 1), which is also regulated by Wnt5a signalling (228, 582, 583). Conversely, the Bcl-2 anti-apoptotic targets of

the Wnt/β-catenin signalling pathway have been shown to actually increase $Ca^{2+}$ uptake without affecting respiration, thereby protecting the mitochondria from excessive $Ca^{2+}$ (584, 585).

The second apoptosis pathway linked to mitochondrial dynamics it that of cytochrome *c* release. As already discussed in section 4.5.2, cytochrome *c* is located in the intermembrane space and in the mitochondrial cristae (265) and it is released into the cytosol in two steps. The first step follows the outer membrane depolarisation. The second step follows activation of the apoptosome during apoptosis and cytochrome *c* is released following the remodelling of the cristae by Opa1 and Parl (the Opa1 regulator) (249, 560, 561, 586). Members of the Bcl-2 family, Bax and Bak, control this release as they regulate mitochondrial membrane permeablisation (265, 266, 587) but, also, by Bid and Bim, which regulate cristae shape (258, 260, 588). It has already been shown that Wnt/β-catenin signalling plays an important role in apoptosis, including the Bcl-2 proteins (350, 494, 503, 589, 590) and in cytochrome *c* release. In addition, this research has already shown that Wnt/β-catenin signalling increases both apoptosis and cytochrome *c* release (see Figures 4.7-4.8) and therefore, could potentially play a role in Opa1 levels (193).

### 6.1.2. Mitophagy

The term mitophagy refers to the selective removal of mitochondria through the process of autophagy (591, 592). Autophagy can occur for a few reasons, but all stem from the basis of metabolic stress (593). It has been posed that autophagy in cancer is likely to be context, tissue and genetically-dependent (547, 594-596). It can act in both a tumour suppressor role (597) as defects in autophagy lead to tumour progression (547), as well as being tumourigenic and promote resistance to anti-cancer treatments (547). Autophagy due to stress is linked to nutrient availability and energy homeostasis. Alternatively, selective mitophagy is activated to remove damaged mitochondria that consume ATP to sustain the mitochondrial membrane potential (598). The removal of mitochondria from the cell is a process that recycles their biomass for reuse to build macromolecules and prevent accumulation of toxic levels of mitochondrial ROS (594, 596, 599).

Mitochondrial fusion is a process dependent on mitochondrial membrane potential. Damaged mitochondria will lose their membrane potential, targeting them for removal, thereby disabling damaged mitochondria (245, 291). It has been shown that mitochondrial fusion will occur even in the absence of a functional respiratory chain or after ATP depletion, but cannot occur when the mitochondrial membrane potential is lost (245). Mitophagy targets mitochondria with a depolarised membrane, although it has been suggested that depolarised mitochondria may remain in the cell, unable to fuse (600). PTEN-induced kinase 1 (Pink1), a mitochondrial kinase (601, 602), is taken into the mitochondria where Parl cleaves it at the N-terminus forming ΔN-Pink1 (602-605). This removes Pink1 from constitutively activating the mitophagy pathway on healthy mitochondria (606). When the membrane potential is diminished, Pink1 is no longer processed and full length Pink1 accumulates on the surface of the mitochondria (242, 602, 607, 608). It has been shown in neuronal cells that knockdown of *PINK1* increased mitochondrial fragmentation and autophagy (601, 603, 609, 610), similar to the findings in Pink1-muatated Parkinson disease cells. Whereas, overexpression of *PINK1* increased mitochondrial networking, elongation, cristae density and reduced autophagy. However, studies in *Drosophila* show the opposite findings (577, 610, 611) where overexpression of PINK1 caused mitochondrial fragmentation and increased autophagy.

In selective mitophagy Parkin, an E3 ubiquitin ligase, is recruited and activated by full-length Pink1. Once at the mitochondria, Parkin ubiquitinates the Mfns on the surface of the mitochondria (612), as well as other OMM proteins (242, 602, 603, 607, 608, 613). It has been stated that Parkin may play different roles in various cancer types (614). As with *PINK1*, *PARK2* (the Parkin gene) overexpression in many cancers has been linked to induction of apoptosis, increased mitophagy and cell cycle arrest (615-617), whereas knockdown is seen to increase mitochondrial fragmentation and reduce ATP production (618). This indicates that activity of Pink1 and Parkin can play a role in metabolism as well as mitochondrial quality control. Parkin has been shown to induce β-catenin ubiquitination and subsequent degradation, therefore reducing Wnt/β-catenin signalling (619, 620). This study by

Rawal *et al*. also showed that downregulation of *PARK2* led to excessive Wnt/β-catenin signalling (619).

Once the Mfns have been ubiquitinated by Parkin, the fusion process is blocked and activates the autophagy machinery (598, 602). A double membrane autophagosome forms surrounding the mitochondria which fuses with lysosomes to form autolysosomes and sequester its contents (591, 595, 621, 622). This process is controlled by a group of Atg proteins that can be divided into three groups according to their function. The first are involved in the initiation step such as ULK1. This is followed by nucleation involving proteins such as Beclin 1. Finally, proteins such as the Microtubule-associated protein 1 light chain 3α (*MAP1LC3A*; LC3), control the elongation and closure of the autophagosome (591, 622).

Nucleoporin p62 (*SQSTM1*) is an adaptor protein that recognises the ubiquitin on the Mfns and subsequently binds LC3 to the ubiquinated proteins ready for degradation (598, 622). LC3 is then cleaved at the C-terminus and binds a phosphatidylethanolamine (PE) to produce its mature form found on the autophagosome membrane (622). Accumulation of p62 has been associated with increased tumourigenesis (595) and knockdown of *SQSTM1* can decrease levels of mitophagy (602). However, autophagy, due to nutrient starvation, increases p62 degradation and, therefore, reduces its intracellular levels (622). Specifically, in melanoma, autophagy is reduced by knockdown of *BECN1*, but during starvation autophagy and Beclin 1 are upregulated (547, 591, 621). Cellular energy levels are regulated by mammalian targets of rapamycin (mTOR) and it has been shown that autophagy can be inhibited via mTOR, due to activation of a number of oncogenes such as Ras and Akt (547, 591, 623). The Wnt/β-catenin pathway is implicated further in autophagy as it is known to regulate p62 transcription (622). During starvation, Wnt3a signalling is decreased due to β-catenin being targeted for degradation by LC3 binding (596). Conversely, knockdown of *MAP1LC3A* or *BECN1* increases Wnt3a activity, indicating that autophagy negatively regulates Wnt3a signalling (595, 624). This is done by promoting degradation of Dvl through p62-mediated aggregation of ubiquitinated Dvl (595, 596, 622, 624, 625). Likewise, Wnt/β-catenin signalling

downregulates autophagy via TCF4 and siRNA knockdown of β-catenin increases numbers of autophagosomes, as measured by increases in LC3-II and p62 in colorectal cancers (596). This suggests that Wnt signalling plays a prominent role in the regulation of autophagy.

### 6.1.3. Aims

In this final chapter, the aim is to identify a mechanism of action that enables the mitochondria of $PTEN^{WT}$ cells to become highly networked with reduced cellular metabolism. Firstly, investigating the genes of mitochondrial dynamics will establish if the mitochondrial networking is due to an increase in mitochondrial fusion or a defect in mitochondrial fission. Following this, the mitochondrial membrane potential was analysed as this plays an important role in the health and function of the mitochondria, directly affecting the mitophagy process. Finally, the genes of mitochondrial quality control and mitophagy were analysed to assess if the reduced metabolism is due to a defect in the removal process of damaged mitochondria.

## 6.2. Wnt/β-Catenin Increases Mitochondrial Fusion Genes

In order to investigate the changes in the mitochondrial shape and networking of $PTEN^{WT}$ cells shown in Chapter 5, it was necessary to investigate the genes of mitochondrial dynamics that control the processes of mitochondrial fusion and fission. There are three genes that control fusion, *MFN1* and *MFN2* on the outer mitochondrial membrane (OMM), and *OPA1* on the inner mitochondrial membrane (570). There is a clear increase in mitochondrial fusion proteins in $PTEN^{WT}$ cells and it was within these cells that activation of the Wnt/β-catenin signalling pathway caused a reduction in migration and invasion. This was confirmed in an *in vivo* tail vein metastasis mouse model (see Chapter 4). Confocal imaging of the fusion genes achieved very clear results. Having been incubated with the Mfn1, Mfn2 or Opa1 antibodies, a secondary antibody in the far-red channel was used for fluorescence imaging (see section 2.3.26.2). As with all previous imaging, the gain settings were kept consistent between controls and Wnt3a overexpression samples. The results are shown in Figure 6.1a. All three mitochondrial fusion proteins show huge up regulation in the Wnt3a samples, indicating an increase in their expression. This was also seen when the cells were analysed by flow cytometry (see section 2.3.15.2). Figure 6.1b shows the flow results for Mfn1, Mfn2 and Opa1 and the subsequently calculated fold change in fluorescence, compared to control as 1.4, 1.5, and 1.3 fold respectively. The up regulation of the fusion proteins Mfn1, Mfn2 and Opa1 can also been seen in total protein samples in Figure 6.2a. However *DNM1L* (the Drp1 gene) is a mitochondrial fission gene. Imaging, flow and protein expression of active Drp1 is not possible as it is in the cytoplasm of the cells and only recruited onto the mitochondria when it is needed during mitochondrial fission (273). Therefore, by extracting the mitochondrial protein (see section 2.3.29) and analysing this by western blot (see section 2.3.13), both the fusion and fission protein levels at the mitochondria can be analysed (see Figure 6.2a). In order to check the purity of the mitochondrial protein extraction, the expression levels of E-cadherin, lamin A/C and α-tubulin were also assessed as shown in Figure 6.2a. E-cadherin is present at the adherens junctions (626) and lamin A/C are scaffolding elements of the nuclear envelope (627). Therefore, neither of these markers

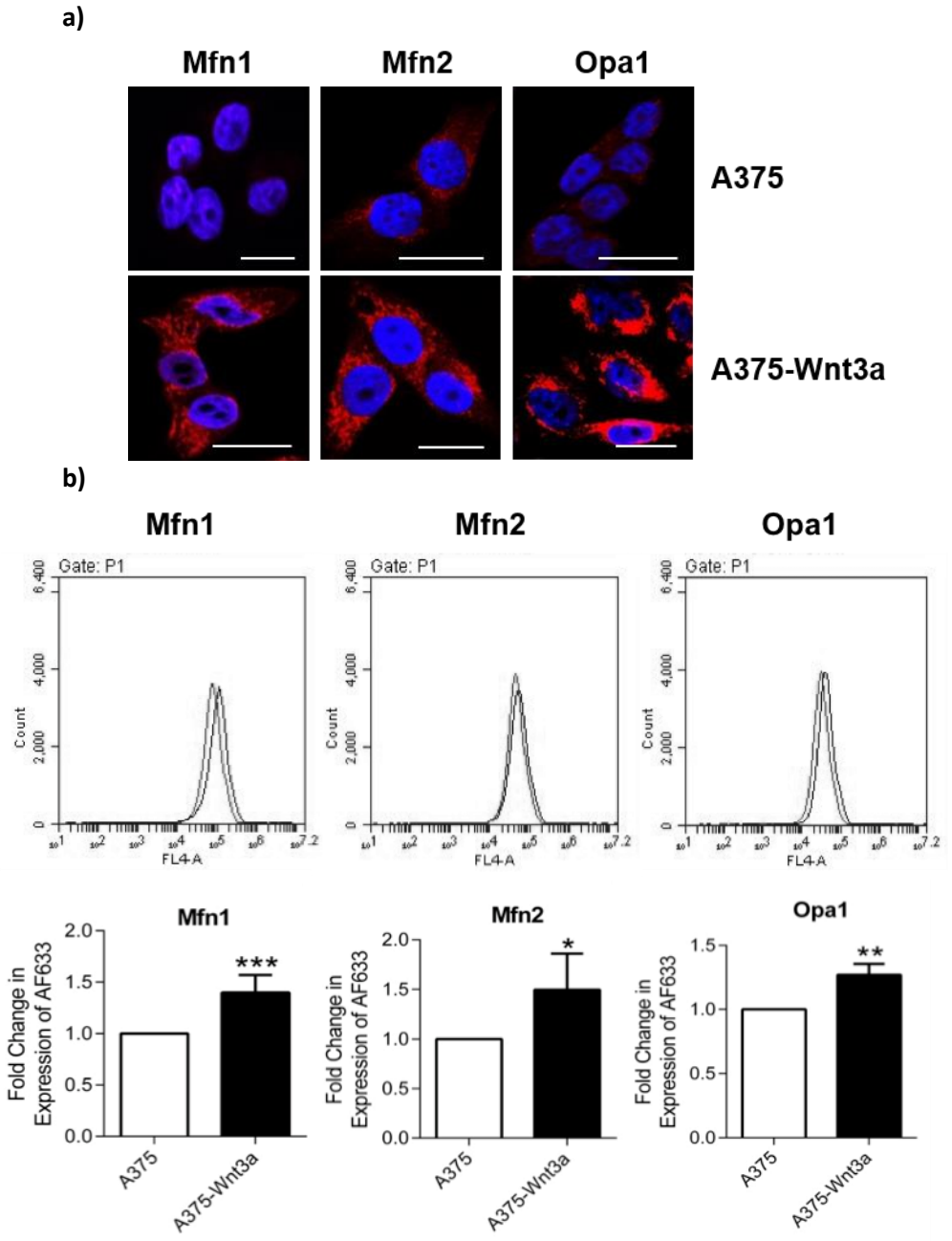


**Figure 6.1: Wnt/β-catenin Signalling Increases Expression of Mitochondrial Fusion Proteins in PTEN$^{WT}$ Cells**

The fusion genes; MFN1, MFN2 and OPA1 were all analysed using confocal microscopy and flow cytometry with the secondary fluorescent antibody AF633. **a)** Wnt3a-overexpression cells were fixed and permeablised before staining with primary antibodies and Far Red secondary antibodies before counter staining with Hoechst (blue). Cells were imaged on a Zeiss LSM510 META with a 63X oil objective. Laser power and gain settings remained constant between control and Wnt3a, but were adjusted for different antibodies. Scale bar = 50 µm. **b)** Cells were analysed on an Accuri C6 flow cytometer for expression of secondary antibody AF633 and fold change in fluorescence calculated. Mean shown ± SD. $p$ = <0.05*. N=4.

should be present at the mitochondria. During the extraction process, cytoskeletal markers such as tubulin or actin are also removed from the protein preparation. Therefore, by comparing the levels of E-cadherin, lamin A/C and α-tubulin in total and mitochondrial extracted protein the purity of the mitochondrial protein can be assessed. Figure 6.2a shows that the levels of E-cadherin, lamin A/C and α-tubulin are very low in the mitochondrial protein and therefore the preparation is pure. In order to qualitatively assess the loading control for the fusion and fission genes, they were compared to Ponceau S staining of the membrane, following transfer. The fusion proteins verify the previously shown results and are all up-regulated in the Wnt3a samples and the active fission protein is down regulated. To verify that this effect was not unique to the overexpression cells, the other $PTEN^{WT}$ cells lines were treated with rWnt3a and the expression levels of Mfn1 are shown in Figure 6.2b. In A375, M202 and Mel501, Mfn1 is upregulated in response to rWnt3a stimulation, confirming the results seen in the Wnt3a overexpression cells using total and mitochondrial extracted protein. In order to quantify the increase in expression in these cells lines, densitometry was carried out and the relative fold increases were calculated at 1.15-fold in the A375 cells, 1.4-fold increase in M202 cells and 1.55-fold increase in the rWnt3a stimulated Mel501 cells (see Figure 6.2c). This data shows that activation of Wnt/β-catenin signalling pathway causes increased mitochondrial fusion and decreased mitochondrial fission protein expression in $PTEN^{WT}$ cells.

### 6.2.1. β-catenin is Vital for Mitochondrial Fusion in $PTEN^{WT}$ Melanoma Cells

It was shown in the previous chapter that, when β-catenin was knocked down in the $PTEN^{WT}$ cells, there was complete fragmentation of the mitochondria (Figure 5.18a). To confirm this, the expression of Mfn1 was measured in the A375 control and Wnt3a overexpression cells treated with scrambled and β-catenin siRNA (see section 2.3.28). The western blot shown in Figure 6.3 clearly shows a reduction in the expression of Mfn1 in the β-catenin siRNA knock down, confirming that

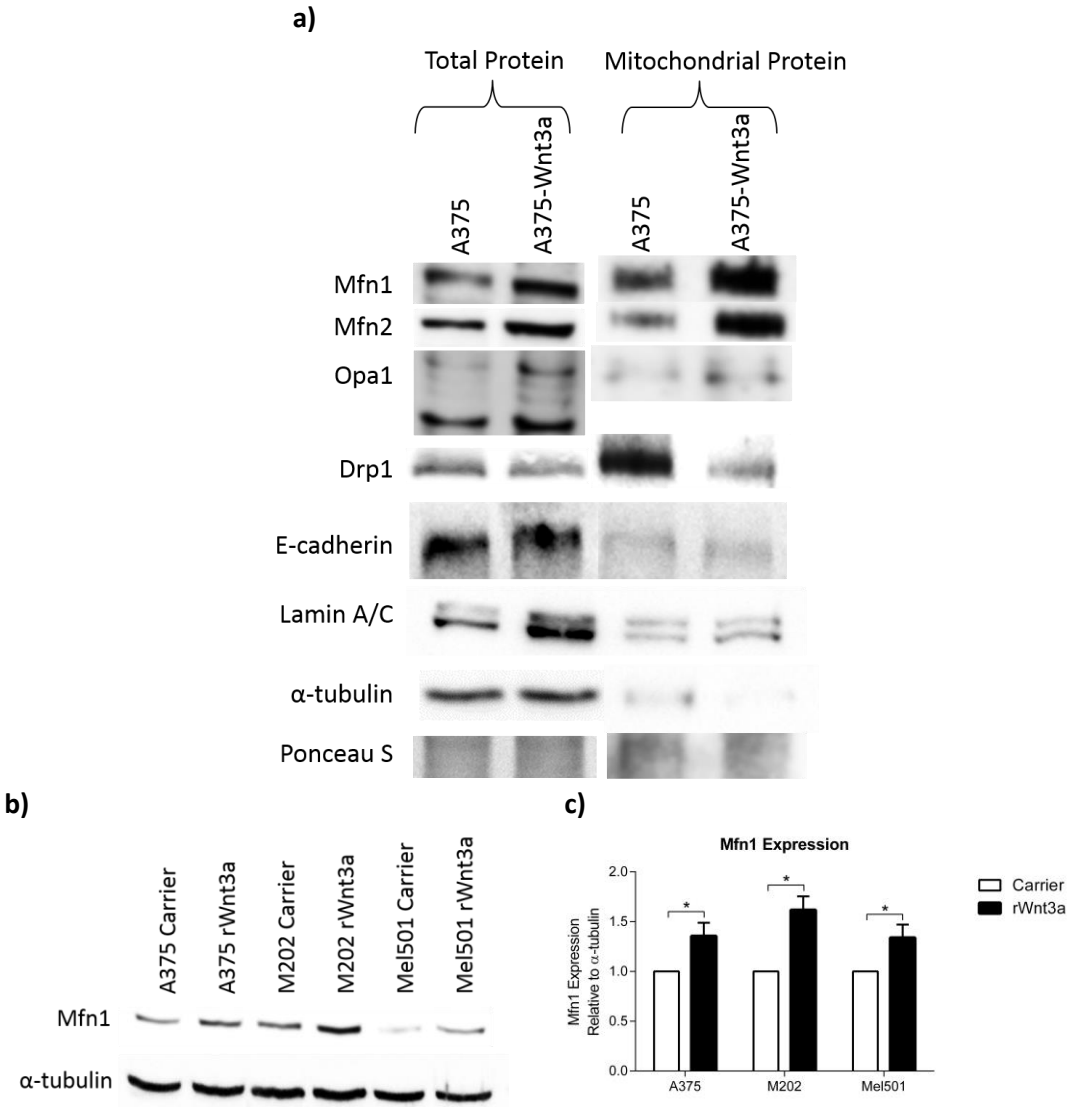


**Figure 6.2: Wnt/β-catenin Signalling Increases Expression of Mitochondrial Fusion Proteins and Reduces Expression of Fission Proteins in PTEN$^{WT}$ Cells**

**a)** Comparing the expression of mitochondrial dynamic proteins in A375 and A375-Wnt3a overexpression cells in total and mitochondrial protein lysates. Levels of E-cadherin and lamin A/C were used to assess the purity of the mitochondrial preparation. α-tubulin and ponceau s staining were used as loading controls. The mitochondria were extracted from 6x10$^7$ A375 Wnt3a overexpression or control cells. Total protein-30 µg. **b)** A375, M202 and Mel501 cells were stimulated with rWnt3a (50 ng/ml) for 48 hours before cells were lysed and BCA for protein concentration was carried out and 30 µg total protein was analysed. **c)** Densitometry was carried out to quantify the increased expression of Mfn1 in rWnt3a treated cell lines. Mean shown ± SD. $p$ = <0.05*. All proteins were run on a 12% Bis-Tris gel and transferred onto a nitrocellulose membrane. Blocking and antibody dilutions were carried out in a 5% Non-Fat Milk solution. Antibody dilution: Mfn1 - 1:500, Mfn2 – 1:500, Opa1 – 1:200, Drp1 – 1:1000, E-cadherin 1:1000, lamin A/C 1:1000. Antibodies were incubated overnight before anti-mouse secondary antibody and ECL development.

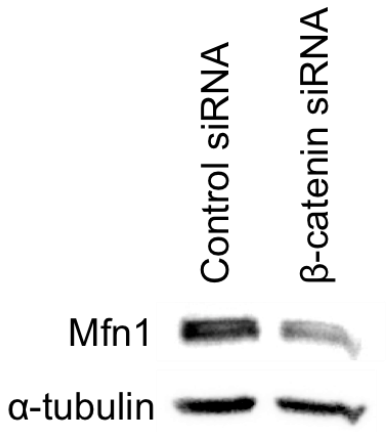


**Figure 6.3: Mfn1 Expression Levels are Controlled by β-catenin**
A375 cells were reverse transfected for 72 hours with β-catenin siRNA. A scrambled control siRNA was used as a control. Cells were lysed and BCA for protein concentration was carried out. 30 µg of protein was run on a 12% Bis-Tris gel and transferred onto nitrocellulose membrane. Blocking and antibody dilutions were carried out in a 5% Non-Fat Milk solution, MFN1 antibody was diluted 1:500 and incubated overnight before anti-mouse secondary antibody and ECL development. α-tubulin was used as a loading control.

depletion of β-catenin causes a reduction in Mfn1 protein. This data indicate that β-catenin regulates fusion proteins in PTEN$^{WT}$ melanoma cells.

### 6.2.2. Knockdown of PTEN Reduces Mitochodnrial Fusion

It was previously shown that PTEN siRNA (see Figure 5.19) also removed the mitochondrial fusion effect from the A375 cells. This effect is confirmed in a reduction of Mfn1 protein expression in A375 cells treated with PTEN siRNA, compared to scrambled siRNA control (see Figure 6.4). The cells were treated with carrier or rWnt3a protein and the increase in Mfn1 seen in the rWnt3a treated sample supports previous results (see Figure 6.1-6.2). These results show that the presence of PTEN is needed for the up regulation of Mfn1 in cells with activated Wnt/β-catenin signalling.

### 6.2.3. β-catenin Does Not Transcriptionally Control The Genes of Mitochondrial Dynamics

As all the levels of fusion and fission genes are affected by the activation of the Wnt/β-catenin pathway and the expression of Mfn1 was reduced by the removal of β-catenin, qPCR (see section 2.3.27) was utilised to see if the fusion and fission genes are controlled at the transcriptional level by β-catenin. There was no statistical significance in the difference at the mRNA level in any of the four genes measured as shown in Figure 6.5. There are large error bars but, following normalisation to three housekeeping genes (β-actin, YWHAZ, UBC), it is possible to conclude that β-catenin does not transcriptionally control expression of these mitochondrial dynamics genes.

## 6.3. Mitochondrial Fusion Accompanies an Increase in Mitochondrial Membrane Potential

A mitochondrial membrane potential is created when free ions generated from the TCA cycle pass through components of the ETC in the mitochondrial membrane (628). Fluorescent dyes, such as JC1 and TMRM, can measure the membrane potential as they accumulate inside the mitochondria in a manner directly

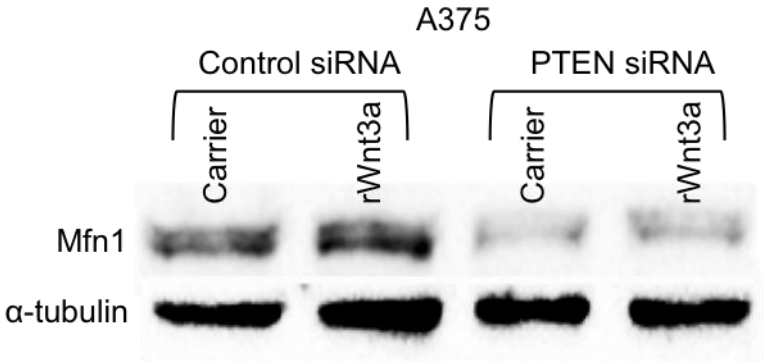


**Figure 6.4: Mfn1 Expression levels are Controlled by PTEN**
A375 cells were reverse transfected for 72 hours with PTEN siRNA. A scrambled control siRNA was used as a control. Cells were lysed and BCA for protein concentration was carried out. 20 µg of protein was run on a 12% Bis-Tris gel and transferred onto nitrocellulose membrane. Blocking and antibody dilutions were carried out in a 5% Non-Fat Milk solution, MFN1 antibody was diluted 1:500 and incubated overnight before anti-mouse secondary antibody and ECL development. α-tubulin was used as a loading control.

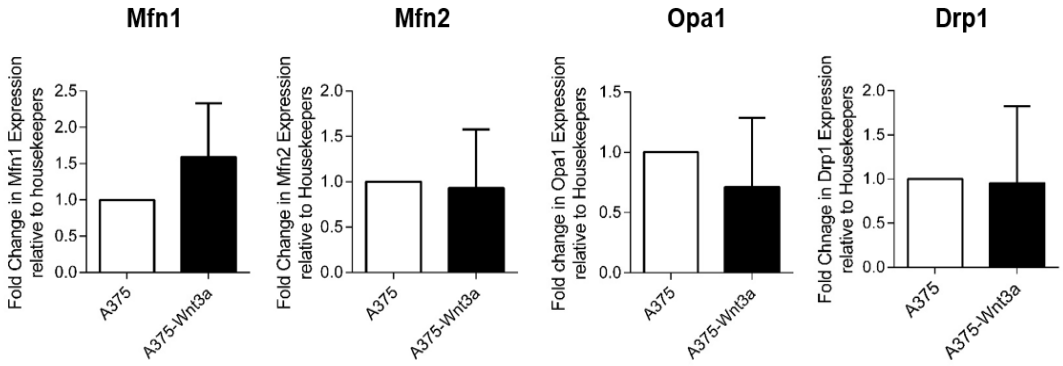


**Figure 6.5: Transcriptional Regulation of Mitochondrial Fusion and Fission Genes in A375 control and Wnt3a Overexpression Cells**
qRT-PCR for MFN1, MFN2, OPA1 and DRP1 in A375 control and Wnt3a overexpression cells. mRNA expression levels were normalized based on the expression of three housekeepers, Ywhaz, UBC and β-actin. RNA was extracted using GeneJet and quantified, RT-PCR was carried out and 2 µg of cDNA was analysed using SYBR green. N=3. Ns.

proportional to the mitochondrial membrane potential (629, 630). Accumulation causes a shift in their fluorescence which can then be analysed by flow cytometry as a measure mitochondrial membrane potential and a subsequent indication of mitochondrial health, fusion and cellular stress.

JC1 (5,5',6,6'-tetrachloro-1,1',3,3'-tetraethylbenzimidazolylcarbocyanine iodide; Invitrogen) is a green fluorescent monomer but, as it accumulates in the mitochondria, it forms red J-aggregates (631). Therefore, the ratio of green to red, when analysed by flow cytometry (see section 2.3.15.4) gives a proportionate analysis of the membrane potential. Figure 6.6a shows a shift in the FL2 (red) channel in A375-overexpression cells. The shift is measured by the percentage of cells in the high FL2 gate-R1 and lower FL2 gate-R2. The A375-Wnt3a overexpression cells show a 13% shift from R2 to R1, indicating an increase in membrane potential, which is represented, by an increase in J-aggregates forming in the mitochondria.

TMRM is a methyl ester of tetramethylrhodamine and, like JC1, is a cationic dye that accumulates in the mitochondria relative to the mitochondrial membrane potential according to the Nernst equation (629, 630). Figure 6.6b shows the flow cytometry staining of TMRM (see section 2.3.15.4) and, as with the JC1 results, the shift in fluorescence is represented in the change of percentage in gates R1 and R2. The Wnt3a overexpression cells increase the percentage of cells in R1 from 87 to 98%, indicating an increase in membrane potential. Taken together the data shows using two different membrane potential dependent dyes, Wnt/β-catenin signalling in $PTEN^{WT}$ cells causes an increase in mitochondrial membrane potential.

## 6.4. Investigations of Mitophagy Control by Canonical Wnt Signalling

As explained in section 6.1.2, the regulation of mitochondrial quality control is governed by two genes called *PINK1* and *PARK2*. It has previously been shown that Pink1 is vital for mitochondrial fusion (603, 609), but along with Parkin, it is also implicated in mitophagy and in the prevention of oxidative stress (632, 633).

**a)**

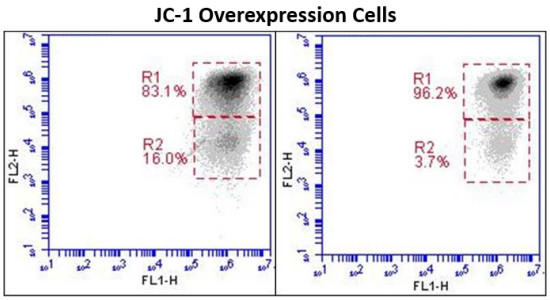


| | R1 | R2 |
|---|---|---|
| A375 | 83.10% | 16.0% |
| A375-Wnt3a | 96.25%* | 3.7%* |

**b)**

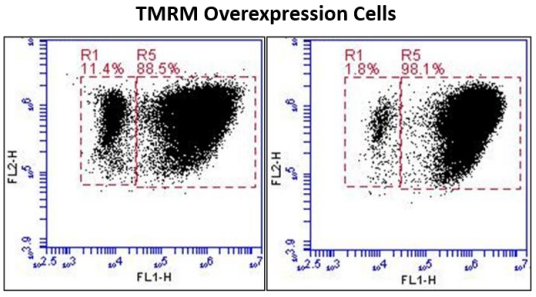


| | R1 | R2 |
|---|---|---|
| A375 | 11.4% | 88.5% |
| A375-Wnt3a | 1.8%* | 98.1%* |

**Figure 6.6: Wnt/β-catenin Increases Mitochondrial Membrane Potential of PTEN$^{WT}$ Cells**
Representative images of Flow Cytometry. A375-Wnt3a overexpression cells were incubated with **a)** 2 µM JC-1 or **b)** 20 µM TMRM diluted in complete media for 2 hours at 37°C, cells were washed in PBS before being resuspended in FACS buffer (PBS +0.01% FCS) and analysed on an Accuri C6 flow cytometer. Mean shown ± SD. $p$ = <0.05*. N=3.

Therefore, understanding the activity of Pink1 and Parkin in these cells could explain the mitochondrial fusion effects and subsequent down regulation of metabolism.

### 6.4.1. Wnt/β-Catenin Reduces Cleavage of Pink1

Typically, Pink1 is taken into the mitochondria where Parl cleaves it at the N-terminus forming ΔN-Pink1 (602-605). This removes Pink1 from constitutively activating the mitophagy pathway on healthy mitochondria (606). During selective mitophagy, cleavage stops allowing full-length Pink1 to accumulate on the mitochondria where it recruits and activates Parkin. Investigating the protein expression (see section 2.3.10-2.3.13) of Pink1 in the Wnt3a overexpressing cells revealed two distinct bands (see Figure 6.7). These two isoforms have previously been published as a full length Pink1 at 63kDa and ΔN-Pink1 at 53kDa (603) which are formed from cleavage of the N-terminus of Pink1 upon entering the mitochondria. Figure 6.7 shows that the control cells have roughly equal expression of both isoforms of Pink1, but the A375-Wnt3a overexpression cells have increased expression of the full-length isoform and reduced levels of the cleaved isoform. These findings indicated a reduction in Pink1 cleavage which could be effecting the recruitment of Parkin to the mitochondria in the mitophagy pathway.

### 6.4.2. β-Catenin Binds Parkin in Melanoma Cells

As Pink1 is vital for recruitment of Parkin, it was important to study the levels of Parkin in both total and mitochondrial extracted protein (613). Figure 6.8a shows that there is no difference in the protein levels of Parkin in the Wnt3a overexpression cells compared to control. Figure 6.8b shows that, as with total protein, there are no differences in the levels of Parkin at the mitochondria, but interestingly there are increased levels of β-catenin at the mitochondria in Wnt3a overexpression cells. It has previously been suggested in neurons that Parkin can bind to β-catenin in a protective role against excessive Wnt/β-catenin signalling (619), as would be the case in the Wnt3a-overexpressing cells where the signalling pathway is constitutively active. Therefore, the potential binding of Parkin to β-

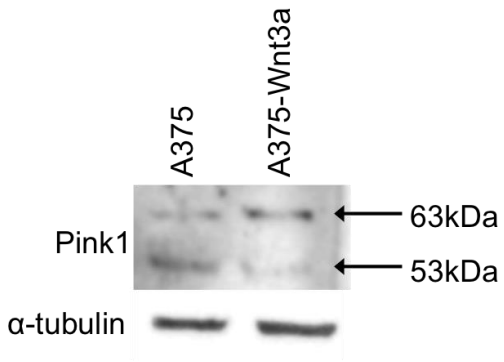


**Figure 6.7: Wnt/β-catenin Signalling Reduces Pink1 Cleavage**
A375 Wnt3a overexpression or control cells were lysed and BCA for protein concentration was carried out and 25 µg total protein was run on a 12% Bis-Tris gel and transferred onto a nitrocellulose membrane. Blocking and antibody dilutions were carried out in a 5% Non-Fat Milk solution, anti-Pink1 1:1000, and incubated overnight before anti-rabbit secondary antibody and ECL development. α-tubulin was used as a loading control. Arrows indicate sizes of full length Pink1 at 63kDa and ΔN-Pink1 at 53kDa.

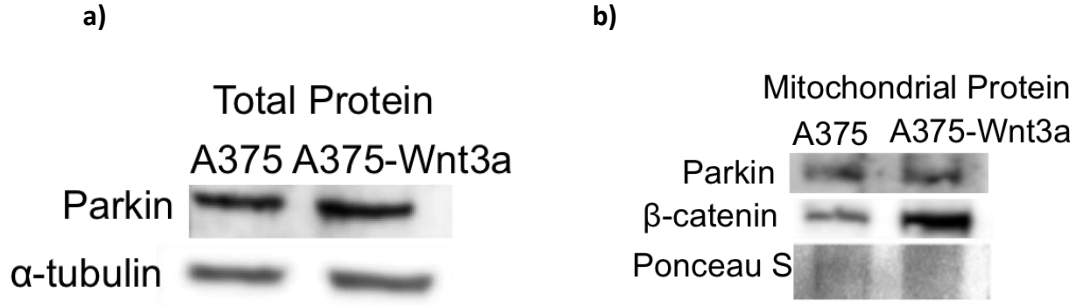


**Figure 6.8: Total and mitochondrial Parkin Expression in Unaffected by Wnt/β-catenin Signalling but β-catenin expression at the Mitochondria is Increased**
**a)** A375 Wnt3a overexpression or control cells were lysed and BCA for protein concentration was carried out and 30 µg total protein was run on a 12% Bis-Tris gel and transferred onto nitrocellulose membrane. Blocking and antibody dilutions were carried out in a 5% Non-Fat Milk solution, Parkin 1:1000, and incubated overnight at 4°C before anti-rabbit secondary antibody and ECL development. α-tubulin was used as a loading control. **b)** The mitochondria were extracted from $6x10^7$ A375 Wnt3a overexpression or control cells. Mitochondrial pellets were resuspended in 1X SDS loading buffer. Concentrations are unknown, Ponceau S staining was used for loading comparisons. Proteins were blotted for Parkin at 1:200 and β-catenin at 1:1000.

catenin in melanoma cells was investigated using co-immunoprecipitation of β-catenin and Parkin (see section 2.3.30). The blot shown in Figure 6.9 shows the results. The levels of Parkin were analysed in the 1/150$^{th}$ of total input of protein, the two pre-clear stages using Concavolin A (399) beads for non-glycosylated β-catenin and IgG control for non-specific binding in the IP samples. Parkin is present in all samples, including the IP samples indicating that Parkin does bind β-catenin in PTEN$^{WT}$ melanoma cells. The level of binding in the Wnt3a samples is higher than that in the control cells indicating that when β-catenin is stabilised, it has higher levels of protein binding to Parkin. As a control for the IP, the samples were all blotted for β-catenin as well. This is shown in the right column of results in Figure 6.9. As expected, β-catenin expression was higher in the total input and the IP of the Wnt3a samples, this implies that Parkin binds to the cytoplasmic portion of β-catenin rather than the adherens junction pool. Also expected was the lower expression in the Wnt3a ConA pre-clear sample, as the Wnt3a samples should have stabilised β-catenin and therefore will have lower levels of non-glycosylated β-catenin. These controls verify the quality of these results showing that β-catenin binds Parkin and that the binding increases in response to Wnt/β-catenin signalling.

### 6.4.3. PTEN$^{WT}$ Melanoma Cells are Autophagy Dependent Which is Blocked by Active Wnt/β-catenin Signalling

As changes to Pink1 cleavage and Parkin binding have been measured, it is necessary to investigate if these have any effect on mitophagy, mitochondrial specific autophagy. As explained in section 6.1.2, the Pink1/Parkin pathway maintains mitochondrial homeostasis by removing damaged mitochondria through the process of autophagosome engulfment (602). LC3 and p62 are two genes involved in this process so their expression levels can indicate levels of autophagy (634).

LC3 expression was analysed in the A375 Wnt3a-overexpression cells (see Figure 6.10a). LC3 (634) is seen in two forms. LC3I (18kDa) is cytosolic and, when activated, is cleaved at the C-terminus to form LC3II (16kDa), which binds to the autophagosomes (591, 622). The control cells only have expression of LC3II,

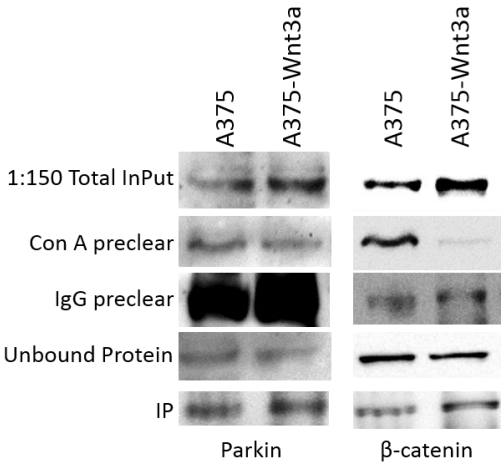


**Figure 6.9: Parkin Binds to β-catenin in PTEN$^{WT}$ Melanoma Cells**
A375 Wnt3a overexpression or control cells were lysed and BCA for protein concentration was carried out. 4 mg of protein was put into a β-catenin IP. Samples: Total protein diluted 1:150, pre-clear with ConA beads for non-glycosylated β-catenin and IgG control for non-specific binding, any unbound protein and IP samples. All samples were blotted for Parkin 1:200 and β-catenin 1:1000.

indicating that it is constantly activated and autophagosomes are constantly present or in the process of forming suggesting that A375 cells are autophagy dependent. However, the results for the Wnt3a overexpression cells show much higher levels of LC3I. This suggests that activation of the Wnt/β-catenin signalling pathway may inhibit autophagy in the $PTEN^{WT}$ melanoma cells.

As the β-catenin siRNA (see section 2.3.28) experiments have previously been very informative and shown that β-catenin is vital in mitochondrial fusion and metabolism, the effects of the siRNA knockdown were also investigated in LC3 expression. Figure 6.10b shows that the A375-Wnt3a-overexpressing cells lose the expression of LC3I when β-catenin is removed from the cells and revert back to the autophagy phenotype that highly expresses LC3II.

Finally, in order to investigate if this effect was specific to the $PTEN^{WT}$ cells, the LC3 expression was analysed in the $PTEN^{Mut}$ cells. Figure 6.10c shows the expression in A2058 control and Wnt3a-overexpression cells. The ratio of LC3I to LC3II is equal in both cell types, indicating that there is no effect of the Wnt/β-catenin pathway on autophagy in these cells. These results suggest that $PTEN^{WT}$ cells have high levels of autophagy, where activation of the Wnt/β-catenin signalling pathway can antagonise the autophagy pathway in these cells and that β-catenin is necessary for this to occur.

The autophagy adaptor p62 is responsible for targeting ubiquinated proteins to the autophagosomes (602). Accumulation of p62 is associated with tumourigenesis (595) and it is accepted that inhibiting autophagy will cause an accumulation of p62 (622) and processes such as hypoxia and nutrient starvation, induce p62 degradation (288, 622). The results in section 6.5.1 show that activation of the Wnt/β-catenin pathway can block autophagy and this process potentially sends the cells into a nutrient poor environment. It has been shown that p62 can bind and interact with the Wnt signalling pathway (see section 6.1.2) and this previous research has led to the finding that Wnt/β-catenin downregulates autophagy and represses p62 (596). Figure 6.11a confirms these findings in $PTEN^{WT}$ melanoma cells. The Wnt3a-overexpression cells have a reduced level of p62 when compared

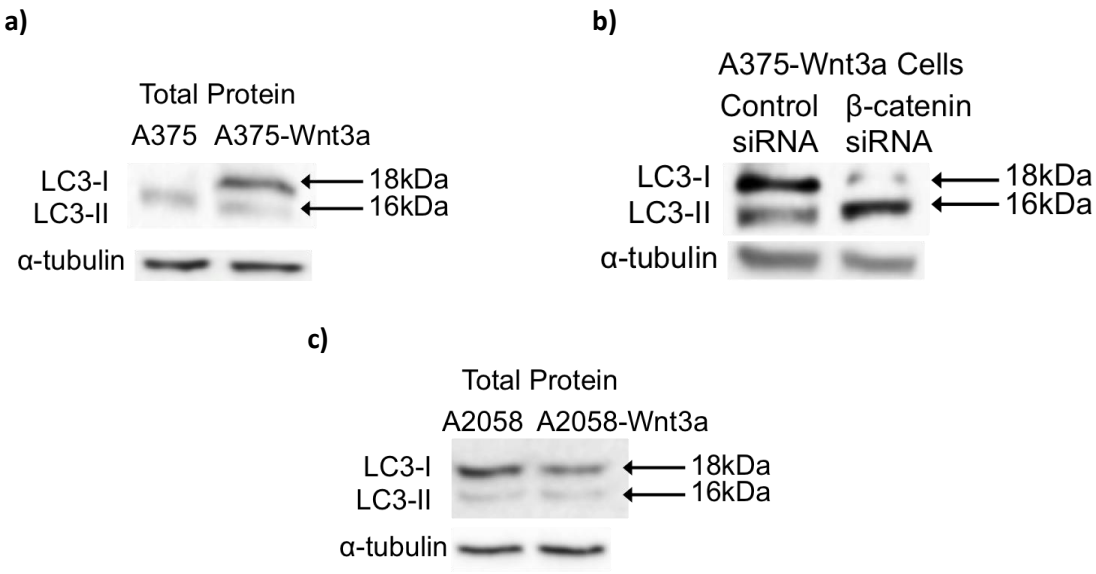


**Figure 6.10: Wnt/β-catenin Signalling Reduces Autophagy in PTEN$^{WT}$ Cells but not in PTEN$^{Mut}$ Cells.**

A375 Wnt3a overexpression or control cells were lysed and BCA for protein concentration was carried out and 25 µg total protein was run on a 12% Bis-Tris gel and transferred onto nitrocellulose membrane. Blocking and antibody dilutions were carried out in a 5% Non-Fat Milk solution, LC3 1:1000, and incubated overnight before anti-rabbit secondary antibody and ECL development. α-tubulin was used as a loading control. **a)** Total protein **b)** Protein treated with β-catenin siRNA. **c)** A2058 control and Wnt3a overexpression cells.

to the control cells and this expression is reversed when β-catenin is removed by siRNA (See Figure 6.11b). These results show that p62 is downregulated by Wnt/β-catenin signalling and, combined with the findings of LC3, confirms previous findings that Wnt/β-catenin signalling reduces autophagy (596) in $PTEN^{WT}$, but not $PTEN^{Mut}$ melanoma cells.

## 6.5. β-Catenin Binds Proteins Involved in Cellular Metabolism

Given β-catenin was found to be present at the mitochondria and it binds to Parkin, in addition to the previous findings that β-catenin knockdown affected metabolism all suggest that it is a major player in cellular metabolism. To investigate this further we decided to analyse the previously described IP samples (see section 6.4.2) by mass spectrometry (MS; see section 2.3.30.1-2.3.30.3). The data was normalised to non-specific IgG binding and then compared to either increased or decreased binding between the control and the Wnt3a overexpression cells. These proteins were subsequently analysed using PANTHER. Listed in Table 6.1 are the 5 proteins with the highest increase and decrease in binding to β-catenin. Of these, 3 of the top 5 proteins with increased binding are linked to metabolism, as are 4 of top 5 proteins with decreased binding to β-catenin. Of specific interest is Microtubule associated protein 1B (MAP1B). This protein had the most reduced level of binding to stabilised β-catenin and it is identified as a protein of cellular process. MAP1B regulates microtuble assembly and has been linked to the axonal movement of mitochondria and autophagosome formation (635, 636). MAP1B is a member of the same family as LC3 (MAP1LC3A) which has previously been measured to be altered by Wnt/β-catenin signalling (see Figure 6.10a). Surprisingly, Parkin was not found in these samples, which would have been expected from previous findings (see Figure 6.9). However, the results provided much new information about β-catenin binding partners. Figure 6.12a shows the GO Biological Processes of proteins with increased binding to β-catenin. Of these genes, 35% were involved in metabolism. These metabolism genes are listed in Table 8.1 (Appendix). Of specific interest from this list are a number of proteins involved in translation, cell cycle and apoptosis, specifically Cytochrome *c*, which as shown in Figure 4.8, is already known

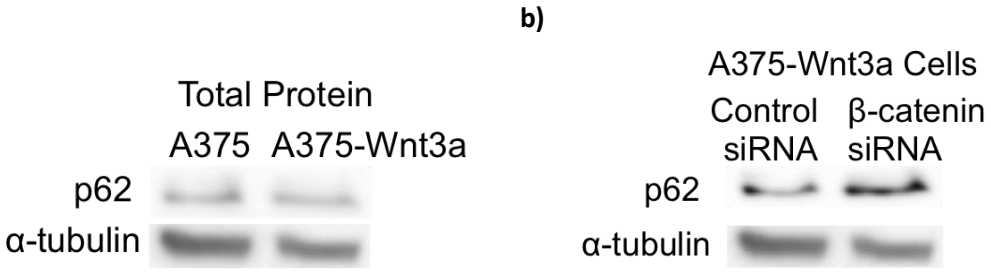


**Figure 6.11: Wnt/β-catenin Signalling Degrades p62 Expression**
A375 Wnt3a overexpression or control cells were lysed and BCA for protein concentration was carried out and 25 µg total protein was run on a 12% Bis-Tris gel and transferred onto nitrocellulose membrane. Blocking and antibody dilutions were carried out in a 5% Non-Fat Milk solution, p62 1:1000, and incubated overnight before anti-rabbit secondary antibody and ECL development. α-tubulin was used as a loading control. **a**) Total protein **b**) Protein treated with β-catenin siRNA.

**Table 6.1: Top 5 Proteins with Increased (green) and Decreased (red) Binding to β-catenin**

| Mapped ID | Gene Name/Symbol | GO Biological Process | Function |
|---|---|---|---|
| Q14692 | Ribosome biogenesis protein BMS1 homolog<br>BMS1<br>ortholog | Metabolic Process | Nucleobase-containing compound metabolic process |
| Q9H0A0 | N-acetlytransferase 10 | Biological Process<br>Metabolic Process | Nucleotide binding |
| Q5BKZ1 | DBIRD complex subunit | Cellular Process | DNA binding |
| Q9Y678 | Coatomer subunit gamma-1 | Localisation | Vesicle coat protein |
| Q9NVP1 | ATP-dependent RNA helicase DDX18<br>DDX18<br>ortholog | Metabolic Process<br>Biological regulation | nucleobase-containing compound metabolic process<br>translation<br>regulation of translation |
| P46821 | Microtubule associated protein 1B | Cellular Process | Non-motor microtubule binding protein |
| P40227 | T-complex protein 1 subunit zeta<br>CCT6A<br>ortholog | Metabolic process<br>Cellular component organisation or biogenesis | Protein folding, protein compex assembly, protein complex biogenesis |
| P09972 | Fructose-bisphosphate aldolase c | Apoptotic Process<br>Metabolic Process | Carbohydrate degradation glycolysis |
| O43175 | D-3-phosphoglycerate dehydrogenase<br>PHGDH<br>ortholog | Metabolic Process | Carbohydrate metabolic process<br>Cellular amino acid biosynthetic process |
| P52209 | 6-phosphogluconate dehydrogenase, decarboxylating<br>PGD<br>ortholog | Metabolic Process | Pentose phospate shunt |

to be released in response to Wnt/β-catenin. The MS analysis also discovered that a number of proteins have lower binding to β-catenin when the Wnt/β-catenin signalling pathway is activated. As shown in Figure 6.12b, 42% of proteins with reduced binding are involved in metabolism, details of which are in Table 8.2 in the Appendix. As with the proteins with increased binding, the list of proteins with reduced binding also has a number of interesting findings, including those involved in glycolysis, amino acid metabolism, the ETC and the TCA cycle. Specifically, there is a reduction in Lactate Dehydrogenase A (LDHA) and Lactate Dehydrogenase B (LDHB), supporting the results as shown in Figure 5.6 where a reduction in lactate secretion was measured in the $PTEN^{WT}$ melanoma cells with active Wnt/β-catenin. Table 8.2 also includes ATP-citrate synthase, supporting the reduction in citrate synthase activity measured in these cells in Figure 5.5. These findings show that β-catenin binds to a number of genes involved in metabolism. As previously shown in Figure 5.18, the removal of β-catenin increased lactate secretion and citrate synthase activity, combined with this data, now implicates β-catenin as a key regulator of melanoma cell metabolism.

**a)**

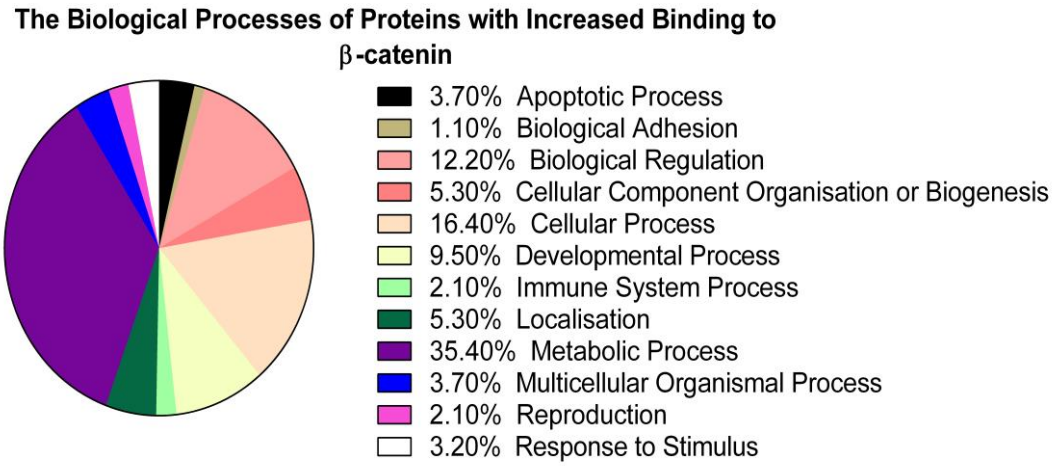


**b)**

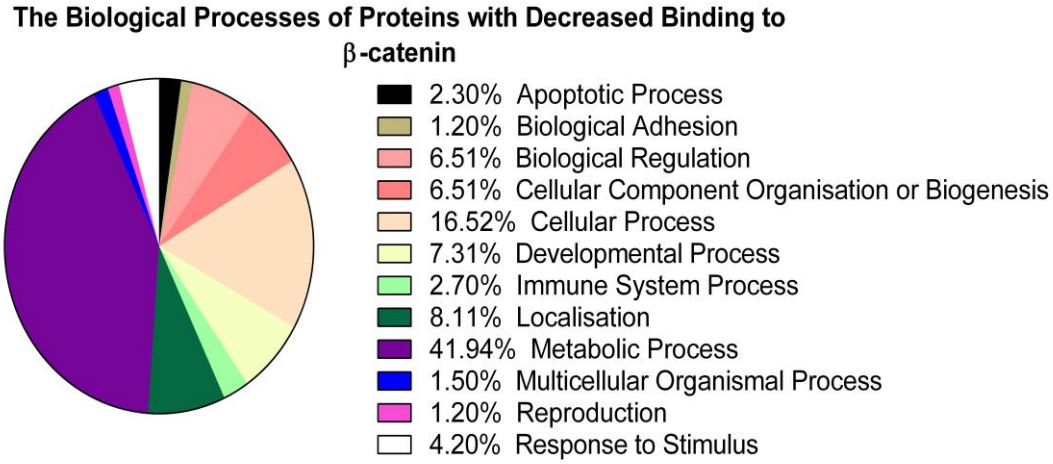


**Figure 6.12: Mass Spectrometry Identifies Novel β-catenin Binding Partners in PTEN$^{WT}$ Melanoma Cells**

A375-Wnt3a overexpression cells used in the β-catenin IP shown in Figure 6.11 were analysed by nano-LC-MS/MS on a Thermo Scientific Q Exactive. Identification and label free quantification of peptides was done with MaxQuant 1.5. Proteins that were significantly regulated between conditions were identified using a permutation-based t-test (S1, FDR 5%) in Perseus 1.4.1.3. GO-terms were analysed using PANTHER 9.0. **a)** GO Biological processes with increased binding to β-catenin. **b)** GO Biological processes with reduced binding to β-catenin.

## 6.6. Discussion

It was previously shown that activation of the Wnt/β-catenin pathway caused the mitochondria of PTEN$^{WT}$ melanoma cells to become highly networked, elongated and perinuclear with reduced cellular metabolism. The aim of this chapter was to investigate a mechanism that controls this process. It was found that PTEN$^{WT}$ melanoma cells have high levels of autophagy providing nutrients for proliferation, invasion and migration. Activation of the Wnt/β-catenin pathway blocks this potentially though the binding of β-catenin to Parkin. This subsequently causes the mitochondria to elongate and cluster near the nucleus in a protective manner against autophagosome formation and sends the cells into a state of starvation. This results in increased expression of mitochonadrial fusion proteins, an increase in glucose intake, potentially as a compensatory mechanism. This results in the reduced OXPHOS, ATP production and glycolysis as previously shown.

The mitochondria of PTEN$^{WT}$ melanoma cells have increased levels of mitochondrial fusion proteins in response to active Wnt/β-catenin signalling, as shown by imaging, flow cytometry (see Figure 6.1), and western blot (see Figure 6.2). This includes the analysis of mitochondrial fusion proteins Mfn1 and Mfn2 on the OMM and Opa1 on the IMM. This was seen in both total protein and, to a greater extent, in mitochondrial extracted protein. It was also seen in cells with overexpressed Wnt3a, to a greater extent to that observed in cells treated with rWnt3a, indicating that constitutively active Wnt/β-catenin signalling prolongs and enhances this effect, probably due to the increased levels of Wnt3a secretion in the overexpression cells. Yoon *et al.* observed increased size and length of mitochondria of Wnt3a treated C2C12 cells (495), potentially implicating Mfns in this model, although the regulators of mitochondrial dynamics were never investigated in this study. In support of the findings shown here, including the increased expression of Mfns and the changes to mitochondrial shape and location seen in PTEN$^{WT}$ melanoma cells in Figure 5.9a, it has previously been shown that the overexpression of both *MFN1* and *MFN2* in COS-7 and HeLa cells causes mitochondrial perinuclear aggregation (239, 562, 572, 581, 637) and, in some cell types (U2OS cells), the mitochondria are observed in

perinuclear clusters under control conditions (561). In HeLa and breast cancer cells, the increased expression of *MFN1* caused the mitochondria to be longer, highly branched and interconnected, which is clearly seen in Figure 5.10 (239, 245). Also, knockdown experiments in MEFs resulted in small, cytoplasmically dispersed, punctate mitochondria (574, 638), indicating *MFN1* plays a specific role in mitochondrial elongation (245, 318). In breast cancer cells, *MFN1* knockdown increased the tumour cells' ability to migrate and invade (239). Likewise, we show here, that cells with increased Mfn expression have reduced invasion and migration as shown in Figures 4.10 and 4.12. Overexpression of *MFN2* has been seen to increase membrane potential, glucose oxidation and inhibit apoptosis (266, 581). Whereas, knockdown of *MFN2* has been shown to reduce the membrane potential, cellular oxygen consumption and glucose oxidation (564, 573), as well as the activity of respiratory complexes I and III (581). The highly fused, perinuclear mitochondria of $PTEN^{WT}$ melanoma cells have increased membrane potential, compared to their controls (see Figure 6.6), measured by two different mitochondrial membrane potential-dependent dyes. Increased membrane potential is expected from highly fused mitochondria (639) as the fusion process itself is dependent on the mitochondrial membrane potential being intact (245, 291). In a variety of cancers including gastric cancer, Mfn2 has been shown to have significantly lower expression levels than in normal tissue (580). However, similar to the results seen in $PTEN^{WT}$ melanoma cells, the overexpression of *MFN2* reduced proliferation, invasion and migration, as well as increasing mitochondrial membrane potential and inducing apoptosis (580, 640-642), indicating that Mfn2 has an anti-tumour effect and that *MFN2* may play a direct role in cellular metabolism by affecting OXPHOS (249). In addition, increased Mfn expression and mitochondrial length have been linked to cell senescence (643, 644), therefore investigating senescence in future work could give more strength to the reduction in proliferation previously seen (see Figure 4.6).

It has been suggested that increased levels of Mfns only tether the outer mitochondrial membrane, causing the mitochondria to cluster, but without the inner mitochondrial membrane fusion (239). This data shows that there is an also increased level of Opa1. Indicating full fusion of the mitochondria (see Figures 6.1-

6.2). To enhance these findings, a photoactivated construct such as Mito-PA-GFP (Addgene) could be used (645). This GFP construct increases its fluorescence 100-fold when activated by 2-photon excitation. It is transfected into cells with mito-DsRed and time-lapse imaging is utilised to capture the mitochondrial fusion. If full fusion occurs, the mitochondrial context will mix, gradually diluting the highly fluorescent PA-GFP. However if full fusion does not occur, fluorescence will remain high (645). This option was not chosen in this research as the fusion effects were visualised following 48 hours of stimulation. Therefore, time-lapse imaging would not have been possible over this period without photobleaching, which could have removed fluorescence results.

Wnt/β-catenin signalling reduced mitochondrial fission in $PTEN^{WT}$ melanoma cells, as shown by levels of active Drp1 in extracted mitochondrial proteins. This further verified the results of cell invasion, migration and metastasis shown in Figures 4.10, 4.12-4.16 and the mitochondrial imaging shown in Figure 5.9a. It is already known that fission is needed to distribute the mitochondria at the leading edge of a tumour for movement (239, 554) as explained in section 5.6. As increased fission is usually seen as a sign of severely damaged mitochondria (561) and loss of membrane potential is often indicative of cell death (265), these results suggest an increase in the health of the mitochondria in response to active Wnt/β-catenin signalling. Drp1 has been shown to be upregulated in metastatic lesions and lymph nodes of breast cancers (239) and the expression levels were directly proportional to the severity of invasiveness and metastasis (239). In breast cancer samples, the mitochondria were found to be more fragmented and expressed lower levels of Mfns (239). Unsurprisingly, inhibition of *DRP1* leads to elongated, perinuclear mitochondria in breast cancer cells (239, 646) with reduced migration and invasion (239) and, in lung cancer samples, has been shown to increase apoptosis (565). This corresponds to results shown here in the $PTEN^{WT}$ melanoma cells where reduced expression of active Drp1 was measured in cells with elongated mitochondria, reduced invasion and migration and increased apoptosis.

None of the genes of mitochondrial dynamics are controlled at the transcriptional level by β-catenin (see Figure 6.5), but siRNA knockdown of β-catenin reduced mitofusin levels (see Figure 6.3) indicating that β-catenin plays a vital role in mitochondrial dynamics, yet not through *de-novo* transcription of the *MFN* genes. It is known that Mfns are degraded by the proteasome (647) following ubiquitination by Parkin (606, 608). However, total and mitochondrial Parkin levels were equal (see Figure 6.8a+b), indicating that there is no direct effect of the Wnt/β-catenin pathway on Parkin recruitment to the mitochondria. However, it is possible that activation of Wnt/β-catenin signalling could perturb the Pink1/Parkin pathway through an alternative mechanism. Pink1 is taken into the mitochondria and cleaved at the N-terminus by Parl (603), but in cells with a reduced mitochondrial membrane potential, Pink1 is no longer cleaved and, instead, full-length Pink1 accumulates on the OMM (605) which subsequently recruits Parkin (604). It has been shown, that the ratio of full-length Pink1 to its cleaved form, ΔN-Pink1, is important and, dysregulation of Pink1 cleavage, can lead to a reduced mitochondrial membrane potential, an increase in ROS and a disrupted mitochondrial network (603). In $PTEN^{WT}$ melanoma cells with activated Wnt/β-catenin signalling, there is an increase in the mitochondrial membrane potential (see Figure 6.6) as well as an increase in the ratio of full-length Pink1 to ΔN-Pink1 (see Figure 6.7). It might be possible that Pink1 is being aberrantly cleaved and, potentially, Parl is downregulated by Wnt/β-catenin signalling, although this would need to be directly investigated. Alternatively, it is already known that Parkin can bind to β-catenin in a protective manner against excessive Wnt/β-catenin signalling in neuronal cells, protecting the cells from Wnt-induced apoptosis and cell cycle dysregulation (619). It is shown here that β-catenin is present at the mitochondria and the level is increased when β-catenin is stabilised (see Figure 6.8b). It is also shown here, for the first time, that Parkin binds β-catenin in melanoma cells. These results indicate that β-catenin binds to Parkin in the cytoplasm of $PTEN^{WT}$ melanoma cells. This is increased as the levels of cytoplasmic, stabilised β-catenin increase, potentially affecting the recruitment of Parkin to the mitochondria. In order to investigate this further, co-IP of Parkin and Pink1 would inform if their interactions were reduced in Wnt/β-catenin cells and an E3 activity

assay could analyse if increased binding of Parkin to β-catenin effects Parkin activity (607).

In order to investigate if the downstream effects of the Pink1/Parkin pathway on mitophagy were altered by aberrant Pink1 cleavage or by increased Parkin/β-catenin binding, markers of autophagy were investigated. LC3 (634) is a protein that plays an important role in the elongation and closure of the autophagosome. Its lipidation converts it from LC3I to LC3II (591, 621, 622). Figure 6.10a shows $PTEN^{WT}$ melanoma cells do not have detectable levels of LC3I. This phenotype has previously been described for cells undergoing autophagy dependency or addiction (541, 599, 623, 648). This implies that these cells, require autophagy to recycle cellular components to use in the biosynthesis of essential amino acids in order to sustain cell survival, metabolism, proliferation and tumourigenesis (541, 547, 599, 621, 623, 648, 649). To fully determine this, siRNA knockdown of autophagy proteins Beclin1 or Atg5 would be needed (541). The expression of LC3 in Wnt3a activated $PTEN^{WT}$ cells shows equal expression of LC3I and LC3II showing that autophagy is inhibited by the active Wnt/β-catenin pathway. This removes the source of nutrients from these cells, ultimately sending them into a state of starvation as depicted in Figure 6.10a. In support of all of this data, others have shown that, in a state of starvation, levels of cAMP increase and subsequently activate PKA, this causes the phosphorylation of Drp1 on Ser637 causing the mitochondria of cancer cells to elongate, become perinuclear (as shown in Figures 5.9a and 5.10) and have reduced levels of autophagy (596, 598, 606). This suggests that investigation into cAMP expression, PKA activity and Drp1 phosphorylation at Ser637 could also confirm autophagy dependency in the $PTEN^{WT}$ cells. The mitochondria respond in this manner to protect themselves from macroautophagy, as they become too large to fit into the autophagosome. Their elongation preserves ATP levels via increased cristae density and, therefore, maintains cell viability (242, 598, 606). In addition, the expression of the adaptor protein p62, plays an important role in regulating cellular autophagy and it is connected to the Wnt/β-catenin pathway though p62-mediated degradation of Dishevelled (595, 596, 622, 624, 625). Its expression is reduced in Wnt3a overexpression cells (see Figure 6.10a), supporting the finding that β-catenin

stabilisation can inhibit the formation of the autophagososme and the subsequent repression of p62 (596), due to degradation during nutrient starvation (622). As in APC driven-colorectal cancers (596), siRNA knockdown of β-catenin reverses the Wnt3a-overexpression cells back to their autophagy dependent state. This increases the levels of p62 in cells with activated Wnt/β-catenin signalling (see Figure 6.10b) in a transcriptional manner through TCF4 (596), adding to the growing support that β-catenin is vital in the regulation of mitochondrial related functions.

To determine if these findings were also dependent on the intact signalling of PTEN, siRNA knockdown of the expression was utilised. PTEN siRNA removed the mitochondrial fusion effect and downregulated Mfn1 expression (see Figures 5.20 and 6.4), showing that the nature of Wnt/β-catenin signalling on the mitochondria is PTEN dependent and presumably this is also the case regarding the effects on cellular metabolism as the LC3 expression is unaffected by Wnt/β-catenin activation in $PTEN^{Mut}$ melanoma cells, as shown in Figure 6.10c.

Autophagy addiction is common in cancers with KRas mutations, such as in lung and pancreatic cancers and this research has shown for the first time, in melanomas with downstream effector mutations such as the $Braf^{V600E}$ or NRas mutations may also be dependent on autophagy to sustain their metabolic requirements (541, 547, 594, 644, 650, 651). In Ras activated cancers, autophagy is a necessary process for mitochondrial metabolic function (599). When autophagy is inhibited there is an accumulation of damaged mitochondria with defective mitochondrial respiration, reduced oxygen consumption and reduced glycolysis (242, 541, 547, 594, 599) as seen in the $PTEN^{WT}$ cells with active Wnt/β-catenin signalling (see Figures 5.1-5.6). Instead of managing pyruvate levels for TCA cycle activity, Ras activates LDH to increase levels of lactate (599). In addition to this, Ras activates PDK1, which inhibits PDH and therefore the conversion of pyruvate to acetyl-CoA, thereby reducing the TCA cycle activity (652). The Ras activation also makes these cells insensitive to glucose levels, by changing the glycolytic requirements of the cells (547, 650). This can be seen in the $PTEN^{WT}$ cells in Figure 5.3 where changes in glucose levels have no effect on the ECAR. This would imply that the cells have become dependent upon

glutamine for respiration, as has previously been seen in Braf driven lung cancers (594). It has also been shown, that decreased autophagy is known to cause an increase in apoptosis and a decrease in proliferation (594, 601), fitting with the data shown in Figures 4.6-4.9. Through multiple pathways, these tumours can reduce acetyl-CoA synthesis, leading to a reduction in citrate available for fatty acid synthesis (653). Therefore, in the $PTEN^{WT}$ cells it would appear that activation of the Wnt/β-catenin pathway inhibits autophagy (596), increasing apoptosis and reducing proliferation to send the cells into starvation mode. The autophagy addicted cells require the recycling of macromolecules for nutrition, by blocking this pathway the cells have no fuel source for mitochondrial metabolism (599). This then causes the large increase in glucose consumption seen in the cells in Figure 5.8. The reduction in autophagy can also explain the reduction in ROS seen in Figure 5.7, as production is linked to the formation of the autophagosome (598, 654), and without autophagy there is also a reduction in substrates used to produce ROS (594).

The role of PTEN further ties autophagy addiction to our model of melanoma. It is known that PTEN can induce autophagy through the negative regulations of Akt and subsequent inactivation of mTOR (655-657). During nutrient rich conditions p62 is known to bind to Raptor, the regulatory-associated protein of mTOR (622, 658), which activates mTORC1 thereby inhibiting autophagy via the PI3K/Akt pathway and phosphorylation of S6K1 (547, 591, 598, 623, 659, 660). Alternatively, deletion of PTEN can phosphorylate and activate Akt (661). Therefore, in $PTEN^{Mut}$ cells with hyperactive PI3K signalling, autophagy addiction is not seen (see Figure 6.10c). However, low AMP levels, due to limited nutrient availability, is sensed by AMPK which phosphorylates TSC2 and negatively regulates mTOR (547, 662), inducing autophagy through to increase the AMP/ATP ratio and prevent metabolic crisis (276, 547, 663). Despite this, autophagy addicted Ras-induced tumours do not show downregulation of mTOR, indicating that the addiction mechanism must be through an mTOR-independent-manner (541) although this is yet to be confirmed in this study. Levels of AMPK and mTORC1 signalling activity would be needed to conclude this through the analysis of phosphorylation of S6K1 (656). This is also surprising as AMPK also regulates PGC1-α, the transcriptional activator of NF-E2-related factor 2

(Nrf2), a modulator of redox homeostasis (664) and known to interact directly with Wnt3a to regulate hepatocyte metabolism (665). It is also understood that β-oxidation and the utilization of fatty acids stores is limited through both the inhibition of AMPK (666) and activation of Ras/MAPK pathways via PI3K (667) both due to Ras activation. This blocks substrate availability and forces the cells towards an autophagy-dependent phenotype (668), in support of the finding that $PTEN^{Mut}$ cells are not autophagy dependent.

The finding that these effects were attenuated by Wnt/β-catenin signalling also fits with a previous study into Salinomycin, a cancer stem cell targeted compound that inhibits Wnt/β-catenin signalling (669) and, has more recently, been shown to induce mitochondrial fragmentation, mitophagy, decrease the membrane potential and reduce cellular ATP levels in prostate and breast cancer (669). It is believed that it does this in a protective manner against excessive apoptosis (669). In prostate and breast cancer, activation of the Wnt/β-catenin signalling pathway is, typically, seen as detrimental to patient prognosis and the opposing effects are often seen in melanoma (670). In melanoma, activation of the Wnt/β-catenin signalling pathway induces mitochondrial fusion with reduced levels of mitophagy and increased membrane potential, findings that are complimentary to the Salinomycin study in other cancer cell types.

It has already been shown how vital β-catenin is to the maintenance and function of the cell as a whole and specifically to the mitochondria. The MS analysis of β-catenin binding partners shown in Table 6.1, Figure 6.12 and Appendix 8.1 provides a number of interesting new targets for future research, but more importantly also supports the findings shown throughout this research. Specifically, proteins with increased binding in response to active Wnt/β-catenin includes cytochrome *c* which, as shown in Figure 4.8, is increased in Wnt3a overexpression cells. This data also includes Insulin-like Growth Factor, which has previously been linked to Mfn2 in diabetes and cancer (671) and Chromatin which is linked to β-catenin transcriptional regulation (672). More interesting are the proteins with reduced binding to β-catenin as these include a number of metabolism proteins. These included; LDHA, LDHB, and ATP-

Citrate Synthase, supporting the reduction in lactate secretion and citrate synthase activity measured in these cells (see Figure 5.5-5.6). In addition, there are a number of proteins involved in glycolysis, such as Glucose-6-phosphate and other members of the PPP pathway supporting the reduction shown in Figures 5.1-5.2. This data suggests that there are a number of major glycolysis and OXPHOS genes that cannot interact with β-catenin when it is not CK-1/GSK3β-phosphorylated or when it is being shuttled to the nucleus. This highlights that β-catenin is a potential master regulator of metabolism as well as mitochondrial dynamics in PTEN$^{WT}$ melanoma cells. There are, also, a number of proteins with reduced binding to stabilised β-catenin that provide much scope for future melanoma research. This includes CDK1 that has been linked to p53 function in Melanoma and β-catenin signalling (673, 674), the Ras-Associated Protein 1 (Rap1) that is linked to Ras/BRAF/ERK activation and integrin-mediated cell adhesion and migration (675). In addition, Table 8.2 includes a number of proteins that could, possibly, have links to the findings shown throughout this research. For example, there is a reduction in the binding of a number of proteins involved in the biosynthesis of amino acids that could be linked to the reduced proliferation. There are, also, leads within this data that will help to further identify the mechanism that is controlling the changes seen in the mitochondria of melanoma cells. This includes the Ubiquitin-like modifier-activating enzyme 1 (UBA1) that could be linked to the reduction in mitophagy.

### 6.6.1. Summary

Taking this data together, it suggests that PTEN$^{WT}$ melanoma cells are autophagy dependent and that β-catenin is a master regulator of both metabolism and mitochondrial dynamics and its stabilisation in PTEN$^{WT}$ cells reduces the tumourigenesis of melanoma cells. The following is a suggested model for Wnt-activated PTEN$^{WT}$ melanoma cells; the PTEN$^{WT}$ melanoma cells rely on the process of autophagy to produce enough nutrients for cellular survival and growth. Activating the Wnt/β-catenin signalling pathway blocks the autophagy pathway and sends the cells into a starvation mode where the mitochondria become highly fused and perinuclear to protect them from mitophagy. Figure 6.13 is a schematic representing

this potential mode of action, it shows In a Wnt 'off' situation β-catenin is degraded in the cytoplasm. Mitochondria are readily sequestered by the autophagy pathway producing amino acids to drive ATP synthesis and sustain proliferation and other cellular activities such as migration. In a Wnt 'on' model, β-catenin is stabilised in the cytoplasm allowing it to bind to the mitochondria to promote mitochondrial fusion protein activity, probably through binding Parkin and leading to increased expression of mitochondrial fusion proteins levels. The mitochondria elongate and become perinuclear evading autophagosome engulfment and sending the cells into starvation mode therefore causing an increase of glucose to potentially compensate. OXPHOS, ATP synthesis and glycolysis are all reduced likely leading to a reduction in cell proliferation and migration. This highlights a novel tumour suppressor function of Wnt/β-catenin signalling in $PTEN^{WT}$ melanoma cells.

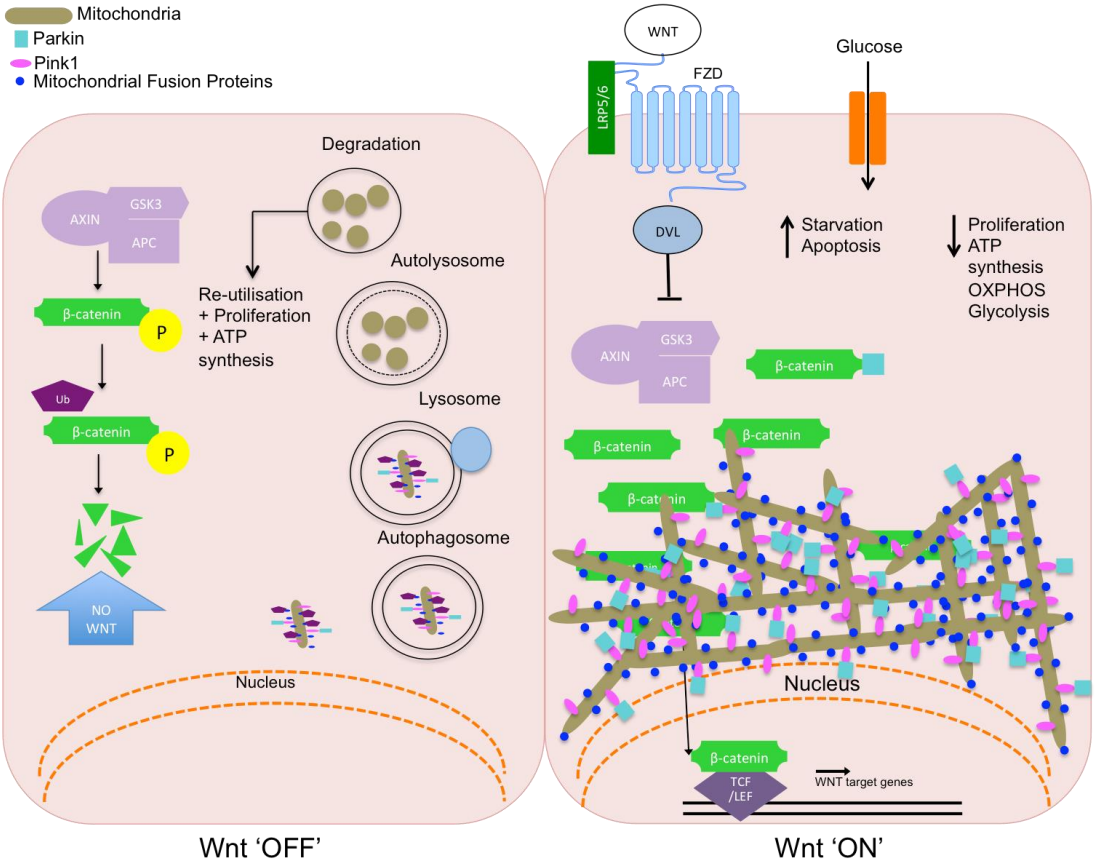


**Figure 6.13: Working Model of Wnt-Activation in PTEN$^{WT}$ Melanoma Cells**
In a Wnt 'off' situation β-catenin is degraded in the cytoplasm. Mitochondria are readily sequestered by the autophagy pathway producing amino acids to drive ATP synthesis and sustain proliferation and other cellular activities such as migration. In a Wnt 'on' model, β-catenin is stabilised in the cytoplasm allowing it to bind to the mitochondria to promote mitochondrial fusion protein activity, probably through binding Parkin and leading to increased expression of mitochondrial fusion proteins levels. The mitochondria elongate and become perinuclear evading autophagosome engulfment and sending the cells into starvation mode therefore causing an increase of glucose to potentially compensate. OXPHOS, ATP synthesis and glycolysis are all reduced likely leading to a reduction in cell proliferation and migration. This highlights a novel tumour suppressor function of Wnt/β-catenin signalling in PTEN$^{WT}$ melanoma cells.

# 7. DISCUSSION

This project combines three extensively studied areas of research, Wnt/β-catenin signalling, melanoma and metabolism, which have all been shown to interact with each other individually but, as yet, have not been directly linked together. It is becoming abundantly clear that cancer is a metabolic disease (294) and the data presented in this thesis shows that, in melanoma, Wnt/β-catenin signalling which is already highly implicated (195), plays an important part in the metabolic alterations of the cancer cells.

Opinions are still mixed on whether stabilisation of β-catenin is beneficial to melanoma progression, with some stating that activation of the pathway leads to increased proliferation, migration and poor patient outcome (404, 436, 437, 439-441). This research, however, agrees with the alternative opinion that activation of the Wnt/β-catenin pathway is beneficial for patient prognosis (20, 166, 203, 384, 430, 442-444). The data supports previous findings that Wnt/β-catenin signalling increases apoptosis (350) and reduces proliferation (203) of melanoma cells, potentially inducing a state of oncogenic senescence and possibly even contributing to the high levels of treatment resistance seen in melanoma (676). This data is also in support of the previous work on the β-catenin-independent Wnt5a signalling pathway that typically has opposing effects on melanoma progression, with higher levels of invasion and migration (222, 228, 337, 450, 453, 461). We have previously shown that Wnt5a increased aerobic glycolysis in melanoma cells (196). Due to this, the hypothesis was made that Wnt3a signalling in a β-catenin-dependent manner can also affect cellular metabolism in melanoma cells. This study found that the effects of Wnt signalling are context dependent and agrees with others that this applies to the cancer type and the genetic background of the tumour (165, 166, 169, 177, 200, 201, 207, 211, 428).

In order to characterise the panel of 29 melanoma cell lines, they were investigated in respect to two different models of melanoma that are theoretically linked to the Wnt/β-catenin signalling pathway. The phenotype switching model is linked through the expression of Wnt pathway genes associated with either the proliferative (MITF and TCF4) or invasive (Wnt5a and LEF1) phenotypes (334, 361, 365). Despite distinct

differences in the 3D Matrigel growth (see Figure 3.4) of melanoma cells, it was not possible to link these differences to the respective phenotypes, nor was it possible to link active Wnt/β-catenin signalling to the regulation of this model. The second model of melanoma progression is that of the tumour initiation/cancer stem cells, identified through cell surface expression of markers associated with hematopoietic stem cells, development of the neural crest and self-renewal capacity (389-394), such as CD271, CD133 and ABCB5. In this study, it was not possible to identify melanoma cells with specific expression of these markers (see Figure 3.9). However, it has been hypothesised that the population of tumour initiating cells could be as small as 2% of the total tumour population (357). Therefore, it would, potentially, be necessary to enrich the tumour initiating cell population before these cells could be identified. This could be done with the use of stem cell media or an in vitro assay that facilitates the separation and isolation of adherent and non-adherent stem cells (409).

This research did, however, identify different melanoma phenotypes based on the genetic background and their response to active Wnt/β-catenin signalling. Melanoma cells with a MAPK signalling pathway activating mutation, either in BRAF or RAS, but with wildtype PTEN expression ($PTEN^{WT}$) significantly reduced invasion (see Figure 4.10), migration (see figure 4.12) and lung metastasis (see Figures 4.13-15) in response to Wnt/β-catenin signalling. The opposite was observed for melanoma cells that contain both a MAPK signalling activating mutation and a PTEN inactivating/reducing mutation ($PTEN^{Mut}$), where an increase in invasion, migration and the number of lung micrometastasis were observed (see Figure 4.16). This is in support of a published transgenic mouse model of melanoma (142, 143). In addition, Wnt/β-catenin signalling had alternate effects on the shape, location and function of the mitochondria in the different genetic backgrounds. $PTEN^{WT}$ cells with active Wnt/β-catenin signalling had decreased aerobic glycolysis and OXPHOS, measured by the Seahorse $XF^{e}96$ Extracellular Flux Analyzer and biochemical analysis of lactate secretion and citrate synthase activity (see Figures 5.2, 5.5, 5.6). The mitochondria of these cells became elongated and perinuclear (see Figure 5.9a and 5.10), with increased expression of mitochondrial fusion markers Mfn1, Mfn2 and Opa1, in addition to decreased expression of mitochondrial fission marker Drp1 (see Figures

6.1-6.2), all factors indicative of nutrient starvation (598, 606). As with the invasion and migration results, the PTEN$^{Mut}$ cells had the opposing response to active Wnt/β-catenin signalling with insignificant trends towards increased aerobic glycolysis and OXPHOS. However, there were no changes observed in the mitochondrial shape or location of the PTEN$^{Mut}$ cells (see Figure 5.9b).

The research indicated that activation of the Wnt/β-catenin pathway was providing an inhibitory effect to cancer cell growth in PTEN$^{WT}$ cells. Analysis of the mitochondrial quality control genes indicated that PTEN$^{WT}$ cells were autophagy addicted (see Figure 6.10a), as shown by the predominant expression of LC3II (541, 594), but, to fully conclude this, siRNA knockdown of autophagy proteins Beclin1 or Atg5 would be needed (541, 677, 678). Autophagy addiction, has previously, been shown for Ras-activated cancers, such as lung and pancreatic cancers. This research, along with that of others (679-683), shows autophagy addiction in melanomas with downstream effector mutations such as the Braf$^{V600E}$ or Nras mutations (541, 547, 594, 644, 650, 651). The expression of LC3 and p62 were reduced in PTEN$^{WT}$ cells with active Wnt/β-catenin signalling indicating that stabilised β-catenin inhibits the autophagy pathway (see Figures 6.10a and 6.11a), potentially through the increased binding to Parkin which has previously been seen in neuronal cells (619), but is shown here for the first time in melanoma cells (see Figure 6.9). This was supported by the finding of increased levels of β-catenin at the mitochondria (see Figure 6.8) and full length Pink1 (see Figure 6.7). However, levels of Parkin were unaffected, indicating that Pink1-mediated Parkin recruitment is possibly impaired as is, the subsequently initiation of mitophagy (633).

These findings were dependent on β-catenin, as shown by DKK1 inhibition (see Figures 5.14-16) and β-catenin siRNA knockdown (see Figures 5.17-18). The absence of β-catenin removed all mitochondrial fusion from the cells, including in the absence of a Wnt ligand, as measured by Mitotracker imaging and the expression of Mfn1 (see Figure 6.3). In addition, removal of β-catenin from the PTEN$^{WT}$ cells reversed their metabolism and migratory capacity in response to Wnt/β-catenin signalling (see Figure 5.19). It also reversed the inhibition of autophagy, sending the cells back into

an autophagy dependent phenotype with the predominant expression of LC3II (see Figure 6.10b). However, the transcriptional regulation that β-catenin has over cell motility, adhesion, differentiation and cell cycle progression, such as Cyclin D1, MYC and CD44 (439, 531, 555), must be taken into consideration in siRNA knockdown results. Despite these considerations, these findings indicate that β-catenin plays an important role in mitochondrial functions. To further verify this statement, MS analysis revealed that a large number of metabolism proteins increase binding to β-catenin in response to its stabilisation and an even larger number of metabolism related proteins lose their binding, including both glycolysis and OXPHOS proteins (see Table 6.1, Figure 6.12 and Appendix 1). This highlights that β-catenin is potentially a master regulator of metabolism, as well as mitochondrial dynamics.

We have already shown that Wnt5a, can increase aerobic glycolysis in melanoma cells via Akt (196) therefore providing cross-talk to the canonical control of autophagy and metabolism through mTOR. However, in the previous study, neither the effect on mitochondrial shape and location or the genetic context of the cells were investigated. Given the results seen in this current research with Wnt3a, it would be interesting to investigate if the non-canonical signalling was as dependent on the genetic context of the tumour.

The majority of this research has focused on the $PTEN^{WT}$ cells that, in the presence of activated Wnt/β-catenin signalling, had an inhibitory effect against melanoma progression. However, also shown in this study was the progressive effect that Wnt/β-catenin had on $PTEN^{Mut}$ melanomas. This data provides the potential for Wnt inhibitor treatments in the right genetic context. Patients would need to be stratified, based on both their BRAF and PTEN genetic status. Those patients that had a MAPK activating mutation and an inactivating PTEN mutation may respond to treatments that reduce Wnt/β-catenin signalling. There are many natural inhibitors of the Wnt/β-catenin pathway, including DKK proteins that were shown in this study to specifically, and successfully, block canonical signalling by competitively binding to the LRP5/6 co-receptor (234, 236, 521, 684). DKK3 has specifically been shown to affect apoptosis and proliferation of solid cancers (684). Secreted frizzled related

proteins (SFRP) and Wnt-inhibitory factor 1 (WIF1) could also be utilised to manipulate excessive Wnt signalling as they bind directly to the Wnt ligand, blocking its binding to receptors (235). They are both commonly down regulated in tumours (173, 234) and, in normal cells, SFRPs act as tumour suppressor genes and, therefore, restoration of their expression could be beneficial against tumour progression as has already been shown in colon cancer (178). However, the mechanism by which WIF1 works is not well understood and it is thought that both SFRPs and WIF1 can also bind to β-catenin-catenin-independent Wnts and, therefore, could potentially increase melanoma progression as has been shown in glioma tumours (178). As well as these, inhibitors acting upon the FZD receptors such as pertussis toxins could also be used (178). The benefits of these treatments are that they act at the cell membrane and, therefore, can alter Wnt signalling even when there are down-stream mutations (178). However, as non-canonical Wnts also bind through FZD receptors and they are necessary for the maintenance of adult stem cells, inhibition of the pathway via the FZD receptors could have detrimental side effects (685). The expression of the Wnt ligands could also be attenuated through the use of small molecules or biologicals. There are antibodies and siRNAs directly targeting the Wnt ligands, including Wnt1 in lung, breast and colon cancer (178, 475, 477) and Wnt2 in melanoma, lung and mesothelioma (178, 389).

Small molecule inhibitors of the Wnt pathway have also been intensively developed in recent years for use in cancer treatment. Wnt ligands have also been shown to be diminished in prostate (484), breast (686) and head and neck cancers by the Porcupine inhibitor which blocks the palmitoylation of Wnts and their subsequent secretion (485-487). β-catenin itself, can also be targeted to prevent transcription (687). Alternatively, inhibiting other aspects of the Wnt/β-catenin pathway has been shown to have success in different cancers, including breast and melanoma. The molecular inhibitor XAV939 inhibits Tankyrases 1 and 2, these are members of the PARP-family and regulate levels of Axin. Their inhibition causes levels of Axin to increase leading to β-catenin degradation (688, 689). Likewise, CK1α can be inhibited by Pyrvinium (690) or the interaction between β-catenin and TCF (691-693) or the CBP (694) can be blocked by small molecular inhibitors. However, the subsequent

lack of β-catenin-regulated transcription must be taken into consideration as adverse effects of these treatments. Each of these treatments would reduce Wnt/β-catenin signalling in melanoma and, therefore, in the specific genetic context, would potentially be beneficial for melanoma patient prognosis.

The effects to $PTEN^{WT}$ melanoma progression shown here, due to active Wnt/β-catenin signalling, also seem to be an attractive treatment option for patients with the appropriate genetic background. However, given that activation of the Wnt/β-catenin pathway is known to induce melanocyte differentiation and initiate melanoma formation, in addition to the fact that β-catenin is involved in a number of other processes (200), constitutive activation of the Wnt/β-catenin pathway would not be a suitable treatment option. Instead, once a tumour has been confirmed as autophagy dependent and as this has been reported for other cancers, including prostate and lung cancer, this applies to any cancer type, the inhibition of autophagy could be a viable treatment option, as currently being tested in clinical trials for a number of cancers (648, 683). These include the use of Chloroquine in lung cancer, which blocks TLR signalling and autolysosomal degradation (695). Hydroxychloroquine works through the same mechanism and is, currently, in use in the treatment of breast and renal cancers (696). In addition, Hydroxychloroquine is used in combination therapies with Bortezomib in Myeloma causing cell cycle arrest, and with the Akt inhibitor MK2206 or the mTOR inhibitor Temsirolimus in melanoma (105, 648, 661, 697, 698). These inhibitor co-therapies act upon the PI3K pathway. The data shown in this study indicated that cells with $PTEN^{WT}$ were autophagy dependent, whereas cells with $PTEN^{Mut}$ were not. This implies that, if the PI3K pathway were blocked or, indeed, PI3K itself were inhibited, the autophagy addiction of $PTEN^{WT}$ cells could be blocked and could, potentially, be beneficial for melanoma patients. Due to this, other PI3K targeted treatments should also be suggested as potential therapies, including wortmannin, LY294002 and 3-methyladenine (591) but, specifically, in the treatment of melanoma, GDC0941 and XL147, which are in ongoing clinical trials (698).

As both Ras-induced autophagy and hyperactive Wnt/β-catenin signalling are seen in a number of different cancers, the treatments detailed above could be considered for the future cancer therapy. In support of the use of these therapies is the finding that Wnt/β-catenin signalling had no effect on the mitochondrial structure of melanocyte cells and, although, the metabolism of the melanocytes was not investigated, this implies that there would be no adverse effects on normal cell metabolism. However, in contrast to this, Sethi *et al.* described very well the complex nature of Wnt signalling in the metabolism of normal cell maintenance and development (195). In addition, Yoon *et al.* showed that Wnt signalling affected the metabolism of normal fibroblasts and myoblasts (495), and Wnt signalling inhibitors have been shown to reduce oxidative metabolism in adipocytes (235). However, as previously discussed in Chapter 1, different cells regulate their mitochondria in proportion to their energetic demands (245). Therefore, given that Wnts, both canonical and non-canonical play such important roles in the regulation of stem cell maintenance, it is easy to assume any alterations to Wnt signalling would also have effects on tissue homeostasis.

In summary, it has been shown here, for the first time, that Ras-activated melanomas with wildtype PTEN signalling are autophagy dependent. I hypothesise that activation of the Wnt/β-catenin signalling pathway can block autophagy and send the cells into starvation mode (see Figure 6.13), causing glycolysis and OXPHOS to be reduced, their mitochondria to elongate, become perinuclear and, subsequently, cause a reduction in proliferation, invasion and migration. The mechanism by which the Wnt/β-catenin pathway does this is still unknown. However, it is possible that stabilised β-catenin binds to Parkin, blocking the mitophagy process and allowing damaged mitochondria to accumulate in the cells. This indicates that autophagy inhibition could be a potentially viable target for melanoma treatments in a specific genetic context. My opinion is highlighted by this research in that detailed genetic profiling of patients is a necessity in order to enable the best, most beneficial treatments, for patients with currently incurable, late stage cancers.

# 8. APPENDIX

**Table 8.1: Metabolic Proteins with Increased Binding to β-catenin**

| Gene ID | Mapped ID | Gene Name/Symbol | GO Biological Process |
|---|---|---|---|
| HUMAN\|Ensembl=ENSG00000021776\|UniProtKB=O60306 | O60306 | Intron-binding protein aquarius<br>AQR<br>ortholog | DNA replication<br>transcription from RNA polymerase II promoter<br>mRNA splicing, via spliceosome<br>tRNA metabolic process<br>RNA catabolic process<br>protein metabolic process<br>cell cycle<br>regulation of transcription from RNA polymerase II promoter |
| HUMAN\|Ensembl=ENSG00000144028\|UniProtKB=O75643 | O75643 | U5 small nuclear ribonucleoprotein 200 kDa helicase<br>SNRNP200<br>ortholog | RNA splicing, via transesterification reactions<br>mRNA splicing, via spliceosome<br>RNA splicing, via transesterification reactions<br>meiosis |
| HUMAN\|Ensembl=ENSG00000100591\|UniProtKB=O95433 | O95433 | Activator of 90 kDa heat shock protein ATPase homolog 1<br>AHSA1<br>ortholog | immune system process<br>protein folding<br>response to stress<br>regulation of catalytic activity |
| HUMAN\|Ensembl=ENSG00000189060\|UniProtKB=P07305 | P07305 | Histone H1.0<br>H1F0<br>ortholog | nucleobase-containing compound metabolic process<br>cellular process<br>chromatin organization |
| HUMAN\|Ensembl=ENSG00000124228\|UniProtKB=Q96GQ7 | Q96GQ7 | Probable ATP-dependent RNA helicase DDX27<br>DDX27<br>ortholog | nucleobase-containing compound metabolic process<br>translation<br>regulation of translation |
| HUMAN\|Ensembl=ENSG00000136271\|UniProtKB=Q9NY93 | Q9NY93 | Probable ATP-dependent RNA helicase DDX56<br>DDX56<br>ortholog | nucleobase-containing compound metabolic process<br>translation<br>regulation of translation |
| HUMAN\|Ensembl=ENSG00000183 | Q9Y3A2 | Probable U3 small nucleolar RNA- | |

| | | | |
|---|---|---|---|
| 20\|UniProtKB=Q9Y3A2 | | associated protein 11<br>UTP11L<br>ortholog | nucleobase-containing compound metabolic process |
| HUMAN\|Ensembl=ENSG00000215301\|UniProtKB=O00571 | O00571 | ATP-dependent RNA helicase DDX3X<br>DDX3X<br>ortholog | nucleobase-containing compound metabolic process<br>translation<br>regulation of translation |
| HUMAN\|Ensembl=ENSG00000102978\|UniProtKB=P19387 | P19387 | DNA-directed RNA polymerase II subunit RPB3<br>POLR2C<br>ortholog | transcription from RNA polymerase II promoter |
| HUMAN\|Ensembl=ENSG00000096746\|UniProtKB=P31942 | P31942 | Heterogeneous nuclear ribonucleoprotein H3<br>HNRNPH3<br>ortholog | mRNA splicing, via spliceosome |
| HUMAN\|Ensembl=ENSG00000143621\|UniProtKB=Q12905 | Q12905 | Interleukin enhancer-binding factor 2<br>ILF2<br>ortholog | spermatogenesis<br>response to interferon-gamma<br>apoptotic process<br>purine nucleobase metabolic process<br>protein metabolic process<br>cell cycle<br>apoptotic process<br>response to stimulus<br>RNA localization<br>regulation of catalytic activity |
| HUMAN\|Ensembl=ENSG00000132153\|UniProtKB=Q7L2E3 | Q7L2E3 | Putative ATP-dependent RNA helicase DHX30<br>DHX30<br>ortholog | mRNA splicing, via spliceosome |
| HUMAN\|Ensembl=ENSG00000151893\|UniProtKB=Q86Y37 | Q86Y37 | CDK2-associated and cullin domain-containing protein 1<br>CACUL1<br>ortholog | induction of apoptosis<br>proteolysis<br>mitosis<br>induction of apoptosis |

| | | | |
|---|---|---|---|
| HUMAN\|Ensembl=ENSG00000119285\|UniProtKB=Q9H583 | Q9H583 | HEAT repeat-containing protein 1<br>HEATR1<br>ortholog | rRNA metabolic process |
| HUMAN\|Ensembl=ENSG00000106344\|UniProtKB=Q9NW13 | Q9NW13 | RNA-binding protein 28<br>RBM28<br>ortholog | DNA replication<br>RNA splicing, via transesterification reactions<br>mRNA splicing, via spliceosome<br>mRNA polyadenylation<br>RNA splicing, via transesterification reactions<br>rRNA metabolic process<br>protein metabolic process<br>cell cycle<br>neurological system process<br>ectoderm development |
| HUMAN\|Ensembl=ENSG00000159217\|UniProtKB=Q9NZI8 | Q9NZI8 | Insulin-like growth factor 2 mRNA-binding protein 1<br>IGF2BP1<br>ortholog | induction of apoptosis<br>RNA splicing, via transesterification reactions<br>transcription from RNA polymerase II promoter<br>mRNA splicing, via spliceosome<br>RNA splicing, via transesterification reactions<br>protein metabolic process<br>cell communication<br>neurological system process<br>induction of apoptosis<br>intracellular protein transport<br>nuclear transport |
| HUMAN\|Ensembl=ENSG00000125970\|UniProtKB=Q9UKM9 | Q9UKM9 | RNA-binding protein Raly<br>RALY<br>ortholog | mRNA splicing, via spliceosome |

| | | | |
|---|---|---|---|
| HUMAN\|Ensembl=ENSG00000153147\|UniProtKB=O60264 | O60264 | SWI/SNF-related matrix-associated actin-dependent regulator of chromatin subfamily A member 5<br>SMARCA5<br>ortholog | DNA repair<br>DNA recombination<br>transcription from RNA polymerase II promoter<br>cellular process<br>regulation of transcription from RNA polymerase II promoter<br>chromatin organization |
| HUMAN\|Ensembl=ENSG00000092199\|UniProtKB=P07910 | P07910 | Heterogeneous nuclear ribonucleoproteins C1/C2<br>HNRNPC<br>ortholog | mRNA splicing, via spliceosome |
| HUMAN\|Ensembl=ENSG00000099783\|UniProtKB=P52272 | P52272 | Heterogeneous nuclear ribonucleoprotein M<br>HNRNPM<br>ortholog | mRNA splicing, via spliceosome |
| HUMAN\|Ensembl=ENSG00000108468\|UniProtKB=P83916 | P83916 | Chromobox protein homolog 1<br>CBX1<br>ortholog | apoptotic process<br>transcription from RNA polymerase II promoter<br>cellular process<br>apoptotic process<br>regulation of transcription from RNA polymerase II promoter<br>chromatin organization |
| HUMAN\|Ensembl=ENSG00000113460\|UniProtKB=Q8TDN6 | Q8TDN6 | Ribosome biogenesis protein BRX1 homolog<br>BRIX1<br>ortholog | rRNA metabolic process |
| HUMAN\|Ensembl=ENSG00000107937\|UniProtKB=Q9BZE4 | Q9BZE4 | Nucleolar GTP-binding protein 1<br>GTPBP4<br>ortholog | translation |
| HUMAN\|Ensembl=ENSG00000134597\|UniProtKB=Q9Y388 | Q9Y388 | RNA-binding motif protein, X-linked 2<br>RBMX2<br>ortholog | RNA splicing, via transesterification reactions<br>mRNA splicing, via spliceosome<br>RNA splicing, via transesterification reactions |

| | | | |
|---|---|---|---|
| HUMAN\|Ensembl=ENSG00000130826\|UniProtKB=O60832 | O60832 | H/ACA ribonucleoprotein complex subunit 4<br>DKC1<br>ortholog | rRNA metabolic process<br>cell cycle |
| HUMAN\|Ensembl=ENSG00000115524\|UniProtKB=O75533 | O75533 | Splicing factor 3B subunit 1<br>SF3B1<br>ortholog | RNA splicing, via transesterification reactions<br>mRNA splicing, via spliceosome<br>RNA splicing, via transesterification reactions |
| HUMAN\|Ensembl=ENSG00000101161\|UniProtKB=O94906 | O94906 | Pre-mRNA-processing factor 6<br>PRPF6<br>ortholog | RNA splicing, via transesterification reactions<br>mRNA splicing, via spliceosome<br>RNA splicing, via transesterification reactions<br>ectoderm development<br>nervous system development |
| HUMAN\|Ensembl=ENSG00000126267\|UniProtKB=P14854 | P14854 | Cytochrome c oxidase subunit 6B1<br>COX6B1<br>ortholog | oxidative phosphorylation<br>respiratory electron transport chain |
| HUMAN\|Ensembl=ENSG00000173801\|UniProtKB=P14923 | P14923 | Junction plakoglobin<br>JUP<br>ortholog | female gamete generation<br>nitrogen compound metabolic process<br>biosynthetic process<br>transcription from RNA polymerase II promoter<br>cell-cell signaling<br>cell adhesion<br>pattern specification process<br>pattern specification process<br>cellular component morphogenesis<br>embryo development<br>cell differentiation |

| | | | |
|---|---|---|---|
| | | | heart development<br>response to stimulus<br>protein localization<br>regulation of transcription from RNA polymerase II promoter<br>cytoskeleton organization |
| HUMAN\|Ensembl=ENSG00000105202\|UniProtKB=P22087 | P22087 | rRNA 2'-O-methyltransferase fibrillarin<br>FBL<br>ortholog | rRNA metabolic process |
| HUMAN\|Ensembl=ENSG00000261236\|UniProtKB=Q14137 | Q14137 | Ribosome biogenesis protein BOP1<br>BOP1<br>ortholog | rRNA metabolic process<br>translation |
| HUMAN\|Ensembl=ENSG00000007968\|UniProtKB=Q14209 | Q14209 | Transcription factor E2F2<br>E2F2<br>ortholog | transcription from RNA polymerase II promoter<br>cell cycle<br>cell communication<br>regulation of transcription from RNA polymerase II promoter |
| HUMAN\|Ensembl=ENSG00000174231\|UniProtKB=Q6P2Q9 | Q6P2Q9 | Pre-mRNA-processing-splicing factor 8<br>PRPF8<br>ortholog | RNA splicing, via transesterification reactions<br>mRNA splicing, via spliceosome<br>RNA splicing, via transesterification reactions |
| HUMAN\|Ensembl=ENSG00000134987\|UniProtKB=Q8NI36 | Q8NI36 | WD repeat-containing protein 36<br>WDR36<br>ortholog | RNA splicing, via transesterification reactions<br>mRNA splicing, via spliceosome<br>RNA splicing, via transesterification reactions |
| HUMAN\|Ensembl=ENSG00000048649\|UniProtKB=Q96T23 | Q96T23 | Remodeling and spacing factor 1<br>RSF1<br>ortholog | induction of apoptosis<br>transcription from RNA polymerase II promoter<br>protein acetylation |

| | | | |
|---|---|---|---|
| | | | cell cycle<br>induction of apoptosis<br>regulation of transcription from RNA polymerase II promoter |
| HUMAN\|Ensembl=ENSG00000185129\|UniProtKB=Q00577 | Q00577 | Transcriptional activator protein Pur-alpha<br>PURA<br>ortholog | transcription from RNA polymerase II promoter |
| HUMAN\|Ensembl=ENSG00000135829\|UniProtKB=Q08211 | Q08211 | ATP-dependent RNA helicase A<br>DHX9<br>ortholog | mRNA splicing, via spliceosome |
| HUMAN\|Ensembl=ENSG00000112739\|UniProtKB=Q13523 | Q13523 | Serine/threonine-protein kinase PRP4 homolog<br>PRPF4B<br>ortholog | glycogen metabolic process<br>protein phosphorylation<br>mitosis<br>cell communication |
| HUMAN\|Ensembl=ENSG00000165733\|UniProtKB=Q14692 | Q14692 | Ribosome biogenesis protein BMS1 homolog<br>BMS1<br>ortholog | nucleobase-containing compound metabolic process |
| HUMAN\|Ensembl=ENSG00000115368\|UniProtKB=Q8IWA0 | Q8IWA0 | WD repeat-containing protein 75<br>WDR75<br>ortholog | RNA splicing, via transesterification reactions<br>transcription from RNA polymerase II promoter<br>mRNA splicing, via spliceosome<br>RNA splicing, via transesterification reactions<br>RNA localization<br>regulation of catalytic activity |
| HUMAN\|Ensembl=ENSG00000096401\|UniProtKB=Q99459 | Q99459 | Cell division cycle 5-like protein<br>CDC5L<br>ortholog | purine nucleobase metabolic process<br>transcription from RNA polymerase II promoter<br>rRNA metabolic process<br>cellular amino acid biosynthetic process<br>cell cycle |

| | | | |
|---|---|---|---|
| | | | regulation of transcription from RNA polymerase II promoter |
| HUMAN\|Ensembl=ENSG00000130810\|UniProtKB=Q9NQ55 | Q9NQ55 | Suppressor of SWI4 1 homolog PPAN ortholog | mRNA splicing, via spliceosome |
| HUMAN\|Ensembl=ENSG00000053372\|UniProtKB=Q9UKD2 | Q9UKD2 | mRNA turnover protein 4 homolog MRTO4 ortholog | translation |
| HUMAN\|Ensembl=ENSG00000065183\|UniProtKB=Q9UNX4 | Q9UNX4 | WD repeat-containing protein 3 WDR3 ortholog | nucleobase-containing compound metabolic process |
| HUMAN\|Ensembl=ENSG00000054118\|UniProtKB=Q9Y2W1 | Q9Y2W1 | Thyroid hormone receptor-associated protein 3 THRAP3 ortholog | transcription from RNA polymerase II promoter<br>regulation of transcription from RNA polymerase II promoter |
| HUMAN\|Ensembl=ENSG00000055044\|UniProtKB=Q9Y2X3 | Q9Y2X3 | Nucleolar protein 58 NOP58 ortholog | rRNA metabolic process |
| HUMAN\|Ensembl=ENSG00000168298\|UniProtKB=P10412 | P10412 | Histone H1.4 HIST1H1E ortholog | nucleobase-containing compound metabolic process<br>cellular process<br>chromatin organization |
| HUMAN\|Ensembl=ENSG00000168036\|UniProtKB=P35222 | P35222 | Catenin beta-1 CTNNB1 ortholog | female gamete generation<br>immune system process<br>apoptotic process<br>nitrogen compound metabolic process<br>biosynthetic process<br>transcription from RNA polymerase II promoter<br>synaptic transmission<br>cell proliferation<br>cell adhesion<br>neurological system process<br>pattern specification process |

| | | | |
|---|---|---|---|
| | | | pattern specification process<br>endoderm development<br>cellular component morphogenesis<br>embryo development<br>apoptotic process<br>cell differentiation<br>skeletal system development<br>angiogenesis<br>nervous system development<br>heart development<br>hemopoiesis<br>response to endogenous stimulus<br>vesicle-mediated transport<br>protein localization<br>regulation of transcription from RNA polymerase II promoter<br>regulation of sequence-specific DNA binding transcription factor activity<br>cytoskeleton organization |
| HUMAN\|Ensembl=ENSG00000253729\|UniProtKB=P78527 | P78527 | DNA-dependent protein kinase catalytic subunit<br>PRKDC<br>ortholog | immune system process<br>induction of apoptosis<br>DNA repair<br>DNA recombination<br>protein phosphorylation<br>cell cycle<br>cell communication<br>induction of apoptosis<br>response to stress<br>chromatin organization |
| HUMAN\|Ensembl=ENSG00000131051\|UniProtKB=Q14498 | Q14498 | RNA-binding protein 39<br>RBM39<br>ortholog | DNA replication<br>RNA splicing, via transesterification reactions<br>mRNA splicing, via spliceosome<br>mRNA polyadenylation |

| | | | |
|---|---|---|---|
| | | | RNA splicing, via transesterification reactions<br>rRNA metabolic process<br>protein metabolic process<br>cell cycle<br>neurological system process<br>ectoderm development<br>nervous system development |
| HUMAN\|Ensembl=ENSG00000108592\|UniProtKB=Q8IY81 | Q8IY81 | pre-rRNA processing protein FTSJ3<br>FTSJ3<br>ortholog | rRNA metabolic process |
| HUMAN\|Ensembl=ENSG00000188976\|UniProtKB=Q9Y3T9 | Q9Y3T9 | Nucleolar complex protein 2 homolog<br>NOC2L<br>ortholog | protein metabolic process<br>protein targeting<br>nuclear transport |
| HUMAN\|Ensembl=ENSG00000172809\|UniProtKB=P63173 | P63173 | 60S ribosomal protein L38<br>RPL38<br>ortholog | translation |
| HUMAN\|Ensembl=ENSG00000115816\|UniProtKB=Q03701 | Q03701 | CCAAT/enhancer-binding protein zeta<br>CEBPZ<br>ortholog | transcription from RNA polymerase II promoter<br>regulation of transcription from RNA polymerase II promoter |
| HUMAN\|Ensembl=ENSG00000111530\|UniProtKB=Q86VP6 | Q86VP6 | Cullin-associated NEDD8-dissociated protein 1<br>CAND1<br>ortholog | transcription from RNA polymerase II promoter |
| HUMAN\|Ensembl=ENSG00000123064\|UniProtKB=Q8TDD1 | Q8TDD1 | ATP-dependent RNA helicase DDX54<br>DDX54<br>ortholog | nucleobase-containing compound metabolic process<br>translation<br>regulation of translation |
| HUMAN\|Ensembl=ENSG00000156697\|UniProtKB=Q9BVJ6 | Q9BVJ6 | U3 small nucleolar RNA-associated protein 14 homolog A<br>UTP14A<br>ortholog | nucleobase-containing compound metabolic process |

| | | | |
|---|---|---|---|
| HUMAN\|Ensembl=ENSG00000089737\|UniProtKB=Q9GZR7 | Q9GZR7 | ATP-dependent RNA helicase DDX24<br>DDX24<br>ortholog | nucleobase-containing compound metabolic process<br>translation<br>regulation of translation |
| HUMAN\|Ensembl=ENSG00000122566\|UniProtKB=P22626 | P22626 | Heterogeneous nuclear ribonucleoproteins A2/B1<br>HNRNPA2B1<br>ortholog | DNA replication<br>RNA splicing, via transesterification reactions<br>mRNA splicing, via spliceosome<br>mRNA polyadenylation<br>RNA splicing, via transesterification reactions<br>rRNA metabolic process<br>protein metabolic process<br>cell cycle<br>neurological system process<br>ectoderm development<br>nervous system development |
| HUMAN\|Ensembl=ENSG00000067066\|UniProtKB=P23497 | P23497 | Nuclear autoantigen Sp-100<br>SP100<br>ortholog | transcription from RNA polymerase II promoter<br>cell communication<br>regulation of transcription from RNA polymerase II promoter<br>chromatin organization |
| HUMAN\|Ensembl=ENSG00000121774\|UniProtKB=Q07666 | Q07666 | KH domain-containing, RNA-binding, signal transduction-associated protein 1<br>KHDRBS1<br>ortholog<br><br>Ribosome biogenesis regulatory protein homolog<br>RRS1<br>ortholog | spermatogenesis<br>RNA splicing, via transesterification reactions<br>mRNA splicing, via spliceosome<br>RNA splicing, via transesterification reactions<br>nucleobase-containing compound metabolic process |
| HUMAN\|Ensembl=ENSG00000179041\|UniProtKB=Q15050 | Q15050 | | |

| | | | |
|---|---|---|---|
| HUMAN\|Ensembl=ENSG00000163811\|UniProtKB=Q15061 | Q15061 | WD repeat-containing protein 43<br>WDR43<br>ortholog | RNA splicing, via transesterification reactions<br>transcription from RNA polymerase II promoter<br>mRNA splicing, via spliceosome<br>RNA splicing, via transesterification reactions<br>ectoderm development<br>RNA localization<br>regulation of catalytic activity |
| HUMAN\|Ensembl=ENSG00000248643\|UniProtKB=Q96PK6 | Q96PK6 | RNA-binding protein 14<br>RBM14<br>ortholog | DNA replication<br>RNA splicing, via transesterification reactions<br>transcription from RNA polymerase II promoter<br>mRNA splicing, via spliceosome<br>mRNA polyadenylation<br>RNA splicing, via transesterification reactions<br>protein metabolic process<br>cell cycle<br>ectoderm development<br>nervous system development |
| HUMAN\|Ensembl=ENSG00000076924\|UniProtKB=Q9HCS7 | Q9HCS7 | Pre-mRNA-splicing factor SYF1<br>XAB2<br>ortholog | RNA splicing, via transesterification reactions<br>mRNA splicing, via spliceosome<br>RNA splicing, via transesterification reactions<br>ectoderm development<br>nervous system development |
| HUMAN\|Ensembl=ENSG000000882 | Q9NVP1 | ATP-dependent RNA helicase DDX18<br>DDX18 | nucleobase-containing compound metabolic process |

| | | | |
|---|---|---|---|
| 05\|UniProtKB=Q9NVP1 | | ortholog | translation<br>regulation of translation |
| HUMAN\|Ensembl=ENSG00000120158\|UniProtKB=Q9Y2P8 | Q9Y2P8 | RNA 3'-terminal phosphate cyclase-like protein<br>RCL1<br>ortholog | mRNA splicing, via spliceosome |

**Table 8.2: Metabolic Proteins with Reduced Binding to β-catenin**

| Gene ID | Mapped ID | Gene Name/Symbol | GO Biological Process |
|---|---|---|---|
| HUMAN\|Ensembl=ENSG00000010244\|UniProtKB=O43670 | O43670 | Zinc finger protein 207<br>ZNF207<br>ortholog | nucleobase-containing compound metabolic process |
| HUMAN\|Ensembl=ENSG00000125166\|UniProtKB=P00505 | P00505 | Aspartate aminotransferase, mitochondrial<br>GOT2<br>ortholog | cellular amino acid metabolic process |
| HUMAN\|Ensembl=ENSG00000111640\|UniProtKB=P04406 | P04406 | Glyceraldehyde-3-phosphate dehydrogenase<br>GAPDH<br>ortholog | glycolysis<br>glycolysis |
| HUMAN\|Ensembl=ENSG00000163902\|UniProtKB=P04843 | P04843 | Dolichyl-diphosphooligosaccharide--protein glycosyltransferase subunit 1<br>RPN1<br>ortholog | translation<br>protein glycosylation |
| HUMAN\|Ensembl=ENSG00000177600\|UniProtKB=P05387 | P05387 | 60S acidic ribosomal protein P2<br>RPLP2<br>ortholog | translation |
| HUMAN\|Ensembl=ENSG00000008018\|UniProtKB=P20618 | P20618 | Proteasome subunit beta type-1<br>PSMB1<br>ortholog | proteolysis |
| HUMAN\|Ensembl=ENSG00000041357\|UniProtKB=P25789 | P25789 | Proteasome subunit alpha type-4<br>PSMA4<br>ortholog | proteolysis |
| HUMAN\|Ensembl=ENSG00000167004\|UniProtKB=P30101 | P30101 | Protein disulfide-isomerase A3<br>PDIA3<br>ortholog | protein folding<br>cellular protein modification process |
| HUMAN\|Ensembl=ENSG00000168906\|UniProtKB=P31153 | P31153 | S-adenosylmethionine synthase isoform type-2<br>MAT2A<br>ortholog | cellular amino acid metabolic process |
| HUMAN\|Ensembl=ENSG00000170606\|UniProtKB=P34932 | P34932 | Heat shock 70 kDa protein 4<br>HSPA4<br>ortholog | immune system process<br>protein folding<br>protein complex assembly<br>response to stress<br>protein complex biogenesis |

| | | | |
|---|---|---|---|
| HUMAN\|Ensembl=ENSG00000150753\|UniProtKB=P48643 | P48643 | T-complex protein 1 subunit epsilon<br>CCT5<br>ortholog | protein folding |
| HUMAN\|Ensembl=ENSG00000100380\|UniProtKB=P50502 | P50502 | Hsc70-interacting protein<br>ST13<br>ortholog | protein folding<br>response to stress |
| HUMAN\|Ensembl=ENSG00000065427\|UniProtKB=Q15046 | Q15046 | Lysine--tRNA ligase<br>KARS<br>ortholog | translation |
| HUMAN\|Ensembl=ENSG00000111196\|UniProtKB=Q96A72 | Q96A72 | Protein mago nashi homolog 2<br>MAGOHB<br>ortholog | female gamete generation<br>nucleobase-containing compound metabolic process<br>sex determination<br>RNA localization |
| HUMAN\|Ensembl=ENSG00000135018\|UniProtKB=Q9UMX0 | Q9UMX0 | Ubiquilin-1<br>UBQLN1<br>ortholog | proteolysis |
| HUMAN\|Ensembl=ENSG00000134333\|UniProtKB=P00338 | P00338 | L-lactate dehydrogenase A chain<br>LDHA<br>ortholog | glycolysis<br>glycolysis<br>tricarboxylic acid cycle |
| HUMAN\|Ensembl=ENSG00000155660\|UniProtKB=P13667 | P13667 | Protein disulfide-isomerase A4<br>PDIA4<br>ortholog | protein folding<br>cellular protein modification process |
| HUMAN\|Ensembl=ENSG00000130985\|UniProtKB=P22314 | P22314 | Ubiquitin-like modifier-activating enzyme 1<br>UBA1<br>ortholog | coenzyme metabolic process<br>cellular protein modification process<br>proteolysis<br>cell communication<br>intracellular protein transport<br>nuclear transport |
| HUMAN\|Ensembl=ENSG00000130741\|UniProtKB=P41091 | P41091 | Eukaryotic translation initiation factor 2 subunit 3<br>EIF2S3<br>ortholog | translation<br>regulation of translation |
| HUMAN\|Ensembl=ENSG00000241837\|UniProtKB=P48047 | P48047 | ATP synthase subunit O, mitochondrial<br>ATP5O<br>ortholog | coenzyme metabolic process<br>nucleobase-containing compound metabolic process<br>cation transport |
| HUMAN\|Ensembl=ENSG00000134 | P54577 | Tyrosine--tRNA ligase, cytoplasmic<br>YARS | translation |

| | | | |
|---|---|---|---|
| 684\|UniProtKB=P54577 | | ortholog | |
| HUMAN\|Ensembl=ENSG00000131467\|UniProtKB=P61289 | P61289 | Proteasome activator complex subunit 3<br>PSME3<br>ortholog | proteolysis |
| HUMAN\|Ensembl=ENSG00000067057\|UniProtKB=Q01813 | Q01813 | 6-phosphofructokinase type C<br>PFKP<br>ortholog | glycolysis<br>glycolysis |
| HUMAN\|Ensembl=ENSG00000104823\|UniProtKB=Q13011 | Q13011 | Delta(3,5)-Delta(2,4)-dienoyl-CoA isomerase, mitochondrial<br>ECH1<br>ortholog | coenzyme metabolic process<br>vitamin biosynthetic process<br>carbohydrate metabolic process<br>fatty acid beta-oxidation |
| HUMAN\|Ensembl=ENSG00000110958\|UniProtKB=Q15185 | Q15185 | Prostaglandin E synthase 3<br>PTGES3<br>ortholog | protein folding<br>protein complex assembly<br>protein complex biogenesis |
| HUMAN\|Ensembl=ENSG00000100836\|UniProtKB=Q86U42 | Q86U42 | Polyadenylate-binding protein 2<br>PABPN1<br>ortholog | mRNA processing |
| HUMAN\|Ensembl=ENSG00000107164\|UniProtKB=Q96I24 | Q96I24 | Far upstream element-binding protein 3<br>FUBP3<br>ortholog | induction of apoptosis<br>RNA splicing, via transesterification reactions<br>transcription from RNA polymerase II promoter<br>mRNA splicing, via spliceosome<br>RNA splicing, via transesterification reactions<br>protein metabolic process<br>cell communication<br>neurological system process<br>induction of apoptosis<br>intracellular protein transport<br>nuclear transport |
| HUMAN\|Ensembl=ENSG00000143401\|UniProtKB=Q9BTT0 | Q9BTT0 | Acidic leucine-rich nuclear phosphoprotein 32 family member E<br>ANP32E<br>ortholog | metabolic process<br>regulation of catalytic activity |

| | | | |
|---|---|---|---|
| HUMAN\|Ensembl=ENSG00000108010\|UniProtKB=O76003 | O76003 | Glutaredoxin-3<br>GLRX3<br>ortholog | respiratory electron transport chain<br>sulfur compound metabolic process<br>response to stress |
| HUMAN\|Ensembl=ENSG00000162813\|UniProtKB=O95861 | O95861 | 3'(2'),5'-bisphosphate nucleotidase 1<br>BPNT1<br>ortholog | sulfur compound metabolic process<br>phospholipid metabolic process<br>nucleobase-containing compound metabolic process<br>phospholipid metabolic process<br>cellular process |
| HUMAN\|Ensembl=ENSG00000121552\|UniProtKB=P01040 | P01040 | Cystatin-A<br>CSTA<br>ortholog | proteolysis<br>regulation of catalytic activity |
| HUMAN\|Ensembl=ENSG00000160213\|UniProtKB=P04080 | P04080 | Cystatin-B<br>CSTB<br>ortholog | proteolysis<br>regulation of catalytic activity |
| HUMAN\|Ensembl=ENSG00000170312\|UniProtKB=P06493 | P06493 | Cyclin-dependent kinase 1<br>CDK1<br>ortholog | glycogen metabolic process<br>protein phosphorylation<br>mitosis<br>cell communication |
| HUMAN\|Ensembl=ENSG00000182199\|UniProtKB=P34897 | P34897 | Serine hydroxymethyltransferase, mitochondrial<br>SHMT2<br>ortholog | nucleobase-containing compound metabolic process<br>cellular amino acid metabolic process |
| HUMAN\|Ensembl=ENSG00000072778\|UniProtKB=P49748 | P49748 | Very long-chain specific acyl-CoA dehydrogenase, mitochondrial<br>ACADVL<br>ortholog | respiratory electron transport chain<br>acyl-CoA metabolic process<br>nitrogen compound metabolic process<br>fatty acid beta-oxidation<br>acyl-CoA metabolic process |
| HUMAN\|Ensembl=ENSG00000127314\|UniProtKB=P61224 | P61224 | Ras-related protein Rap-1b<br>RAP1B<br>ortholog | metabolic process<br>synaptic transmission<br>cell adhesion<br>neurological system process<br>intracellular protein transport<br>receptor-mediated endocytosis |

| | | | |
|---|---|---|---|
| HUMAN\|Ensembl=ENSG00000103257\|UniProtKB=Q01650 | Q01650 | Large neutral amino acids transporter small subunit 1<br>SLC7A5<br>ortholog | cellular amino acid metabolic process<br>amino acid transport |
| HUMAN\|Ensembl=ENSG00000197157\|UniProtKB=Q7KZF4 | Q7KZF4 | Staphylococcal nuclease domain-containing protein 1<br>SND1<br>ortholog | transcription from RNA polymerase II promoter |
| HUMAN\|Ensembl=ENSG00000168872\|UniProtKB=Q9NUU7 | Q9NUU7 | ATP-dependent RNA helicase DDX19A<br>DDX19A<br>ortholog | nucleobase-containing compound metabolic process<br>translation<br>regulation of translation |
| HUMAN\|Ensembl=ENSG00000134440\|UniProtKB=O43776 | O43776 | Asparagine--tRNA ligase, cytoplasmic<br>NARS<br>ortholog | translation |
| HUMAN\|Ensembl=ENSG00000111716\|UniProtKB=P07195 | P07195 | L-lactate dehydrogenase B chain<br>LDHB<br>ortholog | glycolysis<br>glycolysis<br>tricarboxylic acid cycle |
| HUMAN\|Ensembl=ENSG00000175592\|UniProtKB=P15407 | P15407 | Fos-related antigen 1<br>FOSL1<br>ortholog | immune system process<br>induction of apoptosis<br>transcription from RNA polymerase II promoter<br>cell cycle<br>neurological system process<br>induction of apoptosis<br>regulation of transcription from RNA polymerase II promoter |
| HUMAN\|Ensembl=ENSG00000120053\|UniProtKB=P17174 | P17174 | Aspartate aminotransferase, cytoplasmic<br>GOT1<br>ortholog | cellular amino acid metabolic process |
| HUMAN\|Ensembl=ENSG00000125977\|UniProtKB=P20042 | P20042 | Eukaryotic translation initiation factor 2 subunit 2<br>EIF2S2<br>ortholog | translation<br>regulation of translation |
| HUMAN\|Ensembl=ENSG00000152234\|UniProtKB=P25705 | P25705 | ATP synthase subunit alpha, mitochondrial<br>ATP5A1<br>ortholog | respiratory electron transport chain<br>purine nucleobase metabolic process<br>cation transport |

| | | | |
|---|---|---|---|
| HUMAN\|Ensembl=ENSG00000163918\|UniProtKB=P35249 | P35249 | Replication factor C subunit 4<br>RFC4<br>ortholog | DNA replication<br>cell cycle |
| HUMAN\|Ensembl=ENSG00000014641\|UniProtKB=P40925 | P40925 | Malate dehydrogenase, cytoplasmic<br>MDH1<br>ortholog | generation of precursor metabolites and energy<br>carbohydrate metabolic process<br>tricarboxylic acid cycle |
| HUMAN\|Ensembl=ENSG00000109332\|UniProtKB=P61077 | P61077 | Ubiquitin-conjugating enzyme E2 D3<br>UBE2D3<br>ortholog | apoptotic process<br>cellular protein modification process<br>apoptotic process |
| HUMAN\|Ensembl=ENSG00000184640\|UniProtKB=Q9UHD8 | Q9UHD8 | Septin-9<br>ortholog | metabolic process<br>cytokinesis<br>mitosis |
| HUMAN\|Ensembl=ENSG00000091164\|UniProtKB=O43396 | O43396 | Thioredoxin-like protein 1<br>TXNL1<br>ortholog | respiratory electron transport chain<br>sulfur compound metabolic process<br>cell cycle<br>cell communication<br>response to stress |
| HUMAN\|Ensembl=ENSG00000154473\|UniProtKB=O43684 | O43684 | Mitotic checkpoint protein BUB3<br>BUB3<br>ortholog | nucleobase-containing compound metabolic process<br>mitosis<br>chromosome segregation<br>RNA localization |
| HUMAN\|Ensembl=ENSG00000163399\|UniProtKB=P05023 | P05023 | Sodium/potassium-transporting ATPase subunit alpha-1<br>ATP1A1<br>ortholog | metabolic process<br>cation transport<br>cellular calcium ion homeostasis |
| HUMAN\|Ensembl=ENSG00000105220\|UniProtKB=P06744 | P06744 | Glucose-6-phosphate isomerase<br>GPI<br>ortholog | glycolysis<br>gluconeogenesis<br>glycolysis |
| HUMAN\|Ensembl=ENSG00000080824\|UniProtKB=P07900 | P07900 | Heat shock protein HSP 90-alpha<br>HSP90AA1<br>ortholog | protein folding<br>response to stress |
| HUMAN\|Ensembl=ENSG00000096384\|UniProtKB=P08238 | P08238 | Heat shock protein HSP 90-beta<br>HSP90AB1<br>ortholog | immune system process<br>protein folding<br>response to stress |
| HUMAN\|Ensembl=ENSG00000164111\|UniProtKB=P08758 | P08758 | Annexin A5<br>ANXA5<br>ortholog | fatty acid metabolic process |

| | | | |
|---|---|---|---|
| HUMAN\|Ensembl=ENSG00000100567\|UniProtKB=P25788 | P25788 | Proteasome subunit alpha type-3<br>PSMA3<br>ortholog | proteolysis |
| HUMAN\|Ensembl=ENSG00000254772\|UniProtKB=P26641 | P26641 | Elongation factor 1-gamma<br>EEF1G<br>ortholog | immune system process<br>translation<br>cell communication<br>response to toxic substance<br>regulation of translation |
| HUMAN\|Ensembl=ENSG00000143106\|UniProtKB=P28066 | P28066 | Proteasome subunit alpha type-5<br>PSMA5<br>ortholog | proteolysis |
| HUMAN\|Ensembl=ENSG00000100804\|UniProtKB=P28074 | P28074 | Proteasome subunit beta type-5<br>PSMB5<br>ortholog | proteolysis |
| HUMAN\|Ensembl=ENSG00000169710\|UniProtKB=P49327 | P49327 | Fatty acid synthase<br>FASN<br>ortholog | cellular amino acid metabolic process<br>fatty acid biosynthetic process |
| HUMAN\|Ensembl=ENSG00000178952\|UniProtKB=P49411 | P49411 | Elongation factor Tu, mitochondrial<br>TUFM<br>ortholog | translation<br>regulation of translation |
| HUMAN\|Ensembl=ENSG00000090861\|UniProtKB=P49588 | P49588 | Alanine--tRNA ligase, cytoplasmic<br>AARS<br>ortholog | tRNA metabolic process |
| HUMAN\|Ensembl=ENSG00000115484\|UniProtKB=P50991 | P50991 | T-complex protein 1 subunit delta<br>CCT4<br>ortholog | protein folding<br>protein complex assembly<br>protein complex biogenesis |
| HUMAN\|Ensembl=ENSG00000260245\|UniProtKB=P53396 | P53396 | ATP-citrate synthase<br>ACLY<br>ortholog | generation of precursor metabolites and energy<br>coenzyme metabolic process<br>carbohydrate metabolic process<br>tricarboxylic acid cycle<br>lipid metabolic process |
| HUMAN\|Ensembl=ENSG00000124207\|UniProtKB=P55060 | P55060 | Exportin-2<br>CSE1L<br>ortholog | metabolic process<br>intracellular protein transport<br>nuclear transport |
| HUMAN\|Ensembl=ENSG00000136 | Q07065 | Cytoskeleton-associated protein 4<br>CKAP4 | DNA replication<br>DNA repair<br>mitosis |

| | | | |
|---|---|---|---|
| 026\|UniProtKB=Q07065 | | ortholog | meiosis<br>chromosome segregation<br>chromatin organization |
| HUMAN\|Ensembl=ENSG00000187840\|UniProtKB=Q13541 | Q13541 | Eukaryotic translation initiation factor 4E-binding protein 1<br>EIF4EBP1<br>ortholog | translation |
| HUMAN\|Ensembl=ENSG00000263344\|UniProtKB=Q15056 | Q15056 | Eukaryotic translation initiation factor 4H<br>EIF4H<br>ortholog | translation<br>regulation of translation |
| HUMAN\|Ensembl=ENSG00000143870\|UniProtKB=Q15084 | Q15084 | Protein disulfide-isomerase A6<br>PDIA6<br>ortholog | protein folding<br>cellular protein modification process |
| HUMAN\|Ensembl=ENSG00000262812\|UniProtKB=Q9Y4L1 | Q9Y4L1 | Hypoxia up-regulated protein 1<br>HYOU1<br>ortholog | protein folding<br>protein complex assembly<br>response to stress<br>protein complex biogenesis |
| HUMAN\|Ensembl=ENSG00000223639\|UniProtKB=O00299 | O00299 | Chloride intracellular channel protein 1<br>CLIC1<br>ortholog | immune system process<br>translation<br>cell communication<br>response to toxic substance<br>anion transport<br>regulation of translation |
| HUMAN\|Ensembl=ENSG00000136628\|UniProtKB=P07814 | P07814 | Bifunctional glutamate/proline--tRNA ligase<br>EPRS<br>ortholog | translation |
| HUMAN\|Ensembl=ENSG00000160752\|UniProtKB=P14324 | P14324 | Farnesyl pyrophosphate synthase<br>FDPS<br>ortholog | cholesterol metabolic process |
| HUMAN\|Ensembl=ENSG00000166825\|UniProtKB=P15144 | P15144 | Aminopeptidase N<br>ANPEP<br>ortholog | proteolysis |
| HUMAN\|Ensembl=ENSG00000153113\|UniProtKB=P20810 | P20810 | Calpastatin<br>CAST<br>ortholog | proteolysis<br>regulation of catalytic activity |
| HUMAN\|Ensembl=ENSG00000117592\|UniProtKB=P30041 | P30041 | Peroxiredoxin-6<br>PRDX6<br>ortholog | metabolic process |

| | | | |
|---|---|---|---|
| HUMAN\|Ensembl=ENSG00000156261\|UniProtKB=P50990 | P50990 | T-complex protein 1 subunit theta<br>CCT8<br>ortholog | protein folding<br>protein complex assembly<br>protein complex biogenesis |
| HUMAN\|Ensembl=ENSG00000172531\|UniProtKB=P62136 | P62136 | Serine/threonine-protein phosphatase PP1-alpha catalytic subunit<br>PPP1CA<br>ortholog | immune system process<br>apoptotic process<br>glycogen metabolic process<br>transcription from RNA polymerase II promoter<br>mRNA processing<br>protein phosphorylation<br>mitosis<br>meiosis<br>cell communication<br>apoptotic process<br>response to stress<br>regulation of carbohydrate metabolic process<br>regulation of nucleobase-containing compound metabolic process |
| HUMAN\|Ensembl=ENSG00000196262\|UniProtKB=P62937 | P62937 | Peptidyl-prolyl cis-trans isomerase A<br>PPIA<br>ortholog | immune system process<br>protein folding<br>intracellular protein transport<br>nuclear transport |
| HUMAN\|Ensembl=ENSG00000135624\|UniProtKB=Q99832 | Q99832 | T-complex protein 1 subunit eta<br>CCT7<br>ortholog | protein folding<br>protein complex assembly<br>protein complex biogenesis |
| HUMAN\|Ensembl=ENSG00000116161\|UniProtKB=Q9HB71 | Q9HB71 | Calcyclin-binding protein<br>CACYBP<br>ortholog | proteolysis |
| HUMAN\|Ensembl=ENSG00000178896\|UniProtKB=Q9NPD3 | Q9NPD3 | Exosome complex component RRP41<br>EXOSC4<br>ortholog | tRNA metabolic process<br>RNA catabolic process<br>rRNA metabolic process |
| HUMAN\|Ensembl=ENSG00000092621\|UniProtKB=O43175 | O43175 | D-3-phosphoglycerate dehydrogenase<br>PHGDH<br>ortholog | carbohydrate metabolic process<br>cellular amino acid biosynthetic process |
| HUMAN\|Ensembl=ENSG00000110 | P06576 | ATP synthase subunit beta, mitochondrial | respiratory electron transport chain |

| | | | |
|---|---|---|---|
| 955\|UniProtKB=P06576 | | ATP5B<br>ortholog | purine nucleobase metabolic process<br>cation transport |
| HUMAN\|Ensembl=ENSG00000170445\|UniProtKB=P12081 | P12081 | Histidine--tRNA ligase, cytoplasmic<br>HARS<br>ortholog | translation |
| HUMAN\|Ensembl=ENSG00000166598\|UniProtKB=P14625 | P14625 | Endoplasmin<br>HSP90B1<br>ortholog | protein folding<br>response to stress |
| HUMAN\|Ensembl=ENSG00000168374\|UniProtKB=P18085 | P18085 | ADP-ribosylation factor 4<br>ARF4<br>ortholog | metabolic process<br>cell communication<br>intracellular protein transport<br>vesicle-mediated transport |
| HUMAN\|Ensembl=ENSG00000159335\|UniProtKB=P20962 | P20962 | Parathymosin<br>PTMS<br>ortholog | nucleobase-containing compound metabolic process |
| HUMAN\|Ensembl=ENSG00000226589\|UniProtKB=P26640 | P26640 | Valine--tRNA ligase<br>VARS<br>ortholog | translation |
| HUMAN\|Ensembl=ENSG00000146731\|UniProtKB=P40227 | P40227 | T-complex protein 1 subunit zeta<br>CCT6A<br>ortholog | protein folding<br>protein complex assembly<br>protein complex biogenesis |
| HUMAN\|Ensembl=ENSG00000142657\|UniProtKB=P52209 | P52209 | 6-phosphogluconate dehydrogenase, decarboxylating<br>PGD<br>ortholog | pentose-phosphate shunt |
| HUMAN\|Ensembl=ENSG00000087191\|UniProtKB=P62195 | P62195 | 26S protease regulatory subunit 8<br>PSMC5<br>ortholog | proteolysis |
| HUMAN\|Ensembl=ENSG00000088832\|UniProtKB=P62942 | P62942 | Peptidyl-prolyl cis-trans isomerase FKBP1A<br>FKBP1A<br>ortholog | cellular protein modification process<br>cellular process |
| HUMAN\|Ensembl=ENSG00000092010\|UniProtKB=Q06323 | Q06323 | Proteasome activator complex subunit 1<br>PSME1<br>ortholog | proteolysis |
| HUMAN\|Ensembl=ENSG00000099810\|UniProtKB=Q13126 | Q13126 | S-methyl-5'-thioadenosine phosphorylase<br>MTAP<br>ortholog | purine nucleobase metabolic process |
| HUMAN\|Ensembl=ENSG00000090 | Q13310 | Polyadenylate-binding protein 4<br>PABPC4 | DNA replication |

| | | | |
|---|---|---|---|
| 621\|UniProtKB=Q13310 | | ortholog | RNA splicing, via transesterification reactions<br>transcription from RNA polymerase II promoter<br>mRNA splicing, via spliceosome<br>mRNA polyadenylation<br>RNA splicing, via transesterification reactions<br>protein metabolic process<br>cell cycle<br>ectoderm development<br>nervous system development |
| HUMAN\|Ensembl=ENSG00000084623\|UniProtKB=Q13347 | Q13347 | Eukaryotic translation initiation factor 3 subunit I<br>EIF3I<br>ortholog | translation<br>regulation of translation |
| HUMAN\|Ensembl=ENSG00000038274\|UniProtKB=Q9NZL9 | Q9NZL9 | Methionine adenosyltransferase 2 subunit beta<br>MAT2B<br>ortholog | carbohydrate metabolic process |
| HUMAN\|Ensembl=ENSG00000168003\|UniProtKB=P08195 | P08195 | 4F2 cell-surface antigen heavy chain<br>SLC3A2<br>ortholog | glycogen metabolic process |
| HUMAN\|Ensembl=ENSG00000132646\|UniProtKB=P12004 | P12004 | Proliferating cell nuclear antigen<br>PCNA<br>ortholog | DNA replication<br>DNA repair<br>cell cycle<br>regulation of catalytic activity |
| HUMAN\|Ensembl=ENSG00000198959\|UniProtKB=P21980 | P21980 | Protein-glutamine gamma-glutamyltransferase 2<br>TGM2<br>ortholog | cellular protein modification process |
| HUMAN\|Ensembl=ENSG00000101444\|UniProtKB=P23526 | P23526 | Adenosylhomocysteinase<br>AHCY<br>ortholog | purine nucleobase metabolic process |
| HUMAN\|Ensembl=ENSG00000138363\|UniProtKB=P31939 | P31939 | Bifunctional purine biosynthesis protein PURH<br>ATIC<br>ortholog | purine nucleobase metabolic process |
| HUMAN\|Ensembl=ENSG00000167 | P35232 | Prohibitin<br>PHB<br>ortholog | DNA replication<br>cell cycle |

| | | | |
|---|---|---|---|
| 085\|UniProtKB=P35232 | | | |
| HUMAN\|Ensembl=ENSG00000105379\|UniProtKB=P38117 | P38117 | Electron transfer flavoprotein subunit beta<br>ETFB<br>ortholog | respiratory electron transport chain |
| HUMAN\|Ensembl=ENSG00000100983\|UniProtKB=P48637 | P48637 | Glutathione synthetase<br>GSS<br>ortholog | sulfur compound metabolic process |
| HUMAN\|Ensembl=ENSG00000004455\|UniProtKB=P54819 | P54819 | Adenylate kinase 2, mitochondrial<br>AK2<br>ortholog | purine nucleobase metabolic process<br>pyrimidine nucleobase metabolic process |
| HUMAN\|Ensembl=ENSG00000004478\|UniProtKB=Q02790 | Q02790 | Peptidyl-prolyl cis-trans isomerase FKBP4<br>FKBP4<br>ortholog | cellular protein modification process<br>cellular process |

# 9. REFERENCES


1. Society AC. Melanoma Skin cancer Overview. American Cancer Society. 2011.
2. CRUK. All Cancers Combined Key Stats. London: Cancer Research UK, 2015 4/2/15. Report No.
3. Monzon J, Liu L, Brill H, Goldstein A, Tucker M, From L, et al. Cdkn2a Mutations In Multiple Primary Melanomas. NEJM. 1998;338(13):879-87.
4. Gatenby RA, Gawlinski ET, Gmitro AF, Kaylor B, Gillies RJ. Acid-mediated tumor invasion: a multidisciplinary study. Cancer Research. 2006;66(10):5216-23.
5. Antoniou AC, Spurdle AB, Sinilnikova OM, Healey S, Pooley KA, Schmutzler RK, et al. Common Breast Cancer-Predisposition Alleles Are Associated with Breast Cancer Risk in BRCA1 and BRCA2 Mutation Carriers. Am J Hum Genet. 2008;82(4):937-48. Epub 2008 Apr 4 doi:10.1016/j.ajhg.2008.02.008.
6. Jemal A, Siegel R, Xu J, Ward E. Cancer statistics 2010. CA Cancer J Clin. 2010;60:227-300.
7. Beyer M, Schultze JL. Regulatory T cells: major players in the tumor microenvironment. Curr Pharm Des. 2009;15(16):1879-92.
8. Nishida N, Yano H, Nishida T, Kamura T, Kojiro M. Angiogenesis in Cancer. Vasc Health Risk Manag. 2006;2(3):213-9. Epub 2006 Sep.
9. Warburg O. On the origin of cancer cells. Science. 1956;123:309-14.
10. CRUK. Skin Cancer. London: Cancer Research UK, 2013.
11. Madan V, Lear JT, Szeimies RM. Non-melanoma skin cancer. Lancet. 2010;375(9715):673-85. doi: 10.1016/S0140-6736(09)61196-X.
12. Miller SJ, Alam M, Andersen J, Berg D, Bichakjian CK, Bowen G, et al. Basal cell and squamous cell skin cancers. J Natl Compr Canc Netw. 2010;8(8):836-64.
13. Mukhtar H, Setaluri V. Advances in melanocyte and melanoma biology. Archives of Biochemistry and Biophysics. 2014;563(0):1-3.
14. Tachibana M. Sound needs sound melanocytes to be heard. Pigment Cell Res. 1999;12(6):344-54.
15. Brito FC, Kos L. Timeline and distribution of melanocyte precursors in the mouse heart. Pigment Cell Melanoma Res. 2008;21(4):464-70. doi: 10.1111/j.755-148X.2008.00459.x. Epub 2008 Apr 26.
16. Rossetti FbC, Depieri LvV, Bentley MVrLB. Confocal Laser Scanning Microscopy as a Tool for the Investigation of Skin Drug Delivery Systems and Diagnosis of Skin Disorder: *InTech*; 2013. 244 p.
17. Cichorek M, Wachulska M, Stasiewicz A, Tymińska A. Skin melanocytes: biology and development. Advances in Dermatology and Allergology/Postępy Dermatologii I Alergologii. 2013;30(1):30-41.
18. http://apps.nccd.cdc.gov/uscs/index.aspx.
19. Uong A, Zon LI. Melanocytes in development and cancer. Journal of cellular physiology. 2010;222(1):38-41.
20. Larue L, Delmas V. The WNT/Beta-catenin pathway in melanoma. Front Biosci. 2006;11:733-42.

21. Dorsky RI, Moon RT, Raible DW. Control of neural crest cell fate by the Wnt signalling pathway. Nature. 1998;396(6709):370-3.
22. Ksenia Kulikova AK, Nikolay Gnuchev, Georgii Georgiev and Sergey Larin. Research on Melanoma - A Glimpse into Current Directions and Future Trends - Dual Function of Wnts in Human Cutaneous Melanoma. Murph PM, editor: INTECH; 2011.
23. Sauka-Spengler T, Bronner-Fraser M. Evolution of the neural crest viewed from a gene regulatory perspective. Genesis. 2008;46(11):673-82. doi: 10.1002/dvg.20436.
24. Meulemans D, Bronner-Fraser M. Gene-regulatory interactions in neural crest evolution and development. Dev Cell. 2004;7(3):291-9.
25. Liu J, Fukunaga-Kalabis M, Li L, Herlyn M. Developmental pathways activated in melanocytes and melanoma. Archives of Biochemistry and Biophysics. 2014;563(0):13-21.
26. De Calisto J, Araya C, Marchant L, Riaz CF, Mayor R. Essential role of non-canonical Wnt signalling in neural crest migration. Development. 2005;132(11):2587-97.
27. Harris ML, Erickson CA. Lineage specification in neural crest cell pathfinding. Dev Dyn. 2007;236(1):1-19.
28. Thomas AJ, Erickson CA. The making of a melanocyte: the specification of melanoblasts from the neural crest. Pigment Cell Melanoma Res. 2008;21(6):598-610. doi: 10.1111/j.755-148X.2008.00506.x.
29. Goding C. MITF from neural crest to melanoma: signal transduction and transcription in the melanocyte lineage. Genes & Development. 2000;14:16.
30. Imokawa G, Yada Y, Kimura M. Signalling mechanisms of endothelin-induced mitogenesis and melanogenesis in human melanocytes. Biochem J. 1996;314(Pt 1):305-12.
31. Levy C, Khaled M, Fisher DE. MITF: master regulator of melanocyte development and melanoma oncogene. Trends Mol Med. 2006;12(9):406-14. Epub 2006 Aug 8.
32. Yasumoto K, Yokoyama K, Shibata K, Tomita Y, Shibahara S. Microphthalmia-associated transcription factor as a regulator for melanocyte-specific transcription of the human tyrosinase gene. Molecular and Cellular Biology. 1994;14(12):8058-70.
33. McGill GG, Horstmann M, Widlund HR, Du J, Motyckova G, Nishimura EK, et al. Bcl2 regulation by the melanocyte master regulator Mitf modulates lineage survival and melanoma cell viability. Cell. 2002;109(6):707-18.
34. Lang D, Mascarenhas JB, Shea CR. Melanocytes, melanocyte stem cells, and melanoma stem cells. Clin Dermatol. 2013;31(2):166-78. doi:10.1016/j.clindermatol.2012.08.014.
35. Simon JD, Peles D, Wakamatsu K, Ito S. Current challenges in understanding melanogenesis: bridging chemistry, biological control, morphology, and function. Pigment Cell Melanoma Res. 2009;22(5):563-79. doi: 10.1111/j.755-148X.2009.00610.x. Epub 2009 Jul 21.
36. Riley PA. Melanin. Int J Biochem Cell Biol. 1997;29(11):1235-9.
37. Costin GE, Hearing VJ. Human skin pigmentation: melanocytes modulate skin color in response to stress. FASEB J. 2007;21(4):976-94. Epub 2007 Jan 22.
38. Seiji M, Fitzpatrick TB. The reciprocal relationship between melanization and tyrosinase activity in melanosomes (melanin granules). J Biochem. 1961;49:700-6.

39. Raposo G, Marks MS. Melanosomes – dark organelles enlighten endosomal membrane transport. Nat Rev Mol Cell Biol. 2007;8(10):786-97. doi:10.1038/nrm2258.
40. Wasmeier C, Hume AN, Bolasco G, Seabra MC. Melanosomes at a glance. Journal of Cell Science. 2008;121(24):3995-9.
41. Cui R, Widlund HR, Feige E, Lin JY, Wilensky DL, Igras VE, et al. Central role of p53 in the suntan response and pathologic hyperpigmentation. Cell. 2007;128(5):853-64.
42. Griesmann H, Ripka S, Pralle M, Ellenrieder V, Baumgart S, Buchholz M, et al. WNT5A-NFAT Signaling Mediates Resistance to Apoptosis in Pancreatic Cancer.
43. Abdel-Malek Z, Scott MC, Suzuki I, Tada A, Im S, Lamoreux L, et al. The melanocortin-1 receptor is a key regulator of human cutaneous pigmentation. Pigment Cell Res. 2000;13(Suppl 8):156-62.
44. Bertolotto C, Abbe P, Hemesath TJ, Bille K, Fisher DE, Ortonne JP, et al. Microphthalmia gene product as a signal transducer in cAMP-induced differentiation of melanocytes. J Cell Biol. 1998;142(3):827-35.
45. Gaggioli C, Busca R, Abbe P, Ortonne JP, Ballotti R. Microphthalmia-associated transcription factor (MITF) is required but is not sufficient to induce the expression of melanogenic genes. Pigment Cell Res. 2003;16(4):374-82.
46. van Schanke A, Jongsma MJ, Bisschop R, van Venrooij GM, Rebel H, de Gruijl FR. Single UVB overexposure stimulates melanocyte proliferation in murine skin, in contrast to fractionated or UVA-1 exposure. J Invest Dermatol. 2005;124(1):241-7.
47. Hirobe T. Role of keratinocyte-derived factors involved in regulating the proliferation and differentiation of mammalian epidermal melanocytes. Pigment Cell Res. 2005;18(1):2-12.
48. Halaban R. The regulation of normal melanocyte proliferation. Pigment Cell Res. 2000;13(1):4-14.
49. Bandarchi B, Ma L, Navab R, Seth A, Rasty G. From melanocyte to metastatic malignant melanoma. Dermatology Research and Practice. 2010;2010.
50. Kobayashi N, Nakagawa A, Muramatsu T, Yamashina Y, Shirai T, Hashimoto MW, et al. Supranuclear melanin caps reduce ultraviolet induced DNA photoproducts in human epidermis. J Invest Dermatol. 1998;110(5):806-10.
51. Thody AJ, Higgins EM, Wakamatsu K, Ito S, Burchill SA, Marks JM. Pheomelanin as well as eumelanin is present in human epidermis. J Invest Dermatol. 1991;97(2):340-4.
52. Fitzpatrick TB, Miyamoto M, Ishikawa K. The evolution of concepts of melanin biology. Arch Dermatol. 1967;96(3):305-23.
53. Hearing VJ. Determination of melanin synthetic pathways. J Invest Dermatol. 2011;131(E1):E8-E11.
54. Abdel-Malek ZA, Kadekaro AL, Swope VB. Stepping up melanocytes to the challenge of UV exposure. Pigment Cell Melanoma Res. 2010;23(2):171-86. doi: 10.1111/j.755-148X.2010.00679.x. Epub 2010 Feb 1.
55. Mooi WJ, Peeper DS. Oncogene-induced cell senescence--halting on the road to cancer. N Engl J Med. 2006;355(10):1037-46.
56. Zaidi MR, Day CP, Merlino G. From UVs to metastases: modeling melanoma initiation and progression in the mouse. J Invest Dermatol. 2008;128(10):2381-91. doi: 10.1038/jid.2008.177.

57. Shtivelman E, Davies MA, Hwu P, Yang J, Lotem M, Oren M, et al. Pathways and therapeutic targets in melanoma. Oncotarget. 2014;5(7):1701-52.
58. Reymond N, d'Agua BB, Ridley AJ. Crossing the endothelial barrier during metastasis. Nat Rev Cancer. 2013;13(12):858-70. doi: 10.1038/nrc3628.
59. De Giorgi V, Papi F, Giorgi L, Savarese I, Verdelli A, Scarfi F, et al. Skin self-examination and the ABCDE rule in the early diagnosis of melanoma: is the game over? Br J Dermatol. 2013;168(6):1370-1. doi: 10.111/bjd.12250.
60. Abbott NC, Pandeya N, Ong N, McClenahan P, Smithers BM, Green A, et al. Changeable naevi in people at high risk for melanoma. Australas J Dermatol. 2014;20(10):12181.
61. Goldsmith SM. A unifying approach to the clinical diagnosis of melanoma including "D" for "Dark" in the ABCDE criteria. Dermatol Pract Concept. 2014;4(4):75-8. doi: 10.5826/dpc.0404a16. eCollection 2014 Oct.
62. Howlader N NA, Cronin KA (eds). SEER Cancer Statistics Review, 1975-2011. In: Institute NC, editor. Bethesda2014.
63. Jemal A. Cancer statistics, 2003. CA Cancer J Clin. 2003;53:21.
64. de Vries E, Bray FI, Coebergh JWW, Parkin DM. Changing epidemiology of malignant cutaneous melanoma in Europe 1953-1997: Rising trends in incidence and mortality but recent stabilizations in Western Europe and decreases in Scandinavia. International Journal of Cancer. 2003;107(1):119-26.
65. Dennis LK. Analysis of the melanoma epidemic, both apparent and real: Data from the 1973 through 1994 surveillance, epidemiology, and end results program registry. Archives of Dermatology. 1999;135(3):275-80.
66. Linos E, Swetter SM, Cockburn MG, Colditz GA, Clarke CA. Increasing burden of melanoma in the United States. J Invest Dermatol. 2009;129(7):1666-74.
67. de Vries E, Coebergh JW. Cutaneous malignant melanoma in Europe. Eur J Cancer. 2004;40(16):2355-66.
68. de Vries E, Coebergh J-WW. Melanoma incidence has risen in Europe. BMJ : British Medical Journal. 2005;331(7518):698-.
69. Gandini S, Autier P, Boniol M. Reviews on sun exposure and artificial light and melanoma. Prog Biophys Mol Biol. 2011;107(3):362-6.
70. Armstrong BK, Kricker A. How much melanoma is caused by sun exposure? Melanoma Res. 1993;3(6):395-401.
71. Parkin DM, Mesher D, Sasieni P. 13. Cancers attributable to solar (ultraviolet) radiation exposure in the UK in 2010. British Journal of Cancer. 2011;105(Suppl 2):S66-S9.
72. Purdue MP, Freeman LE, Anderson WF, Tucker MA. Recent trends in incidence of cutaneous melanoma among US Caucasian young adults. J Invest Dermatol. 2008;128(12):2905-8.
73. Diffey BL. A quantitative estimate of melanoma mortality from ultraviolet A sunbed use in the U.K. Br J Dermatol. 2003;149(3):578-81.
74. El Ghissassi F, Baan R, Straif K, Grosse Y, Secretan B, Bouvard V, et al. A review of human carcinogens—Part D: radiation. The Lancet Oncology.10(8):751-2.
75. Marks R. Campaigning for melanoma prevention: a model for a health education program. J Eur Acad Dermatol Venereol. 2004;18(1):44-7.

76. Hill D, White V, Marks R, Borland R. Changes in sun-related attitudes and behaviours, and reduced sunburn prevalence in a population at high risk of melanoma. Eur J Cancer Prev. 1993;2(6):447-56.
77. Leiter U, Garbe C. Epidemiology of melanoma and nonmelanoma skin cancer--the role of sunlight. Adv Exp Med Biol. 2008;624:89-103.
78. Bharath AK, Turner RJ. Impact of climate change on skin cancer. Journal of the Royal Society of Medicine. 2009;102(6):215-8.
79. MacLennan R, Green AC, McLeod GRC, Martin NG. Increasing Incidence of Cutaneous Melanoma in Queensland, Australia. Journal of the National Cancer Institute. 1992;84(18):1427-32.
80. Stubblefield J, Kelly B. Melanoma in Non-Caucasian Populations. Surgical Clinics of North America. 2014;94(5):1115-26.
81. Cress RD, Holly EA. Incidence of cutaneous melanoma among non-Hispanic whites, Hispanics, Asians, and blacks: an analysis of california cancer registry data, 1988-93. Cancer Causes Control. 1997;8(2):246-52.
82. Hu S, Soza-Vento RM, Parker DF, Kirsner RS. COmparison of stage at diagnosis of melanoma among hispanic, black, and white patients in miami-dade county, florida. Archives of Dermatology. 2006;142(6):704-8.
83. Gloster HM, Jr., Neal K. Skin cancer in skin of color. J Am Acad Dermatol. 2006;55(5):741-60.
84. Balch CM, Gershenwald JE, Soong SJ, Thompson JF, Atkins MB, Byrd DR, et al. Final version of 2009 AJCC melanoma staging and classification. Journal of clinical oncology : official journal of the American Society of Clinical Oncology. 2009;27(36):6199-206.
85. Hinrichs CS, Gibbs JF, Driscoll D, Kepner JL, Wilkinson NW, Edge SB, et al. The effectiveness of complete decongestive physiotherapy for the treatment of lymphedema following groin dissection for melanoma. J Surg Oncol. 2004;85(4):187-92.
86. Starritt EC, Joseph D, McKinnon JG, Lo SK, de Wilt JHW, Thompson JF. Lymphedema After Complete Axillary Node Dissection for Melanoma: Assessment Using a New, Objective Definition. Ann Surg. 2004;240(5):866-74. doi:10.1097/01.sla.0000143271.32568.2b.
87. Mocellin S, Pasquali S, Rossi CR, Nitti D. Interferon alpha adjuvant therapy in patients with high-risk melanoma: a systematic review and meta-analysis. J Natl Cancer Inst. 2010;102(7):493-501.
88. Hauschild A. Adjuvant interferon alfa for melanoma: new evidence-based treatment recommendations?
89. Paulsen IF, Chakera AH, Drejoe JB, Klyver H, Dahlstrom K, Oturai PS, et al. Tumour response after hyperthermic isolated limb perfusion for locally advanced melanoma. Dan Med J. 2014;61(1).
90. Liu-Smith F, Dellinger R, Meyskens Jr FL. Updates of reactive oxygen species in melanoma etiology and progression. Archives of Biochemistry and Biophysics. 2014;563(0):51-5.
91. Bhatia S, S.Tykodi, Thompson J. Treatment of Metastatic Melanoma An Overview. Oncology. 2009;23(6):488-96.

92. Chapman PB, Einhorn LH, Meyers ML, Saxman S, Destro AN, Panageas KS, et al. Phase III multicenter randomized trial of the Dartmouth regimen versus dacarbazine in patients with metastatic melanoma. J Clin Oncol. 1999;17(9):2745-51.
93. Ives NJ, Stowe RL, Lorigan P, Wheatley K. Chemotherapy compared with biochemotherapy for the treatment of metastatic melanoma: a meta-analysis of 18 trials involving 2,621 patients. J Clin Oncol. 2007;25(34):5426-34.
94. Ascierto PA, Kirkwood JM. Adjuvant therapy of melanoma with interferon: lessons of the past decade. J Transl Med. 2008;6(62):1479-5876.
95. Proebstle TM, Fuchs T, Scheibenbogen C, Sterry W, Keilholz U. Long-term outcome of treatment with dacarbazine, cisplatin, interferon-alpha and intravenous high dose interleukin-2 in poor risk melanoma patients. Melanoma Res. 1998;8(6):557-63.
96. Hao MZ, Zhou WY, Du XL, Chen KX, Wang GW, Yang Y, et al. Novel anti-melanoma treatment: focus on immunotherapy.
97. Ott PA, Hodi FS, Robert C. CTLA-4 and PD-1/PD-L1 blockade: new immunotherapeutic modalities with durable clinical benefit in melanoma patients. Clin Cancer Res. 2013;19(19):5300-9. doi: 10.1158/078-0432.CCR-13-143.
98. Pardoll DM. The blockade of immune checkpoints in cancer immunotherapy. Nat Rev Cancer. 2012;12(4):252-64. doi: 10.1038/nrc3239.
99. Hodi FS, O'Day SJ, McDermott DF, Weber RW, Sosman JA, Haanen JB, et al. Improved survival with ipilimumab in patients with metastatic melanoma. N Engl J Med. 2010;363(8):711-23. doi: 10.1056/NEJMoa1003466. Epub 2010 Jun 5.
100. O'Day SJ, Maio M, Chiarion-Sileni V, Gajewski TF, Pehamberger H, Bondarenko IN, et al. Efficacy and safety of ipilimumab monotherapy in patients with pretreated advanced melanoma: a multicenter single-arm phase II study. Ann Oncol. 2010;21(8):1712-7. doi: 10.093/annonc/mdq013. Epub 2010 Feb 10.
101. Wolchok JD, Neyns B, Linette G, Negrier S, Lutzky J, Thomas L, et al. Ipilimumab monotherapy in patients with pretreated advanced melanoma: a randomised, double-blind, multicentre, phase 2, dose-ranging study. Lancet Oncol. 2010;11(2):155-64. doi: 10.1016/S470-2045(09)70334-1. Epub 2009 Dec 8.
102. Weber J, Thompson JA, Hamid O, Minor D, Amin A, Ron I, et al. A randomized, double-blind, placebo-controlled, phase II study comparing the tolerability and efficacy of ipilimumab administered with or without prophylactic budesonide in patients with unresectable stage III or IV melanoma. Clin Cancer Res. 2009;15(17):5591-8. Epub 2009 Aug 11.
103. Bhatia S, Thompson JA. Melanoma: immune checkpoint blockade story gets better. Lancet. 2014;384(9948):1078-9. doi: 10.16/S0140-6736(14)61140-5. Epub 2014 Jul 15.
104. Wolchok JD, Kluger H, Callahan MK, Postow MA, Rizvi NA, Lesokhin AM, et al. Nivolumab plus ipilimumab in advanced melanoma. N Engl J Med. 2013;369(2):122-33. doi: 10.1056/NEJMoa1302369. Epub 2013 Jun 2.
105. Health NCIatNIo. Clinical Trials [29/01/15]. Available from: http://www.cancer.gov/clinicaltrials.
106. He J, Yin Y, Luster TA, Watkins L, Thorpe PE. Antiphosphatidylserine antibody combined with irradiation damages tumor blood vessels and induces tumor immunity in a rat model of glioblastoma. Clin Cancer Res. 2009;15(22):6871-80. doi: 10.1158/078-0432.CCR-09-1499. Epub 2009 Nov 3.

107. Meier F, Schittek B, Busch S, Garbe C, Smalley K, Satyamoorthy K, et al. The RAS/RAF/MEK/ERK and PI3K/AKT signaling pathways present molecular targets for the effective treatment of advanced melanoma. Front Biosci. 2005;10:2986-3001.
108. Anforth RM, Blumetti TCMP, Kefford RF, Sharma R, Scolyer RA, Kossard S, et al. Cutaneous manifestations of dabrafenib (GSK2118436): a selective inhibitor of mutant BRAF in patients with metastatic melanoma.
109. Sosman JA, Kim KB, Schuchter L, Gonzalez R, Pavlick AC, Weber JS, et al. Survival in BRAF V600–Mutant Advanced Melanoma Treated with Vemurafenib. N Engl J Med. 2012;366:707-14.
110. Flaherty KT, Puzanov I, Kim KB, Ribas A, McArthur GA, Sosman JA, et al. Inhibition of Mutated, Activated BRAF in Metastatic Melanoma.
111. Helmbach H, Rossmann E, Kern MA, Schadendorf D. Drug-resistance in human melanoma. Int J Cancer. 2001;93(5):617-22.
112. Chen KG, Valencia JC, Gillet JP, Hearing VJ, Gottesman MM. Involvement of ABC Transporters in Melanogenesis and the Development of Multidrug Resistance of Melanoma.
113. Schadendorf D, Makki A, Stahr C, van Dyck A, Wanner R, Scheffer GL, et al. Membrane transport proteins associated with drug resistance expressed in human melanoma. Am J Pathol. 1995;147(6):1545-52.
114. Berger W, Hauptmann E, Elbling L, Vetterlein M, Kokoschka EM, Micksche M. Possible role of the multidrug resistance-associated protein (MRP) in chemoresistance of human melanoma cells. Int J Cancer. 1997;71(1):108-15.
115. Sun C, Wang L, Huang S, Heynen GJ, Prahallad A, Robert C, et al. Reversible and adaptive resistance to BRAF(V600E) inhibition in melanoma. Nature. 2014;508(7494):118-22.
116. Atefi M, von Euw E, Attar N, Ng C, Chu C, Guo D, et al. Reversing Melanoma Cross-Resistance to BRAF and MEK Inhibitors by Co-Targeting the AKT/mTOR Pathway. PLoS ONE. 2011;6(12):e28973.
117. Flaherty KT, Infante JR, Daud A, Gonzalez R, Kefford RF, Sosman J, et al. Combined BRAF and MEK inhibition in melanoma with BRAF V600 mutations. N Engl J Med. 2012;367(18):1694-703.
118. Jang S, Atkins MB. Treatment of BRAF-mutant melanoma: the role of vemurafenib and other therapies. Clin Pharmacol Ther. 2014;95(1):24-31.
119. Bombelli FB, Webster CA, Moncrieff M, Sherwood V. The scope of nanoparticle therapies for future metastatic melanoma treatment. Lancet Oncol. 2014;15(1):70333-4.
120. Sztiller-Sikorska M, Koprowska K, Jakubowska J, Zalesna I, Stasiak M, Duechler M, et al. Sphere formation and self-renewal capacity of melanoma cells is affected by the microenvironment. Melanoma Research. 2012;22(3):215-24.
121. Schatton T, Frank MH. REVIEW ARTICLE: Cancer stem cells and human malignant melanoma. Pigment Cell & Melanoma Research. 2007;21(1):39-55.
122. Rich BE, Ramgolam K, Lauriol J, Lalou C, Lauden L, Michel L, et al. Melanoma Spheroids Grown Under Neural Crest Cell Conditions Are Highly Plastic Migratory/Invasive Tumor Cells Endowed with Immunomodulator Function. PLoS ONE. 2011;6(4):e18784.
123. H D. Mutations of the BRAF gene in human cancer. Nature. 2002;417:949-54.

124. Goodall J, Wellbrock C, Dexter TJ, Roberts K, Marais R, Goding CR. The Brn-2 Transcription Factor Links Activated BRAF to Melanoma Proliferation. Mol Cell Biol. 2004;24(7):2923-31. doi:10.1128/MCB.24.7.2923-31.004.
125. Yajima I, Kumasaka MY, Thang ND, Goto Y, Takeda K, Yamanoshita O, et al. RAS/RAF/MEK/ERK and PI3K/PTEN/AKT Signaling in Malignant Melanoma Progression and Therapy. Dermatol Res Pract. 2012;2012:354191.
126. Gray-Schopfer V, Wellbrock C, Marais R. Melanoma biology and new targeted therapy. Nature. 2007;445(7130):851-7.
127. Carracedo A, Pandolfi PP. The PTEN-PI3K pathway: of feedbacks and cross-talks. Oncogene. 2008;27(41):5527-41.
128. Ogawara Y, Kishishita S, Obata T, Isazawa Y, Suzuki T, Tanaka K, et al. Akt enhances Mdm2-mediated ubiquitination and degradation of p53. J Biol Chem. 2002;277(24):21843-50. Epub 2002 Mar 28.
129. Maehama T, Dixon JE. PTEN: a tumour suppressor that functions as a phospholipid phosphatase. Trends Cell Biol. 1999;9(4):125-8.
130. Sekulic A, Haluska P, Jr., Miller AJ, Genebriera De Lamo J, Ejadi S, Pulido JS, et al. Malignant melanoma in the 21st century: the emerging molecular landscape. Mayo Clin Proc. 2008;83(7):825-46.
131. Dhawan P, Singh AB, Ellis DL, Richmond A. Constitutive activation of Akt/protein kinase B in melanoma leads to up-regulation of nuclear factor-kappaB and tumor progression. Cancer Res. 2002;62(24):7335-42.
132. Curtin J, Fridyland J, Kageshita T, H P. Distinct sets of genetic alterations in melanoma. NEJM. 2005;353(20):2135-47.
133. Si L, Kong Y, Xu X, Flaherty KT, Sheng X, Cui C, et al. Prevalence of BRAF V600E mutation in Chinese melanoma patients: large scale analysis of BRAF and NRAS mutations in a 432-case cohort. European Journal of Cancer. 2012;48(1):94-100.
134. Bucheit AD, Syklawer E, Jakob JA, Bassett RL, Jr., Curry JL, Gershenwald JE, et al. Clinical characteristics and outcomes with specific BRAF and NRAS mutations in patients with metastatic melanoma. Cancer. 2013;119(21):3821-9.
135. Ekedahl H, Cirenajwis H, Harbst K, Carneiro A, Nielsen K, Olsson H, et al. The clinical significance of BRAF and NRAS mutations in a clinic-based metastatic melanoma cohort. Br J Dermatol. 2013;169(5):1049-55.
136. Liu D, Liu X, Xing M. Activities of multiple cancer-related pathways are associated with BRAF mutation and predict the resistance to BRAF/MEK inhibitors in melanoma cells. Cell Cycle. 2014;13(2):208-19.
137. Banerji U, Affolter A, Judson I, Marais R, Workman P. BRAF and NRAS mutations in melanoma: potential relationships to clinical response to HSP90 inhibitors. Molecular Cancer Therapeutics. 2008;7(4):737-9.
138. Rubinstein JC, Sznol M, Pavlick AC, Ariyan S, Cheng E, Bacchiocchi A, et al. Incidence of the V600K mutation among melanoma patients with BRAF mutations, and potential therapeutic response to the specific BRAF inhibitor PLX4032.
139. Niault TS, Baccarini M. Targets of Raf in tumorigenesis. Carcinogenesis. 2010;31(7):1165-74.
140. Wellbrock C, Karasarides M, Marais R. The RAF proteins take centre stage. Nature reviews Molecular cell biology. 2004;5(11):875-85.

141. Ascierto P, Kirkwood J, Grob J, Simeone E, Grimaldi A, Maio M et al. The role of BRAF V600 mutation in melanoma. Journal of Translational Medicine. 2012;10(85).
142. Dankort D, Curley DP, Cartlidge RA, Nelson B, Karnezis AN, Damsky Jr WE, et al. BrafV600E cooperates with Pten loss to induce metastatic melanoma. Nature Genetics. 2009;41(5):544-52.
143. Damsky William E, Curley David P, Santhanakrishnan M, Rosenbaum Lara E, Platt James T, Gould Rothberg Bonnie E, et al. β-Catenin Signaling Controls Metastasis in Braf-Activated Pten-Deficient Melanomas. Cancer Cell. 2011;20(6):741-54.
144. Xing F, Persaud Y, Pratilas CA, Taylor BS, Janakiraman M, She QB, et al. Concurrent loss of the PTEN and RB1 tumor suppressors attenuates RAF dependence in melanomas harboring V600EBRAF. Oncogene. 2011;31(4):446-57.
145. Tsao H, Zhang X, Fowlkes K, al. e. Relative reciprocity of NRAS and PTEN-MMAC1 Alterations in Cutaneous Melanoma Cell Lines. Cancer Res. 2000;60:1800-4.
146. Wu H, Goel V, Haluska FG. PTEN signaling pathways in melanoma. Oncogene. 2003;22(20):3113-22.
147. Blouin M-J, Zhao Y, Zakikhani M, Algire C, Piura E, Pollak M. Loss of function of PTEN alters the relationship between glucose concentration and cell proliferation, increases glycolysis, and sensitizes cells to 2-deoxyglucose. Cancer Letters. 2010;289(2):246-53.
148. Madhunapantula SV, Robertson GP. The PTEN-AKT3 signaling cascade as a therapeutic target in melanoma. Pigment Cell & Melanoma Research. 2009;22(4):400-19.
149. Davies MA, Stemke-Hale K, Tellez C, Calderone TL, Deng W, Prieto VG, et al. A novel AKT3 mutation in melanoma tumours and cell lines. British Journal of Cancer. 2008;99(8):1265-8.
150. Cheung M, Sharma A, Madhunapantula SV, Robertson GP. Akt3 and Mutant V600E B-Raf Cooperate to Promote Early Melanoma Development. Cancer Research. 2008;68(9):3429-39.
151. Govindarajan B, Sligh JE, Vincent BJ, Li M, Canter JA, Nickoloff BJ, et al. Overexpression of Akt converts radial growth melanoma to vertical growth melanoma.
152. Tsao H, Chin L, Garraway LA, Fisher DE. Melanoma: from mutations to medicine. Genes & Development. 2012;26(11):1131-55.
153. Goldstein AM. Familial melanoma, pancreatic cancer and germline CDKN2A mutations. Hum Mutat. 2004;23(6):630.
154. Ryu B, Kim DS, Deluca AM, Alani RM. Comprehensive expression profiling of tumor cell lines identifies molecular signatures of melanoma progression. PLoS ONE. 2007;2(7):e594.
155. Willmore-Payne C, Holden JA, Tripp S, Layfield LJ. Human malignant melanoma: detection of BRAF- and c-kit–activating mutations by high-resolution amplicon melting analysis. Human Pathology. 2005;36(5):486-93.
156. Curtin JA, Busam K, Pinkel D, Bastian BC. Somatic Activation of KIT in Distinct Subtypes of Melanoma. Journal of Clinical Oncology. 2006;24(26):4340-6.
157. Kennedy C, ter Huurne J, Berkhout M, Gruis N, Bastiaens M, Bergman W, et al. Melanocortin 1 receptor (MC1R) gene variants are associated with an increased

risk for cutaneous melanoma which is largely independent of skin type and hair color. J Invest Dermatol. 2001;117(2):294-300.
158. Palmer JS, Duffy DL, Box NF, Aitken JF, O'Gorman LE, Green AC, et al. Melanocortin-1 receptor polymorphisms and risk of melanoma: is the association explained solely by pigmentation phenotype?
159. Garraway LA, Widlund HR, Rubin MA, Getz G, Berger AJ, Ramaswamy S, et al. Integrative genomic analyses identify MITF as a lineage survival oncogene amplified in malignant melanoma. Nature. 2005;436(7047):117-22.
160. Du J, Widlund HR, Horstmann MA, Ramaswamy S, Ross K, Huber WE, et al. Critical role of CDK2 for melanoma growth linked to its melanocyte-specific transcriptional regulation by MITF. Cancer Cell. 2004;6(6):565-76.
161. Busca R, Berra E, Gaggioli C, Khaled M, Bille K, Marchetti B, et al. Hypoxia-inducible factor 1{alpha} is a new target of microphthalmia-associated transcription factor (MITF) in melanoma cells. J Cell Biol. 2005;170(1):49-59. Epub 2005 Jun 27.
162. Hoek KS, Schlegel NC, Eichhoff OM, Widmer DS, Praetorius C, Einarsson SO, et al. Novel MITF targets identified using a two-step DNA microarray strategy. Pigment Cell Melanoma Res. 2008;21(6):665-76. doi: 10.1111/j.755-148X.2008.00505.x.
163. Chen B, Tardell C, Higgins B, Packman K, Boylan JF, Niu H. BRAFV600E negatively regulates the AKT pathway in melanoma cell lines. PLoS ONE. 2012;7(8):e42598.
164. Rimm DL, Caca K, Hu G, Harrison FB, Fearon ER. Frequent Nuclear/Cytoplasmic Localization of β-Catenin without Exon 3 Mutations in Malignant Melanoma. The American Journal of Pathology. 1999;154(2):325-9.
165. O'Connell MP, Weeraratna AT. Hear the Wnt Ror: how melanoma cells adjust to changes in Wnt. Pigment Cell & Melanoma Research. 2009;22(6):724-39.
166. Lucero OM, Dawson DW, Moon RT, Chien AJ. A Re-evaluation of the "Oncogenic" Nature of Wnt/β-catenin Signaling in Melanoma and Other Cancers. Current Oncology Reports. 2010;12(5):314-8.
167. Komiya Y, Habas R. Wnt signal transduction pathways. Organogenesis. 2008;4(2):68-75.
168. Clevers H. Wnt/beta-catenin signaling in development and disease. Cell. 2006;127(3):469-80.
169. Clevers H, Nusse R. Wnt/β-Catenin Signaling and Disease. Cell. 2012;149(6):1192-205.
170. Martinez Arias A. Wnts as morphogens? The view from the wing of Drosophila. Nature reviews Molecular cell biology. 2003;4(4):321-5.
171. Mikels AJ, Nusse R. Wnts as ligands: processing, secretion and reception. Oncogene. 2006;25(57):7461-8.
172. Coudreuse D, Korswagen HC. The making of Wnt: new insights into Wnt maturation, sorting and secretion. Development. 2007;134(1):3-12. Epub 2006 Nov 30.
173. Chien AJ, Conrad WH, Moon RT. A Wnt Survival Guide: From Flies to Human Disease. Journal of Investigative Dermatology. 2009;129(7):1614-27.
174. Schulte G, Bryja V. The Frizzled family of unconventional G-protein-coupled receptors. Trends Pharmacol Sci. 2007;28(10):518-25. Epub 2007 Sep 19.

175. Senior AE, Nadanaciva S, Weber J. The molecular mechanism of ATP synthesis by F1F0-ATP synthase. Biochim Biophys Acta. 2002;1553(3):188-211.
176. Janda CY, Waghray D, Levin AM, Thomas C, Garcia KC. Structural basis of Wnt recognition by Frizzled. Science. 2012;337(6090):59-64. doi: 10.1126/science.1222879. Epub 2012 May 31.
177. Moon RT, Kohn AD, Ferrari GVD, Kaykas A. WNT and [beta]-catenin signalling: diseases and therapies. Nat Rev Genet. 2004;5(9):691-701.
178. Chien AJ, Moon RT. WNTS and WNT receptors as therapeutic tools and targets in human disease processes. Front.12:448-57.
179. van Meurs JBJ, Trikalinos TA, Ralston SH, Balcells S, Brandi ML, Brixen K, et al. Large-Scale Analysis of Association Between LRP5 and LRP6 Variants and Osteoporosis. JAMA. 2008;299(11):1277-90. doi:10.001/jama.299.11..
180. Mani A, Radhakrishnan J, Wang H, Mani MA, Nelson-Williams C, Carew KS, et al. LRP6 mutation in a family with early coronary disease and metabolic risk factors. Science. 2007;315(5816):1278-82.
181. De Ferrari GV, Papassotiropoulos A, Biechele T, Wavrant De-Vrieze F, Avila ME, Major MB, et al. Common genetic variation within the Low-Density Lipoprotein Receptor-Related Protein 6 and late-onset Alzheimer's disease. Proc Natl Acad Sci U S A. 2007;104(22):9434-9. Epub 2007 May 21.
182. Grant SF, Thorleifsson G, Reynisdottir I, Benediktsson R, Manolescu A, Sainz J, et al. Variant of transcription factor 7-like 2 (TCF7L2) gene confers risk of type 2 diabetes. Nat Genet. 2006;38(3):320-3. Epub 2006 Jan 15.
183. Kanazawa A, Tsukada S, Sekine A, Tsunoda T, Takahashi A, Kashiwagi A, et al. Association of the gene encoding wingless-type mammary tumor virus integration-site family member 5B (WNT5B) with type 2 diabetes. Am J Hum Genet. 2004;75(5):832-43. Epub 2004 Sep 21.
184. Christodoulides C, Scarda A, Granzotto M, Milan G, Dalla Nora E, Keogh J, et al. WNT10B mutations in human obesity. Diabetologia. 2006;49(4):678-84. Epub 2006 Feb 14.
185. Benzing T, Simons M, Walz G. Wnt Signaling in Polycystic Kidney Disease. Journal of the American Society of Nephrology. 2007;18(5):1389-98.
186. Simons M, Mlodzik M. Planar Cell Polarity Signaling: From Fly Development to Human Disease. Annu Rev Genet. 2008;42:517.(doi).
187. Li B, Zhong L, Yang X, Andersson T, Huang M, Tang SJ. WNT5A Signaling Contributes to Aβ-Induced Neuroinflammation and Neurotoxicity. PLoS One. 2011;6(8):e22920.
188. Chocarro-Calvo A, García-Martínez Jose M, Ardila-González S, De la Vieja A, García-Jiménez C. Glucose-Induced β-Catenin Acetylation Enhances Wnt Signaling in Cancer. Molecular Cell. 2013;49(3):474-86.
189. An JH, Yang J-Y, Ahn BY, Cho SW, Jung JY, Cho HY, et al. Enhanced mitochondrial biogenesis contributes to Wnt induced osteoblastic differentiation of C3H10T1/2 cells. Bone. 2010;47(1):140-50.
190. Cadoret A, Ovejero C, Terris B, Souil E, Lévy L, Lamers WH, et al. New targets of b-catenin signaling in the liver are involved in the glutamine metabolism. Oncogene. 2002;21(54):8293-301.

191. Pate KT, Stringari C, Sprowl-Tanio S, Wang K, TeSlaa T, Hoverter NP, et al. Wnt signaling directs a metabolic program of glycolysis and angiogenesis in colon cancer. The EMBO Journal. 2014.
192. Liu H, Fergusson MM, Wu JJ, Rovira II, Liu J, Gavrilova O, et al. Wnt Signaling Regulates Hepatic Metabolism. Science Signaling. 2011;4(158):ra6-ra.
193. Lee SY, Jeon HM, Ju MK, Kim CH, Yoon G, Han SI, et al. Wnt/Snail Signaling Regulates Cytochrome c Oxidase and Glucose Metabolism. Cancer Research. 2012;72(14):3607-17.
194. Elstrom RL, Bauer DE, Buzzai M, Karnauskas R, Harris MH, Plas DR, et al. Akt stimulates aerobic glycolysis in cancer cells.
195. Sethi Jaswinder K, Vidal‐Puig A. Wnt signalling and the control of cellular metabolism. Biochemical Journal. 2010;427(1):1-17.
196. Sherwood V, Chaurasiya SK, Ekstrom EJ, Guilmain W, Liu Q, Koeck T, et al. WNT5A-mediated B-catenin-independent signalling is a novel regulator of cancer cell metabolism. Carcinogenesis. 2013.
197. Kikuchi A, Yamamoto H. Tumor formation due to abnormalities in the beta-catenin-independent pathway of Wnt signaling. Cancer Sci. 2008;99(2):202-8. doi: 10.1111/j.349-7006.2007.00675.x.
198. Katoh M. WNT/PCP signaling pathway and human cancer (review). Oncol Rep. 2005;14(6):1583-8.
199. Klemm F, Bleckmann A, Siam L, Chuang HN, Rietkotter E, Behme D, et al. beta-catenin-independent WNT signaling in basal-like breast cancer and brain metastasis. Carcinogenesis. 2011;32(3):434-42. doi: 10.1093/carcin/bgq269. Epub 2010 Dec 20.
200. Valenta T, Hausmann G, Basler K. The many faces and functions of beta-catenin. The EMBO Journal. 2012;31(12):2714-36.
201. MacDonald BT, Tamai K, He X. Wnt/beta-catenin signaling: components, mechanisms, and diseases. Developmental Cell. 2009;17(1):9-26.
202. Karim R, Tse G, Putti T, Scolyer R, Lee S. The significance of the Wnt pathway in the pathology of human cancers.
203. Chien AJ, Moore EC, Lonsdorf AS, Kulikauskas RM, Rothberg BG, Berger AJ, et al. Activated Wnt/B-catenin signaling in melanoma is associated with decreased proliferation in patient tumors and a murine melanoma model. Proceedings of the National Academy of Sciences. 2009;106(4):1193-8.
204. Katoh M, Katoh M. WNT Signaling Pathway and Stem Cell Signaling Network. Clinical Cancer Research. 2007;13(14):4042-5.
205. Niehrs C. The complex world of WNT receptor signalling. Nat Rev Mol Cell Biol. 2012;13(12):767-79. doi: 10.1038/nrm3470. Epub 2012 Nov 15.
206. MacDonald BT, He X. Frizzled and LRP5/6 receptors for Wnt/beta-catenin signaling. Cold Spring Harb Perspect Biol. 2012;4(12).(pii):a007880. doi: 10.1101/cshperspect.a.
207. Huelsken J. The Wnt signalling pathway. Journal of Cell Science. 2002;115(21):3977-8.
208. Akiyama T. Wnt bcatenin signaling.pdf. Cytokine and Growth Factor Reviews. 2000:273-82.

209. Cavallo RA, Cox RT, Moline MM, Roose J, Polevoy GA, Clevers H, et al. Drosophila Tcf and Groucho interact to repress Wingless signalling activity. Nature. 1998;395:604-8.
210. Arce L, Yokoyama NN, Waterman ML. Diversity of LEF/TCF action in development and disease. Oncogene. 2006;25(57):7492-504.
211. Brown JD, Moon RT. Wnt signaling: why is everything so negative? Current Opinion in Cell Biology. 1998;10:182-7.
212. Archbold HC, Yang YX, Chen L, Cadigan KM. How do they do Wnt they do?: regulation of transcription by the Wnt/beta-catenin pathway. Acta physiologica. 2012;204(1):74-109.
213. Cadigan KM, Waterman ML. TCF/LEFs and Wnt Signaling in the Nucleus. Cold Spring Harbor Perspectives in Biology. 2012;4(11).
214. Daniels DL, Weis WI. [beta]-catenin directly displaces Groucho/TLE repressors from Tcf/Lef in Wnt-mediated transcription activation. Nat Struct Mol Biol. 2005;12(4):364-71.
215. Yamamoto H, Kishida S, Kishida M, Ikeda S, Takada S, Kikuchi A. Phosphorylation of Axin, a Wnt Signal Negative Regulator, by Glycogen Synthase Kinase-3 Regulates Its Stability. Journal of Biological Chemistry. 1999;274(16):10681-4.
216. Fagotto F, Gluck U, Gumbiner BM. Nuclear localization signal-independent and importin/karyopherin-independent nuclear import of beta-catenin. Curr Biol. 1998;8(4):181-90.
217. Gordon MD, Nusse R. Wnt Signaling: Multiple Pathways, Multiple Receptors, and Multiple Transcription Factors. Journal of Biological Chemistry. 2006;281(32):22429-33.
218. Ishitani T, Ninomiya-Tsuji J, Matsumoto K. Regulation of Lymphoid Enhancer Factor 1/T-Cell Factor by Mitogen-Activated Protein Kinase-Related Nemo-Like Kinase-Dependent Phosphorylation in Wnt/β-Catenin Signaling. Molecular and Cellular Biology. 2003;23(4):1379-89.
219. Kioussi C, Briata P, Baek SH, Rose DW, Hamblet NS, Herman T, et al. Identification of a Wnt/Dvl/beta-Catenin --> Pitx2 pathway mediating cell-type-specific proliferation during development. Cell. 2002;111(5):673-85.
220. Olson LE, Tollkuhn J, Scafoglio C, Krones A, Zhang J, Ohgi KA, et al. Homeodomain-mediated beta-catenin-dependent switching events dictate cell-lineage determination. Cell. 2006;125(3):593-605.
221. Grossmann H, Yoo JH, Clancy J, Sorensen LK, Sedgwick A, Tong Z, et al. The Small GTPase ARF6 Stimulates β-Catenin Transcriptional Activity During WNT5A-Mediated Melanoma Invasion and Metastasis. Science Signalling. 2008;265(6).
222. Jenei V, Sherwood V, Howlin J, Linnskog R, Safholm A, Axelsson L, et al. A t-butyloxycarbonyl-modified Wnt5a-derived hexapeptide functions as a potent antagonist of Wnt5a-dependent melanoma cell invasion. Proc Natl Acad Sci U S A. 2009;106(46):19473-8.
223. Anastas JN, Kulikauskas RM, Tamir T, Rizos H, Long GV, von Euw EM, et al. WNT5A enhances resistance of melanoma cells to targeted BRAF inhibitors. The Journal of Clinical Investigation. 2014;124(7):2877-90.
224. De A. Wnt/Ca2+ signaling pathway: a brief overview. Acta Biochimica et Biophysica Sinica. 2011;43(10):745-56.

225. Kohn AD, Moon RT. Wnt and calcium signaling: beta-catenin-independent pathways. Cell Calcium. 2005;38(3-4):439-46.
226. Dissanayake SK, Weeraratna AT. Detecting PKC phosphorylation as part of the Wnt/calcium pathway in cutaneous melanoma. Methods Mol Biol. 2008;468:157-72.(doi).
227. Luna-Ulloa LB, Hernandez-Maqueda JG, Castaneda-Patlan MC, Robles-Flores M. Protein kinase C in Wnt signaling: implications in cancer initiation and progression. IUBMB Life. 2011;63(10):915-21. doi: 10.1002/iub.559. Epub 2011 Sep 9.
228. Dissanayake SK, Wade M, Johnson CE, O'Connell MP, Leotlela PD, French AD, et al. The Wnt5A/Protein Kinase C Pathway Mediates Motility in Melanoma Cells via the Inhibition of Metastasis Suppressors and Initiation of an Epithelial to Mesenchymal Transition. Journal of Biological Chemistry. 2007;282(23):17259-71.
229. Hutchins BI, Li L, Kalil K. Wnt/calcium signaling mediates axon growth and guidance in the developing corpus callosum. Dev Neurobiol. 2011;71(4):269-83. doi: 10.1002/dneu.20846.
230. George SJ. Wnt pathway: a new role in regulation of inflammation. Arterioscler Thromb Vasc Biol. 2008;28(3):400-2. doi: 10.1161/ATVBAHA.107.160952.
231. Couchonnal LF, Anderson ME. The role of calmodulin kinase II in myocardial physiology and disease. Physiology (Bethesda). 2008;23:151-9.(doi):10.1152/physiol.00043.2007.
232. Malinauskas T, Aricescu AR, Lu W, Siebold C, Jones EY. Modular mechanism of Wnt signaling inhibition by Wnt inhibitory factor 1. Nat Struct Mol Biol.18(8):886-93. doi:10.1038/nsmb.2081.
233. Logan CY, Nusse R. The Wnt signaling pathway in development and disease. Annu Rev Cell Dev Biol. 2004;20:781-810.
234. Kawano Y, Kypta R. Secreted antagonists of the Wnt signalling pathway. Journal of Cell Science. 2003;116(Pt 13):2627-34.
235. Mori H. Secreted frizzled-related protein 5 suppresses adipocyte mitochondrial metabolism through WNT inhibition. The Journal of Clinical Investigation. 2012;122(7).
236. Fedi P, Bafico A, Soria AN, Burgess WH, Miki T, Bottaro DP, et al. Isolation and Biochemical Characterization of the Human Dkk-1 Homologue, a Novel Inhibitor of Mammalian Wnt Signaling. Journal of Biological Chemistry. 1999;274(27):19465-72.
237. Cruciat CM, Niehrs C. Secreted and transmembrane wnt inhibitors and activators. Cold Spring Harb Perspect Biol. 2013;5(3):a015081. doi: 10.1101/cshperspect.a.
238. Cereghetti GM, Scorrano L. The many shapes of mitochondrial death. Oncogene. 2006;25(34):4717-24.
239. Zhao J, Zhang J, Yu M, Xie Y, Huang Y, Wolff DW, et al. Mitochondrial dynamics regulates migration and invasion of breast cancer cells. Oncogene. 2013;32(40):4814-24.
240. Carew JS, Huang P. Mitochondrial defects in cancer. Molecular Cancer. 2002.
241. Theodosakis N, Micevic G, Kelly DP, Bosenberg M. Mitochondrial function in melanoma. Archives of Biochemistry and Biophysics. 2014;563(0):56-9.
242. Nunnari J, Suomalainen A. Mitochondria: In Sickness and in Health. Cell. 2012;148(6):1145-59.

243. Palade GE. An electron microscope study of the mitochondrial structure. J Histochem Cytochem. 1953;1(4):188-211.
244. Anesti V, Scorrano L. The relationship between mitochondrial shape and function and the cytoskeleton. Biochim Biophys Acta. 2006;1757(5-6):692-9. Epub 2006 Apr 19.
245. Legros F. Mitochondrial Fusion in Human Cells Is Efficient, Requires the Inner Membrane Potential, and Is Mediated by Mitofusins. Molecular Biology of the Cell. 2002;13(12):4343-54.
246. Matsui Y, Kitade H, Kamiya T, Kanemaki T, Hiramatsu Y, Okumura T, et al. Adenylate energy charge of rat and human cultured hepatocytes. In Vitro Cell Dev Biol Anim. 1994;30A(9):609-14.
247. Zhang ZW, Cheng J, Xu F, Chen YE, Du JB, Yuan M, et al. Red blood cell extrudes nucleus and mitochondria against oxidative stress. IUBMB Life. 2011;63(7):560-5. doi: 10.1002/iub.490.
248. Searcy DG. Metabolic integration during the evolutionary origin of mitochondria. Cell Res. 2003;13(4):229-38.
249. Pellegrini L, Scorrano L. A cut short to death: Parl and Opa1 in the regulation of mitochondrial morphology and apoptosis. Cell Death and Differentiation. 2007;14(7):1275-84.
250. CK M, KE vH. Biochemistry 2/E: Menlo Park, Ca. Benjamin/Cummings 1996.; 1996.
251. Hoppins S, Lackner L, Nunnari J. The machines that divide and fuse mitochondria. Annu Rev Biochem. 2007;76:751-80.
252. Campello S, Scorrano L. Mitochondrial shape changes: orchestrating cell pathophysiology. EMBO Rep. 2010;11(9):678-84. Epub 2010 Aug 20.
253. Shoshan-Barmatz V, De Pinto V, Zweckstetter M, Raviv Z, Keinan N, Arbel N. VDAC, a multi-functional mitochondrial protein regulating cell life and death. Mol Aspects Med. 2010;31(3):227-85. doi: 10.1016/j.mam.2010.03.002. Epub Mar 23.
254. Schatz G. The Protein Import System of Mitochondria. Journal of Biological Chemistry. 1996;271(50):31763-6.
255. Frey TG, Mannella CA. The internal structure of mitochondria. Trends Biochem Sci. 2000;25(7):319-24.
256. Zick M, Rabl R, Reichert AS. Cristae formation-linking ultrastructure and function of mitochondria. Biochim Biophys Acta. 2009;1793(1):5-19.
257. Zheng J. Energy metabolism of cancer: Glycolysis versus oxidative phosphorylation (Review). Oncol Lett. 2012;4(6):1151-7.
258. Cogliati S, Frezza C, Soriano Maria E, Varanita T, Quintana-Cabrera R, Corrado M, et al. Mitochondrial Cristae Shape Determines Respiratory Chain Supercomplexes Assembly and Respiratory Efficiency. Cell. 2013;155(1):160-71.
259. Hackenbrock CR. ULTRASTRUCTURAL BASES FOR METABOLICALLY LINKED MECHANICAL ACTIVITY IN MITOCHONDRIA : I. Reversible Ultrastructural Changes with Change in Metabolic Steady State in Isolated Liver Mitochondria: J Cell Biol. 1966 Aug 1;30(2):269-97.
260. Frezza C, Cipolat S, Martins de Brito O, Micaroni M, Beznoussenko GV, Rudka T, et al. OPA1 Controls Apoptotic Cristae Remodeling Independently from Mitochondrial Fusion. Cell. 2006;126(1):177-89.

261. Pearce S, Nezich CL, Spinazzola A. Mitochondrial diseases: translation matters. Mol Cell Neurosci. 2013;55:1-12.
262. Falkenberg M, Larsson NG, Gustafsson CM. DNA replication and transcription in mammalian mitochondria. Annu Rev Biochem. 2007;76:679-99.
263. Iborra FJ, Kimura H, Cook PR. The functional organization of mitochondrial genomes in human cells. BMC Biol. 2004;2:9.(doi).
264. Christian BE, Spremulli LL. Mechanism of Protein Biosynthesis in Mammalian Mitochondria: Biochim Biophys Acta. 2012 Sep;1819(9-10):1035-54.; 2011.
265. Alirol E, Martinou JC. Mitochondria and cancer: is there a morphological connection? Oncogene. 2006;25(34):4706-16.
266. Karbowski M, Norris KL, Cleland MM, Jeong S-Y, Youle RJ. Role of Bax and Bak in mitochondrial morphogenesis. Nature. 2006;443(7112):658-62.
267. Youle RJ, Strasser A. The BCL-2 protein family: opposing activities that mediate cell death. Nature reviews Molecular cell biology. 2008;9(1):47-59.
268. Roskoski R. Bioenergetics 3: Nicholls, David G., and Ferguson, Stuart J. Biochemistry and Molecular Biology Education. 2003;31(3):215-6.
269. Gogvadze V, Orrenius S, Zhivotovsky B. Multiple pathways of cytochrome c release from mitochondria in apoptosis. Biochimica et Biophysica Acta (BBA) - Bioenergetics. 2006;1757(5–6):639-47.
270. Gao W, Pu Y, Luo KQ, Chang DC. Temporal relationship between cytochrome c release and mitochondrial swelling during UV induced apoptosis in living HeLa cells. Journal of Cell Science. 2001;114:2855-62.
271. Goodsell DS. The Molecular Perspective: Cytochrome c and Apoptosis. The Oncologist. 2004;9(2):226-7.
272. Karbowski M, Lee Y-J, Gaume B, Jeong S-Y, Frank S, Nechushtan A, et al. Spatial and temporal association of Bax with mitochondrial fission sites, Drp1, and Mfn2 during apoptosis. The Journal of Cell Biology. 2002;159(6):931-8.
273. Liesa M, Palaci´N M, Zorzano A. Mitochondrial Dynamics in Mammalian Health and Disease. Physiol Rev. 2009;89:799-845.
274. Horowitz MP, Greenamyre JT. Mitochondrial iron metabolism and its role in neurodegeneration. J Alzheimers Dis. 2010;20(Suppl 2):S551-68. doi: 10.3233/JAD-2010-100354.
275. L. ND, M. CM. *Lehninger principles of biochemistry* (4th ed.). 4th Edition ed. New York, New York: W.H. Freeman; 2005.
276. Vander Heiden MG, Cantley LC, Thompson CB. Understanding the Warburg Effect: The Metabolic Requirements of Cell Proliferation. Science. 2009;324(5930):1029-33.
277. Chen J-Q, Russo J. Dysregulation of glucose transport, glycolysis, TCA cycle and glutaminolysis by oncogenes and tumor suppressors in cancer cells. Biochimica et Biophysica Acta (BBA) - Reviews on Cancer. 2012;1826(2):370-84.
278. Hirschhaeuser F, Sattler UGA, Mueller-Klieser W. Lactate: A Metabolic Key Player in Cancer. Cancer Research. 2011;71(22):6921-5.
279. Kruger NJ, von Schaewen A. The oxidative pentose phosphate pathway: structure and organisation. Curr Opin Plant Biol. 2003;6(3):236-46.
280. Qu W, Oya S, Lieberman BP, Ploessl K, Wang L, Wise DR, et al. Preparation and Characterization of l-[5-11C]-Glutamine for Metabolic Imaging of Tumors. Journal of Nuclear Medicine. 2012;53(1):98-105.

281. Filipp FV, Ratnikov B, De Ingeniis J, Smith JW, Osterman AL, Scott DA. Glutamine-fueled mitochondrial metabolism is decoupled from glycolysis in melanoma. Pigment Cell & Melanoma Research. 2012;25(6):732-9.
282. DeBerardinis RJ, Mancuso A, Daikhin E, Nissim I, Yudkoff M, Wehrli S, et al. Beyond aerobic glycolysis: Transformed cells can engage in glutamine metabolism that exceeds the requirement for protein and nucleotide synthesis. Proc Natl Acad Sci U S A. 2007;104(49):19345-50. Epub 2007 Nov 21.
283. Filipp FV, Scott DA, Ronai ZA, Osterman AL, Smith JW. Reverse TCA cycle flux through isocitrate dehydrogenases 1 and 2 is required for lipogenesis in hypoxic melanoma cells. Pigment Cell Melanoma Res. 2012;25(3):375-83.
284. Scott DA, Richardson AD, Filipp FV, Knutzen CA, Chiang GG, Ronai ZA, et al. Comparative Metabolic Flux Profiling of Melanoma Cell Lines: BEYOND THE WARBURG EFFECT. Journal of Biological Chemistry. 2011;286(49):42626-34.
285. Brandt U. Energy converting NADH:quinone oxidoreductase (complex I). Annu Rev Biochem. 2006;75:69-92.
286. Oyedotun KS, Lemire BD. The quaternary structure of the Saccharomyces cerevisiae succinate dehydrogenase. Homology modeling, cofactor docking, and molecular dynamics simulation studies. J Biol Chem. 2004;279(10):9424-31. Epub 2003 Dec 12.
287. Rieske JS. Composition, structure, and function of complex III of the respiratory chain. Biochim Biophys Acta. 1976;456(2):195-247.
288. Klionsky DJ, Abdalla FC, Abeliovich H, Abraham RT, Acevedo-Arozena A, Adeli K, et al. Guidelines for the use and interpretation of assays for monitoring autophagy. Autophagy. 2012;8(4):445-544.
289. Capaldi RA. Structure and function of cytochrome c oxidase. Annu Rev Biochem. 1990;59:569-96.
290. Boyer PD. The ATP synthase--a splendid molecular machine. Annu Rev Biochem. 1997;66:717-49.
291. Mattenberger Y, James DI, Martinou J-C. Fusion of mitochondria in mammalian cells is dependent on the mitochondrial inner membrane potential and independent of microtubules or actin. FEBS Letters. 2003;538(1–3):53-9.
292. Cui H, Kong Y, Zhang H. Oxidative stress, mitochondrial dysfunction, and aging. J Signal Transduct. 2012;646354(10):2.
293. Dimauro S, Davidzon G. Mitochondrial DNA and disease. Ann Med. 2005;37(3):222-32.
294. Seyfried TN, Shelton LM. Cancer as a metabolic disease. Nutrition & Metabolism. 2010;7:7-.
295. Seyfried TN, Flores RE, Poff AM, D'Agostino DP. Cancer as a metabolic disease: implications for novel therapeutics. Carcinogenesis. 2013.
296. Park CB, Larsson N-G. Mitochondrial DNA mutations in disease and aging. The Journal of Cell Biology. 2011;193(5):809-18.
297. Johns DR. Seminars in medicine of the Beth Israel Hospital, Boston. Mitochondrial DNA and disease. N Engl J Med. 1995;333(10):638-44.
298. Mattson MP, Gleichmann M, Cheng A. Mitochondria in Neuroplasticity and Neurological Disorders. Neuron. 2008;60(5):748-66.

299. Hashimoto M, Rockenstein E, Crews L, Masliah E. Role of protein aggregation in mitochondrial dysfunction and neurodegeneration in Alzheimer's and Parkinson's diseases. Neuromolecular Med. 2003;4(1-2):21-36.
300. Lin MT, Beal MF. Mitochondrial dysfunction and oxidative stress in neurodegenerative diseases. Nature. 2006;443(7113):787-95.
301. Gaude E, Frezza C. Defects in mitochondrial metabolism and cancer. Cancer Metab. 2014;2(10).
302. Schlichtholz B, Turyn J, Goyke E, Biernacki M, Jaskiewicz K, Sledzinski Z, et al. Enhanced citrate synthase activity in human pancreatic cancer. Pancreas. 2005;30(2):99-104.
303. Simonnet H, Alazard N, Pfeiffer K, Gallou C, Beroud C, Demont J, et al. Low mitochondrial respiratory chain content correlates with tumor aggressiveness in renal cell carcinoma. Carcinogenesis. 2002;23(5):759-68.
304. Lin CC, Cheng TL, Tsai WH, Tsai HJ, Hu KH, Chang HC, et al. Loss of the respiratory enzyme citrate synthase directly links the Warburg effect to tumor malignancy. Scientific Reports. 2012;2:785.
305. Wang P, Mai C, Wei YL, Zhao JJ, Hu YM, Zeng ZL, et al. Decreased expression of the mitochondrial metabolic enzyme aconitase (ACO2) is associated with poor prognosis in gastric cancer. Med Oncol. 2013;30(2):552. Epub 2013 Apr 2.
306. Kavanagh JP. Sodium, potassium, calcium, magnesium, zinc, citrate and chloride content of human prostatic and seminal fluid. J Reprod Fertil. 1985;75(1):35-41.
307. Parsons DW, Jones S, Zhang X, Lin JC, Leary RJ, Angenendt P, et al. An integrated genomic analysis of human glioblastoma multiforme. Science. 2008;321(5897):1807-12. doi: 10.126/science.1164382. Epub 2008 Sep 4.
308. Mardis ER, Ding L, Dooling DJ, Larson DE, McLellan MD, Chen K, et al. Recurring mutations found by sequencing an acute myeloid leukemia genome. N Engl J Med. 2009;361(11):1058-66. doi: 10.6/NEJMoa0903840. Epub 2009 Aug 5.
309. Kang MR, Kim MS, Oh JE, Kim YR, Song SY, Seo SI, et al. Mutational analysis of IDH1 codon 132 in glioblastomas and other common cancers. Int J Cancer. 2009;125(2):353-5. doi: 10.1002/ijc.24379.
310. Ricketts C, Woodward ER, Killick P, Morris MR, Astuti D, Latif F, et al. Germline SDHB mutations and familial renal cell carcinoma. J Natl Cancer Inst. 2008;100(17):1260-2. doi: 10.093/jnci/djn254. Epub 2008 Aug 26.
311. Kim S, Kim do H, Jung WH, Koo JS. Succinate dehydrogenase expression in breast cancer. Springerplus. 2013;2(1):299.
312. Janeway KA, Kim SY, Lodish M, Nose V, Rustin P, Gaal J, et al. Defects in succinate dehydrogenase in gastrointestinal stromal tumors lacking KIT and PDGFRA mutations. Proc Natl Acad Sci U S A. 2011;108(1):314-8. doi: 10.1073/pnas.1009199108. Epub 2010 Dec 20.
313. Khalil AA. Biomarker discovery: a proteomic approach for brain cancer profiling. Cancer Sci. 2007;98(2):201-13.
314. Fieuw A, Kumps C, Schramm A, Pattyn F, Menten B, Antonacci F, et al. Identification of a novel recurrent 1q42.2-1qter deletion in high risk MYCN single copy 11q deleted neuroblastomas. Int J Cancer. 2012;130(11):2599-606. doi: 10.1002/ijc.26317. Epub 2011 Aug 29.

315. Tomlinson IP, Alam NA, Rowan AJ, Barclay E, Jaeger EE, Kelsell D, et al. Germline mutations in FH predispose to dominantly inherited uterine fibroids, skin leiomyomata and papillary renal cell cancer. Nat Genet. 2002;30(4):406-10. Epub 2002 Feb 25.
316. Hansford RG, Lehninger AL. Active oxidative decarboxylation of malate by mitochondria isolated from L-1210 ascites tumor cells. Biochem Biophys Res Commun. 1973;51(2):480-6.
317. Ren JG, Seth P, Everett P, Clish CB, Sukhatme VP. Induction of erythroid differentiation in human erythroleukemia cells by depletion of malic enzyme 2. PLoS One. 2010;5(9).(pii):e12520. doi: 10.1371/journal.pone.0012520.
318. Kroemer G. Mitochondria in cancer. Oncogene. 2006;25(34):4630-2.
319. Cairns RA, Harris IS, Mak TW. Regulation of cancer cell metabolism. Nature reviews Cancer. 2011;11(2):85-95.
320. Dakubo G. Mitochondrial Genetic and cancer: Springer; 2010.
321. Gatenby RA, Gillies RJ. Why do cancers have high aerobic glycolysis? Nat Rev Cancer. 2004;4(11):891-9.
322. Yang L, Moss T, Mangala LS, Marini J, Zhao H, Wahlig S, et al. Metabolic shifts toward glutamine regulate tumor growth, invasion and bioenergetics in ovarian cancer. Molecular Systems Biology. 2014;10(5):728-.
323. Daye D, Wellen KE. Metabolic reprogramming in cancer: Unraveling the role of glutamine in tumorigenesis. Seminars in Cell & Developmental Biology. 2012;23(4):362-9.
324. Patra KC, Hay N. The pentose phosphate pathway and cancer. Trends Biochem Sci. 2014;39(8):347-54. doi: 10.1016/j.tibs.2014.06.005. Epub Jul 15.
325. Duvel K, Yecies JL, Menon S, Raman P, Lipovsky AI, Souza AL, et al. Activation of a metabolic gene regulatory network downstream of mTOR complex 1. Mol Cell. 2010;39(2):171-83. doi: 10.1016/j.molcel.2010.06.022.
326. Ying H, Kimmelman AC, Lyssiotis CA, Hua S, Chu GC, Fletcher-Sananikone E, et al. Oncogenic Kras maintains pancreatic tumors through regulation of anabolic glucose metabolism. Cell. 2012;149(3):656-70. doi: 10.1016/j.cell.2012.01.058.
327. Santos CR, Schulze A. Lipid metabolism in cancer. FEBS J. 2012;279(15):2610-23.
328. Elf SE, Chen J. Targeting glucose metabolism in patients with cancer. Cancer. 2014;120(6):774-80.
329. Tennant DA, Durán RV, Gottlieb E. Targeting metabolic transformation for cancer therapy. Nature Reviews Cancer. 2010;10(4):267-77.
330. Freshney RI, editor. Basic Principles of cell culture: Wiley-Liss; 2000.
331. van Kuppeveld FJ, Johansson KE, Galama JM, Kissing J, Bölske G, Hjelm E, et al. 16S rRNA based polymerase chain reaction compared with culture and serological methods for diagnosis of mycoplasma pneumoniae infection.pdf. European Journal of Clinical Microbiology & Infectious Diseases. 1994;13(5):5.
332. van Kuppeveld FJ, van der Logt JT, Angulo AF, van Zoest MJ, Quint WG, Niesters HG, et al. Genus- and species-specific identification of mycoplasmas by 16S rRNA amplification. Applied and Environmental Microbiology. 1992;58(8):2606-15.
333. Louis K, Siegel A. Cell Viability Analysis Using Trypan Blue: Manual and Automated Methods. In: Stoddart MJ, editor. Mammalian Cell Viability. Methods in Molecular Biology. 740: Humana Press; 2011. p. 7-12.

334. Zipser MC, Eichhoff OM, Widmer DS, Schlegel NC, Schoenewolf NL, Stuart D, et al. A proliferative melanoma cell phenotype is responsive to RAF/MEK inhibition independent of BRAF mutation status. Pigment Cell & Melanoma Research. 2011;24(2):326-33.
335. Divieto C, Revel L, Sassi G, Sassi MP. Uncertainty analysis of cell counting by metabolic assays. Journal of Physics: Conference Series. 2013;459:012051.
336. Grun B, Benjamin E, Sinclair J, Timms JF, Jacobs IJ, Gayther SA, et al. Three-dimensional in vitro cell biology models of ovarian and endometrial cancer. Cell Proliferation. 2009;42(2):219-28.
337. Hotchin NA, Ekström EJ, Sherwood V, Andersson T. Methylation and Loss of Secreted Frizzled-Related Protein 3 Enhances Melanoma Cell Migration and Invasion. PLoS ONE. 2011;6(4):e18674.
338. Safholm A, Leandersson K, Dejmek J, Nielsen CK, Villoutreix BO, Andersson T. A formylated hexapeptide ligand mimics the ability of Wnt-5a to impair migration of human breast epithelial cells. The Journal of biological chemistry. 2006;281(5):2740-9.
339. Lawrenson K, Benjamin E, Turmaine M, Jacobs I, Gayther S, Dafou D. In vitro three-dimensional modelling of human ovarian surface epithelial cells. Cell Proliferation. 2009;42(3):385-93.
340. Vinci M, Gowan S, Boxall F, Patterson L, Zimmermann M, Court W, et al. Advances in establishment and analysis of three-dimensional tumor spheroid-based functional assays for target validation and drug evaluation. BMC Biol. 2012;10:29.
341. Wang G, Li X, Huang F, Zhao J, Ding H, Cunningham C, et al. Antitumor effect of beta-elemene in non-small-cell lung cancer cells is mediated via induction of cell cycle arrest and apoptotic cell death. Cell Mol Life Sci. 2005;62(7-8):881-93.
342. Thomas P, Bagrij T, Campos-Toimil M, Edwardson JM. Mitochondria play a critical role in shaping the exocytotic response of rat pancreatic acinar cells. Cell Calcium. 2006;39(1):57-63.
343. Vincan E. Wnt Signalling; chapter 8; Assaying B-catenin-TCF Transscription with Bcatenin-TCF Transcription Based Reporter Constructs. 2008.
344. Korinek V. Constitutive Transcriptional Activation by a beta -Catenin-Tcf Complex in APC-/- Colon Carcinoma. Science. 1997;275(5307):1784-7.
345. Deb J, Majumder J, Bhattacharyya S, Jana SS. A novel naproxen derivative capable of displaying anti-cancer and anti-migratory properties against human breast cancer cells. BMC Cancer. 2014;14.
346. McClatchey AI. Modeling metastasis in the mouse. Oncogene. 1999;18:5334-9.
347. Bustos RI, Jensen EL, Ruiz LM, Rivera S, Ruiz S, Simon F, et al. Copper deficiency alters cell bioenergetics and induces mitochondrial fusion through up-regulation of MFN2 and OPA1 in erythropoietic cells. Biochemical and Biophysical Research Communications. 2013;437(3):426-32.
348. Wu M, Neilson A, Swift AL, Moran R, Tamagnine J, Parslow D, et al. Multiparameter metabolic analysis reveals a close link between attenuated mitochondrial bioenergetic function and enhanced glycolysis dependency in human tumor cells. Am J Physiol Cell Physiol. 2007;292:C125–C36.

349. Mathieu J, Zhou W, Xing Y, Sperber H, Ferreccio A, Agoston Z, et al. Hypoxia-inducible factors have distinct and stage-specific roles during reprogramming of human cells to pluripotency. Cell Stem Cell. 2014;14(5):592-605.
350. Zimmerman ZF, Kulikauskas RM, Bomsztyk K, Moon RT, Chien AJ. Activation of Wnt/beta-catenin signaling increases apoptosis in melanoma cells treated with trail. PLoS One. 2013;8(7):e69593.
351. Conrad W, Major M, Cleary M, Ferrer M, Roberts B, Marine S, et al. FAM129B is a novel regulator of Wnt/β-catenin signal transduction in melanoma cells. F1000 Research. 2013;2(134).
352. Nelson J, Denisenko O, Bomsztyk K. The fast chromatin immunoprecipitation method. Methods in molecular biology. 2009;567:45-57.
353. Biechele TL, Kulikauskas RM, Toroni RA, Lucero OM, Swift RD, James RG, et al. Wnt/B-Catenin Signaling and AXIN1 Regulate Apoptosis Triggered by Inhibition of the Mutant Kinase BRAFV600E in Human Melanoma. Science Signaling. 2012;5(206):ra3-ra.
354. Bonifacino JS, Dell'Angelica, E. C. and Springer, T. A, editor. Immunoprecipitation: Wiley; 2001.
355. Luber CA, Cox J, Lauterbach H, Fancke B, Selbach M, Tschopp J, et al. Quantitative proteomics reveals subset-specific viral recognition in dendritic cells. Immunity. 2010;32(2):279-89.
356. Rosenberg IM, editor. Protein Analysis and Purification: Benchtop Techniques. 2 ed: Birkhauser Verlag; 2004.
357. Visvader JE, Lindeman GJ. Cancer stem cells in solid tumours: accumulating evidence and unresolved questions. Nat Rev Cancer. 2008;8(10):755-68.
358. Yancovitz M, Litterman A, Yoon J, Ng E, Shapiro RL, Berman RS, et al. Intra- and Inter-Tumor Heterogeneity of BRAF Mutations in Primary and Metastatic Melanoma. PLoS ONE. 2012;7(1).
359. Hoek KS, Goding CR. Cancer stem cells versus phenotype-switching in melanoma. Pigment Cell & Melanoma Research. 2010;23(6):746-59.
360. Porta C. Cancer Stem Cells: Lessons From Melanoma. Stem Cell Reviews and Reports. 2008;5(1):61-5.
361. Eichhoff OM, Weeraratna A, Zipser MC, Denat L, Widmer DS, Xu M, et al. Differential LEF1 and TCF4 expression is involved in melanoma cell phenotype switching. Pigment Cell & Melanoma Research. 2011;24(4):631-42.
362. Quintana E, Shackleton M, Sabel MS, Fullen DR, Johnson TM, Morrison SJ. Efficient tumour formation by single human melanoma cells. Nature. 2008;456(7222):593-8.
363. Perego M, Tortoreto M, Tragni G, Mariani L, Deho P, Carbone A, et al. Heterogeneous Phenotype of Human Melanoma Cells with In Vitro and In Vivo Features of Tumor-Initiating Cells. Journal of Investigative Dermatology. 2010;130(7):1877-86.
364. Schatton T, Murphy GF, Frank NY, Yamaura K, Waaga-Gasser AM, Gasser M, et al. Identification of cells initiating human melanomas. Nature. 2008;451(7176):345-9.
365. Hoek KS, Eichhoff OM, Schlegel NC, Dobbeling U, Kobert N, Schaerer L, et al. In vivo Switching of Human Melanoma Cells between Proliferative and Invasive States. Cancer Research. 2008;68(3):650-6.

366. Girouard SD, Murphy GF. Melanoma stem cells: not rare, but well done. Laboratory Investigation. 2011;91(5):647-64.
367. Klein WM, Wu BP, Zhao S, Wu H, Klein-Szanto AJP, Tahan SR. Increased expression of stem cell markers in malignant melanoma. Modern Pathology. 2006;20(1):102-7.
368. Dou J. Isolation and identification of cancer stem-like cells from murine melanoma cell lines. Cellular and Molecular Immunology. 2007.
369. Roesch A, Fukunaga-Kalabis M, Schmidt EC, Zabierowski SE, Brafford PA, Vultur A, et al. A Temporarily Distinct Subpopulation of Slow-Cycling Melanoma Cells Is Required for Continuous Tumor Growth. Cell. 2010;141(4):583-94.
370. Fang D. A Tumorigenic Subpopulation with Stem Cell Properties in Melanomas. Cancer Research. 2005;65(20):9328-37.
371. Sáez-Ayala M, Montenegro María F, Rodríguez-López José N, amp, amp. Directed Phenotype Switching as an Effective Antimelanoma Strategy. Cancer Cell. 2013;24(1):105-19.
372. Enderling H. Cancer stem cells and tumor dormancy. Adv Exp Med Biol. 2013;734:55-71.
373. Lapidot T. A Cell initiating human acute myeloid leukaemia after transplantation into SCID mice.pdf. Nature. 1994;367:645-8.
374. Dick JE. Breast cancer stem cells revealed. Proceedings of the National Academy of Sciences. 2003;100(7):3547-9.
375. Al-Hajj M. From the Cover: Prospective identification of tumorigenic breast cancer cells. Proceedings of the National Academy of Sciences. 2003;100(7):3983-8.
376. Clarke MF, Dick JE, Dirks PB, Eaves CJ, Jamieson CHM, Jones DL, et al. Cancer Stem Cells--Perspectives on Current Status and Future Directions: AACR Workshop on Cancer Stem Cells. Cancer Research. 2006;66(19):9339-44.
377. Hanahan D. The hallmarks of cancer 2000.pdf. Cell. 2000;100:57-70.
378. Yang S WX, Contino G, et al. Pancreatic cancers require autophagy for tumor growth. *Genes & Develop*ment 2011, doi:10.1101/gad.2016111. -.
379. O'Brien CA, Kreso A, Jamieson CHM. Cancer Stem Cells and Self-renewal. Clinical Cancer Research. 2010;16(12):3113-20.
380. La Porta CA, Zapperi S. Human breast and melanoma cancer stem cells biomarkers. Cancer Letters. 2013;338(1):69-73.
381. Medema JP. Cancer stem cells: The challenges ahead. Nat Cell Biol. 2013;15(4):338-44.
382. Smalley KSM. Life isn't flat; taking cancer biology to the next dimension. In Vitro Cell Dev Biol. 2006;42:5.
383. Guzman ML, Rossi RM, Karnischky L, Li X, Peterson DR, Howard DS, et al. The sesquiterpene lactone parthenolide induces apoptosis of human acute myelogenous leukemia stem and progenitor cells. Blood. 2005;105(11):4163-9.
384. Arozarena I, Bischof H, Gilby D, Belloni B, Dummer R, Wellbrock C. In melanoma, beta-catenin is a suppressor of invasion. Oncogene. 2011;30(45):4531-43.
385. Hoek KS, Schlegel NC, Brafford P, Sucker A, Ugurel S, Kumar R, et al. Metastatic potential of melanomas defined by specific gene expression profiles with no BRAF signature. Pigment Cell Research. 2006;19(4):290-302.

386. SAITO H. MITF in the wnt signalling pathway. Pigment Cell Research. 2003;16:4.
387. Eastman Q, Grosschedl R. Regulation of LEF-1/TCF transcription factors by Wnt and other signals. Current Opinion in Cell Biology. 1999;11(2):233-40.
388. O'Connell MP, Marchbank K, Webster MR, Valiga AA, Kaur A, Vultur A, et al. Hypoxia Induces Phenotypic Plasticity and Therapy Resistance in Melanoma via the Tyrosine Kinase Receptors ROR1 and ROR2. Cancer Discovery. 2013;3(12):1378-93.
389. Takahashi-Yanaga F, Kahn M. Targeting Wnt Signaling: Can We Safely Eradicate Cancer Stem Cells? Clinical Cancer Research. 2010;16(12):3153-62.
390. Reya T, Clevers H. Wnt signalling in stem cells and cancer. Nature. 2005;434(7035):843-50.
391. Taipale J, Beachy PA. The Hedgehog and Wnt signalling pathways in cancer. Nature. 2001;411(6835):349-54.
392. Reya T, Morrison SJ, Clarke MF, Weissman IL. Stem cells, cancer, and cancer stem cells. Nature. 2001;414(6859):105-11.
393. Izrailit J, Reedijk M. Developmental pathways in breast cancer and breast tumor-initiating cells: Therapeutic implications. Cancer Letters. 2012;317(2):115-26.
394. Hartman ML, Talar B, Noman MZ, Gajos-Michniewicz A, Chouaib S, Czyz M. Gene expression profiling identifies microphthalmia-associated transcription factor (MITF) and Dickkopf-1 (DKK1) as regulators of microenvironment-driven alterations in melanoma phenotype. PLoS ONE. 2014;9(4):e95157.
395. S. BM, Patricia V, Michael F. BRAF and Ras mutations in lung cancer and melanoma. Cancer Res. 2002;62:6997-7000.
396. Giuliano S, Cheli Y, Ohanna M, Bonet C, Beuret L, Bille K, et al. Microphthalmia-Associated Transcription Factor Controls the DNA Damage Response and a Lineage-Specific Senescence Program in Melanomas. Cancer Research. 2010;70(9):3813-22.
397. Tap WD. Pharmacodynamic Characterization of the Efficacy Signals Due to Selective BRAF Inhibition with PLX4032 in Malignant Melanoma. Neoplasia. 2010;12(8):18.
398. ŠVEC J. VESELOVSKÁ Z. KESZEGHOVÁ V. MAŤOŠKA J. MARCHETTI A. SQUARTIXI1 F. Biological and immunological properties of the 1П1В-2 human melanoma cell line. Neoplasma. 1988;35(6):665-81.
399. Søndergaard JN, Nazarian R, Wang Q, Guo D, Hsueh T, Mok S, et al. Differential sensitivity of melanoma cell lines with BRAFV600E mutation to the specific Raf inhibitor PLX4032. Journal of Translational Medicine. 2010;8(1):39.
400. Euw Ev, Atefi M, Attar N, Chu C, Zachariah S, Burgess BL, et al. Antitumor effects of the investigational selective MEK inhibitor TAK733 against cutaneous and uveal melanoma cell lines. Molecular Cancer. 2012;11(22):9.
401. Joseph EW, Pratilas CA, Poulikakos PI, Tadi M, Wang W, Taylor BS, et al. The RAF inhibitor PLX4032 inhibits ERK signaling and tumor cell proliferation in a V600E BRAF-selective manner. Proc Natl Acad Sci U S A. 2010;107(33):14903-8.
402. Halaban R, Zhang W, Bacchiocchi A, Cheng E, Parisi F, Ariyan S, et al. PLX4032, a selective BRAF(V600E) kinase inhibitor, activates the ERK pathway and enhances cell migration and proliferation of BRAF melanoma cells. Pigment Cell & Melanoma Research. 2010;23(2):190-200.

403. Panka DJ, Wang W, Atkins MB, Mier JW. The Raf inhibitor BAY 43-9006 (Sorafenib) induces caspase-independent apoptosis in melanoma cells. Cancer Research. 2006;66(3):1611-9.
404. Webster MR, Weeraratna AT. A Wnt-er Migration: The Confusing Role of -Catenin in Melanoma Metastasis. Science Signaling. 2013;6(268):pe11-pe.
405. Liao J, Qian F, Tchabo N, Mhawech-Fauceglia P, Beck A, Qian Z, et al. Ovarian cancer spheroid cells with stem cell-like properties contribute to tumor generation, metastasis and chemotherapy resistance through hypoxia-resistant metabolism. PLoS ONE. 2014;9(1):e84941.
406. Monzani E, Facchetti F, Galmozzi E, Corsini E, Benetti A, Cavazzin C, et al. Melanoma contains CD133 and ABCG2 positive cells with enhanced tumourigenic potential. European Journal of Cancer. 2007;43(5):935-46.
407. Frank NY. ABCB5-Mediated Doxorubicin Transport and Chemoresistance in Human Malignant Melanoma. Cancer Research. 2005;65(10):4320-33.
408. Boiko AD, Razorenova OV, van de Rijn M, Swetter SM, Johnson DL, Ly DP, et al. Human melanoma-initiating cells express neural crest nerve growth factor receptor CD271. Nature. 2010;466(7302):133-7.
409. Chandrasekaran S, DeLouise LA. Enriching and characterizing cancer stem cell sub-populations in the WM115 melanoma cell line. Biomaterials. 2011;32(35):9316-27.
410. Boonyaratanakornkit JB, Yue L, Strachan LR, Scalapino KJ, LeBoit PE, Lu Y, et al. Selection of Tumorigenic Melanoma Cells Using ALDH. Journal of Investigative Dermatology. 2010;130(12):2799-808.
411. Shanhai Xie ML, Suyun Huang, et al. Expression of MCAM,MUC18 by human melanoma cells leads to increased tumour growth and metastasis. Cancer Research. 1997;57:2295-303.
412. Pirozzi G, CD40 Expressed on human melanoma cells mediates T cell co-stimulation and tumor cell growth, Oxford Journals,. CD40 expressed on humnan melanoma cells mediates T cell co-stimulation and tumour cell growth. The Japanese Society for Immunology. 2000;12(6):787-95.
413. Thomas WD. Expression of the costimulatory molecule CD40 on melanoma cells. International Journal of Cancer. 1996;68:795-801.
414. Keshet GI, Goldstein I, Itzhaki O, Cesarkas K, Shenhav L, Yakirevitch A, et al. MDR1 expression identifies human melanoma stem cells. Biochemical and Biophysical Research Communications. 2008;368(4):930-6.
415. Al Dhaybi R, Sartelet H, Powell J, Kokta V. Expression of CD133+ cancer stem cells in childhood malignant melanoma and its correlation with metastasis. Modern Pathology. 2010;23(3):376-80.
416. Civenni G, Walter A, Kobert N, Mihic-Probst D, Zipser M, Belloni B, et al. Human CD271-Positive Melanoma Stem Cells Associated with Metastasis Establish Tumor Heterogeneity and Long-term Growth. Cancer Research. 2011;71(8):3098-109.
417. Zimmerer R, Korn P, Tavassol F, amp.., amp.. Functional features of cancer stem cells in melanoma cell lines. Cancer Cell International. 2012;13(78):13.
418. Arnoult D, Grodet A, Lee Y-J, Estaquier J, Blackstone C. Release of OPA1 during Apoptosis Participates in the Rapid and Complete Release of Cytochrome c and

Subsequent Mitochondrial Fragmentation. Journal of Biological Chemistry. 2005;280(42):35742-50.
419. Gallas JM, Eisner M. FLUORESCENCE OF MELANIN-DEPENDENCE UPON EXCITATION WAVELENGTH AND CONCENTRATION. Photochemistry and Photobiology. 1987;45(5):595-600.
420. Khaitan D, Chandna S, Arya MB, Dwarakanath BS. Establishment and characterization of multicellular spheroids from a human glioma cell line; Implications for tumor therapy. Journal of Translational Medicine. 2006;4:12.
421. Robertson FM, Ogasawara MA, Ye Z, Chu K, Pickei R, Debeb BG, et al. Imaging and Analysis of 3D Tumor Spheroids Enriched for a Cancer Stem Cell Phenotype. Journal of Biomolecular Screening. 2010;15(7):820-9.
422. Hong X, Chedid K, Kalkanis SN. Glioblastoma cell line-derived spheres in serumcontaining medium versus serum-free medium: a comparison of cancer stem cell properties. Int J Oncol. 2012;41(5):1693-700.
423. Hirschhaeuser F, Menne H, Dittfeld C, West J, Mueller-Klieser W, Kunz-Schughart LA. Multicellular tumor spheroids: an underestimated tool is catching up again. J Biotechnol. 2010;148(1):3-15.
424. Yuzugullu H, Benhaj K, Ozturk N, Senturk S, Celik E, Toylu A, et al. Canonical Wnt signaling is antagonized by noncanonical Wnt5a in hepatocellular carcinoma cells. Molecular Cancer. 2009;8(1):90.
425. Ju X, Ishikawa T-o, Naka K, Ito K, Ito Y, Oshima M. Context-dependent activation of Wnt signaling by tumor suppressor RUNX3 in gastric cancer cells. Cancer Science. 2014;105(4):418-24.
426. Cselenyi CS, Lee E. Context-Dependent Activation or Inhibition of Wnt-β-Catenin Signaling by Kremen2008 2008-02-26 00:00:00. pe10-pe p.
427. Oh EC, Katsanis N. Context-Dependent Regulation of Wnt Signaling through the Primary Cilium. Journal of the American Society of Nephrology. 2013;24(1):10-8.
428. Polakis P. Wnt signaling and cancer. Genes & Development. 2000;14:1837-51.
429. Herr P, Hausmann G, Basler K. WNT secretion and signalling in human disease. Trends in Molecular Medicine. 2012;18(8):483-93.
430. Gottardi C, Sinnberg T, Menzel M, Ewerth D, Sauer B, Schwarz M, et al. β-Catenin Signaling Increases during Melanoma Progression and Promotes Tumor Cell Survival and Chemoresistance. PLoS ONE. 2011;6(8):e23429.
431. Jin E-J, Erickson CA, Takada S, Burrus LW. Wnt and BMP Signaling Govern Lineage Segregation of Melanocytes in the Avian Embryo. Developmental Biology. 2001;233(1):22-37.
432. Thomas AJ, Erickson CA. FOXD3 regulates the lineage switch between neural crest-derived glial cells and pigment cells by repressing MITF through a non-canonical mechanism. Development. 2009;136(11):1849-58.
433. Yamaguchi Y, Brenner M, Hearing VJ. The Regulation of Skin Pigmentation. Journal of Biological Chemistry. 2007;282(38):27557-61.
434. Larue L, Luciani F, Kumasaka M, Champeval D, Demirkan N, Bonaventure J, et al. Bypassing melanocyte senescence by beta-catenin: a novel way to promote melanoma. Pathol Biol (Paris). 2009;57(7-8):543-7.
435. Delmas V, Beermann F, Martinozzi S, Carreira S, Ackermann J, Kumasaka M, et al. Beta-catenin induces immortalization of melanocytes by suppressing p16INK4a

expression and cooperates with N-Ras in melanoma development. Genes & Development. 2007;21(22):2923-35.
436. Kielhorn E, Provost E, Olsen D, D'Aquila TG, Smith BL, Camp RL, et al. Tissue microarray-based analysis shows phospho-beta-catenin expression in malignant melanoma is associated with poor outcome. Int J Cancer. 2003;103(5):652-6.
437. Widlund HR, Horstmann MA, Price ER, Cui J, Lessnick SL, Wu M, et al. Beta-catenin-induced melanoma growth requires the downstream target Microphthalmia-associated transcription factor. The Journal of Cell Biology. 2002;158(6):1079-87.
438. Sanders DSA, Blessing K, Hassan G, Bruton R, Marsden J, J J. Alterations in cadherin and catenin expression during the biological progression of melanocytic tumours. J Clin Pathol: Mol Pathol. 1999;52:151-7.
439. Vlad-Fiegen A, Langerak A, Eberth S, Muller O. The Wnt pathway destabilizes adherens junctions and promotes cell migration via beta-catenin and its target gene cyclin D1. FEBS Open Bio. 2012;2:26-31.
440. Murakami T, Toda S, Fujimoto M, Ohtsuki M, Byers HR, Etoh T, et al. Constitutive Activation of Wnt/β-Catenin Signaling Pathway in Migration-Active Melanoma Cells: Role of LEF-1 in Melanoma with Increased Metastatic Potential. Biochemical and Biophysical Research Communications. 2001;288(1):8-15.
441. Qi J, Chen N, Wang J, Siu CH. Transendothelial migration of melanoma cells involves N-cadherin-mediated adhesion and activation of the beta-catenin signaling pathway. Molecular Biology of the Cell. 2005;16(9):4386-97.
442. Mælandsmo GM, Holm R, Jahn M. Nesland ea. Reduced B-catenin expression in the cytoplasm of advanced stage superficial spreading malignant melanoma. Clinical Cancer Research. 2003;9:3383-8.
443. Kageshita T, Hamby C, Ishihara T, Matsumoto K, Ono T. Loss of beta-catenin expression associated with disease progression in malignant melanoma. British Journal of Dermatology. 2001;145:210-6.
444. Bachmann IM, Straume O, Puntervoll HE, Kalvenes MB, Akslen LA. Importance of P-cadherin, beta-catenin, and Wnt5a/frizzled for progression of melanocytic tumors and prognosis in cutaneous melanoma. Clin Cancer Res. 2005;11(24 Pt 1):8606-14.
445. Bellei B, Flori E, Izzo E, Maresca V, Picardo M. GSK3beta inhibition promotes melanogenesis in mouse B16 melanoma cells and normal human melanocytes. Cell Signal. 2008;20(10):1750-61.
446. Takahashi Y, Nishikawa M, Suehara T, Takiguchi N, Takakura Y. Gene silencing of beta-catenin in melanoma cells retards their growth but promotes the formation of pulmonary metastasis in mice. Int J Cancer. 2008;123(10):2315-20.
447. Zhang J, Li Y, Wu Y, Yang T, Yang K, Wang R, et al. Wnt5a Inhibits the Proliferation and Melanogenesis of Melanocytes. International Journal of Medical Sciences. 2013;10(6):699-706.
448. Sherwood V, Chaurasiya SK, Ekstrom EJ, Guilmain W, Liu Q, Koeck T, et al. WNT5A-mediated -catenin-independent signalling is a novel regulator of cancer cell metabolism. Carcinogenesis. 2013.
449. Bittner M, Meltzer P, Trent J, amp., amp. Molecular classifcation of cutaneous malignant melanoma by gene expression profling. nature. 2000;406:536-40.

450. Da Forno PD, Pringle JH, Hutchinson P, Osborn J, Huang Q, Potter L, et al. WNT5A expression increases during melanoma progression and correlates with outcome. Clin Cancer Res. 2008;14(18):5825-32.
451. Nemeth MJ, Topol L, Anderson SM, Yang Y, Bodine DM. Wnt5a inhibits canonical Wnt signaling in hematopoietic stem cells and enhances repopulation. Proc Natl Acad Sci U S A. 2007;104(39):15436-41.
452. Topol L, Jiang X, Choi H, Garrett-Beal L, Carolan PJ, Yang Y. Wnt-5a inhibits the canonical Wnt pathway by promoting GSK-3-independent beta-catenin degradation. The Journal of Cell Biology. 2003;162(5):899-908.
453. Weeraratna AT, Jiang Y, Hostetter G, Rosenblatt K, Duray P, Bittner M, et al. Wnt5a signaling directly affects cell motility and invasion of metastatic melanoma. Cancer Cell. 2002;1:279-88.
454. O'Connell MP, Fiori JL, Xu M, Carter AD, Frank BP, Camilli TC, et al. The orphan tyrosine kinase receptor, ROR2, mediates Wnt5A signaling in metastatic melanoma. Oncogene. 2010;29(1):34-44.
455. Julia Billiard DSW, Laura M. Seestaller-Wehr, Robert A. Moran, Annamarie Mangine, and Peter V. N. Bodine. The Orphan Receptor Tyrosine Kinase Ror2 Modulates Canonical Wnt Signaling in Osteoblastic Cells. Molecular Endocrinology. 2005;19(1):90-101.
456. Oishi I, Suzuki H, Onishi N, Takada R, Kani S, Ohkawara B, et al. The receptor tyrosine kinase Ror2 is involved in non-canonical Wnt5a/JNK signalling pathway. Genes to Cells. 2003;8:645-54.
457. Bakker ER, Das AM, Helvensteijn W, Franken PF, Swagemakers S, van der Valk MA, et al. Wnt5a promotes human colon cancer cell migration and invasion but does not augment intestinal tumorigenesis in Apc1638N mice. Carcinogenesis. 2013;34(11):2629-38.
458. Cheng R, Sun B, Liu Z, Zhao X, Qi L, Li Y, et al. Wnt5a suppresses colon cancer by inhibiting cell proliferation and epithelial-mesenchymal transition. Journal of cellular physiology. 2014;229(12):1908-17.
459. Weeraratna AT, Becker D, Carr KM, Duray PH, Rosenblatt KP, Yang S, et al. Generation and analysis of melanoma SAGE libraries: SAGE advice on the melanoma transcriptome. Oncogene. 2004;23(12):2264-74.
460. Witze ES, Litman ES, Argast GM, Moon RT, Ahn NG. Wnt5a control of cell polarity and directional movement by polarized redistribution of adhesion receptors. Science. 2008;320(5874):365-9.
461. O'Connell MP, French AD, Leotlela PD, Weeraratna AT. Assaying Wnt5A-mediated invasion in melanoma cells. Methods in molecular biology. 2008;468:243-53.
462. Herlyn M, Berking C, Li G, Satyamoorthy K. Lessons from melanocyte development for understanding the biological events in naevus and melanoma formation. Melanoma Res. 2000;10(4):303-12.
463. Bendas G, Borsig L. Cancer Cell Adhesion and Metastasis: Selectins, Integrins, and the Inhibitory Potential of Heparins. International Journal of Cell Biology. 2012;2012:10.
464. Rubinfeld B. Stabilization of beta -Catenin by Genetic Defects in Melanoma Cell Lines. Science. 1997;275(5307):1790-2.

465. Hanahan D, Weinberg Robert A. Hallmarks of Cancer: The Next Generation. Cell. 2011;144(5):646-74.
466. Tyurina YY, Tyurin VA, Zhao Q, Djukic M, Quinn PJ, Pitt BR, et al. Oxidation of phosphatidylserine: a mechanism for plasma membrane phospholipid scrambling during apoptosis? Biochemical and Biophysical Research Communications. 2004;324(3):1059-64.
467. Evan GI, Vousden KH. Proliferation, cell cycle and apoptosis in cancer. NATURE. 2001;411:342-8.
468. Cooper G.M, Hausma R.E. The Cell A molecular approach, Chapter 16 The Eukaryotic Cell Cycle. 6th ed2013.
469. Shu CH, Yang WK, Shih YL, Kuo ML, Huang TS. Cell cycle G2/M arrest and activation of cyclin-dependent kinases associated with low-dose paclitaxel-induced sub-G1 apoptosis. Apoptosis. 1997;2(5):463-70.
470. Friedl P, Wolf K. Tumour-cell invasion and migration: diversity and escape mechanisms. Nat Rev Cancer. 2003;3(5):362-74.
471. Cory G. Scratch-Wound Assay. In: Wells CM, Parsons M, editors. Cell Migration. Methods in Molecular Biology. 769: Humana Press; 2011. p. 25-30.
472. Elkin M, Vlodavsky I. Tail Vein Assay of Cancer Metastasis. Current Protocols in Cell Biology: John Wiley & Sons, Inc.; 2001.
473. Nakajima T, Watanabe S, Sato Y, Kameya T, Shimosato Y, Ishihara K. Immunohistochemical Demonstration of S 100 Protein in Malignant Melanoma and Pigmented Nevus, and Its Diagnostic Application. Cancer. 1982;50:912-8.
474. Schatton T, Frank MH. The in vitro spheroid melanoma cell culture assay: cues on tumor initiation? J Invest Dermatol. 2010;130(7):1769-71.
475. He B, You L, Uematsu K, Xu Z, Lee AY, Matsangou M, et al. A Monoclonal Antibody against Wnt-1 Induces Apoptosis in Human Cancer Cells.
476. You L, He B, Xu Z, Uematsu K, Mazieres J, Mikami I, et al. Inhibition of Wnt-2-mediated signaling induces programmed cell death in non-small-cell lung cancer cells.
477. He B, Reguart N, You L, Mazieres J, Xu Z, Lee AY, et al. Blockade of Wnt-1 signaling induces apoptosis in human colorectal cancer cells containing downstream mutations. Oncogene. 2005;24(18):3054-8.
478. Hartwell LH, Kastan MB. Cell cycle control and cancer. Science. 1994;266(5192):1821-8.
479. Zbytek B, Carlson JA, Granese J, Ross J, Mihm MC, Slominski A. Current concepts of metastasis in melanoma.
480. Alimonti A. PTEN breast cancer susceptibility: a matter of dose. Ecancermedicalscience. 2010;4:192.
481. Barker N, Morin PJ, Clevers H. The Yin-Yang of TCF/beta-catenin signaling. Adv Cancer Res. 2000;77:1-24.
482. Fokas E, Engenhart-Cabillic R, Daniilidis K, Rose F, An HX. Metastasis: the seed and soil theory gains identity. Cancer Metastasis Rev. 2007;26(3-4):705-15.
483. Paget S. THE DISTRIBUTION OF SECONDARY GROWTHS IN CANCER OF THE BREAST. The Lancet. 1889;133(3421):571-3.
484. Kypta RM, Waxman J. Wnt/beta-catenin signalling in prostate cancer. Nat Rev Urol. 2012;9(8):418-28. doi: 10.1038/nrurol.2012.116. Epub Jun 19.

485. Liu J, Pan S, Hsieh MH, Ng N, Sun F, Wang T, et al. Targeting Wnt-driven cancer through the inhibition of Porcupine by LGK974. Proc Natl Acad Sci U S A. 2013;110(50):20224-9. doi: 10.1073/pnas.1314239110. Epub 2013 Nov 25.
486. Lu J, Ma Z, Hsieh JC, Fan CW, Chen B, Longgood JC, et al. Structure/Activity Relationship Studies of Small-Molecule Inhibitors of Wnt Response. Bioorg Med Chem Lett. 2009;19(14):3825-7. Epub 2009 Apr 18 doi:10.1016/j.bmcl.2009.04.040.
487. Takebe N, Harris PJ, Warren RQ, Ivy SP. Targeting cancer stem cells by inhibiting Wnt, Notch, and Hedgehog pathways. Nat Rev Clin Oncol. 2011;8(2):97-106. doi: 10.1038/nrclinonc.2010.196. Epub Dec 14.
488. Schulze A, Harris AL. How cancer metabolism is tuned for proliferation and vulnerable to disruption. Nature. 2012;491(7424):364-73.
489. Fritz V, Fajas L. Metabolism and proliferation share common regulatory pathways in cancer cells. Oncogene. 2010;29(31):4369-77.
490. Nadolski MJ, Linder ME. Protein lipidation. Febs J. 2007;274(20):5202-10.
491. Xue L, Gollapalli DR, Maiti P, Jahng WJ, Rando RR. A palmitoylation switch mechanism in the regulation of the visual cycle. Cell. 2004;117(6):761-71.
492. J. Andersen S. Kornbluth. The tangled circuitry of metabolism and apoptosis. Mol Cell. 2013;49(3):399-410.
493. Chen S, Guttridge DC, You Z, Zhang Z, Fribley A, Mayo MW, et al. Wnt-1 Signaling Inhibits Apoptosis by Activating B-Catenin-T Cell Factor–mediated Transcription. JCB. 2001;152(1):87-96.
494. Pecina-Slaus N. Wnt signal transduction pathway and apoptosis: a review. Cancer Cell International. 2010;10:22.
495. Yoon JC, Ng A, Kim BH, Bianco A, Xavier RJ, Elledge SJ. Wnt signaling regulates mitochondrial physiology and insulin sensitivity. Genes & Development. 2010;24(14):1507-18.
496. McDonald SL, Silver A. The opposing roles of Wnt-5a in cancer. British Journal of Cancer. 2009;101(2):209-14.
497. D. Schwartz R. Wu S. Kardia A. Levin C. Huang K. Shedden R. Kuick et al. Novel candidate targets of beta-catenin/T-cell factor signaling identified by gene expression profiling of ovarian endometrioid adenocarcinomas. Cancer Res. 2003;63(11):2913-22.
498. Dickinson A, Yeung KY, Donoghue J, Baker MJ, Kelly RD, McKenzie M, et al. The regulation of mitochondrial DNA copy number in glioblastoma cells. Cell Death and Differentiation. 2013;20(12):1644-53.
499. Scott I, Youle RJ. Mitochondrial fission and fusion. Essays in biochemistry. 2010;47:85-98.
500. Godoy JA, Arrazola MS, Ordenes D, Silva-Alvarez C, Braidy N, Inestrosa NC. Wnt-5a Modulates Mitochondrial Fission-Fusion in Rat Hippocampal Neurons. The Journal of biological chemistry. 2014.
501. Serrat Rn, pez-Dome´nech GL, Mirra S, Quevedo M, Garcia- J, Ferna`ndez4, et al. The Non-Canonical Wnt/PKC Pathway Regulates Mitochondrial Dynamics through Degradation of the Arm-Like Domain-Containing Protein Alex3. PLoS ONE. 2013;8(7).
502. Kasahara A, Scorrano L. Mitochondria: from cell death executioners to regulators of cell differentiation. Trends in Cell Biology. 2014.
503. Ming M, Wang S, Wu W, Senyuk V, Le Beau MM, Nucifora G, et al. Activation of Wnt/beta-catenin protein signaling induces mitochondria-mediated apoptosis in

hematopoietic progenitor cells. The Journal of biological chemistry. 2012;287(27):22683-90.
504. Martinou JC, Youle RJ. Mitochondria in apoptosis: Bcl-2 family members and mitochondrial dynamics. Developmental Cell. 2011;21(1):92-101.
505. Zeilstra J, Joosten SP, Wensveen FM, Dessing MC, Schutze DM, Eldering E, et al. WNT signaling controls expression of pro-apoptotic BOK and BAX in intestinal cancer. Biochemical and Biophysical Research Communications. 2011;406(1):1-6.
506. Yeh CT, Yao CJ, Yan JL, Chuang SE, Lee LM, Chen CM, et al. Apoptotic Cell Death and Inhibition of Wnt/beta-Catenin Signaling Pathway in Human Colon Cancer Cells by an Active Fraction (HS7) from Taiwanofungus camphoratus. Evid Based Complement Alternat Med. 2011;2011:750230.
507. Yizhak K, Le Devedec SE, Rogkoti VM, Baenke F, de Boer VC, Frezza C, et al. A computational study of the Warburg effect identifies metabolic targets inhibiting cancer migration. Mol Syst Biol. 2014;10(8):744.
508. Dairaku N, Kato K, Honda K, Koike T, Iijima K, Imatani A, et al. Oligomycin and antimycin A prevent nitric oxide-induced apoptosis by blocking cytochrome C leakage. The Journal of laboratory and clinical medicine. 2004;143(3):143-51.
509. Pendergrass W, Wolf N, Poot M. Efficacy of MitoTracker Green and CMXrosamine to measure changes in mitochondrial membrane potentials in living cells and tissues. Cytometry A. 2004;61(2):162-9.
510. Oliva CR, Moellering DR, Gillespie GY, Griguer CE. Acquisition of chemoresistance in gliomas is associated with increased mitochondrial coupling and decreased ROS production. PLoS One. 2011;6(9):9.
511. Brand Martin D, Nicholls David G. Assessing mitochondrial dysfunction in cells. Biochemical Journal. 2011;435(2):297-312.
512. Li N, Ragheb K, Lawler G, Sturgis J, Rajwa B, Melendez JA, et al. Mitochondrial Complex I Inhibitor Rotenone Induces Apoptosis through Enhancing Mitochondrial Reactive Oxygen Species Production. Journal of Biological Chemistry. 2003;278(10):8516-25.
513. Wick AN, Drury DR, Nakada HI, Wolfe JB. Localization of the primary metabolic block produced by 2-deoxyglucose. The Journal of biological chemistry. 1957;224(2):963-9.
514. Dickinson BC, Chang CJ. Chemistry and biology of reactive oxygen species in signaling or stress responses. Nat Chem Biol. 2011;7(8):504-11.
515. Wiegand G, Remington SJ. Citrate synthase- structure, control, and mechanism. Ann Rev Biophys Chem. 1986;15:97-117.
516. Kuznetsov AV, Kehrer I, Kozlov AV, Haller M, Redl H, Hermann M, et al. Mitochondrial ROS production under cellular stress: comparison of different detection methods. Analytical and bioanalytical chemistry. 2011;400(8):2383-90.
517. Loson OC, Song Z, Chen H, Chan DC. Fis1, Mff, MiD49, and MiD51 mediate Drp1 recruitment in mitochondrial fission. Mol Biol Cell. 2013;24(5):659-67.
518. Poot M, Zhang YZ, Krämer JA, Wells KS, Jones LJ, Hanzel DK, et al. Analysis of mitochondrial morphology and function with novel fixable fluorescent stains. Journal of Histochemistry & Cytochemistry. 1996;44(12):1363-72.
519. Presley AD, Fuller KM, Arriaga EA. MitoTracker Green labeling of mitochondrial proteins and their subsequent analysis by capillary electrophoresis

with laser-induced fluorescence detection. J Chromatogr B Analyt Technol Biomed Life Sci. 2003;793(1):141-50.
520. Rowland AA, Voeltz GK. Endoplasmic reticulum-mitochondria contacts: function of the junction. Nature reviews Molecular cell biology. 2012;13(10):607-25.
521. Wang K, Zhang Y, Li X, Chen L, Wang H, Wu J, et al. Characterization of the Kremen-binding site on Dkk1 and elucidation of the role of Kremen in Dkk-mediated Wnt antagonism. The Journal of biological chemistry. 2008;283(34):23371-5.
522. Jastroch M, Divakaruni AS, Mookerjee S, Treberg JR, Brand MD. Mitochondrial proton and electron leaks. Essays in biochemistry. 2010;47:53-67.
523. Solaini G, Sgarbi G, Baracca A. Oxidative phosphorylation in cancer cells. Biochim Biophys Acta. 2011;1807(6):534-42.
524. Wang X. The expanding role of mitochondria in apoptosis. Genes & Development. 2001;15(22):2922-33.
525. Ricci J-E, Gottlieb RA, Green DR. Caspase-mediated loss of mitochondrial function and generation of reactive oxygen species during apoptosis. The Journal of Cell Biology. 2003;160(1):65-75.
526. DeBerardinis RJ, Lum JJ, Hatzivassiliou G, Thompson CB. The Biology of Cancer: Metabolic Reprogramming Fuels Cell Growth and Proliferation. Cell Metabolism. 2008;7(1):11-20.
527. Ng SS, Mahmoudi T, Danenberg E, Bejaoui I, de Lau W, Korswagen HC, et al. Phosphatidylinositol 3-kinase (PI3K) signaling does not activate the Wnt cascade. Journal of Biological Chemistry. 2009.
528. Voskas D, Ling LS, Woodgett JR. Does GSK-3 provide a shortcut for PI3K activation of Wnt signalling?
529. Manning BD, Cantley LC. AKT/PKB Signaling: Navigating Downstream. Cell2007. p. 1261–74.
530. Dang CV. Links between metabolism and cancer. Genes & Development. 2012;26(9):877-90.
531. Zhang S, Li Y, Wu Y, Shi K, Bing L, Hao J. Wnt/beta-catenin signaling pathway upregulates c-Myc expression to promote cell proliferation of P19 teratocarcinoma cells. Anat Rec. 2012;295(12):2104-13.
532. Tan S, Sagara Y, Liu Y, Maher P, Schubert D. The regulation of Reactive Oxygen Species production during programmed cell death. The Journal of Cell Biology. 1998;141(6):1423-32.
533. Schumacker PT. Reactive oxygen species in cancer cells: live by the sword, die by the sword. Cancer Cell. 2006;10(3):175-6.
534. Wellen KE, Thompson CB. Cellular metabolic stress: considering how cells respond to nutrient excess. Mol Cell. 2010;40(2):323-32.
535. Shlevkov E, Schwarz TL. Have you seen? For parkin, it's not all or nothing. EMBO J. 2014;33(4):277-9.
536. Costa A, Scholer-Dahirel A, Mechta-Grigoriou F. The role of reactive oxygen species and metabolism on cancer cells and their microenvironment. Seminars in cancer biology. 2014;25:23-32.
537. Kohchi C, Inagawa H, Nishizawa T, Soma G-I. ROS and innate Immunity. Anticancer Research. 2009;29:817-22.
538. Kim JS, Huang TY, Bokoch GM. Reactive oxygen species regulate a slingshot-cofilin activation pathway. Mol Biol Cell. 2009;20(11):2650-60.

539. Gianni D, Taulet N, DerMardirossian C, Bokoch GM. c-Src-mediated phosphorylation of NoxA1 and Tks4 induces the reactive oxygen species (ROS)-dependent formation of functional invadopodia in human colon cancer cells. Mol Biol Cell. 2010;21(23):4287-98.
540. Bellot GL, Liu D, Pervaiz S. ROS, autophagy, mitochondria and cancer: Ras, the hidden master? Mitochondrion. 2013;13(3):155-62.
541. Guo JY, Chen HY, Mathew R, Fan J, Strohecker AM, Karsli-Uzunbas G, et al. Activated Ras requires autophagy to maintain oxidative metabolism and tumorigenesis. Genes & Development. 2011;25(5):460-70.
542. Kongara S, Karantza V. The interplay between autophagy and ROS in tumorigenesis. Frontiers in oncology. 2012;2:171.
543. Karantza-Wadsworth V, Patel S, Kravchuk O, Chen G, Mathew R, Jin S, et al. Autophagy mitigates metabolic stress and genome damage in mammary tumorigenesis. Genes Dev. 2007;21(13):1621-35.
544. Mathew R, Kongara S, Beaudoin B, Karp CM, Bray K, Degenhardt K, et al. Autophagy suppresses tumor progression by limiting chromosomal instability. Genes & Development. 2007;21(11):1367-81.
545. Liang C. Negative regulation of autophagy. Cell Death Differ. 2010;17(12):1807-15.
546. Scherz-Shouval R, Elazar Z. Regulation of autophagy by ROS: physiology and pathology. Trends Biochem Sci. 2011;36(1):30-8.
547. Lozy F, Karantza V. Autophagy and cancer cell metabolism. Seminars in Cell & Developmental Biology. 2012;23(4):395-401.
548. Funato Y, Michiue T, Asashima M, Miki H. The thioredoxin-related redox-regulating protein nucleoredoxin inhibits Wnt-beta-catenin signalling through dishevelled. Nat Cell Biol. 2006;8(5):501-8.
549. Korswagen HC. Regulation of the Wnt/beta-catenin pathway by redox signaling. Dev Cell. 2006;10(6):687-8.
550. Li Z, Xu J, Xu P, Liu S, Yang Z. Wnt/beta-catenin signalling pathway mediates high glucose induced cell injury through activation of TRPC6 in podocytes. Cell Prolif. 2013;46(1):76-85.
551. Lin C-L, Wang J-Y, Huang Y-T, Kuo Y-H, Surendran K, Wang F-S. Wnt/β-Catenin Signaling Modulates Survival of High Glucose–Stressed Mesangial Cells. Journal of the American Society of Nephrology. 2006;17(10):2812-20.
552. Marin-Valencia I, Yang C, Mashimo T, Cho S, Baek H, Yang X-L, et al. Analysis of Tumor Metabolism Reveals Mitochondrial Glucose Oxidation in Genetically Diverse Human Glioblastomas in the Mouse Brain In Vivo. Cell Metabolism. 2012;15(6):827-37.
553. Serkova NJ, Glunde K. Metabolomics of cancer. Methods Mol Biol. 2009;520:273-95.
554. Desai SP, Bhatia SN, Toner M, Irimia D. Mitochondrial localization and the persistent migration of epithelial cancer cells. Biophys J. 2013;104(9):2077-88.
555. Marhaba R, Zoller M. CD44 in cancer progression: adhesion, migration and growth regulation. J Mol Histol. 2004;35(3):211-31.
556. Lathrop KL, Steketee MB. Mitochondrial Dynamics in Retinal Ganglion Cell Axon Regeneration and Growth Cone Guidance. J Ocul Biol. 2013;1(2):9.

557. Kreis P, Leondaritis G, Lieberam I, Eickholt BJ. Subcellular targeting and dynamic regulation of PTEN: implications for neuronal cells and neurological disorders. Front Mol Neurosci. 2014;7:23.(doi):10.3389/fnmol.2014.00023. eCollection 2014.
558. Liang H, He S, Yang J, Jia X, Wang P, Chen X, et al. PTENalpha, a PTEN isoform translated through alternative initiation, regulates mitochondrial function and energy metabolism. Cell Metab. 2014;19(5):836-48.
559. Zlotorynski E. Organelle dynamics: (P)TEN-ding to mitochondria. Nat Rev Mol Cell Biol. 2014;15(6):366-7.
560. LIESA M, PALACI´N M, ZORZANO A. Mitochondrial Dynamics in Mammalian Health and Disease. Physiol Rev. 2009;89:799-845.
561. Shirihai OS, Westrate LM, Drocco JA, Martin KR, Hlavacek WS, MacKeigan JP. Mitochondrial Morphological Features Are Associated with Fission and Fusion Events. PLoS ONE. 2014;9(4):e95265.
562. Santel A, Fuller MT. Control of mitochondrial morphology by a human mitofusin. Journal of Cell Science. 2000;114:867-74.
563. Huang P, Galloway CA, Yoon Y. Control of Mitochondrial Morphology Through Differential Interactions of Mitochondrial Fusion and Fission Proteins. PLoS ONE. 2011;6.
564. Zorzano A, Liesa M, Sebastián D, Segalés J, Palacín M. Mitochondrial fusion proteins: Dual regulators of morphology and metabolism. Seminars in Cell & Developmental Biology. 2010;21(6):566-74.
565. Rehman J, Zhang HJ, Toth PT, Zhang Y, Marsboom G, Hong Z, et al. Inhibition of mitochondrial fission prevents cell cycle progression in lung cancer. The FASEB Journal. 2012;26(5):2175-86.
566. Guo X, Chen KH, Guo Y, Liao H, Tang J, Xiao RP. Mitofusin 2 Triggers Vascular Smooth Muscle Cell Apoptosis via Mitochondrial Death Pathway. Circulation Research. 2007;101(11):1113-22.
567. Huang JSCaP. Mitochondrial defects in cancer.pdf. Molecular Cancer. 2002.
568. Mitra K, Wunder C, Roysam B, Lin G, Lippincott-Schwartz J. A hyperfused mitochondrial state achieved at G1–S regulates cyclin E buildup and entry into S phase. Proceedings of the National Academy of Sciences. 2009;106(29):11960-5.
569. Qian W, Choi S, Gibson GA, Watkins SC, Bakkenist CJ, Van Houten B. Mitochondrial hyperfusion induced by loss of the fission protein Drp1 causes ATM-dependent G2/M arrest and aneuploidy through DNA replication stress. J Cell Sci. 2012;125(Pt 23):5745-57.
570. Park SL, Le Marchand L, Wilkens LR, Kolonel LN, Henderson BE, Zhang Z-F, et al. Risk Factors for Malignant Melanoma in White and Non-White/Non-African American Populations: The Multiethnic Cohort. Cancer prevention research (Philadelphia, Pa). 2012;5(3):423-34.
571. Ishihara N. Mitofusin 1 and 2 play distinct roles in mitochondrial fusion reactions via GTPase activity. Journal of Cell Science. 2004;117(26):6535-46.
572. Santel A. Mitofusin-1 protein is a generally expressed mediator of mitochondrial fusion in mammalian cells. Journal of Cell Science. 2003;116(13):2763-74.
573. Bach D, Pich S, Soriano FX, Vega N, Baumgartner B, Oriola J, et al. Mitofusin-2 Determines Mitochondrial Network Architecture and Mitochondrial Metabolism: A

novel regulatory mechanism altered in obesity. Journal of Biological Chemistry. 2003;278(19):17190-7.
574. Chen H, Detmer SA, Ewald AJ, Griffin EE, Fraser SE, Chan DC. Mitofusins Mfn1 and Mfn2 coordinately regulate mitochondrial fusion and are essential for embryonic development. The Journal of Cell Biology. 2003;160(2):189-200.
575. de Brito OM, Scorrano L. Mitofusin 2 tethers endoplasmic reticulum to mitochondria. Nature. 2008;456(7222):605-10.
576. Zhang Z, Wakabayashi N, Wakabayashi J, Tamura Y, Song W-J, Sereda S, et al. The dynamin-related GTPase Opa1 is required for glucose-stimulated ATP production in pancreatic beta cells. Molecular Biology of the Cell. 2011;22(13):2235-45.
577. Poole AC, Thomas RE, Yu S, Vincow ES, Pallanck L. The Mitochondrial Fusion-Promoting Factor Mitofusin Is a Substrate of the PINK1/Parkin Pathway. PLoS ONE. 2010;5(4):8.
578. Koch A, Yoon Y, Bonekamp NA, McNiven MA, Schrader M. A role for Fis1 in both mitochondrial and peroxisomal fission in mammalian cells. Mol Biol Cell. 2005;16(11):5077-86.
579. Gilad Twig, Alvaro Elorza, Anthony JA Molina, Hibo Mohamed, Jakob D Wikstrom GW, Linsey, Stiles SEH, Steve Katz, Guy Las JA, Min Wu, Be´ne´ dicte F Py5 JY, et al. Fission and selective fusion govern mitochondrial segregation and elimination by autophagy. The EMBO Journal. 2008;27:433-46.
580. Zhang G, Jin H, Lin X, Chen C, Liu X, Zhang Q, et al. Anti-tumor effects of Mfn2 in gastric cancer. Translational Gastrointestinal Cancer. 2013.
581. Pich S, Bach D, Briones P, Liesa M, Camps M, Testar X, et al. The Charcot–Marie–Tooth type 2A gene product, Mfn2, up-regulates fuel oxidation through expression of OXPHOS system. Human Molecular Genetics. 2005;14(11):1405-15.
582. Silva-Alvarez C, Arrázola MS, Godoy JA, Ordenes D, Inestrosa NC. Canonical Wnt signaling protects hippocampal neurons from Aβ oligomers: role of non-canonical Wnt-5a/Ca2+ in mitochondrial dynamics. Frontiers in Cellular Neuroscience. 2013;7.
583. Qi X, Disatnik MH, Shen N, Sobel RA, Mochly-Rosen D. Aberrant mitochondrial fission in neurons induced by protein kinase C{delta} under oxidative stress conditions in vivo. Mol Biol Cell. 2011;22(2):256-65.
584. Zhu L, Ling S, Yu X-D, Venkatesh LK, Subramanian T, Chinnadurai G, et al. Modulation of Mitochondrial Ca2+ Homeostasis by Bcl-2. Journal of Biological Chemistry. 1999;274(47):33267-73.
585. Murphy AN, Bredesen DE, Cortopassi G, Wang E, Fiskum G. Bcl-2 potentiates the maximal calcium uptake capacity of neural cell mitochondria. Proceedings of the National Academy of Sciences. 1996;93(18):9893-8.
586. Jourdain A, Martinou J-C. Mitochondrial outer-membrane permeabilization and remodelling in apoptosis. The International Journal of Biochemistry & Cell Biology. 2009;41(10):1884-9.
587. Antignani A, Youle RJ. How do Bax and Bak lead to permeabilization of the outer mitochondrial membrane? Curr Opin Cell Biol. 2006;18(6):685-9.
588. Scorrano L. Mitochondrial Apoptosis Regulation by Bcl-2 Family Members. In: Mitchell LMMN, editor. Pathobiology of Human Disease. San Diego: Academic Press; 2014. p. 170-4.

589. Zeilstra J, Joosten SP, Wensveen FM, Dessing MC, Schutze DM, Eldering E, et al. WNT signaling controls expression of pro-apoptotic BOK and BAX in intestinal cancer. Biochem Biophys Res Commun. 2011;406(1):1-6.
590. Biechele TL, Kulikauskas RM, Toroni RA, Lucero OM, Swift RD, James RG, et al. Wnt/beta-catenin signaling and AXIN1 regulate apoptosis triggered by inhibition of the mutant kinase BRAFV600E in human melanoma. Sci Signal. 2012;5(206):ra3.
591. Kim I, Rodriguez-Enriquez S, Lemasters JJ. Selective degradation of mitochondria by mitophagy. Archives of Biochemistry and Biophysics. 2007;462(2):245-53.
592. J. L. Selective Mitochondrial Autophagy, or Mitophagy, as a Targeted Defense Against Oxidative Stress, Mitochondrial Dysfunction, and Aging. Rejuvenation Research. 2005;8(1):3-5.
593. Mathew R, Karantza-Wadsworth V, White E. Role of autophagy in cancer. Nat Rev Cancer. 2007;7(12):961-7.
594. Strohecker A M, Jessie Yanxiang Guo, Gizem Karsli-Uzunbas, Sandy M. Price, Guanghua Jim Chen, Robin Mathew, et al. Autophagy sustains mitochondrial glutamine metabolism and growth of BRAFv600E driven lung tumors. Caner Discovery. 2013.
595. Gao C, Cao W, Bao L, Zuo W, Xie G, Cai T, et al. Autophagy negatively regulates Wnt signalling by promoting Dishevelled degradation. Nature Cell Biology. 2010;12(8):781-90.
596. Petherick KJ, Williams AC, Lane JD, Ordóñez-Morán P, Huelsken J, Collard TJ, et al. Autolysosomal β-catenin degradation regulates Wnt-autophagy-p62 crosstalk. The EMBO Journal. 2013;32(13):1903-16.
597. Vincent M. Aita, Liang XH, Murty VVVS, Pincus DL, Yu W, Cayanis E, et al. Cloning and Genomic Organization of B*eclin 1,* a Candidate Tumor Suppressor Gene on Chromosome 17q21. Genomics. 1999;59(1):59-65.
598. Gomes LC, Di Benedetto G, Scorrano L. During autophagy mitochondria elongate, are spared from degradation and sustain cell viability. Nat Cell Biol. 2011;13(5):589-98.
599. Mathew R, White E. Autophagy, Stress, and Cancer Metabolism: What Doesn't Kill You Makes You Stronger. Cold Spring Harbor Symposia on Quantitative Biology. 2011;76:389-96.
600. Twig G, Hyde B, Shirihai OS. Mitochondrial fusion, fission and autophagy as a quality control axis: The bioenergetic view. Biochimica et Biophysica Acta (BBA) - Bioenergetics. 2008;1777(9):1092-7.
601. Fimia GM, Parganlija D, Klinkenberg M, Domínguez-Bautista J, Hetzel M, Gispert S, et al. Loss of PINK1 Impairs Stress-Induced Autophagy and Cell Survival. PLoS ONE. 2014;9(4):e95288.
602. Jin SM, Youle RJ. PINK1- and Parkin-mediated mitophagy at a glance. Journal of Cell Science. 2012;125(4):795-9.
603. Deas E, Plun-Favreau H, Gandhi S, Desmond H, Kjaer S, Loh SHY, et al. PINK1 cleavage at position A103 by the mitochondrial protease PARL. Human Molecular Genetics. 2010;20(5):867-79.
604. Green DR, Narendra DP, Jin SM, Tanaka A, Suen D-F, Gautier CA, et al. PINK1 Is Selectively Stabilized on Impaired Mitochondria to Activate Parkin. PLoS Biology. 2010;8(1):e1000298.

605. Zheng X, Hunter T. Pink1, the first ubiquitin kinase. The EMBO Journal. 2014.
606. Kanamaru Y, Sekine S, Ichijo H, Takeda K. The phosphorylation-dependent regulation of mitochondrial proteins in stress responses. J Signal Transduct. 2012;2012:931215.
607. Zheng X, Hunter T. Pink1, the first ubiquitin kinase. EMBO J. 2014.
608. Shlevkov E, Schwarz TL. For Parkin, it's not all or nothing. The EMBO Journal. 2014;33(4):277-9.
609. Dagda RK, Cherra SJ, Kulich SM, Tandon A, Park D, Chu CT. Loss of PINK1 Function Promotes Mitophagy through Effects on Oxidative Stress and Mitochondrial Fission. Journal of Biological Chemistry. 2009;284(20):13843-55.
610. Yang et al. Pink1 regulates mitochondrial dynamics through interaction with the fission/fusion machinery. Proceedings of the National Academy of Sciences. 2008;105(45):17585-.
611. Poole AC, Thomas RE, Andrews LA, McBride HM, Whitworth AJ, Pallanck LJ. The PINK1/Parkin pathway regulates mitochondrial morphology. Proceedings of the National Academy of Sciences. 2008;105(5):1638-43.
612. Gegg ME, Cooper JM, Chau K-Y, Rojo M, Schapira AHV, Taanman J-W. Mitofusin 1 and mitofusin 2 are ubiquitinated in a PINK1/parkin-dependent manner upon induction of mitophagy. Human Molecular Genetics. 2010;19(24):4861-70.
613. Narendra D, Tanaka A, Suen DF, Youle RJ. Parkin is recruited selectively to impaired mitochondria and promotes their autophagy. The Journal of Cell Biology. 2008;183(5):795-803.
614. Lee K-H, Lee M-H, Kang Y-W, Rhee K-J, Kim T-U, Kim Y-S. Parkin induces apoptotic cell death in TNF-α-treated cervical cancer cells. BMB reports. 2012;45(9):526-31.
615. Poulogiannis G, McIntyre RE, Dimitriadi M, Apps JR, Wilson CH, Ichimura K, et al. PARK2 deletions occur frequently in sporadic colorectal cancer and accelerate adenoma development in Apc mutant mice. Proceedings of the National Academy of Sciences. 2010;107(34):15145-50.
616. Wang F, Denison S, Lai J-P, Philips LA, Montoya D, Kock N, et al. Parkin gene alterations in hepatocellular carcinoma. Genes, Chromosomes and Cancer. 2004;40(2):85-96.
617. Picchio MC, Martin ES, Cesar R. Alterations of the tumor supressor gene Parkin in non-small cell lung cancer. Clinical Cancer Research. 2004;10:2720-4.
618. Lutz AK, Exner N, Fett ME, Schlehe JS, Kloos K, Lammermann K, et al. Loss of Parkin or PINK1 Function Increases Drp1-dependent Mitochondrial Fragmentation. Journal of Biological Chemistry. 2009;284(34):22938-51.
619. Rawal N, Corti O, Sacchetti P, Ardilla-Osorio H, Sehat B, Brice A, et al. Parkin protects dopaminergic neurons from excessive Wnt/β-catenin signaling. Biochemical and Biophysical Research Communications. 2009;388(3):473-8.
620. Berwick DC, Harvey K. The regulation and deregulation of Wnt signaling by PARK genes in health and disease. Journal of Molecular Cell Biology. 2013;6(1):3-12.
621. Mizushima N. Autophagy: process and function. Genes & Development. 2007;21(22):2861-73.
622. Puissant A, Fenouille N, Auberger P. When autophagy meets Cancer through p62-SQSTM1. Am J Cnacer Res. 2012;2(4):397-413.

623. Strohecker A M, Guo J, Karsli-Uzunbas G, Price S, Chen G, Mathew R, et al. Autophagy sustains mitochondrial glutamine metabolism and growth of BRAFv600E driven lung tumors. Caner Discovery. 2013.
624. Gao C, Chen Y-G. Selective removal of dishevelled by autophagy- a role of p62. Autophagy. 2010;7(3):334-5.
625. Gao C, Chen Y-G. Dishevelled: The hub of Wnt signaling. Cell Signal. 2010;22(5):717-27.
626. Behrens J. Cadherins and catenins Role in signal transduction and tumor progression. Cancer and Metastasis Reviews. 1999;18:15-30.
627. Dechat T, Adam SA, Goldman RD. Nuclear Lamins and Chromatin: When Structure Meets Function. Advances in Enzyme Regulation. 2009;49(1):157-66.
628. Hüttemann M, Lee I, Pecinova A, Pecina P, Przyklenk K, Doan JW. Regulation of oxidative phosphorylation, the mitochondrial membrane potential, and their role in human disease. Journal of Bioenergetics and Biomembranes. 2008;40(5):445-56.
629. Farkas DL, Wei MD, Febbroriello P, Carson JH, Loew LM. Simultaneous imaging of cell and mitochondrial membrane potentials. Biopsy J. 1989;56(6):1053-69.
630. Ehrenberg B, Montana V, Wei MD, Wuskell JP, Loew LM. Membrane potential can be determined in individual cells from the nernstian distribution of cationic dyes. Biophys J. 1988;53(5):785-94.
631. Reers M, Smith TW, Chen LB. J-aggregate formation of a carbocyanine as a quantitative fluorescent indicator of membrane potential. Biochemistry. 1991;30(18):4480-6.
632. Pridgeon JW, Olzmann JA, Chin LS, Li L. PINK1 Protects against Oxidative Stress by Phosphorylating Mitochondrial Chaperone TRAP1: PLoS Biol. 2007 Jul;5(7):e172. Epub 2007 Jun 19 doi:10.1371/journal.pbio.0050172.
633. Vives-Bauza C, Zhou C, Huang Y, Cui M, de Vries RLA, Kim J, et al. PINK1-dependent recruitment of Parkin to mitochondria in mitophagy. Proceedings of the National Academy of Sciences. 2009;107(1):378-83.
634. Pankiv S, Clausen TH, Lamark T, Brech A, Bruun J-A, Outzen H, et al. p62/SQSTM1 Binds Directly to Atg8/LC3 to Facilitate Degradation of Ubiquitinated Protein Aggregates by Autophagy. Journal of Biological Chemistry. 2007;282(33):24131-45.
635. Jiménez-Mateos E, González-Billault C, Dawson H N, Vitek M P, Avila J. Role of MAP1B in axonal retrograde transport of mitochondria. Biochem J. 2006;397(Pt 1):53-9. Epub 2006 Jun 14 doi:10.1042/BJ20060205.
636. Wang QJ, Ding Y, Kohtz DS, Mizushima N, Cristea IM, Rout MP, et al. Induction of autophagy in axonal dystrophy and degeneration. J Neurosci. 2006;26(31):8057-68.
637. Huang P, Yu T, Yoon Y. Mitochondrial clustering induced by overexpression of the mitochondrial fusion protein Mfn2 causes mitochondrial dysfunction and cell death. European Journal of Cell Biology. 2007;86(6):289-302.
638. Benard G, Karbowski M. Mitochondrial fusion and division: regulation and role in cell viability. Seminars in Cell & Developmental Biology. 2009;20(3):365-74.
639. Chan DC. Mitochondria: Dynamic Organelles in Disease, Aging, and Development. Cell. 2006;125(7):1241-52.

640. Wang W, Lu J, Zhu F, Wei J, Jia C, Zhang Y, et al. Pro-apoptotic and anti-proliferative effects of mitofusin-2 via Bax signaling in hepatocellular carcinoma cells. Med Oncol. 2012;29(1):70-6.
641. Wu L, Li Z, Zhang Y, Zhang P, Zhu X, Huang J, et al. Adenovirus-expressed human hyperplasia suppressor gene induces apoptosis in cancer cells. Molecular Cancer Therapeutics. 2008;7(1):222-32.
642. Jin B, Fu G, Pan H, Cheng X, Zhou L, Lv J, et al. Anti-tumour efficacy of mitofusin-2 in urinary bladder carcinoma. Med Oncol. 2011;28(1):373-80.
643. Lee S, Jeong S-Y, Lim W-C, Kim S, Park Y-Y, Sun X, et al. Mitochondrial Fission and Fusion Mediators, hFis1 and OPA1, Modulate Cellular Senescence. Journal of Biological Chemistry. 2007;282(31):22977-83.
644. Yoon YS, Yoon DS, Lim IK, Yoon SH, Chung HY, Rojo M, et al. Formation of elongated giant mitochondria in DFO-induced cellular senescence: involvement of enhanced fusion process through modulation of Fis1. Journal of cellular physiology. 2006;209(2):468-80.
645. Song Z, Ghochani M, McCaffery JM, Frey TG, Chan DC. Mitofusins and OPA1 Mediate Sequential Steps in Mitochondrial Membrane Fusion. Molecular Biology of the Cell. 2009;20(15):3525-32.
646. Smirnova E, Shurland D-L, Ryazantsev SN, van der Bliek AM. A Human Dynamin-related Protein Controls the Distribution of Mitochondria. The Journal of Cell Biology. 1998;143(2):351-8.
647. Wiedemann N, Stiller Sebastian B, Pfanner N. Activation and Degradation of Mitofusins: Two Pathways Regulate Mitochondrial Fusion by Reversible Ubiquitylation. Molecular Cell. 2013;49(3):423-5.
648. Mancias JD, Kimmelman AC. Targeting Autophagy Addiction in Cancer2011.
649. Buchser WJ, Laskow TC, Pavlik PJ, Lin H-M, Lotze MT. Cell-Mediated Autophagy Promotes Cancer Cell Survival. Cancer Research. 2012;72(12):2970-9.
650. Lock R, Roy S, Kenific CM, Su JS, Salas E, Ronen SM, et al. Autophagy facilitates glycolysis during Ras-mediated oncogenic transformation. Molecular Biology of the Cell. 2011;22(2):165-78.
651. Yang S WX, Contino G, et al. Pancreatic cancers require autophagy for tumor growth. *Genes & Develop*ment. 2011;25(7):717-29.
652. Chun SY, Johnson C, Washburn JG, Cruz-Correa MR, Dang DT, Dang LH. Oncogenic KRAS modulates mitochondrial metabolism in human colon cancer cells by inducing HIF-1α and HIF-2α target genes. Molecular Cancer. 2010;9:293-.
653. White E. Exploiting the bad eating habits of Ras-driven cancers. Genes Dev. 2013;27(19):2065-71. doi:10.1101/gad.228122.113.
654. Scherz‐Shouval R, Shvets E, Fass E, Shorer H, Gil L, Elazar Z. Reactive oxygen species are essential for autophagy and specifically regulate the activity of Atg42007 2007-04-04 00:00:00. 1749-60 p.
655. Huang J, Dibble CC, Matsuzaki M, Manning BD. The TSC1-TSC2 Complex Is Required for Proper Activation of mTOR Complex 2. Molecular and Cellular Biology. 2008;28(12):4104-15.
656. Inoki K, Corradetti MN, Guan K-L. Dysregulation of the TSC-mTOR pathway in human disease. Nat Genet. 2005;37(1):19-24.

657. Degtyarev M, De Maziere A, Orr C, Lin J, Lee BB, Tien JY, et al. Akt inhibition promotes autophagy and sensitizes PTEN-null tumors to lysosomotropic agents. J Cell Biol. 2008;183(1):101-16. doi: 10.1083/jcb.200801099.
658. Moscat J, Diaz-Meco MT. p62: a versatile multitasker takes on cancer. Trends Biochem Sci. 2012;37(6):230-6.
659. Jangamreddy JR, Ghavami S, Grabarek J, Kratz G, Wiechec E, Fredriksson B-A, et al. Salinomycin induces activation of autophagy, mitophagy and affects mitochondrial polarity: Differences between primary and cancer cells. Biochimica et Biophysica Acta (BBA) - Molecular Cell Research. 2013;1833(9):2057-69.
660. Esen E, Chen J, Karner Courtney M, Okunade Adewole L, Patterson Bruce W, Long F. WNT-LRP5 Signaling Induces Warburg Effect through mTORC2 Activation during Osteoblast Differentiation. Cell Metabolism. 2013;17(5):745-55.
661. Riggio M, Polo ML, Blaustein M, Colman-Lerner A, Luthy I, Lanari C, et al. PI3K/AKT pathway regulates phosphorylation of steroid receptors, hormone independence and tumor differentiation in breast cancer. Carcinogenesis. 2011;33(3):509-18.
662. Luo J, Manning BD, Cantley LC. targeting the PI3K-Akt pathway in human cancer rational and promise. Cancer Cell. 2003;4:257-62.
663. Altman BJ, Rathmell JC. Metabolic Stress in Autophagy and Cell Death Pathways. Cold Spring Harbor Perspectives in Biology. 2012;4(9):a008763-a.
664. Mitsuishi Y, Taguchi K, Kawatani Y, Shibata T, Nukiwa T, Aburatani H, et al. Nrf2 Redirects Glucose and Glutamine into Anabolic Pathways in Metabolic Reprogramming. Cancer Cell. 2012;22(1):66-79.
665. Rada P, Rojo AI, Offergeld A, Feng GJ, Velasco-Martin JP, Gonzalez-Sancho JM, et al. WNT-3A Regulates an Axin1/NRF2 Complex That Regulates Antioxidant Metabolism in Hepatocytes. Antioxid Redox Signal. 2014;21:21.
666. Zheng B, Jeong JH, Asara JM, Yuan YY, Granter SR, Chin L, et al. Oncogenic B-RAF negatively regulates the tumor suppressor LKB1 to promote melanoma cell proliferation. Mol Cell. 2009;33(2):237-47.
667. DeBerardinis RJ, Lum JJ, Thompson CB. Phosphatidylinositol 3-Kinase-dependent Modulation of Carnitine Palmitoyltransferase 1A Expression Regulates Lipid Metabolism during Hematopoietic Cell Growth. Journal of Biological Chemistry. 2006;281(49):37372-80.
668. White E. Deconvoluting the context-dependent role for autophagy in cancer. Nature reviews Cancer. 2012;12(6):401-10.
669. Lu D, Choi MY, Yu J, Castro JE, Kipps TJ, Carson DA. Salinomycin inhibits Wnt signaling and selectively induces apoptosis in chronic lymphocytic leukemia cells. Proceedings of the National Academy of Sciences. 2011;108(32):13253-7.
670. Anastas JN, Moon RT. WNT signalling pathways as therapeutic targets in cancer. Nature Reviews Cancer. 2012;13(1):11-26.
671. Sebastián D, Hernández-Alvarez MI, Segalés J, Sorianello E, Muñoz JP, Sala D, et al. Mitofusin 2 (Mfn2) links mitochondrial and endoplasmic reticulum function with insulin signaling and is essential for normal glucose homeostasis. Proc Natl Acad Sci U S A. 2012;109(14):5523-8.
672. Mosimann C, Hausmann G, Basler K. Beta-catenin hits chromatin: regulation of Wnt target gene activation. Nature reviews Molecular cell biology. 2009;10(4):276-86.

673. Lu M, Breyssens H, Salter V, Zhong S, Hu Y, Baer C, et al. Restoring p53 function in human melanoma cells by inhibiting MDM2 and cyclin B1/CDK1-phosphorylated nuclear iASPP. Cancer Cell. 2013;23(5):618-33. doi: 10.1016/j.ccr.2013.03.013. Epub Apr 25.
674. Lim S, Kaldis P. Cdks, cyclins and CKIs: roles beyond cell cycle regulation. Development. 2013;140(15):3079-93.
675. Gao L, Feng Y, Bowers R, Becker-Hapak M, Gardner J, Council L, et al. Ras-Associated Protein-1 Regulates Extracellular Signal-Regulated Kinase Activation and Migration in Melanoma Cells: Two Processes Important to Melanoma Tumorigenesis and Metastasis. Cancer Research. 2006;66(16):7880-8.
676. Gordon RR, Nelson PS. Cellular senescence and cancer chemotherapy resistance. Drug Resistance Updates. 2012;15(1–2):123-31.
677. Qu X, Yu J, Bhagat G, Furuya N, Hibshoosh H, Troxel A, et al. Promotion of tumorigenesis by heterozygous disruption of the beclin 1 autophagy gene. J Clin Invest. 2003;112(12):1809-20. Epub 2003 Nov 24.
678. Miracco C, Cevenini G, Franchi A, Luzi P, Cosci E, Mourmouras V, et al. Beclin 1 and LC3 autophagic gene expression in cutaneous melanocytic lesions. Hum Pathol. 2010;41(4):503-12. doi: 10.1016/j.humpath.2009.09.004. Epub Dec 11.
679. Ma XH, Piao S, Wang D, McAfee QW, Nathanson KL, Lum JJ, et al. Measurements of tumor cell autophagy predict invasiveness, resistance to chemotherapy, and survival in melanoma. Clin Cancer Res. 2011;17(10):3478-89. doi: 10.1158/078-0432.CCR-10-2372. Epub 011 Feb 15.
680. Lazova R, Klump V, Pawelek J. Autophagy in cutaneous malignant melanoma. J Cutan Pathol. 2010;37(2):256-68. doi: 10.1111/j.600-0560.2009.01359.x. Epub 2009 Jul 14.
681. Lazova R, Camp RL, Klump V, Siddiqui SF, Amaravadi RK, Pawelek JM. Punctate LC3B expression is a common feature of solid tumors and associated with proliferation, metastasis, and poor outcome. Clin Cancer Res. 2012;18(2):370-9. doi: 10.1158/078-0432.CCR-11-1282. Epub 2011 Nov 11.
682. Hersey P, Zhang XD. Adaptation to ER stress as a driver of malignancy and resistance to therapy in human melanoma. Pigment Cell Melanoma Res. 2008;21(3):358-67. doi: 10.1111/j.755-148X.2008.00467.x.
683. Corazzari M, Fimia GM, Lovat P, Piacentini M. Why is autophagy important for melanoma? Molecular mechanisms and therapeutic implications. Semin Cancer Biol. 2013;23(5):337-43. doi: 10.1016/j.semcancer.2013.07.001. Epub Jul 12.
684. Veeck J, Dahl E. Targeting the Wnt pathway in cancer: The emerging role of Dickkopf-3. Biochimica et Biophysica Acta (BBA) - Reviews on Cancer. 2012;1825(1):18-28.
685. Sugimura R, Li L. Noncanonical Wnt signaling in vertebrate development, stem cells, and diseases. Birth Defects Res C Embryo Today. 2010;90(4):243-56. doi: 10.1002/bdrc.20195.
686. Proffitt KD, Madan B, Ke Z, Pendharkar V, Ding L, Lee MA, et al. Pharmacological Inhibition of the Wnt Acyltransferase PORCN Prevents Growth of WNT-Driven Mammary Cancer. Cancer Research. 2013;73(2):502-7.
687. Ewan K, Pajak B, Stubbs M, Todd H, Barbeau O, Quevedo C, et al. A useful approach to identify novel small-molecule inhibitors of Wnt-dependent

transcription. Cancer Res. 2010;70(14):5963-73. doi: 10.1158/0008-5472.CAN-10-1028. Epub 2010 Jul 7.
688. Bao R, Christova T, Song S, Angers S, Yan X, Attisano L. Inhibition of Tankyrases Induces Axin Stabilization and Blocks Wnt Signalling in Breast Cancer Cells. PLoS One. 2012;7(11):e48670. doi:10.1371/journal.pone.0048670.
689. Huang SM, Mishina YM, Liu S, Cheung A, Stegmeier F, Michaud GA, et al. Tankyrase inhibition stabilizes axin and antagonizes Wnt signalling. Nature. 2009;461(7264):614-20. doi: 10.1038/nature08356. Epub 2009 Sep 16.
690. Thorne CA, Hanson AJ, Schneider J, Tahinci E, Orton D, Cselenyi CS, et al. Small-molecule inhibition of Wnt signaling through activation of casein kinase 1α. Nat Chem Biol. 2010;6(11):829-36. Epub 2010 Oct 3 doi:10.1038/nchembio.453.
691. Gonsalves FC, Klein K, Carson BB, Katz S, Ekas LA, Evans S, et al. An RNAi-based chemical genetic screen identifies three small-molecule inhibitors of the Wnt/wingless signaling pathway. Proc Natl Acad Sci U S A. 2011;108(15):5954-63.
692. Lepourcelet M, Chen YN, France DS, Wang H, Crews P, Petersen F, et al. Small-molecule antagonists of the oncogenic Tcf/beta-catenin protein complex. Cancer Cell. 2004;5(1):91-102.
693. Wang W, Liu H, Wang S, Hao X, Li L. A diterpenoid derivative 15-oxospiramilactone inhibits Wnt/beta-catenin signaling and colon cancer cell tumorigenesis. Cell Res. 2011;21(5):730-40. doi: 10.1038/cr.2011.30. Epub Feb 15.
694. Emami KH, Nguyen C, Ma H, Kim DH, Jeong KW, Eguchi M, et al. A small molecule inhibitor of beta-catenin/CREB-binding protein transcription [corrected]. Proc Natl Acad Sci U S A. 2004;101(34):12682-7. Epub 2004 Aug 16.
695. Fan C, Wang W, Zhao B, Zhang S, Miao J. Chloroquine inhibits cell growth and induces cell death in A549 lung cancer cells. Bioorg Med Chem. 2006;14(9):3218-22. Epub 2006 Jan 18.
696. Cook KL, Warri A, Soto-Pantoja DR, Clarke PA, Cruz MI, Zwart A, et al. Hydroxychloroquine inhibits autophagy to potentiate antiestrogen responsiveness in ER+ breast cancer. Clin Cancer Res. 2014;20(12):3222-32. doi: 10.1158/078-0432.CCR-13-3227.
697. Rangwala R, Chang YC, Hu J, Algazy KM, Evans TL, Fecher LA, et al. Combined MTOR and autophagy inhibition: phase I trial of hydroxychloroquine and temsirolimus in patients with advanced solid tumors and melanoma. Autophagy. 2014;10(8):1391-402. doi: 10.4161/auto.29119. Epub 2014 May 20.
698. Flaherty KT, Hodi FS, Fisher DE. From genes to drugs: targeted strategies for melanoma. Nature reviews Cancer. 2012;12(5):349-61.